Genesis of Stratabound Scheelite and Stratiform Pb-Zn Mineralisation Chitral, Northern Pakistan, and its Comparison with S-W England Tin-Tungsten Deposits.

Thesis submitted for the degree of
Doctor of Philosophy
at the University of Leicester

by

Mohammad Zahid Khan
Department of Geology
University of Leicester

September 1996

ProQuest LLC
789 East Eisenhower Parkway
P.O. Box 1346
Ann Arbor, MI 48106-1346

Genesis of Stratabound Scheelite and Stratiform Pb-Zn Mineralisation Chitral, Northern Pakistan, and its Comparison with S-W England Tin-Tungsten Deposits.

Mohammad Zahid Khan

Abstract

Tungsten mineralisation lies within the Asian plate to the north-west of Main Karakoram Thrust, which marks the suture zone between the Kohistan complex (Northern Pakistan) and Asian plate. Scheelite has been found mainly in the calc-silicate quartzites and subordinate tourmalinites associated with metapelites at Miniki Gol. This succession is intruded by leucogranites emplaced after the culmination of amphibolite facies metamorphism followed by retrogression. The area has undergone at least two deformational events and scheelite seems to be structurally controlled.

Miniki Gol leucogranites are exposed 400 m away from the scheelite mineralisation and tungsten appears to be genetically related to these leucogranites. The chemistry of these leucogranites particularly high levels of Li, Be, W, Sn and Ta fairly coordinate with the specialised granite.

The trace element chemistry and the chemical composition of clinozoisite, sphene, amphibole, grossular garnet, biotite, chlorite and scheelite of the calc-silicate rocks indicate a pronounced hydrothermal activity at Miniki Gol. The chemical composition of the tourmaline and spessartine-rich garnet of the tourmalinites is similar to that of tourmaline and spessartine-rich garnet of the leucogranite reflecting a genetic linkage. The occurrence of scheelite-bearing skarn at Miniki Gol further support a genetic relationship between scheelite mineralisation and leucogranite.

In addition, the geochemical data of the Miniki Gol tourmalinites have been found similar to that of schist and hence can not be considered as siliceous chemical precipitates. Background level of tungsten is slightly higher than those of the average shale but not anomalous that rules out the possibility of the pre-granitic enrichment of tungsten at the study area.

The consistency of the fluid inclusions both within leucogranites and calc-silicate rocks also signify a genetic link between the scheelite mineralisation and the possible post-magmatic hydrothermal fluids.

The Miniki Gol W mineralisation has been compared with Cornubian Sn-W deposits. In both the areas tungsten seems to be enriched after the emplacement of granites.

The stratiform and stratabound lead-zinc mineralisation is mainly confined to the marble horizon at Besti Gol. The conformability of the sulphide mineralisation with the host marble indicates that these mineralisations have been precipitated in synsedimentary environment.

Acknowledgements

This study was completed with the help and encouragement from a number of individuals and organisations. The financial assistance was provided by the Association of Commonwealth Universities and administered by the British Council. The University of Peshawar (Pakistan) is acknowledged by granting a leave of absence from the employment. The Sarhad Development Authority contributed an assistance in the field work in many ways.

I would like to thank Dr. C. J. Moon for the critical review of the manuscript and supervision of thesis project. Due regards are extended to all members of the academic staff at the Department of Geology, Leicester University, particularly Steve Temperley, M. J. Le Bas, Jeremy Richards and M. J. Norry for their valuable suggestions and fruitful discussion.

I wish to express my profound gratitude to D. H. M. Alderton for helping in fluid inclusion study and permission to use the fluid inclusion stage at Royal Holloway and Bedford New College, University of London. All the members of clerical and technical staffs at the Department of Geology, Leicester University, especially Bill Teasdale, Colin Cunnigham, Rod Branson, Nick Marsh, Rob Wilson, Rob Kelly, Chris Beckett, Paul Ayto, Pat Herbert, Emma Mansley, Linda Marvin, Andrew Smith and Douglas Martin are gratefully acknowledged for providing assistance in many ways.

I also would like to thank Shakirullah, Zahid Ahmad Sahibzada and Zafar, employees of the Sarhad Development Authority, Peshawar, Pakistan for their help and assistance during the field work.

Finally, I like to express my gratitude to my wife and four children, who have been very helpful and supportive during the entire course of this study.

Genesis of Stratabound Scheelite and Stratiform Pb-Zn Mineralisation Chitral, Northern Pakistan, and its Comparison with S-W England Tin-Tungsten Deposits.

Contents

Page Number

Abstract
Acknowledgements
List of Figures i
List of Tables iii
List of Appendices iv

Chapter One Introduction

1.1 Introduction 1
1.1.1 Brief description of the thesis area 1
1.1.2 Previous work 4
1.1.3 Thesis focus 5
1.1.4 Field work 5
1.1.5 Thesis layout 6
1.2 Classification of tungsten deposits 6
1.2.1 Granitoid-related deposits. 6
1.2.2 Tungsten-bearing granitoid or specialised granite 6
1.2.3 Greisen or hydrothermal deposits 7
1.2.4 Tungsten skarn deposits 7
1.2.5 Metamorphosed volcanogenic or exhalative W deposits 8
1.3 Occurrences of lead-zinc mineralisation 9

Chapter Two Regional and local geological setting

2.1 Regional geology 10
2.1.1 Tectonic history of Pakistan 10
2.1.2 Himalayas 10
2.1.2A Zanskar Range 10
2.1.2B High Himalaya 11
2.1.2C Lesser and Sub-Himalaya 11
2.1.3 Indus suture zone 11
2.1.4 Kohistan island arc 13
2.1.4A Jijal and Chilas complexes 13
2.1.4B Kamila amphibolites 13
2.1.4C Kohistan batholith 13
2.1.4D Island arc volcanics and metasediments 14
2.1.5 Northern suture zone 14
2.1.6 The Karakoram terrane 14
2.1.6A Northern Karakoram terrane 15
2.1.6B The Karakoram batholith 15
2.1.6C Leucogranite 17
2.1.6D Karakoram metamorphic complex 17
2.1.6E Deformational and metamorphic history 18

2.2 Local geology 18
2.2.1 Western Karakoram and Hindu Kush 18
2.2.2 Central Unit 20
2.2.2A Gahiret Lime stone 20
2.2.2B Koghozi greenschist 20
2.2.2C Chitral Slate 21
2.2.2D Reshun Formation 21
2.2.2E Shoghor Limestone 21
2.2.3 Northwestern Unit 21
2.2.4 Tirich Mir and Kafiristan plutons 23
2.2.5 Other mineralisations 23

Chapter Three Field relations and structure

3.1 Introduction 25
3.2 Field relations 25
3.2.1 Schistose rocks 25
3.2.2 Quartzitic rocks 26
3.2.3 Leucogranite 26
3.3 Structure 28
3.3.1 First deformation 28
3.3.2 Second deformation 28
3.3.3 Veins 28
3.3.4 Metamorphism and paragenetic sequence of minerals 31
3.4 Mineralisation in the area 31
3.4.1 Tungsten mineralisation 31
3.4.2 Lead-zinc mineralisation 34
3.5 Discussion 36

Chapter Four Petrographic and mineralogical studies

4.1 Introduction 38
4.2 Samples and methods 38
4.3 Lithology and petrography 38
4.3.1 Mica schist 42
4.3.2 Phyllite 42
4.3.3 Mica quartzite and micaeous psammite 42
4.3.4 Calc-silicate quartzite 42
4.3.5 Tourmalinite 48
4.3.6 Marble 48
4.3.7 Porphyritic granodiorites 51
4.3.8 Leucogranite and pegmatite 51
4.4 Mineral chemistry 51
4.4.1 Tourmaline 55
4.4.2 Clinozoisite 61
4.4.3 Garnet 65
4.4.4 Amphibole 71
4.4.5 Chlorite 80
4.4.6 Biotite 80
4.4.7 Titanite 88
4.4.8 Plagioclase 92
4.4.9 Scheelite 92
4.4.10 Sphalerite 96
4.5 Discussion 100

4.5.1 Calc-silicate quartzite 100
4.5.2 Tourmalinite 104
4.5.3 Leucogranite 106
4.5.4 Pb-Zn mineralisation 107
4.6 Summary 108

Chapter Five Geochemistry

5.1 Introduction 109
5.2 Geochemistry of Miniki Gol granite 109
5.2.1 Petrographic and mineralogical features of the Miniki Gol leucogranite 109
5.2.2 Major element geochemistry 110
5.2.3 Trace element geochemistry 115
5.2.4 Specialised granite 119
5.3 Schist 121
5.4 Background level of tungsten at Miniki Gol 121
5.4.1 Background level of tungsten at SW England 124
5.4.2 Levels of Li, W and Sn 124
5.5 Calc-silicate quartzite and psammite 128
5.5.1 Trace element chemistry 131
5.6 Tourmalinite 131
5.7 Marble-hosted stratiform Pb-Zn mineralisation 133
5.8 REE 136
5.8.1 Leucogranite 136
5.8.2 Schist 139
5.8.3 Calc-silicate rocks 139
5.8.4 Tourmalinite 142
5.8.5 Marble 142
5.9 Conclusion 142

Chapter Six Fluid inclusions

6.1 Introduction 144
6.2 Sample preparation 144
6.3 Analytical techniques 145
6.4 Fluid inclusions characteristics 146
6.4.1 Primary inclusions 147
6.4.1A Quartz veins 147
6.4.1B Pegmatites 147
6.4.1C Leucogranite 147
6.4.1D Scheelite-bearing calc-silicate quartzites 147
6.4.2 Secondary inclusions 148
6.4.3 Microthermometry 148
6.5 Discussion 158
6.6 Conclusion 161

Chapter Seven Discussion and conclusions

7.1 Discussion 163
7.1.1 Introduction 163
7.1.2 Deformation and metamorphism 163
7.1.3 Leucogranite 164
7.1.4 Hydrothermal alteration 165
7.1.4 A Leucogranite 165

7.1.4 B Schist 166
7.1.4 C Calc-silicate rocks 166
7.1.4 D Tourmalinite 167
7.1.5 Tourmalinisation 167
7.1.6 Nature of the mineralising fluid 169
7.1.7 Pressure-temperature estimates 171
7.1.8 Evolution of calc-silicate quartzite 172
7.1.9 Scheelite mineralisation 173
7.1.10 Source of tungsten 174
7.1.11 Marble-hosted stratiform Pb-Zn mineralisation 174
7.1.12 Comparison of Miniki Gol mineralisation with SW England deposits 176
7.2 Conclusion 177
7.2.1 Genesis of Miniki Gol scheelite 177
7.2.1 A Tourmalinites 177
7.2.1 B Calc-silicates 178
7.2.1 C Granite chemistry 178
7.2.1 D Fluid inclusions 179
7.2.1 E Deformation 179
7.2.2 Other conclusions 179
7.3 Recommendation for future studies 179

Appendices 181

References 209

List of Figures

Page

Number

Chapter One Introduction

Figure 1.1 Topographic frame work of N. Pakistan 2
Figure 1.2 Geological map of the Miniki Gol area 2
Figure 1.3 Geological map of the Besti Gol area 3

Chapter Two Regional and local geological setting

Figure 2.1 Geological map of Himalaya and Karakoram 12
Figure 2.2 Geological map of the Central Karakoram 16
Figure 2.3 Geological map of the Chitral area 19
Figure 2.4 Geological map of the Garam Chashma area 22

Chapter Three Field relations and structure

Figure 3.1 Photographs of (a) tourmaline-mica schist (b) calc-silicate quartzite 27
Figure 3.2a-b Contact relationship of granite with schist 29
Figure 3.2c Boudinage structure in scheelite-bearing quartzite 29
Figure 3.2d Chevron folds in schist 29
Figure 3.3a Scheelite patches in calc-silicate quartzite 30
Figure 3.3b Scheelite patches in tourmalinites 30
Figure 3.4 Scheelite fluorescence (a) in calc-silicate quartzite (b) tourmalinite 33
Figure 3.5a Marble-hosted stratiform Pb-Zn mineralisation 35
Figure 3.5b Fluorescence of sphalerite-hydrozincite under UV lamp 35

Chapter Four Petrographic and mineralogical studies

Figure 4.1 A Sample location map of the Miniki Gol area (ZC series) 39
Figure 4.1 B Sample location map of the Miniki Gol area (ZM series) 40
Figure 4.1 C Sample location map of the Besti Gol area 41
Figure 4.2 A Photomicrograph showing garnet and staurolite porphyroblasts 44
Figure 4.2 B Photomicrograph showing clinozoisite grains 44
Figure 4.3 A Photomicrograph showing chlorite veins 45
Figure 4.3 B Photomicrograph showing alteration of plagioclase 45
Figure 4.4 A Photomicrograph showing spherulitic amphibole 46
Figure 4.4 B Photomicrograph showing secondary biotite and chlorite 46
Figure 4.5 A Photomicrograph showing alteration of biotite 47
Figure 4.5 B SEM Photograph showing scheelite associated with clinozoisite 47
Figure 4.6 A Photomicrograph showing scheelite intergrown with clinozoisite 49
Figure 4.6 B Photomicrograph showing scheelite veins 49
Figure 4.7 A Photomicrograph showing tourmaline grains 50
Figure 4.7 B Photomicrograph showing garnet grains 50
Figure 4.8 A Photomicrograph showing alteration of sphalerite 52
Figure 4.8 B SEM Photograph showing texture of sphalerite 52
Figure 4.9 A Photomicrograph showing alteration of galena 53
Figure 4.9 B Photomicrograph showing alteration of pyrite 53
Figure 4.10 A Photomicrograph showing alteration of biotite in leucogranite 54
Figure 4.10 B Photomicrograph showing alteration of biotite into kaolin 54

Figure 4.11 Compositional characteristics of tourmaline 59
Figure 4.12 Compositional characteristics of tourmaline 60
Figure 4.13 Chemical composition of clinozoisite 64
Figure 4.14 Chemical characteristics of garnet 72
Figure 4.15 Composition of amphibole 78
Figure 4.16 Chemical characteristics of amphibole 79
Figure 4.17 Chemistry of chlorite 83
Figure 4.18 Chemical characteristics of biotite 87
Figure 4.19 Composition of sphene 91

Chapter Five Geochemistry

Figure 5.1A Composition of muscovite from leucogranite 111
Figure 5.1 Major and trace elements relationship within the granodiorite and leucogranite 111
Figure 5.2 Relationship of FeO with Major elements 116
Figure 5.3 Relationship of FeO with Major and trace elements, Ta vs. Sn 117
Figure 5.4 Samples location map of the background pelites at Garam Chashma 123
Figure 5.5 Concentrations of Sn-W against distance 125
Figure 5.6 Samples location map of the background pelites at SW England 126
Figure 5.7 Major and trace elements relationship within the calc-silicate and tourmalinite 130
Figure 5.8 Chondrite normalised REE pattern of the studied rocks 137
Figure 5.9 Relationship of La with Zr, Hf, Be and W in leucogranite and tourmalinite 138
Figure 5.10 Correlation of REE with other elements in calc-silicate rocks 141

Chapter Six Fluid inclusions

Figure 6.1 Photomicrographs showing CO_2-bearing fluid inclusions 149
Figure 6.2 Photomicrographs showing aqueous inclusions in leucogranites 150
Figure 6.3 Photomicrographs showing inclusions in calc-silicate rocks 151
Figure 6.4 Photomicrographs showing inclusions in granite and pegmatite 152
Figure 6.5 Charts showing homogenisation temperature 156
Figure 6.6 Charts showing homogenisation temperature and salinity 157

List of Tables

Number Page

Chapter Three Field relations and structure

Table 3.1 Summary of structure and mineralisation in the study area 32

Chapter Four Petrographic and mineralogical studies

Table 4.1 Microprobe analyses of tourmaline 56
Table 4.2 Microprobe analyses of clinozoisite 62
Table 4.3 Microprobe analyses of garnet 66
Table 4.4 Microprobe analyses of amphibole 73
Table 4.5 Microprobe analyses of chlorite 81
Table 4.6 Microprobe analyses of biotite 85
Table 4.7 Microprobe analyses of titanite 89
Table 4.8 Microprobe analyses of plagioclase 93
Table 4.9 Microprobe analyses of scheelite 97
Table 4.10 Microprobe analyses of sphalerite, arsenopyrite and galena 101

Chapter Five Geochemistry

Table 5.1 Major and trace element geochemistry of the leucogranite 112
Table 5.2 Geochemical data of the granodiorite 114
Table 5.3 Major and trace element geochemistry of schist 122
Table 5.4 Li, W and Sn concentration in SW England pelites 127
Table 5.5 Geochemical data of the calc-silicate quartzite and psammite 129
Table 5.6 Major and trace element chemistry of tourmalinite 132
Table 5.7 Trace elements analyses of marble 134

Chapter Six Fluid inclusions

Table 6.1 Description of the samples 145
Table 6.2 Microthermometric analyses 154

List of Appendices

Number		Page
Appendix 4.1	List of the samples studied	181
Appendix 4.2	Analytical techniques for microprobe analyses	188
Appendix 5.1	Analytical techniques for geochemical analyses	190
Appendix 5.2	Major and trace element chemistry of the leucogranite	194
Appendix 5.3	Major and trace element geochemical data of schist	196
Appendix 5.4	Major and trace element chemistry of psammite and calc-silicate rocks	199
Appendix 5.5	Major and trace element composition of the tourmalinite	204
Appendix 5.6	Description of the samples from SW England	205
Appendix 5.7	Trace element chemistry of the studied rocks from SW England	207

Chapter One

INTRODUCTION

1.1 Introduction

1.1.1 Brief description of the thesis area

The study area, largely the catchment of Miniki Gol and Besti Gol rivers, Chitral District, Northern Pakistan lies within the Hindu Kush range, approximately 50 km to the northwest of the Main Karakoram Thrust between Afghanistan border and Shoghor Limestone (Fig. 1.1, 2.3, 2.4). The project area can be approached from Chitral to Garam Chashma by a 45 km jeepable road. Further access to the main mineralised area can be made from Garam Chashma to the Miniki Gol by a 7 km foot trails along the right bank of Murdan Gol. The Besti Gol Pb-Zn mineralisation zone lies about 7 km further north of Miniki Gol. Both the Miniki Gol and Besti Gol areas lie at an elevation of about 3500 m (Topographic sheet 37 P / 12) and are characterised by rugged mountains and V-shaped canyons.

The Arkari Formation hosts the stratabound tungsten and stratiform lead-zinc mineralisation at Miniki Gol and Besti Gol respectively (Fig. 1.2, 1.3). The Formation is dominantly composed of garnet mica schist, phyllite, calc-silicate quartzites, marble and subordinate tourmalinites (Fig. 1.2). These rocks have undergone at least two phases of deformation and metamorphism, and are related to continent-arc collisions during the Cretaceous and Eocene respectively (Leake et al. 1989). Metamorphism within the Arkari Formation is highly variable, ranging from lower greenschist grade to amphibolite facies. The age of the Arkari Formation is still unclear, however Tipper (in Pascoe 1924) recovered belemnites from the Besti Gol phyllite and suggested a Jurassic age.

Tungsten mineralisation is mainly represented by scheelite in the study area and has been found in various rocks but is mainly concentrated in calc-silicate quartzite and subordinate tourmalinites. Although minor occurrences and showings extended up to Garam Chashma area, the best grade tungsten mineralisation zone has been found within a 2-3 km belt in the vicinity of Miniki Gol. Two mica leucogranite is emplaced at the mouth of Miniki Gol, approximately 400 meters to the southeast of mineralised zone (Fig. 1.2) but is generally unmineralised. Although the leucogranites and tungsten mineralisation do not appear to be spatially associated at least at the surface, however, the possible genetic relationship between the two can not be ruled out (see Chapter 5).

Tungsten mineralisation elsewhere in Pakistan has been reported at Saindak area, Baluchistan and Oghi, Hazara, southern Himalaya, by Siddiqui et al. (1986) and Asrarullah (1982). In Saindak area scheelite is associated with a pyroclastic sequence, dyke-like

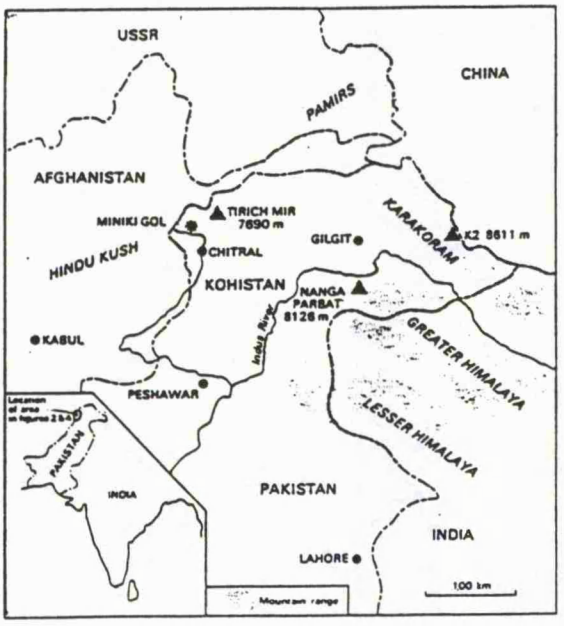

Fig. 1.1: Topographic frame work of N. Pakistan showing the location of tungsten mineralisation at Miniki Gol within the Hindu Kush range (after Fletcher 1985).

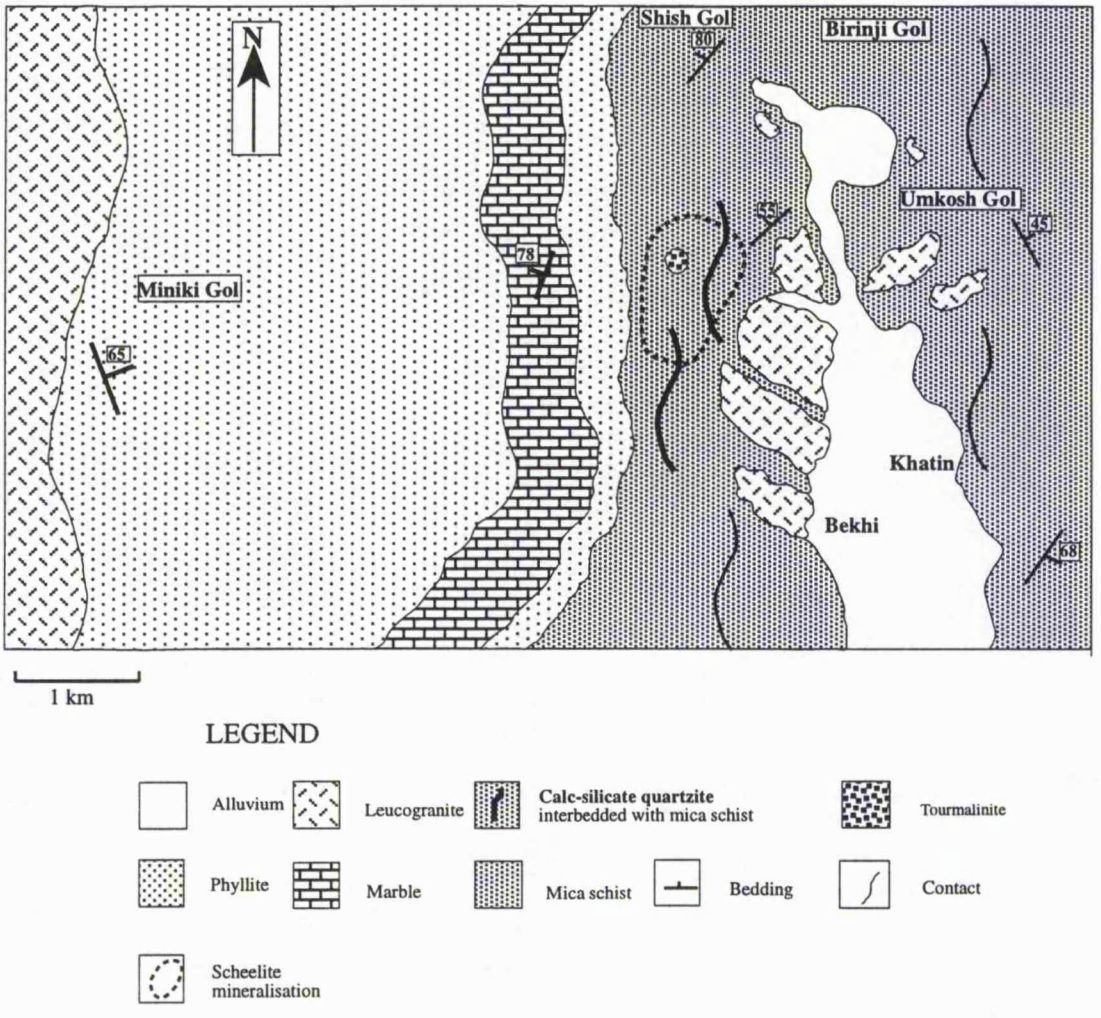

Fig. 1.2: Simplified geological map of the Miniki Gol and surrounding area.

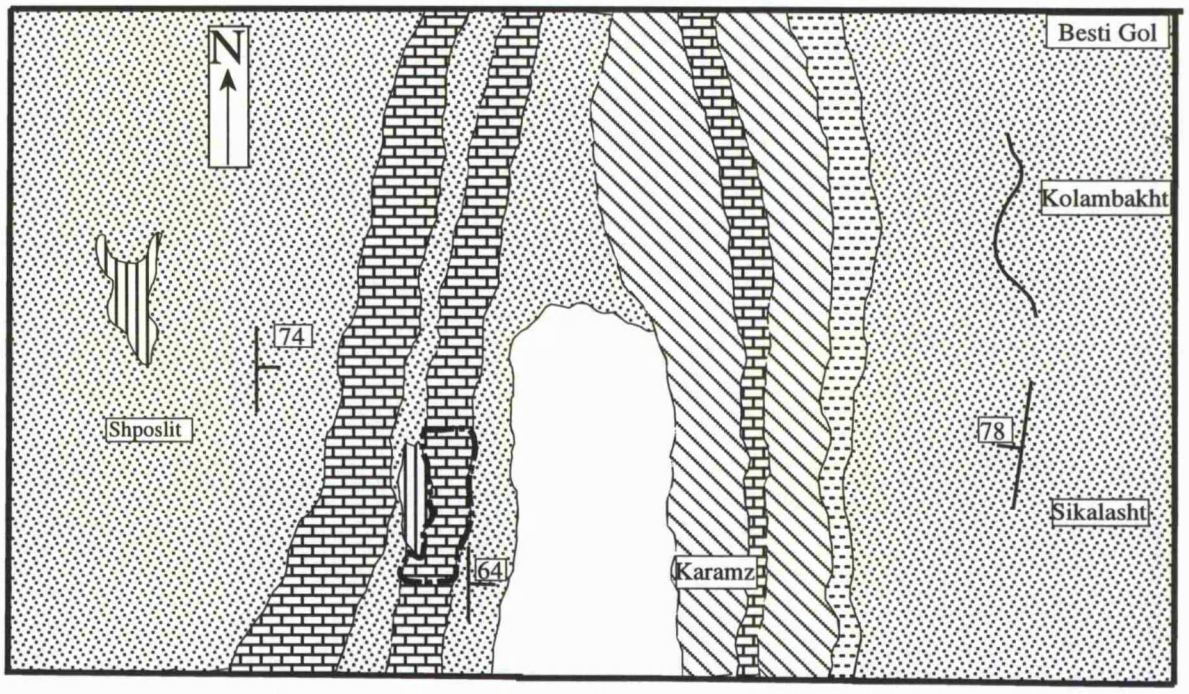

LEGEND

- Alluvium
- Phyllitic schist
- Quartz veins
- Quartzite
- Marble
- Bedding
- Green schist
- Contact
- Calcareous schist
- Pb-Zn mineralisation

Fig. 1.3: Simplified geological map of the Besti Gol and adjoining area.

quartz porphyry intrusion and tourmaline intrusive breccia pipes (Siddiqui et al. 1986). These authors have considered it as a hypogene tungsten mineralisation associated with Chagai calc-alkaline magmatic belt. Scheelite in Oghi area has been found in granite gneiss and seems to be related to the surrounding Mansehra granite (Asrarullah 1982).

Stratiform lead-zinc mineralisation is confined to a prominent belt of marble extending from Hot springs to Besti area within the Arkari Formation (Fig. 1.3, 2.4). Sphalerite and galena are the main phases identified which occur as more or less continuous layers along the strike of the enclosing marble. The extension of Pb-Zn mineralisation along its strike length at Besti Gol is unknown. No leucogranite plutons have been found in the near vicinity, however, quartz veins that are generally unmineralised, are associated with the mineralised zone.

1.1.2 Previous work

Tungsten in the form of scheelite was first reported in the Hindu Kush range of northern Pakistan by Zeschke (1961) as grains in a regional stream sediment panned concentrate survey. Austromineral (1978) discovered scheelite within the Garam Chashma area using a regional geochemical stream sediments survey, although they were unable to locate the source of mineralisation. A detailed panned concentrate survey of the area by the Sarhad Development Authority and the British Geological Survey (Leake 1983) was more successful and traced the source of the mineralisation in the Miniki Gol area. Further exploration, whole rock geochemical studies and petrological studies were carried out under the auspices of Sarhad Development Authority, by Soquem (1984), Leake and Haslam (1985), Dames and Moore (1987) and Sultan (1990). The work to date has managed to locate the host of scheelite as calc-silicate quartzites, tourmalinites and tourmaline gneisses in the Miniki Gol area.

Fletcher (1985) focused on the structural setting of the area and recognised two major deformational events in the Miniki Gol area, and also proposed that the emplacement of the Miniki Gol leucogranite is contemporaneous with the second deformational phase in the area.

Fletcher (1985) and Dames and Moore (1987) argued that the Miniki Gol leucogranite may have remobilised the pre-existing primary scheelite, however the latter author preferred the hot springs origin. Leake (1983) proposed a volcanic-exhalative origin for the Miniki Gol scheelite and considered it as stratabound scheelite. On the basis of tourmaline, garnet mineral chemistry and whole rock analyses, Leake and Haslam (1985) interpreted the Miniki Gol sequence as a metamorphosed playa lake sequence. Later work by Leake et al. (1989) concluded that Miniki Gol stratabound scheelite has

crystallised prior to the intrusion of leucogranite and they regarded it clearly of diagenetic-metamorphic origin.

1.1.3 Thesis focus

The basic aim of the present investigation is to evolve a comprehensive genetic model of tungsten and lead-zinc mineralisations in Chitral, northern Pakistan. In spite of substantial geological and geochemical work on the tungsten mineralisation at Miniki Gol, Chitral, its genesis is still unclear. The role of the Miniki Gol leucogranite in the reconcentration of these metals has not been addressed in the past. Moreover the genesis of newly discovered Pb-Zn mineralisation in the project area is also unresolved.

Mineral chemistry, fluid inclusions, and trace element geochemical studies of the host rocks and associated leucogranites have been performed. The study will enable us to understand the behaviour of ore bearing fluids and its source. The thesis also includes the comparison and correlation of Chitral tungsten mineralisation with SW England tungsten mineralisation. The tungsten mineralisation, almost always in the form of wolframite, is spatially and genetically associated with most of the SW England leucogranites, particularly the fractionated parts and of greisen.

Another important geochemical exploration work regarding these mineralisations is to study the background levels of tungsten in surrounding host rocks both in Chitral and SW England.

The primary aims of this project can be summarised as:

- Proposing a complete genetic model for Chitral W and Pb-Zn mineralisation.
- Geochemical exploration by determining the levels of tungsten and other pathfinders elements in the country rocks.
- Comparison of Chitral tungsten mineralisation with SW England tungsten mineralisation.

1.1.4 Field work

In order to know field relations of the scheelite mineralisation, form and its relation to the enclosing rocks and leucogranites, two field trips have been made. The first one week field work was carried out prior to the commencement of the study and a second four weeks field trip was arranged during July 1992 to Chitral. Initially, scheelite mineralisation at Miniki Gol was selected for this study, however, during the second field trip, Pb-Zn mineralisation was discovered at Besti Gol. The lead-zinc mineralisation was marked previously as tungsten mineralisation due to same coloration and fluorescence by Sarhad Development Authority. Little attention has been given to the marble-hosted Pb-

Zn mineralisation during the course of this study. The field relations based on these trips are presented in Chapter 3. A third one week field trip was made during September 1992 to the SW England. Besides field observation and geological mapping, about 300 representative rock samples were collected from different locality of the project area (see Fig. 4.1A-C, 5.4, 5.6).

1.1.5 Thesis layout

An outline of the regional tectonic setting of northern Pakistan and local geology of the project area are presented in Chapter Two. Chapter Three describes the mineralisation, field relations and structures in the thesis area. Mineral chemical composition of the silicate, oxide and sulphide phases are discussed in Chapter Four. Chapter Five explains geochemical characteristics and signature of the rocks, whereas Chapter Six reports the fluid inclusion study. Finally, Chapter Seven presents a genetic model for the mineralisation, interpretations and conclusion of the project.

1.2 Classification of tungsten deposits

Tungsten deposits may be broadly classified into granitoid-related and non granitoid-related deposits. The tungsten deposits which are directly or indirectly related to granitoid include tungsten-bearing granitoid, greisens and tungsten skarn deposits (e.g. Hosking 1982; Raith and Prochaska 1995). In contrast, non granitoid deposits include volcanogenic or exhalative tungsten deposits, which may be reconcentrated by subsequent metamorphism.

1.2.1 Granitoid-related deposits

1.2.2 Tungsten-bearing granitoid or specialised granite

Most tungsten and tin deposits are spatially and genetically associated with the granitoids, mostly granodiorites, monzogranites and two mica leucogranites (Lehmann 1990). The pegmatite-hosted W-Sn mineralisation of Thailand is considered to be of primary magmatic origin formed by magmatic fractionation from a late stage volatile rich aqueous melt (Manning 1986). Scheelite has also been found in pegmatite at Colorado and Wyoming, USA (Tweto 1960). However, no economic tungsten deposits of primary magmatic origin within granite have been found in the world. Some of the granitic dykes in Auvergne (France) and Nigde Massif (Turkey) do contain tungsten mineralisation but they are not of commercial interest (Alexandrov 1962; Akcay 1994).

The genetic relationship between the composition of the granitoid and the nature of associated mineralisation has been addressed by many authors. The geochemical behaviour and the concentration of W and Sn along with other trace elements of the granite have led to the establishment of criteria in distinguishing between ore-bearing granite and barren granite. Authors such as Stemprok et al. (1977), Tischendorf (1977) and Rossi et al. (1988) have categorically used the terminology of specialised granite to delineate it from normal granite. These specialised granites are characterised by high levels of elements particularly Rb, F, B, Li, Be, Sn, W, Ta, U and Th (see section 5.2.4). Tungsten mineralisation is commonly associated with S-type granite, however, scheelite has also been found associated with I-type granite in King Island, Australia and Sierra Nevada, USA.

1.2.3 Greisen or hydrothermal deposits

This class includes all other hydrothermal deposits (except skarn), that are associated with igneous intrusion and their effusives. Greisen is one of the most spectacular members of the hydrothermal deposits and contributes a substantial amount of tungsten production. Cligga Head (SW England), Mount Mulgine (Western Australia) and Mawchi deposits (Burma) fall into this category (Hosking 1982; Beer and Ball 1987; Migisha and Both 1991). Greisen is usually composed of quartz and muscovite (or zinnwaldite) with variable amounts of accessory tourmaline, topaz and fluorite (Hall 1971; Roberts 1983). During greisenisation the hydrothermal fluids break down feldspar and mica of the leucogranite, leaching tungsten from these minerals and depositing in veins at higher levels within the hydrothermal system (Alderton and Moore 1981). Alterations, such as tourmalisation, sericitisation, silicification, kaolinisation and albitization are closely associated with the greisenisation. Greisens usually develop within the granite or close to the apical-granitic contacts but may also penetrate into the surrounding country rocks. In these hydrothermal deposits wolframite and scheelite are commonly associated with quartz veins, occurring as network of veins (stockwork vein system) or lodes occupying the apices of granitic cusps.

The other important hydrothermal deposits include Ashio Mine, Japan, Climax deposits of Colorado and Jiangxi province, China (Hosking 1982; Giuliani et al. 1988).

1.2.4 Tungsten skarn deposits

Skarns consist of Ca-Fe-Mg-Mn silicates formed by replacement of carbonate-bearing rocks accompanying regional or contact metamorphism and metasomatism (Einaudi et al. 1981). Tungsten skarn mineralisation is closely related to the hydrothermal

activity associated with the more basic members of the granite series (Einaudi and Burt 1982). Scheelite comprises at least 95 % by volume of all the tungsten minerals in skarn. The mineralisation tends to concentrate around the marble replacement front and depleted away from marble (Newberry 1982; Kwak 1987). Common gangue calc-silicate minerals include epidote, clinozoisite, actinolite, grossularite, andradite, wollastonite and vesuvianite. Einaudi et al. (1981) and Kwak (1987) observed that W (Mo-Cu) skarns are typically related to granodiorite to quartz monzonite plutons (I-type), whereas the Sn (W-F-Be-Li) skarns are typically related to S-type leucogranites. Deposits in the Sierra Nevada, California and MacTung, Canada are the classical tungsten skarn deposits, the latter is considered as the largest deposit containing 65 Mt of tungsten with 1.5 % WO_3 (Kwak 1987).

Stratabound tungsten mineralisation, confined to a regional metamorphic terrain, has been reported by Larsen (1991) in the Bjellatind area, northern Norway. This mineralisation has been classified as an example of regional tungsten skarn in accordance with the classification established by Kwak (1987).

1.2.5 Metamorphosed volcanogenic or exhalative tungsten deposits

Volcanogenic or exhalative volcanogenic deposits are stratiform and stratabound mineral deposits that have formed by volcanic processes or precipitated from submarine hot springs.

Stratiform and stratabound tungsten mineralisation in the Sangdong, South Korea (Hosking 1982), carbonate-hosted scheelite and wolframite of the Nock mountains, Austria (Neinavaie et al. 1989), Western Hohe Tauern, Eastern Alps (Niedermayr and Schroll 1983) and Mittersill and Bohemian Massif, Austria (Thalhammer et al. 1989; Beran et al. 1985), all are considered to have been primarily related to submarine exhalation or / and associated with mafic-ultramafic volcanic activity. Mittersill scheelite, the largest known stratabound scheelite deposit in the world, occurs exclusively within the hornblendites and amphibolites of boninitic parentage and gneisses of rhyolitic to dacitic affinities (Thalhammer et al. 1989). In contrast, scheelite in the Bohemian Massif and Eastern Alps is associated with the calc-silicate rocks, pelitic metasediments, quartzite and tourmalinite of higher amphibolite facies (Beran et al. 1985; Niedermayr and Schroll 1983). Plimer (1980 and 1987 a) and Niedermayr and Schroll (1983) argued that the pre-existing magmatic, volcano-sedimentary and synsedimentary tungsten has been remobilised and accumulated during different metamorphic events and multiple episodes of deformation and anatexis.

No economic tungsten deposits either of volcano-sedimentary origin or exhalative origin elsewhere in the world have been found where scheelite and wolframite are precipitated as primary minerals. However up to 3 % W has been found in siliceous sinters associated with active hot springs from Frying Pan Lake, New Zealand (Dames and Moore 1987). Similarly, the evaporites of Searle Lake, California, contains 70 ppm WO_3 and alkaline tungsteniferous brines are thought to be responsible for the precipitation of these Lake deposits (Hosking 1982).

1.3 Occurrences of lead-zinc mineralisation

Lead-zinc mineralisation occurs in different geological environments, and can be broadly grouped into sediment-hosted deposits, magmatic-hydrothermal and skarn deposits (see Edwards and Atkinson 1986).

The most important of which is the sediment-hosted (sedimentary exhalative) Pb-Zn deposits. Broken Hill, Mount Isa and McArthur River, Australia, western Newfoundland, Pine Point District, Canada and carbonate-hosted Pb-Zn deposits (Mississippi valley-type) USA are the good examples of these stratiform and non-stratiform sulphide mineralisations (Edwards and Atkinson 1986; Large 1981; Saunders et al. 1992). The common host rocks include carbonates (dolomite and limestone), breccia, conglomerate and shale of various ages, ranging from Proterozoic to late Paleozoic. Gustafson and Williams (1981) suggested that the brines generated, fault controlled sedimentary basin are responsible for the precipitation of these deposits during diagenesis.

Magmatic hydrothermal deposits include examples such as Butte, Montana and Kuroko, Japan. Butte, Montana is an excellent example of mesothermal mineralisation. This magmatic hydrothermal Cu-Zn-Pb-Ag-Au mineralisation is the world's most famous vein type deposit occurring in granodiorite (Evans 1993). Volcanic-associated massive sulphide mineralisation is another class of Pb-Zn mineralisation probably formed on the sea floor near the discharge site of hydrothermal fluids (Franklin et al. 1981). The sulphide mineralisation at Kuroko, Japan is the typical volcanic-hosted massive sulphide deposit, that exhibits primary igneous features. It occurs in the Green Tuff Belt, which contains rhyolite domes, acid tuff breccia and ferruginous chert, accumulated during Miocene (Edwards and Atkinson 1986).

Skarn also host Zn-Pb mineralisation that are associated with granodioritic to granitic magmatism. Examples include Washington Camp, Arizona, and Santa Eulalia, Mexico (cf. Edwards and Atkinson 1985).

Chapter Two

REGIONAL AND LOCAL GEOLOGICAL SETTING

2.1 Regional geology

2.1.1 Tectonic history of Pakistan

The India-Asia collision is considered to be one of the major tectonic events of the Cenozoic time. Prior to the collision, the Kohistan island arc developed in response to the northward subduction of the Tethys ocean. Paleomagnetic and sea-floor spreading data from the Indian ocean suggest that the Indo-Pakistan plate started moving towards Asia at least 130 Ma ago (Powell 1979). The first contact of the Kohistan arc with the Karakoram terrane occurred between 100 and 80 Ma ago (Coward et al. 1986; Pudsey 1986), which corresponds to the initiation of the northward subduction and consumption of Tethys ocean. The closure of the back-arc basin north of the Kohistan complex along the northern suture zone was completed by about 75 Ma ago (Pudsey et al. 1985). Subduction of Indo-Pakistan plate continued in the direction of north and northeast at a rate between 10 and 20 cm / yr (Patriat and Achache 1984), and has rotated anticlockwise by about 33^{o} (Dewey et al. 1989). The final collision of the Indo-Pakistan plate with the Asian plate along the Main Mantle Thrust took place between 50 and 40 Ma ago (Molnar and Tapponnier 1975; Pierce 1978; Petterson and Windley 1985).

To accommodate the post-collisional northwards movement of India, three basic models have been proposed; crustal shortening and thickening (England and McKenzie 1982), underthrusting of India beneath Asia (Barazangi and Ni 1982) and lateral eastward expulsion of Asia (Molnar and Tapponnier 1975).

The India-Asia collision produced the most spectacular mountain chains in the world, Himalayas, Karakoram and Hindu Kush. These are described below:

2.1.2 Himalayas

The Himalayan mountain chains have been subdivided into a number of geographical domains. The central and northwestern part of the Himalayas comprise the Zanskar Range, Higher Himalaya, Lesser Himalaya, and Sub-Himalaya from north to south (Fig. 2.1). These terranes represent a complex history of deformation and metamorphism.

2.1.2 (A) Zanskar Range

Zanskar Range lies immediately south of the Main Mantle Thrust in the Indian Himalaya (Fig. 2.1), and is composed largely of sedimentary shelf facies rocks forming

the northern continental margin of Indian plate. The succession of the Zanskar fossiliferous marine sediments is stratigraphically divided into Paleozoic Lahoul Supergroup and Mesozoic Zanskar Supergroup separated by the Permian Panjal Traps (Garzanti et al. 1987). The latter represents tholeiitic volcanic and volcanoclastic rocks (Searle et al. 1987).

2.1.2 (B) High Himalaya

The High Himalaya or Tibetan crystalline slab crops out to the south of the Zanskar Range bounded to the south by the Main Central Thrust and to the north by a major normal fault (Fig. 2.1). The Main Central Thrust is a major southward-verging shear zone developed during Eocene (Thakur 1980). The rocks of the High Himalaya include varying proportion of metapelite, amphibolite, marble, quartzite and orthogneiss, ranging in age from Precambrian to Mesozoic (Tahirkheli 1982; Yeats and Lawrence 1983). These rocks have undergone several phases of regional metamorphism and deformation (Honegger et al. 1982) followed by retrogression. The inverted metamorphic isograds appear to be related directly to the movement along the Main Central Thrust (Le Fort 1986).

2.1.2 (C) Lesser and Sub-Himalaya

The Lesser Himalaya comprises the Precambrian and Paleozoic sedimentary cover to the Indian basement and is bounded in its hanging wall by the Main Central Thrust and along its foot wall by Main Boundary Thrust (Fig. 2.1). The rocks of the Lesser Himalaya include paragneiss, metapelite, sandstone, conglomerate, quartzite, and limestone (Tahirkheli 1982). These rocks are intruded by cordierite-bearing granites along the length of Lesser Himalaya (Le Fort et al. 1980).

The Main Boundary Thrust places the rocks of Lesser Himalaya over the late Tertiary Siwalik molasse deposits of the Sub-Himalayan zone (Fig. 2.1). These unmetamorphosed fluvial sediments extend from the Sulaiman Range in Pakistan to Assam in the eastern India and range in age from late Miocene to Pleistocene (Raynolds et al. 1980).

2.1.3 Indus suture zone

The Indus suture, commonly known as Main Mantle Thrust, marks the zone of collision between Indian plate and Kohistan Complex, extends eastwards from Kohistan across Ladakh and southern Tibet (Fig. 2.1). In Pakistan, the Indus suture zone consists of Mingora-Shangla (Swat) melange and Allai-Kohistan (Hazara) ophiolitic melange. The former includes subduction-related Shangla blueschist melange, Charbagh greenschist melange and Mingora ophiolitic melange (Kazmi et al. 1984).

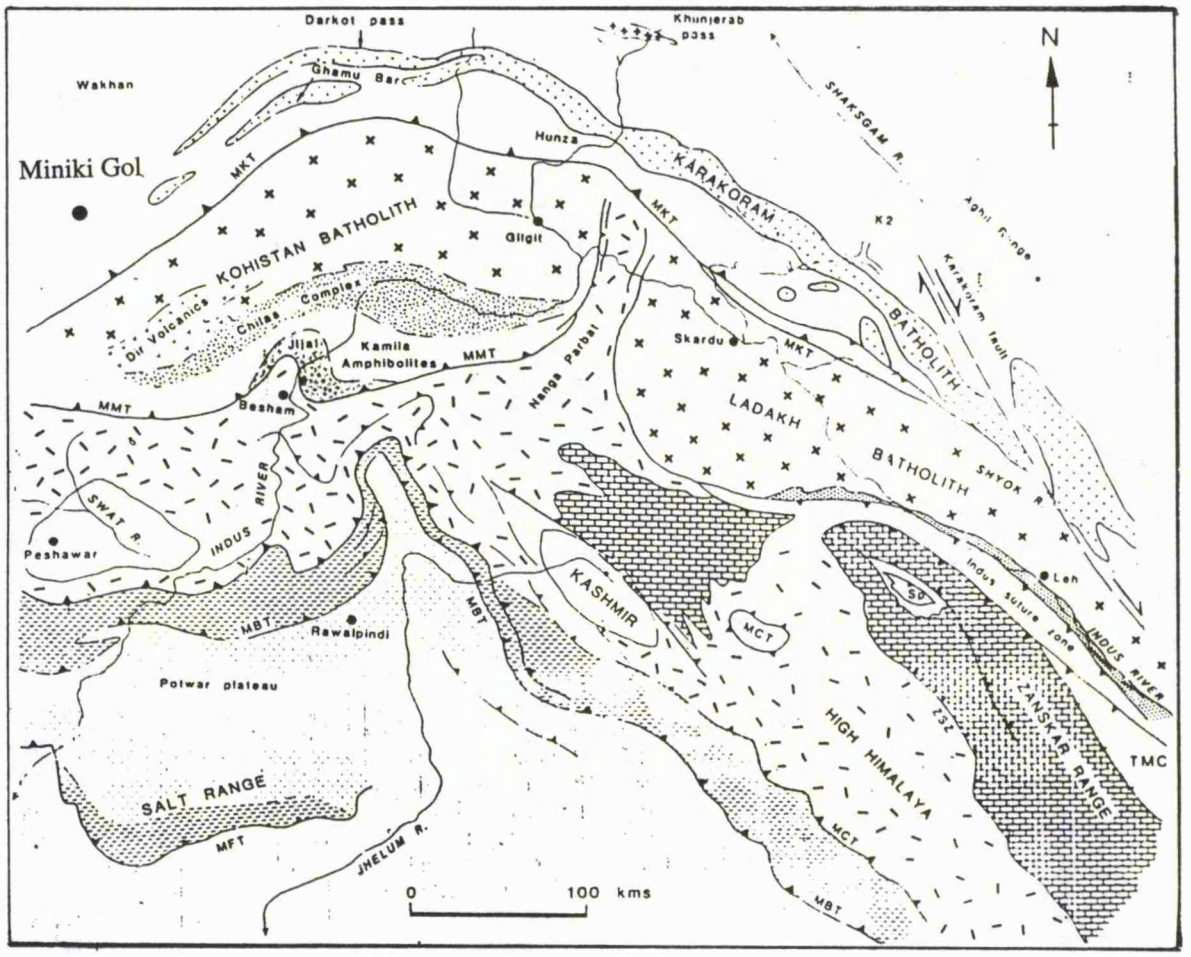

Figure 2.1: Geological sketch map of the western Himalaya and Karakoram showing Karakoram batholith, Kohistan-Ladakh island arc and tectonic zones of Himalaya (after Searle et al. 1988).

In Ladakh, the Indus suture zone consists of three major linear thrust belt, separated by ophiolitic melange (Searle et al. 1988). The Indus suture zone at Ladakh, composed of calc-alkaline basaltic lava, agglomerate, shale, limestone and radiolarian chert.

2.1.4 Kohistan island arc

The Kohistan terrane extends at least, 1000 km, cropping out in the western Himalaya, southern Karakoram and eastern Hindu Kush (Fig. 2.1). The terrane which has been proposed as island arc is bounded by major thrust, along the south (Main Mantle Thrust) and along the north by Main Karakoram Thrust (Shyok suture zone) see (Fig. 2.1). The Kohistan terrane has undergone varying degrees of deformation and metamorphism. Tahirkheli (1982) and Coward et al. (1982) divided the Kohistan island arc into six structural and stratigraphic units. These are as follows:

2.1.4 (A) Jijal and Chilas complexes

Jijal complex lies on the southern margin of the Kohistan island arc between Patan and Jijal, and occupies about 200 km^2 (Fig. 2.1). The complex is composed of garnet granulites and alpine ultramafics including diopsidite, peridotite, dunite and websterite. These serpentinised ultramafics represent a metamorphosed ophiolitic mantle or deformed cumulate sequence (Jan 1980; Coward et al. 1982).

Chilas complex is a large mafic-ultramafic body, extends between Nanga Parbat and Dir volcanics (Fig. 2.1). Chilas complex is composed principally of two-pyroxene gabbro, norite, anorthosite, troctolite and quartz diorite (Jan 1979; Coward et al. 1982; Khan et al. 1989). It has been interpreted as the root zone magma chamber of the Kohistan island arc or magma generated by diapirism during the intra-arc rifting (Khan et al. 1989).

2.1.4 (B) Kamila amphibolites

Kamila amphibolites crop out to the South of Chilas complex (Fig. 2.1) and consists of fine and coarse grained amphibolites. These amphibolites are considered as metamorphic equivalents of the metavolcanic and Chilas metagabbro (Jan 1988). Kamila amphibolite represents relics of oceanic crust on which arc was built (Bard et al. 1980) .

2.1.4 (C) Kohistan batholith

The northern part of the Kohistan terrane is dominated by plutonic rocks of Kohistan batholith (Fig. 2.1). The composition of the batholith varies from hornblende gabbro to leucogranite, but is dominantly composed of granodiorite to quartz-diorite (Petterson and Windley 1985). Many of the early plutons have undergone greenschist

facies metamorphism, however, two-thirds of the plutons are undeformed and post-date the deformation associated with the northern suture zone (Searle 1991). Kohistan batholith gives a whole rock (Rb-Sr) age of 102 ± 12 Ma (Petterson and Windley 1985).

2.1.4 (D) Island arc volcanics and metasediments

Kohistan volcanic arc includes three volcanic belts namely Chalt, Shamran and Dir volcanic groups, that are exposed on the northern periphery of the Kohistan complex (Fig. 2.1). The former two groups represent pre-collisional island arc signature, whereas the later forms the roof zone of the post-collision Kohistan batholith (Searle 1991). The volcanic rocks of the island arc include basalt, andesite, dacite, rhyolite, boninite and agglomerate (Tahirkheli 1982).

Metasediments crop out throughout the Kohistan domain and, at places, are interbedded with the volcanic rocks of the complex. These include metapelites such as slate, phyllite, chlorite schist and garnet mica schist as well as psammites consisting of metamorphosed sandstone, quartzite and metagreywacke (Tahirkheli 1982).

2.1.5 Northern suture zone

The Main Karakoram Thrust (now termed as Shyok suture) marks the suture zone between the Kohistan sequence and the Asian plate. This suture zone is best exposed just east of the Chalt village and Coward et al. (1982) therefore referred it as the Chalt melange. In the western Karakoram the melange is up to 4 km thick, but is reduced to just a 150 m wide fault zone near Yasin. The Northern suture melange is characterised by brecciated and serpentinised volcanics with pale green tuff, limestone, red shale, quartzite, conglomerate and cleaved slate (Pudsey et al. 1985). Most of these rocks are derived from Kohistan island arc, however, some of the quartzites and conglomerates appear to be derived from Karakoram terrane (Searle 1991).

The Northern suture melange has been interpreted as tectonic melange by Coward et al. (1986) and Pudsey et al. (1985). In contrast, Pudsey (1986) argued that the occurrences of thick granule sandstones and pebble conglomerate interbedded with slate represent a part of the sedimentary sequence rather than tectonic slices. Based on the presence of Orbitolina sp. and rudist fragments in the limestone, Pudsey et al. (1985) considered it as lower Cretaceous in age.

2.1.6 The Karakoram terrane

The Karakoram plate extends from Afghanistan, through northern Pakistan and northern Ladakh to western Tibet (Desio and Zanettin 1970). Its boundaries are defined as

the PaleoTethyan Rushan-Pshart suture zone within the southern Pamirs (Shvolman 1978) to the north, and the Shyok (northern) Suture Zone to the south. Within the central Karakoram three main tectonic zones from north to south are recognised: a northern karakoram terrane, the Karakoram batholith and the Karakoram metamorphic complex (Rex et al. 1988).

The Western Karakoram continues southwestward and merges into the Hindu Kush range along the Afghan-Pakistan border near Chitral. Western Karakoram includes many high mountains, notably Tirich Mir and Noshaq (Searle 1991).

2.1.6 (A) Northern Karakoram terrane

Northern Karakoram terrane crops out to the north and northeast of Karakoram batholith (Fig. 2.2). This terrane is represented by Gasherbrum sedimentary group, Broad Peak quartz diorite and K2 gneiss (Rex et al. 1988). The Gasherbrum sedimentary succession includes Carboniferous black shale that is overlain by a thick Permian and Mesozoic carbonate sequence with interbedded conglomerate, shale and tuffaceous horizons (Rex et al. 1988). These sedimentary rocks are intruded by the Broad Peak hornblende-bearing quartz diorite and lamprophyric dikes of calc-alkaline signatures (Searle et al. 1989). The plutonic units of northern Karakoram are probably related to the Andean-type magmatism prior to India-Asia collision (Searle 1991).

2.1.6 (B) The Karakoram batholith

The Karakoram axial batholith runs roughly east-west across the Karakoram mountains of northern Pakistan (Fig. 2.2). This composite batholith is approximately 600 km long and up to 30 km wide and can be divided into seven main magmatic units, the Kande complex, Muztagh Tower unit, Baltoro plutonic unit, Masherbrum pluton, Hunza plutonic complex, Darkot pass and Ghamu Bar pluton (Searle 1991). The Kande complex is represented by a composite magmatic units including amphibolite, hornblende tonalite, granodiorite and K-feldspar porphyritic granite, yielding a hornblende K-Ar age of 24 ± 1 Ma (Searle et al. 1989). The Muztagh Tower unit is characterised by narrow belt of Late Cretaceous tonalitic to granodioritic gneiss outcrops along the northern margin of Baltoro plutonic unit (Crawford and Searle 1992). The Miocene Baltoro plutonic unit and Masherbrum pluton (Fig. 2.2) represent monzogranite, garnet-two mica leucogranite, leucogranitic pegmatite and aplites (Desio and Zanettin 1970; Searle 1991).

The Hunza plutonic complex dominates the Karakoram batholith in the west (Fig. 2.1) and is composed of quartz diorite-granodiorite plutons, yielding U-Pb Zircon age of 95 ± 5 Ma (Crawford 1988; Searle 1991).

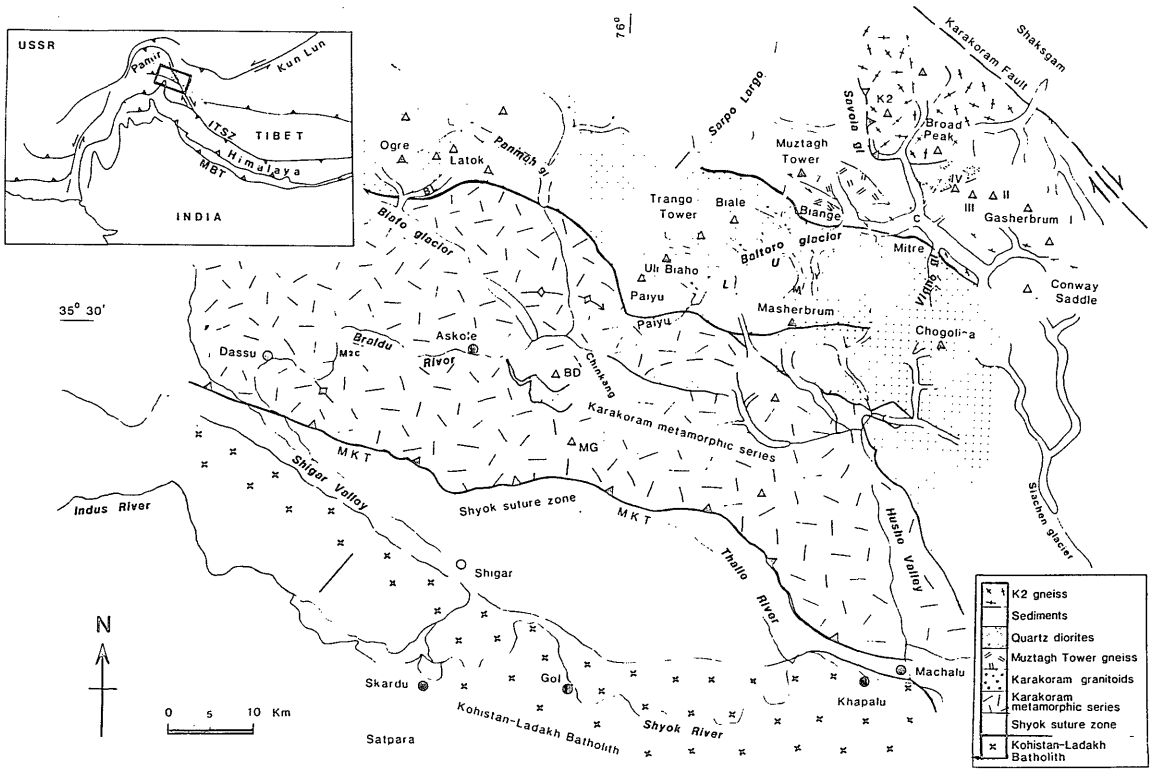

Figure 2.2: Simplified geological map of the central Karakoram showing northern Karakoram terrane, Karakoram batholith and Karakoram metamorphic complex (after Searle 1991).

Further west the main Karakoram batholith splits into two plutons, Darkot pass (or Dobargar) pluton and Ghamu Bar (or Zagar-Umalsit) pluton (Fig. 2.1). The former extends southwestwards along the Yarkhun River towards the village of Mastuj (Pudsey et al. 1985). The Darkot pass granitoid ranges from quartz monzodiorite to leucogranite in composition and has been dated at 111 ± 6 Ma by Rb-Sr method (Debon et al. 1987). The Ghamu Bar pluton crops out on the southern branch of the Karakoram batholith (Fig. 2.1) and is dominantly composed of a medium to fine grained porphyritic granite with K-feldspar megacrysts (Pudsey et al. 1985).

2.1.6 (C) Leucogranite

Numerous leucogranitic stocks and dikes within both the Asian and Indian plates have been emplaced after the culmination of Barrovian-type of metamorphism. These granites occur as an anastomosing network throughout the Karakoram terrane and are characterised by the presence of quartz, plagioclase, alkali feldspar, muscovite, biotite, garnet, accessory apatite, zircon and beryl (Searle et al. 1989). Tourmaline has been found in minor amounts in few plutons but is generally absent in the Karakoram leucogranite (Crawford and Searle 1993). In contrast, Himalayan leucogranites contain appreciable amounts of tourmaline and lithium-bearing mica (Le Fort 1981), and differ considerably in their mineralogy, geochemistry and isotopic composition from Karakoram leucogranites.

Minimum melt composition, low crystallisation temperature and water saturated nature of the Karakoram leucogranites suggest that they were generated by melting of pelitic metamorphic assemblage similar to deeper level equivalent of the Karakoram metamorphic complex (Crawford and Searle 1993). U-Pb dating of the Baltoro granite, Karakoram gives age of 21.5 ± 0.5 Ma (Parish and Tirrul 1989), whereas Brookfield and Reynolds (1990) have reported an Ar^{40}/Ar^{39} age ranging from 8 Ma up to 13.5 Ma for Baltoro leucogranite. Schärer (1984) obtained U-Pb dates of 21.9 ± 0.2 for the Himalayan leucogranite.

2.1.6 (D) Karakoram metamorphic complex

Between the Main Karakoram Thrust and south of the Karakoram batholith is a high grade metamorphic terrane (Desio 1979), termed as Karakoram metamorphic complex (see Fig. 2.2). The diverse lithological units of the complex include dominantly metasedimentary sequence, tonalitic Dassu orthogneiss, Hushe orthogneiss, Askole amphibolite and Panmah ultramafic unit (Rex et al. 1988). The multiple episodes of metamorphism and polyphase deformation have obscured most of the primary sedimentary structures and relationships.

2.1.6 (E) Deformational and metamorphic history

According to Searle and Tirrul (1991) the Karakoram terrane has suffered four phases of metamorphism with relevant deformation during its evolution. Andalusite grade metamorphism is considered to be the earliest metamorphic event (M1) in the Karakoram terrane, which occurred prior to the collision of India with Asia. The age of the M1 metamorphism is interpreted to be roughly synchronous with the Jurassic magmatism (Searle and Tirrul 1991). The earlier small scale folds represent the first phase of deformation in these rocks (Searle 1991).

The post-collision thermal history and the intense crustal shortening and thickening of the Karakoram plate is represented by the dominant regional sillimanite grade Barrovian metamorphism (M2). This metamorphic event occurred between 50-37 Ma, with the peak of metamorphic temperatures around 650-700^{o}C (Patriat and Achache 1984). The M2 metamorphism is clearly synchronous with D2 deformation as aluminosilicates and mica have grown along the foliation planes (Searle and Tirrul 1991).

Early Miocene sillimanite grade thermal metamorphism (M3) is associated with large-scale crustal melting at 21 ± 0.5 Ma around the Baltoro granite (Parrish and Tirrul 1989). This metamorphic event is genetically related to the emplacement of Baltoro leucogranite.

Local retrogressive metamorphism in the Karakoram metamorphic complex is thought to be related to the post-Miocene thrusting along the Main Karakoram Thrust zone (Searle 1991). The retrogressive minerals such as actinolite, chlorite, epidote and secondary muscovite in these metamorphic rocks display pervasive foliation parallel to post-Miocene thrusting (Searle and Tirrul 1991).

Similar metamorphic and deformational events with relatively different time period and cooling history have been reported in the Himalayas (DiPietro and Lawrence 1991; Le Fort 1986).

2.2 Local geology

2.2.1 Western Karakoram and Hindu Kush

The Hindu Kush terrane merges into western Karakoram along the Afghan-Pakistan border near Chitral. The terrane, in the easternmost most part of which lies the thesis area, stretches southwest from the Pamirs in Russia across the north-western extremities of Pakistan and passes into Afghanistan (Fig. 1.1). Tirich Mir (7706 m) is the highest peak in the Hindu Kush and overlooks the town of Chitral. Based on the stratigraphical sequence and structural evolution, Pudsey et al. (1985) divided the geology

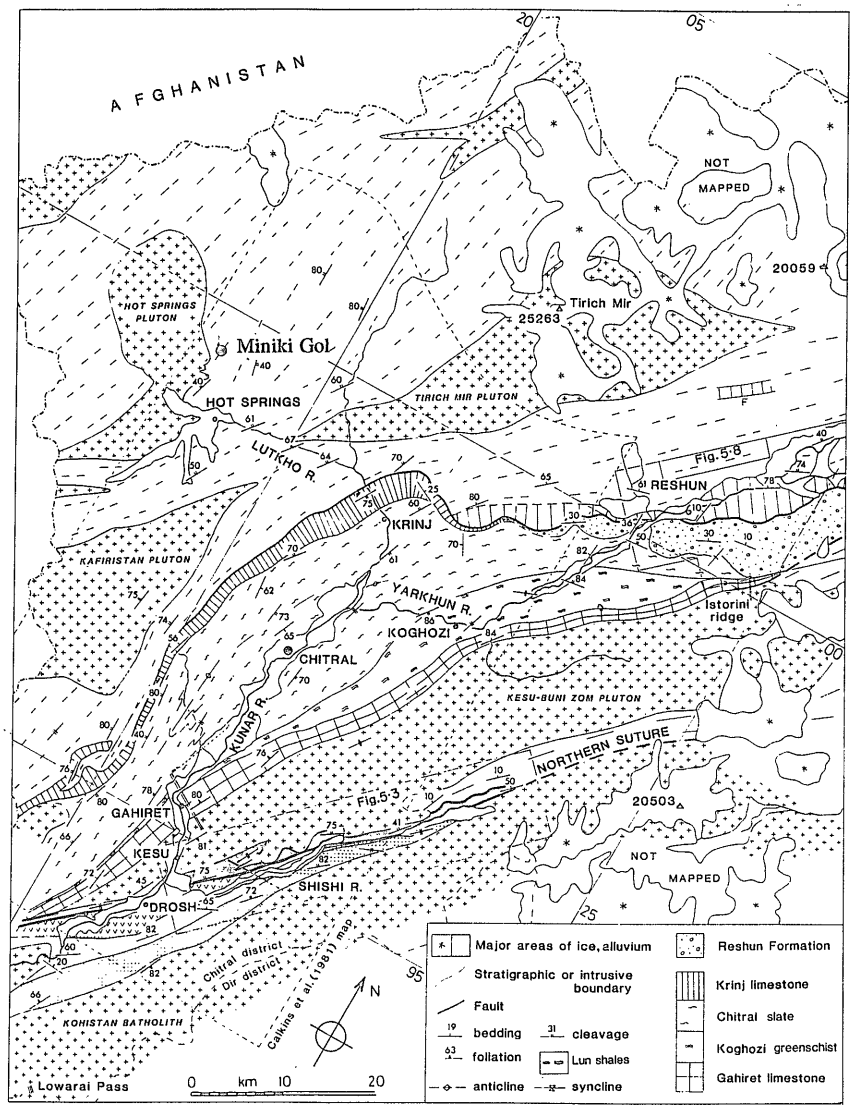

Figure 2.3: Geological map of the Chitral and adjoining area showing the lithological units between Northern suture zone and Pakistan-Afghanistan border (after Calkins et al. 1981; Pudsey et al. 1985).

of Western Karakoram and Hindu Kush (in the Chitral and surrounding area), between the Pakistan-Afghanistan border and northern suture into two tectonic units (Fig. 2.3): (1) the northwestern unit between Afghan-Pakistan border and the Reshun Fault, (2) the Central unit between Reshun Fault and northern suture. Leake et al. (1989) subdivided the former unit into three lithostratigraphic formations separated by faults.

2.2.2 Central unit

The Central unit, predominantly composed of Paleozoic-Mesozoic metasediments, forms a narrow (20-40 km) strip between Reshun Fault and northern suture. This unit comprises Gahiret Limestone, Koghozi greenschist, Chitral Slate and Shoghor Limestone from south to north in the Chitral and surrounding areas.

2.2.2 (A) Gahiret Limestone

Gahiret Limestone is a thick massive (3 km) and coarse crystalline marble that crops out at the southern periphery of the Central unit (Fig. 2.3). The northwesternmost Gahiret Limestone overlies the Koghozi greenschist conformably but may be faulted against mica schist on its southeastern side (Pudsey et al. 1985). The Gahiret Limestone is composed of almost pure calcite with chalcopyrite, graphite and traces of phlogopite and is interbedded with dark phyllite and calcareous shale. Hayden (1915) and Calkins et al. (1981) reported Orbitolina from the Gahiret Limestone and considered it as Cretaceous in age. Structural and stratigraphical evidence are both compatible with the Cretaceous age (Pudsey et al. 1985).

2.2.2 (B) Koghozi greenschist

Koghozi greenschist is a continuous belt which extends between Chitral Slate and Gahiret Limestone (Fig 2.3) and lies stratigraphically above the former unit (Pudsey et al. 1985). The fine-grained and thinly laminated greenschist is represented by varying amounts of albite, actinolite, epidote, chlorite and quartz (Calkins et al. 1981). The occurrence of non-laminated layers containing relict feldspar phenocryst and chalcopyrite probably represent altered tuffs (Calkins et al. 1981; Pudsey et al. 1985). No fossils have been found in the Koghozi greenschist, however, structurally and stratigraphically the greenschist appears to occupy the same position as do the Chitral Slate (Pudsey et al. 1985).

2.2.2 (C) Chitral Slate

The "slate series of Chitral" was first mentioned by Hayden (1915), and later by Tipper in Pascoe (1924) who referred it to as Chitral Slate. The slate forms a northeast-trending belt extending from Pakistan-Afghanistan border along the Chitral and Mastuj river up to Reshun (Fig. 2.3, 2.4). The Chitral Slate attains a maximum thickness of 6 km in central part of Chitral valley and its eastern margin has been found gradational with the Koghozi greenschist (Calkins et al. 1981). The unit represents a rather uniform sequence of fine-grained dark grey slate and laminated phyllite, interbedded with thick units of quartzitic sandstone and metavolcanics (Buchroithner and Gamerith 1986). The only reference to fossils recovered from the Chitral Slate is by Pascoe (1924) who interpreted it as Permian in age whereas, based on the stratigraphical and structural evidences, Calkins et al. (1981) regarded it as Cretaceous in age.

2.2.2 (D) Reshun Formation

Reshun Formation was originally named by Hayden (1915) as the Reshun Conglomerate and is exposed to the south of Reshun between Chitral and Mastuj village (Fig. 2.3). The Reshun Formation is composed of conglomerate, limestone, calcareous phyllite, sandstone, quartzite and greenstone. The thickness of conglomerate beds varies between 3 and 15 m. Desio (1959) assigned Cretaceous age to the Reshun Formation on the basis of Orbitolina findings.

2.2.2 (E) Shoghor Limestone

Shoghor Limestone (also called Krinj Limestone) extends from Pakistan-Afghanistan border in the southeast of Chitral up to Partsan area (Fig. 2.3). In the Lutkho gorge near Shoghor village, the limestone is approximately 2 km thick, and is represented by light grey to pink recrystallised marble (Fletcher 1985). Shoghor Limestone is bounded on its northwestern side by the Reshun Fault which runs parallel to the northern suture (Fig. 2.3, 2.4). This limestone is lower Cretaceous as shown by the presence of Orbitolinas and rudistids at Krinj mine (Desio 1959).

2.2.3 Northwestern Unit

This tectonic unit extends northwestwards from Reshun Fault to the Pakistan-Afghanistan border and probably to the Pamirs (Pudsey et al. 1985). This Northwestern unit has been divided into different lithostratigraphic units termed as Shogram Formation, Wakhan Formation, Sarikol Shale, Lun Shales. (Hayden 1915; Desio 1959; Calkins et al. 1981; Pudsey et al. 1985; Buchroithner and Gamerith 1986). According to Buchroithner

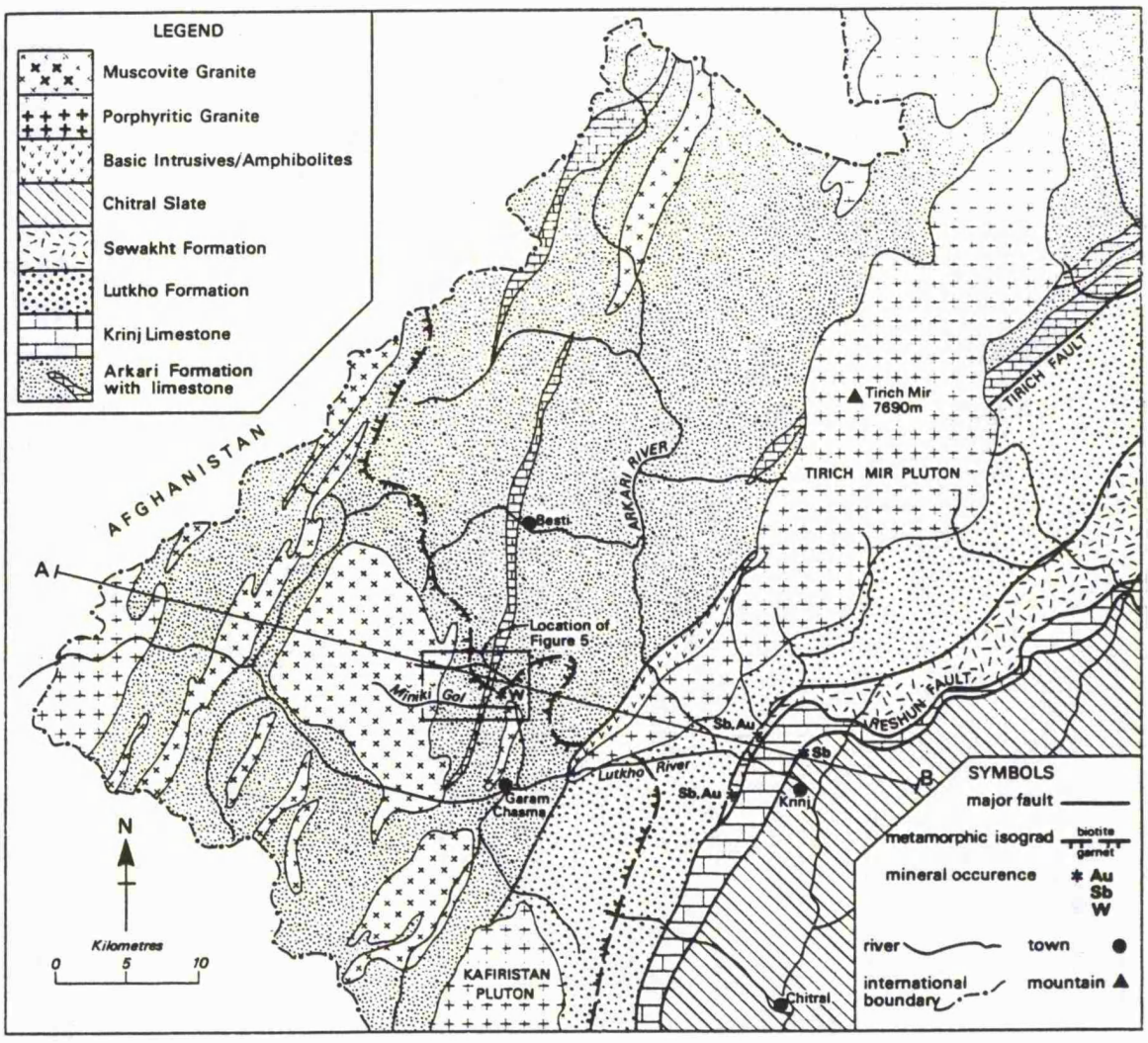

Figure 2.4: Geological map of the Garam Chashma area showing Arkari Formation that hosts W and Pb-Zn mineralisation (after Leake et al. 1989).

and Gamerith (1986), the Wakhan Formation extends to the west of Tirich Mir and they considered it as lower Triassic based on the conodont fauna. On the basis of fossils found in the metasediments from Reshun Fault to the Pakistan-Afghanistan border, Calkins et al. (1981) termed these rocks as Devonian to Jurassic in age. Leake et al. (1989) separated the metasediments to the northwest of Shoghor Limestone into three lithostratigraphic Formations, Sewakht, Lutkho and Arkari Formations (Fig. 2.4). The latter two are probably subdivisions of the Lun Shales which overlies the Shogram Formation in the Tirich and Mastuj valleys as described by Hayden (1915) and Talent et al. (1982). The Sewakht Formation, that lies adjacent to the Krinj Limestone (Fig 2.4), is characterised by greenschist, micritic limestone, cherts, ferruginous dolomitic carbonate, phyllite, sandstone and breccia. This sequence probably correlates with the Shogram Formation of Devonian age, however, in the type locality Shogram Formation is composed predominantly of limestone and sandstones (Leake et al. 1989). A major tectonic break to the northwest, delineates Sewakht Formation from the monotonous sequence of light green phyllite of Lutkho Formation (Fig 2.4). This is followed by Arkari Formation which extends up to the northwest of the Tirich Mir pluton. Arkari Formation consists of mica schist, dark grey phyllite and subordinate quartzites and has been metamorphosed up to amphibolite facies.

2.2.4 Tirich Mir and Kafiristan plutons

Tirich Mir pluton forms an elongate northeast trending belt that pinches out in a southwestward direction near Lutkho River (Fig. 2.4). This pluton predominantly consists of biotite granodiorite and coarse grained plagioclase augen gneiss (Buchroithner and Gamerith 1986). Desio et al. (1964) obtained a Rb-Sr biotite age of 115 ± 4 Ma for these granites. The Kafiristan granite extends to the south of Garam Chashma, and is similar in composition to that of Tirich Mir granite but has an younger K-AR biotite cooling age of 48 ± 2 Ma (Searle 1991).

2.2.5 Other mineralisations

Gold and antimony mineralisations in the area of the Krinj limestone such as Shoghor have been described by many authors (such as Austromineral 1978; Leake 1983; Soquem 1984; Fletcher 1985; Khaliq 1991). Antimony has been mined at several localities since 1939 and the Krinj antimony mine is still intermittently in operation.

Antimony mineralisation in the form of stibnite occurs at the southern faulted contact between Shoghor Limestone and Chitral Slate. In the Krinj area stibnite is associated with a narrow zone of quartz veining within the phyllite breccia sequence (Calkins et al. 1981; Fletcher 1985). Fletcher (1985) argued that the mineralisation seems

to be controlled by faulting with stibnite being introduced from the surrounding phyllite into the fault plane and redistributed by subsequent deformation.

Antimony-rich sulphosalt mineralisation has been found at the faulted contact between Shoghor Limestone and Sewakht Formation. The richest gold mineralisation is contained within a thin discontinuous boulangerite vein associated with the faulted northwestern contact of the Shoghor Limestone. Although extremely enriched in gold (up to 59 g / t Au), the mineralisation is localised and discontinuous (Austromineral 1978; Fletcher 1985; Khaliq 1991).

Low grade gold mineralisation associated with As-Sb-Ag-Hg mineralisation has also been found in altered siliceous dolomitic limestone (red carbonate) unit of Sewakht Formation. Leake (1983) and Fletcher (1985) concluded that mineralisation seems to be related to the calcite-filled tension gashes within the Shoghor Limestone which postdates the main thrusting episode between Shoghor and Sewakht Formations.

Chapter Three

FIELD RELATIONS AND STRUCTURE

3.1 Introduction

As mentioned in the first chapter, the Arkari Formation that hosts the stratabound tungsten and stratiform lead-zinc mineralisation, is mainly composed of mica schist, phyllite, marble and quartzitic rocks. These rock units are conformable to each other and strike persistent. Scheelite mineralisation in the study area has been found mainly in calc-silicate quartzite and tourmalinite. A two mica leucogranite is emplaced at the mouth of Miniki Gol, 400 meters to the southeast of mineralised zone (Fig. 1.2).

In this chapter the field relations of the mineralisation with the enclosing rocks as well as deformational history and metamorphism are discussed. The field relations have been observed during the field work. The main objective of this chapter is, the structure of the thesis area. This is important as shown by Dames and Moore (1987) that the scheelite mineralisation is apparently controlled by structure.

3.2 Field relations

3.2.1 Schistose rocks

Schistose rocks comprise mica schist, greenschist, graphitic schist, calcareous schist, tourmaline-bearing schist and phyllite, among them the mica schist is the dominant rock type within the Miniki Gol and surrounding area. These schists are highly weathered, fractured and intercalated with each others and is difficult to separate these schists on a map. Both concordant and discordant quartz veins as well as pegmatites are also observed throughout the schistose rocks in the Miniki Gol and Besti Gol area (Fig 3.2 D, 3.3 B). The schist is medium to coarse grained, blackish grey to reddish brown in colour, the brownish tent indicates iron leaching and chemical weathering in these rocks.

Garnet porphyroblast up to 0.5 cm in diameter, muscovite, biotite, tourmaline, chlorite, calcite, carbonaceous material, graphite, quartz and feldspar can easily be recognised in these schists. Garnet and staurolite porphyroblasts are wrapped in the foliation defined by mainly muscovite.

Mica schist grades into phyllite towards the western side of Miniki Gol (Fig. 1.2). The schist at Besti Gol appears to be of low-grade metasediments and predominantly consist of phyllitic schist. The fine-grained phyllitic schist at Besti Gol grades into greenschist and calcareous schist with abundant green minerals such as chlorite, epidote and occasionally actinolite and calcite respectively (Fig. 1.3). Hornblende gneiss is also

observed within the phyllitic schist near the mineralised zone. Calc-silicate rocks are rare at Besti Gol and similarly leucogranite has not been exposed in the vicinity of lead-zinc mineralisation. However, quartz veins are abundant along the marble and within the phyllitic schist (Fig. 1.3).

3.2.2 Quartzitic rocks

Quartzitic rocks consist of calc-silicate quartzite, mica quartzite and micaceous psammite; the former is more common and contains scheelite mineralisation. Calc-silicate quartzite beds range from 1 to 4 meters in thickness and occur within the schistose rocks, particularly mica schist, throughout Miniki Gol, Besti Gol and surrounding areas (Fig. 3.1 B). These quartzites are conformable to the enclosing schist, although, the individual beds may not be strike persistent, being disturbed by the tectonic activity in the area. The calc-silicate quartzite beds are quite abundant to the western side of Miniki Gol above the marble horizon and are generally unmineralised (Fig. 1.2). The quartzite is fine to medium grained, greenish grey and light buff in colour. Mica and quartz can easily be identified in these rocks while dark portions of the calc-silicate quartzite indicate clinozoisite and amphiboles. Minor isoclinal and ptygmatic folds are found in these rocks, whereas micaceous minerals mark the foliations in the foliated quartzite.

3.2.3 Leucogranite

Numerous bodies of leucogranite are exposed in the vicinity of Miniki Gol, Garam Chashma and adjoining areas. These plutons are also called Hot Springs plutons (see Fig. 2.3). According to Fletcher (1985) the Miniki Gol leucogranite is an elongate stock measuring approximately 7 km by 0.5 to 1 km, with the long axis being orientated NNE. Miniki Gol gorge exposes the contact relationship of the granite with the enclosing rocks at the extreme north of the stock. Along the contact granite forms a network of sills and dikes extending outward from the main stock (Fig. 3.2 A). The contact of these apophyses has been controlled by both (S1) and (S2) foliation (Fig. 3.2 A-B), associated with the second deformation folds in the schist (Fletcher 1985; Leake et al. 1989).

Miniki Gol granite is medium to coarse grained, milky white to buff in colour and its texture varies from equigranular to foliated, with coarse muscovite flakes defining the penetrative foliation. Quartz, muscovite, garnet and plagioclase can easily be recognised by the naked eye in these granites. Pinkish garnet is more abundant in the granite to the west of Miniki Gol as compared to the granite exposed at the mouth of Miniki Gol.

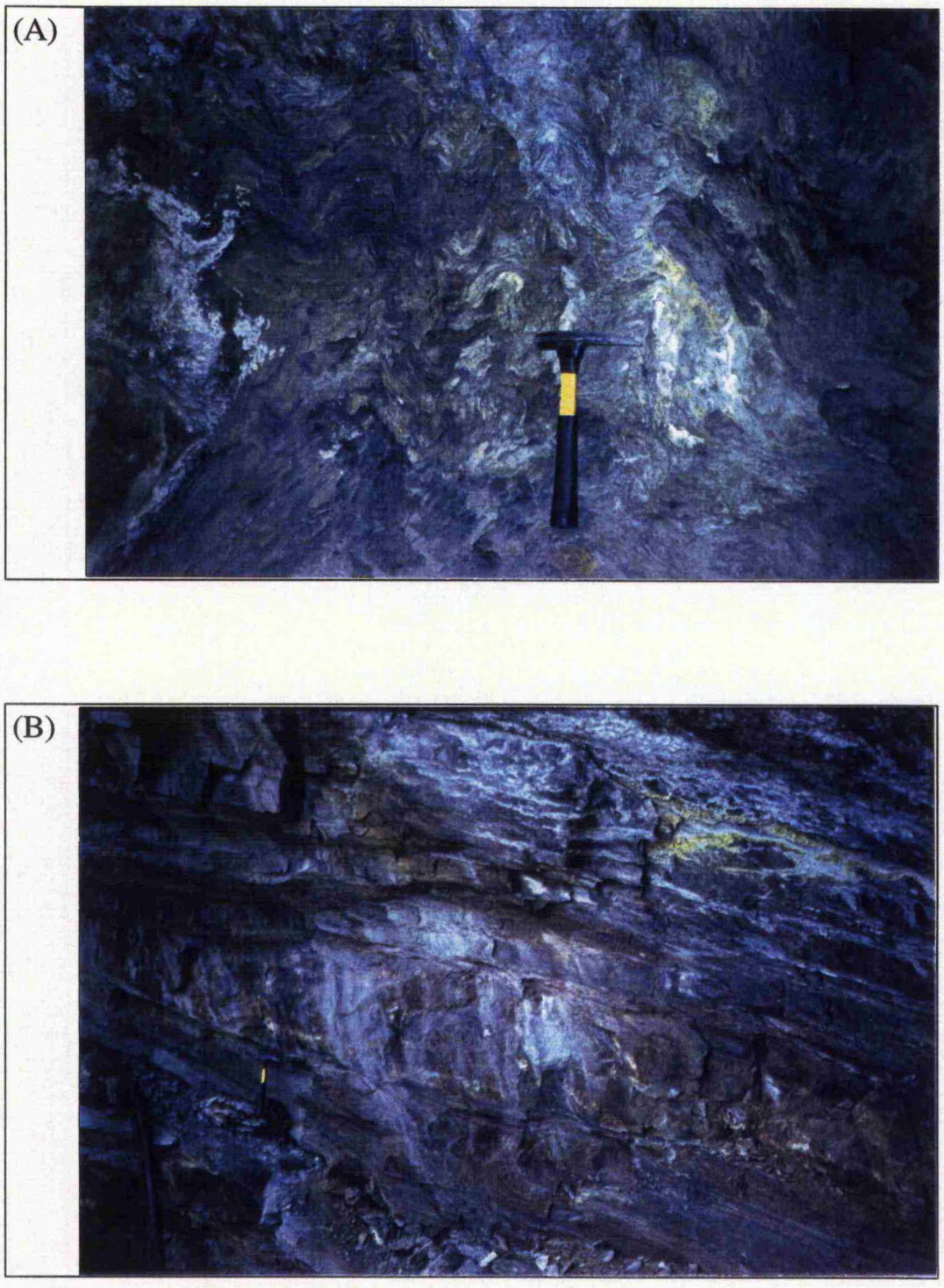

Fig. 3.1: Field relations: **(A)** Intercalated tourmaline and mica schist indicating S1 and S2 foliation. **(B)** Scheelite-bearing calc-silicate quartzite within the Miniki Gol.

3.3 Structure

The study area has undergone at least two major deformational events (D1, D2) associated with foliations (S1, S2) and with the formation of folds (F1 and F2) see (Fig. 3.1, 3.2, 3.3). According to Leake et al. (1989) the first deformation is related to the collision between Kohistan complex and Asian plate along the Northern suture during the late Cretaceous. The second deformation is associated with regional metamorphism and granite emplacement as result of collision between Indian plate and Kohistan complex along the Main Mantle Thrust during the Eocene.

3.3.1 First deformation

The primary foliation is defined by the parallel alignment of muscovite flakes in the phyllite and schist (Fig. 3.2, 3.3). According to Fletcher (1985), the other structural features associated with D1 includes deformed quartz veins, boudins of competent layers including scheelite-bearing quartzite (Fig. 3.2 C)

3.3.2 Second deformation

The chevron or kink folds and crenulation foliation (S2) in the studied rocks mark the secondary deformational event (Fig. 3.2 D, 3.3 B). According to Fletcher (1985), the effect of (D2) can also be recognised by the parallel alignment of xenoliths and muscovite laths within the granite to the (S2) crenulation foliation in the surrounding schist (Fig. 3.2 B). This, in turn, imply a relationship between the granite emplacement and second deformation in the thesis area.

3.3.3 Veins

Three types of veins were observed in Miniki Gol and surrounding area. The first type consists of buff-coloured quartz veins which have been deformed into augen-shaped bodies. According to Leake et al. (1989) these veins have been emplaced during the final stages of the first deformation and are still contained within the dominant penetrative foliation (S1) of the schist. These veins are generally unmineralised. The second variety of veins consist of quartz ± tourmaline crystals (Fig. 3.2 D), and some of these veins are intruded within tourmalinites along the axial planes of the second deformation folds (Fig. 3.3 B). The orientation of these veins appears to be controlled by both the penetrative foliation and secondary foliation in the study area. These veins contain some scheelite grains. The muscovite-bearing pegmatite is the third variety of veins, and occurs within the leucogranite at the mouth of Miniki Gol and surrounding area.

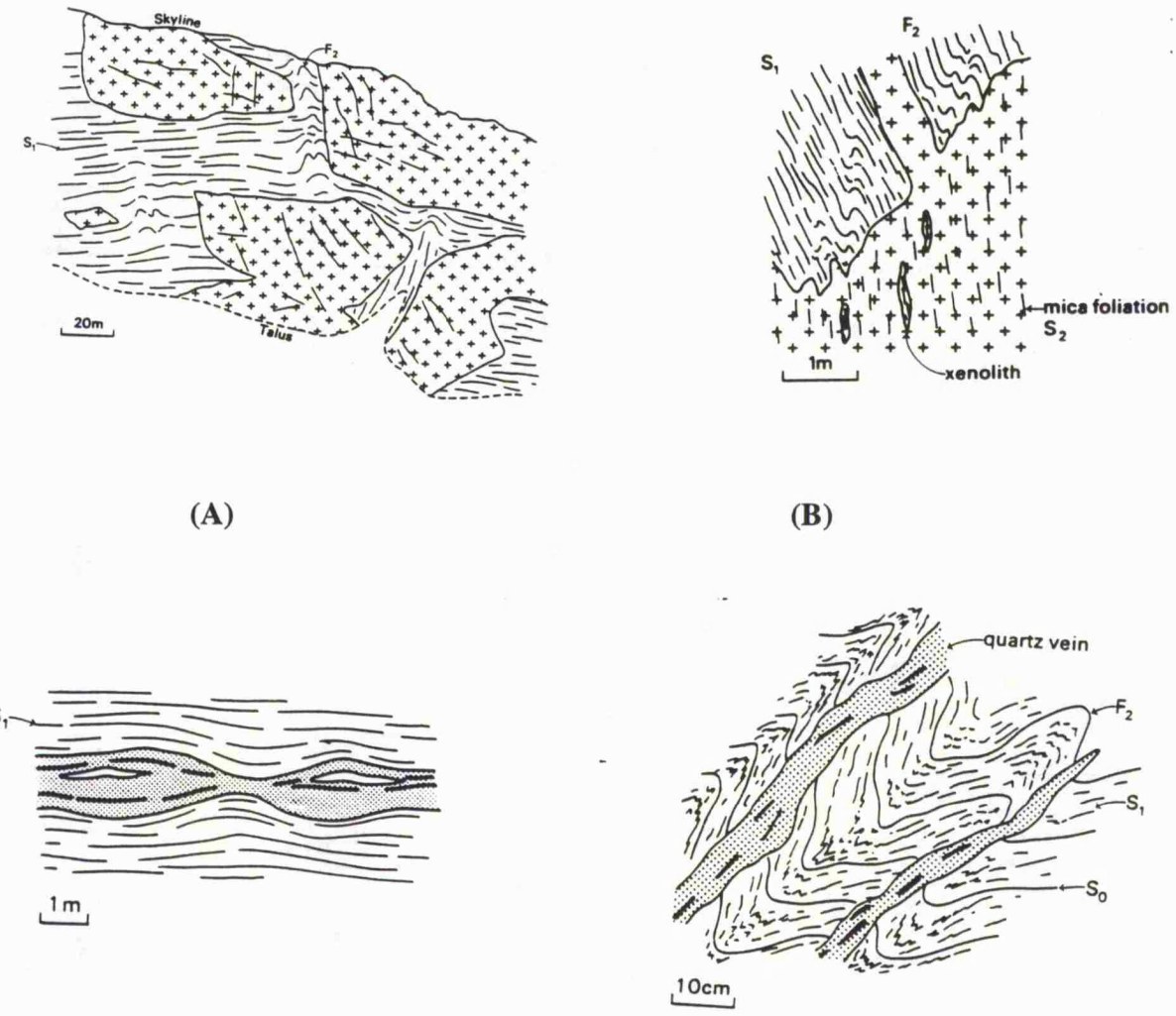

Fig 3.2: Contact relationships of the Miniki Gol granite (after Fletcher 1985). **(A)** Sheet-like granite bodies intruded into schist sequence on the northern side of Miniki Gol, showing apophyses. (B) Contact relationship between granite and schist, main granite contact is at high angle to S1 but a minor dyke has been intruded along S1. Xenolith and mica foliation in granite are subparallel to the axial plane of F2. **(C)** Boudinage structures in scheelite-bearing quartzite within the schistose succession. **(D)** Chevron folds (D2) and associated crenulation have deformed S1 in the schist. Quartz veins with tourmaline have been intruded along the axial plane of F2.

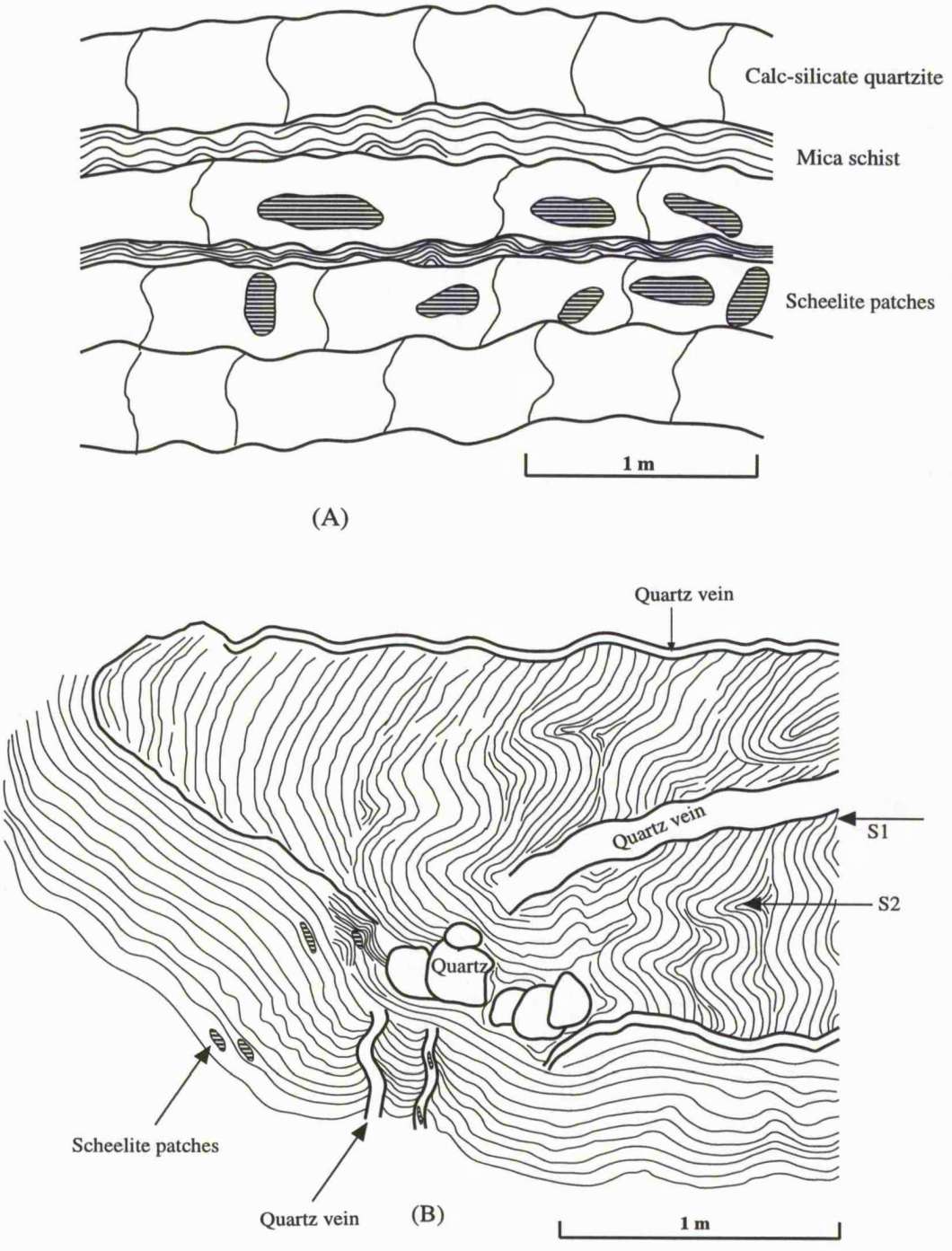

Fig. 3.3 (**A**) Sketch of calc-silicate quartzite interlayered with mica schist showing concordant and discordant scheelite patches. (**B**) Sketch of tourmalinite outcrop indicating overprint foliation (S1), crenulation foliation (S2), quartz veins and scheelite patches. Note that some scheelite grains are emplaced within the quartz vein and (S2) foliation.

These pegmatites are the late evolved stage of felsic intrusion and postdate the veins of the second type. The latter two types appear to be related to the intrusion of Miniki Gol leucogranite (Fletcher 1985).

3.3.4 Metamorphism and paragenetic sequence of minerals

According to Leake et al. (1989) the metamorphism in the Miniki Gol area is of Barrovian type. The garnet isograd lies to the north of valley and staurolite to the west and south of the area. The metapelites vary from phyllite to mica schist reflecting differences in initial bulk rock composition rather than metamorphic grade. In contrast, the lack of staurolite and garnet in the phyllitic schist at Besti Gol demonstrate lower grade metasediments than at Miniki Gol. On the basis of petrographic and mineralogical study and deformational history (see Fletcher 1985; Leake et al. 1989), the following paragenetic sequence is listed below (Table 3.1).

Muscovite: seems to have crystallised during S1 and continued during D2.

Biotite and chlorite: crystallised and recrystallised during D1, D2, their growth as secondary alteration product continued to post-D2 phase.

Staurolite and garnet: Staurolite precipitated mainly during D1 event, however garnet contains linear and sigmoidal internal schistosity, representing both post-and syn-D2 crystallisation.

Clinozoisite and scheelite: developed mimetically along the foliation (Leake et al. 1989), must have formed post-D1. Scheelite in addition cross cuts clinozoisite grains and its growth seems to be continued syn-and post-D2.

Tourmaline: euhedral crystals overprint S1 foliation and were broken during D2.

Amphibole: prismatic and laths of amphibole in the banded calc-silicate quartzite overprint S1 foliation and its sieve texture indicates that they formed during D2. The spherulitic or radiating appearance of actinolitic-hornblende indicates that it may be formed after D2 phase.

3.4 Mineralisation in the area

3.4.1 Tungsten mineralisation

Scheelite is the only tungsten mineral identified with the help of UV lamp in the Miniki Gol area, and occurs in a variety of rocks, the most important of which is calc-silicate quartzite. Tourmalinites also contain substantial amount of scheelite but the lateral extension of tourmalinite is very limited. Leake et al. (1989) have also reported some scheelite grains in the quartz calcite schist, albite quartzite and at the contact between quartzite and graphitic schist.

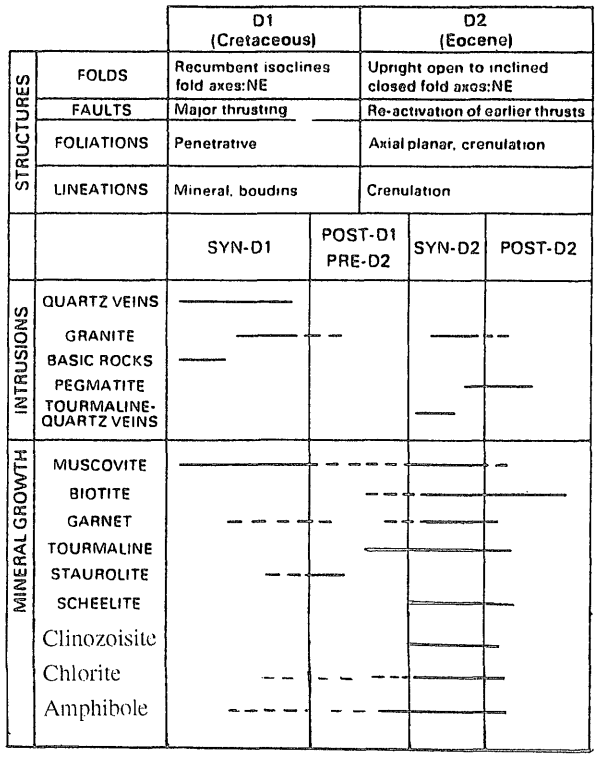

Table 3.1: Summary of tectonic, intrusive, metamorphic and mineralisation history of the Miniki Gol area after (Fletcher 1985) with modified paragenetic sequence of minerals.

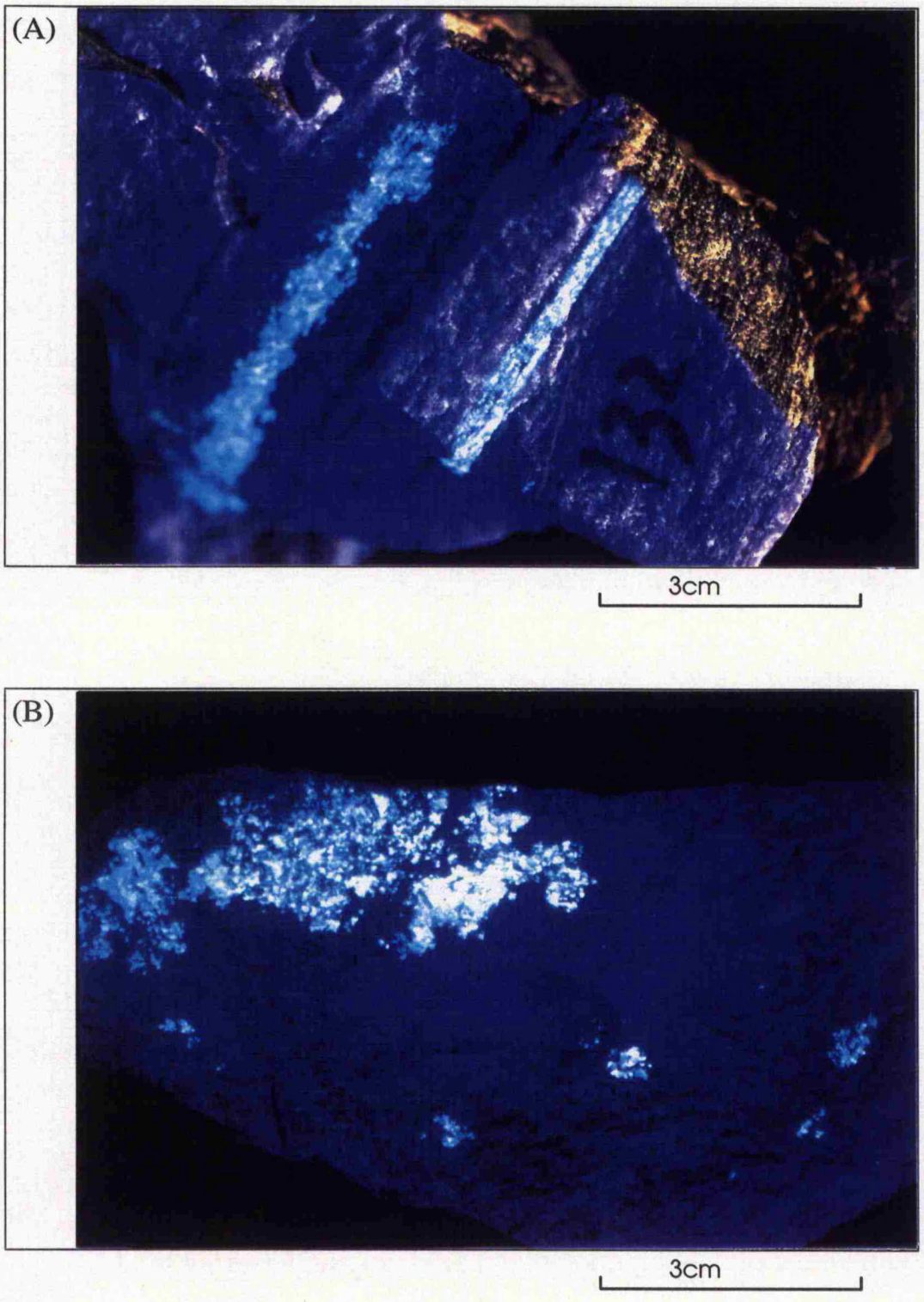

Fig. 3.4: Scheelite fluorescence **(A)** Scheelite veins within the calc-silicate quartzite along the bedding. **(B)** Discrete scheelite patches in tourmalinite. These photographs were taken from hand specimens under the UV light.

Scheelite occurs as discontinuous patches, stringers and conformable small veins within the calc-silicate quartzite (Fig. 3.3 A, 3.4 A) and can be considered as stratabound scheelite. Some minor scheelite veins also cut across the calc-silicate quartzite beds (Fig. 3.3 A). It should be noted that not all the calc-silicate quartzite beds are mineralised and also there is a considerable variation in the concentration of scheelite along and across the calc-silicate quartzite beds.

Tourmalinites display deformation phases (D1) and (D2) more prominently than do the calc-silicate quartzites (Fig. 3.3 B). Scheelite, here seems to be concentrated along both overprint penetrative foliation as well as crenulation foliation. Some of the cross-cutting quartz veins also contain scheelite patches.

3.4.2 Lead-zinc mineralisation

Lead-zinc mineralisation was mapped as scheelite in the field by Sarhad Development Authority because of same coloration and fluorescence to that of scheelite. Zinc mineralisation (sphalerite and hydrozincite) is more common and widespread than the Pb mineralisation (galena) in the Besti Gol area. The mineralisation is confined to a 65 m thick marble horizon at Singlasht in the Besti Gol area, whereas other marble beds in the Besti Gol area are unmineralised (see Fig. 1.3). Moreover, the one kilometre thick marble unit at Miniki Gol, is also devoid of any lead-zinc mineralisation.

Lead-zinc mineralisation is concordant with the enclosing marble and occurs as conformable continuous veins within the marble beds (Fig. 3.5 A-B). Based on the continuity and conformability of these mineralised veins, it can be considered as stratiform and stratabound mineralisation. Some small mineralised veins cut across the marble and form a network of the mineralised veins or stockwork adjacent to the stratiform sulphide at Singlasht. The individual veins range from 0.5 cm to 9.3 cm in thickness and the overall thickness of the mineralisation within the marble varies from 30 m to 65 m.

Some of the mineralised veins along with marble beds, show a stylolitic appearance, where the susceptible carbonates have been dissolved during the intense chemical weathering, giving a zigzag aspect to these mineralised veins (Fig. 3.5 A).

Several quartz veins are exposed in the vicinity of Besti Gol area and some of the quartz veins are closely associated with the rich zone of mineralisation at Singlasht (Fig. 1.3). These veins are generally unmineralised but one sample contains zinc mineralisation, which can be considered as the local remobilisation during the injection of these veins.

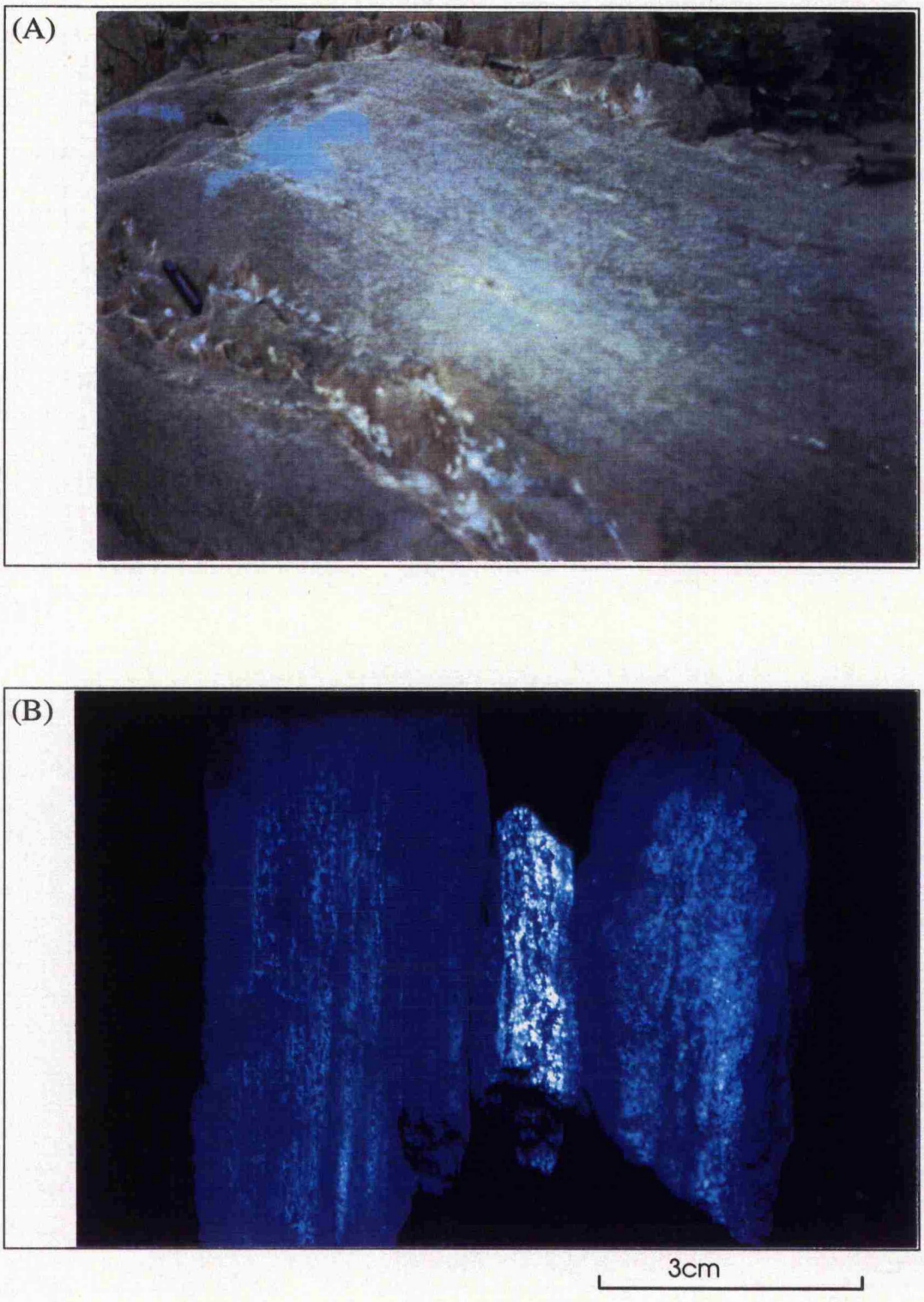

3.5: Lead zinc mineralisation **(A)** Stratiform Pb-Zn mineralisation conformable with enclosing marble. **(B)** Fluorescence of hydrozincite and possible sphalerite under the UV light, indicating stratiform layers.

3.5 Discussion

The compositional layering in the schist, the abundance of chlorite in the greenschist (Miyashiro 1973) and the general conformability of different lithological units at the Miniki Gol and Besti Gol area, signify a sedimentary protolith for these rock. Moreover the deformed cross bedding in the mica quartzite (Leake and Haslam 1985) also establishes a sedimentary parentage for these rocks.

The occurrence of black biotite, muscovite, staurolite, garnet and clinozoisite in these rocks probably reflect iron and aluminium rich pelitic environment in the project area. The occurrence of garnet and staurolite porphyroblasts wrapped in the foliated rock and the acicular crystals of tourmaline in the schist imply a high growth rate as compared to nucleation rate (Barker 1990).

Scheelite mineralisation in the Miniki Gol area seems to be structurally controlled. According to Leake et al. (1989), the compositional layering within the calc-silicate quartzite is assumed to be transposed bedding. Scheelite together with clinozoisite and garnet crystals developed mimetically along this foliation and therefore must have formed post D1. Moreover, Dames and Moore (1987) have also reported scheelite grains in the drag-folded sequence of calc-silicate quartzite. The concentration of some scheelite grains in the hinges of the kink folds (Fig. 3.3 B) can also be explained by the fractured hinges acting as loci for the epigenetic mineralising fluids (see also Dames and Moore 1987). The epigenetic mineralising fluids appear to follow the weak structural zones or, in other words, the foliation planes probably acted as channel ways for the epigenetic mineralising fluids. Both the continuity and distribution of mineralisation seems to be influenced by the structure in the study area. Source of these epigenetic mineralising fluids will be discussed in the Chapter 6.

It is tentatively concluded that the primary scheelite grains were crystallised post or during the late-stage of the second deformation. The cross-cutting scheelite crystals (Fig. 3.3 A) appear to form at an even later stage. The concentration of scheelite in the drag folded sections and the emplacement of scheelite bearing quartz veins along the axial plane of F2 probably suggest a genetic relationship between the scheelite mineralisation during the second deformation and intrusion of Miniki Gol granite.

As far as Pb-Zn mineralisation is concerned, on the basis of field relationship (continuity and conformability of the mineralised veins with the host marble), it can be concluded primarily that the Pb-Zn mineralisation in the Besti Gol area precipitated syngenitically at the time of the deposition of limestone. Subsequent metamorphism has coarsened the grain size of these mineralisations and also disturbed, at places, the concordance of these mineralised veins.

No skarn assemblages have been observed along the contact between the pegmatite and marble.

Chapter Four

PETROGRAPHIC AND MINERALOGICAL STUDIES

4.1 Introduction

The composition of the silicate minerals provide some constraints on the origin of tungsten mineralisation. To ascertain chemical variation in the silicate minerals and also to determine the environment of growth and pressure-temperature conditions of crystallisation, the chemistry of the silicate minerals is discussed in this chapter. Silicate minerals include tourmaline, clinozoisite, garnet, amphibole, chlorite, biotite, sphene and plagioclase. Whereas scheelite, sphalerite, galena, arsenopyrite and pyrite are the ore minerals. Objects of this chapter are summarised as follow:

- To understand mineral chemistry and paragenesis.
- To establish the protolith of the metamorphic rocks.
- To know the metamorphic history using pressure-temperature estimates.
- To understand mineralogy of the leucogranites and associated phases.

4.2 Samples and methods

During three separate field trips, the study area was sampled through a number of systematic traverses and a total of about 294 rock samples were collected. The location of some of these samples has been shown in the (Fig. 4.1 A, B, C, 5.4, 5.6). A complete list of the rock samples together with mineralogy is given in Appendix 4.1 and 5.6. The samples collected, predominantly consist of mica schist, calc-silicate quartzite and leucogranites. Other collected samples include psammite, mica quartzite, phyllite, tourmalinite, calcareous schist, feldspathic gneiss, amphibolite, pegmatite, marble, Kafiristan and Tirich Mir porphyritic granodiorites. Samples of the majority of calc-silicate quartzites, micaceous psammite, mica quartzite, mica schist, tourmalinites and leucogranite together with a sample each from Kafiristan and Tirich Mir granodiorite were studied using microscope, SEM and microprobe. The other rock units were studied through thin sections and megascopic observations.

4.3 Lithology and petrography

The study area is predominantly composed of metasediments such as mica schist, phyllite, micaceous psammite, together with calc-silicate quartzites, tourmalinites and marble. Feldspathic gneiss and thin layers of amphibolite were also interlayered with the metasediments.

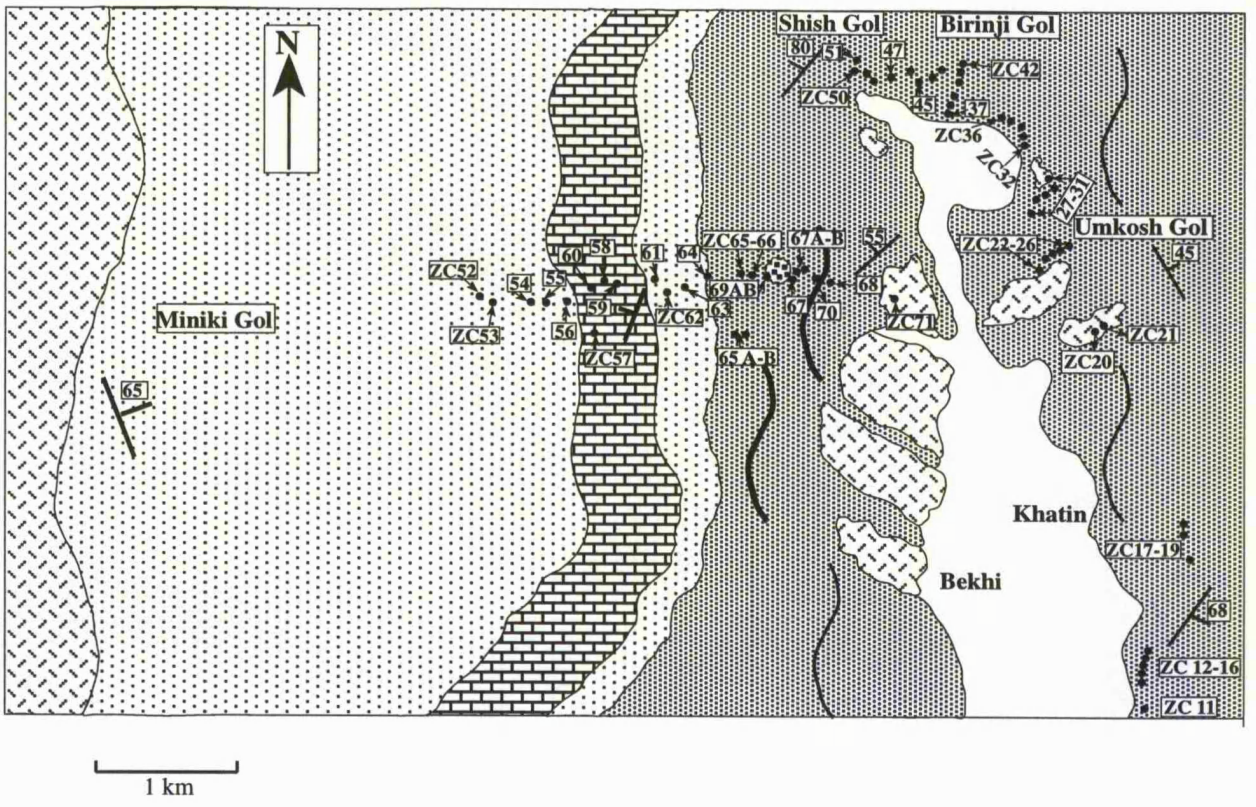

LEGEND

- Alluvium
- Leucogranite
- **Calc-silicate quartzite** interbedded with mica schist
- Tourmalinite
- Phyllite
- Marble
- Mica schist
- Bedding
- Contact

Fig. 4.1 A: Sample location map of the Miniki Gol and adjoining area (ZC series).

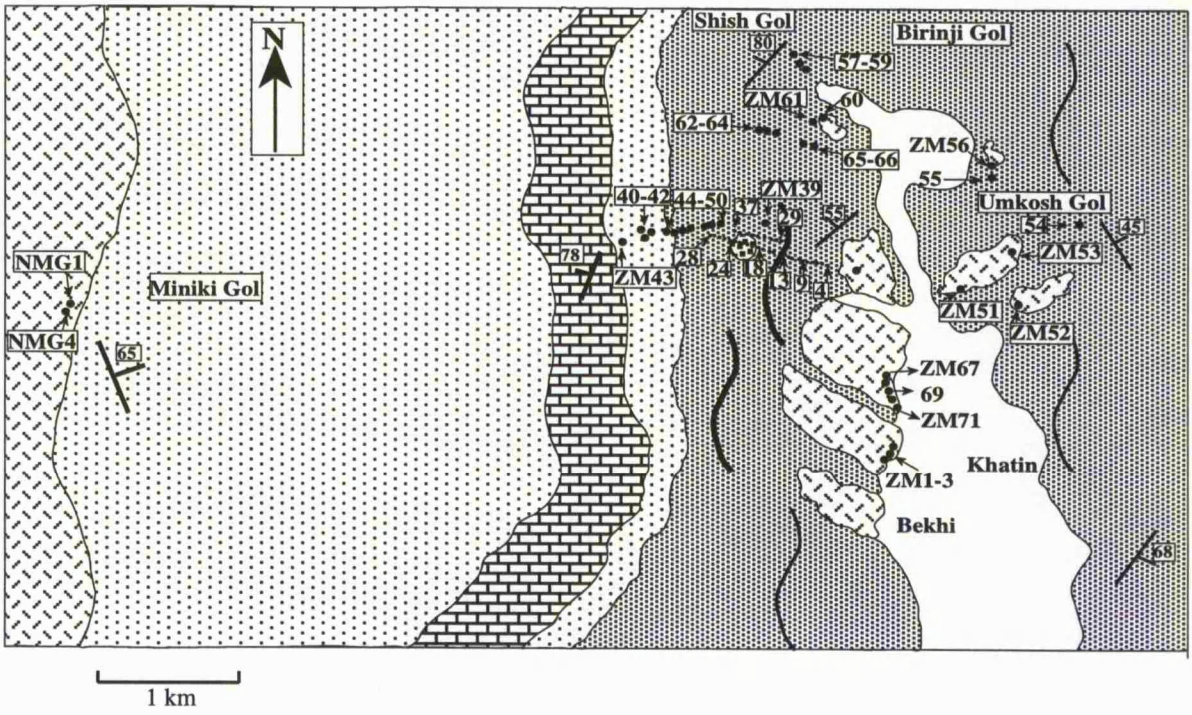

LEGEND

- Alluvium
- Leucogranite
- Calc-silicate quartzite interbedded with mica schist
- Tourmalinite
- Phyllite
- Marble
- Mica schist
- Bedding
- Contact

Fig. 4.1 B: Sample location map of the Miniki Gol and surrounding area (ZM series).

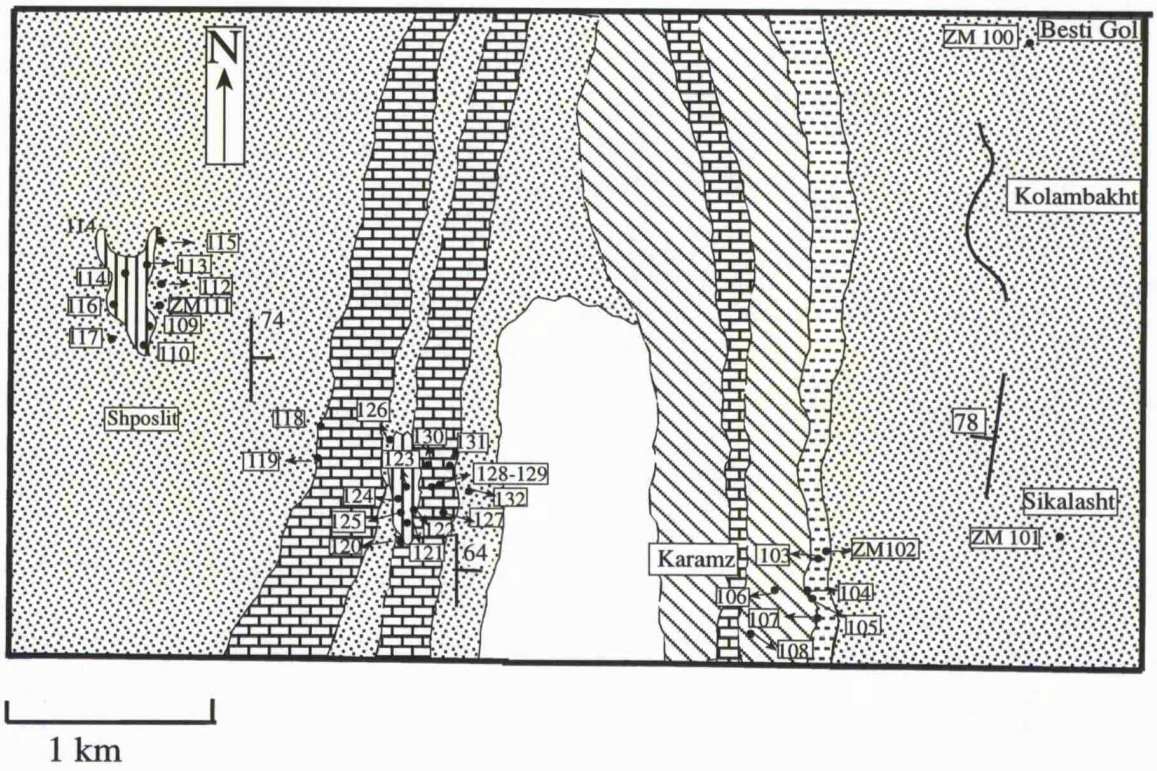

LEGEND

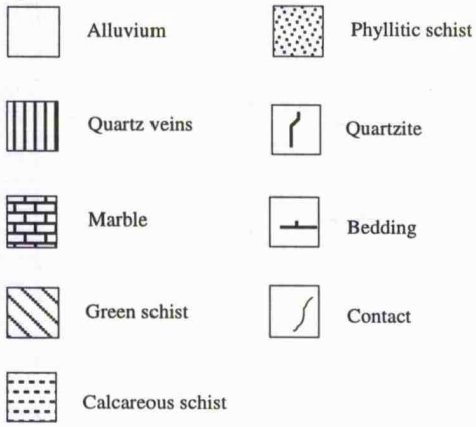

Fig. 4.1 C: Sample location map of the Besti Gol and adjoining area.

The metasediments have been intruded by relatively early porphyritic granodiorites and later leucogranites.

4.3.1 Mica schist

Mica schist is composed of variable amounts of quartz, plagioclase, muscovite, biotite, graphite and tourmaline with porphyroblasts of garnet and staurolite. Kyanite, cordierite and andalusite have been reported by Leake et al. (1989). Accessory minerals include titanite, ilmenite and zircon. Garnet and staurolite porphyroblasts are enclosed by muscovite, biotite, chlorite and graphite bands (Fig. 4.2 A).

4.3.2 Phyllite

The phyllite is a finely-foliated rock containing quartz, muscovite, biotite, chlorite and graphite. Although, phyllites are of lower metamorphic grade than the schist, they contain porphyroblasts of garnet and rare staurolite. Bedding is defined by the relative abundance of muscovite, graphite and occasionally chlorite.

4.3.3 Mica quartzite and micaceous psammite

Mica quartzite is composed of granular quartz > 90 %, biotite, muscovite, plagioclase (mostly albite) and chlorite. The micaceous psammite is almost similar in mineralogy but containing < 90 % quartz and as well as relatively high plagioclase. A mosaic of anhedral to subhedral quartz and albite forms the ground mass, the foliation being defined by biotite flakes and minor muscovite and chlorite. Some calc-silicate bands also cross-cut the psammite and hence postdate the psammite. No scheelite has been located in these rocks.

4.3.4 Calc-silicate quartzite

The calc-silicate rocks are composed of clinozoisite, quartz, amphibole, plagioclase, chlorite, biotite, calcite, sphene, garnet, anthophyllite, scheelite and accessories such as diopside, ilmenite and muscovite. Calcite in one sample of scheelite-bearing rock, ZC 65 B, C (Appendix 4.1) reaches over 50 % by volume. Pyrite (partly altered to geothite), chalcopyrite, pyrrhotite and melnikovite were also identified by Leake et al. (1989). Some varieties of calc-silicate rocks are banded with the darker layers being mainly composed of amphibole chlorite and clinozoisite. The non-banded or granular variety is mainly characterised by quartz and clinozoisite and the scheelite grains are mostly found in this non-banded variety. It is also worth mentioning that at the onset of clinozoisite and scheelite grains, calc-silicate quartzites lose the foliations (Fig. 4.2 B). In some rocks later

veins consisting of chlorite, titanite and epidote cross-cut the pre-existing clinozoisite and quartz (Fig. 4.3 A)

Clinozoisite in the granular calc-silicate quartzite, occurs as subhedral to euhedral grains and is associated with quartz and scheelite grains. The percentage of the clinozoisite varies but reaches up to 60 % by volume. The granular nature of clinozoisite with clear grain boundaries, suggest that clinozoisite is completely recrystallised and it appears to have formed at the expense of plagioclase. In one sample of scheelite-bearing calc-silicate quartzite, the clinozoisite (replacing plagioclase) shows relicts of the plagioclase twinning (Fig. 4.3 B). This is a transitional phase between parent plagioclase and secondary clinozoisite.

Quartz grains in these calc-silicate quartzite occur as medium to large grains. They show no deformation (Fig 4.2 B), indicating annealing which is consistent with retrogression.

The amphibole (actinolitic hornblende) in these rocks occurs as spherulites, needle or fibrous flakes radiating from a common centre (Fig. 4.4 A). The non-spherulitic tschermakitic-hornblende occurs as laths associated with scheelite, anorthite and in places clinozoisite and sphene. Some of the hornblende grains are found as euhedral grains, long axes of blade are not aligned with the foliation. Some thin layers of amphibole crosscut the main amphibole layers. The stellate form of actinolitic amphibole appears to be crystallised later than clinozoisite (Leake et al. 1989), although the tschermakitic hornblende predates the clinozoisite phase.

Biotite occur as minute flakes exhibiting a feathery appearance and seems to be secondary (Fig. 4.4 B) unlike in schists, where it occurs as bands defining primary schistosity. Biotite in the scheelite-bearing rocks is also associated with clinozoisite.

Chlorite has been found as small flakes or laths and was found at an angle to the main schistosity (Fig. 4.4 B). Chlorite fibres replace biotite, actinolite and even clinozoisite (Fig. 4.5 A), where additional Fe and Mg in chlorite are probably provided by the associated amphibole. These secondary chlorites exhibit grey birefringence compared with schist, giving blue color in transmitted light. Scheelite grains are concentrated in calc-silicate quartzites, that also contain substantial amounts of amphibole and clinozoisite. In addition, scheelite-bearing calc-silicate quartzites are schistosless than barren calc-silicate quartzite. Scheelite patches, stringers and discrete grains are intergrown with clinozoisite and quartz grains (4.5 B), and occur mostly as anhedral grains of irregular shape.

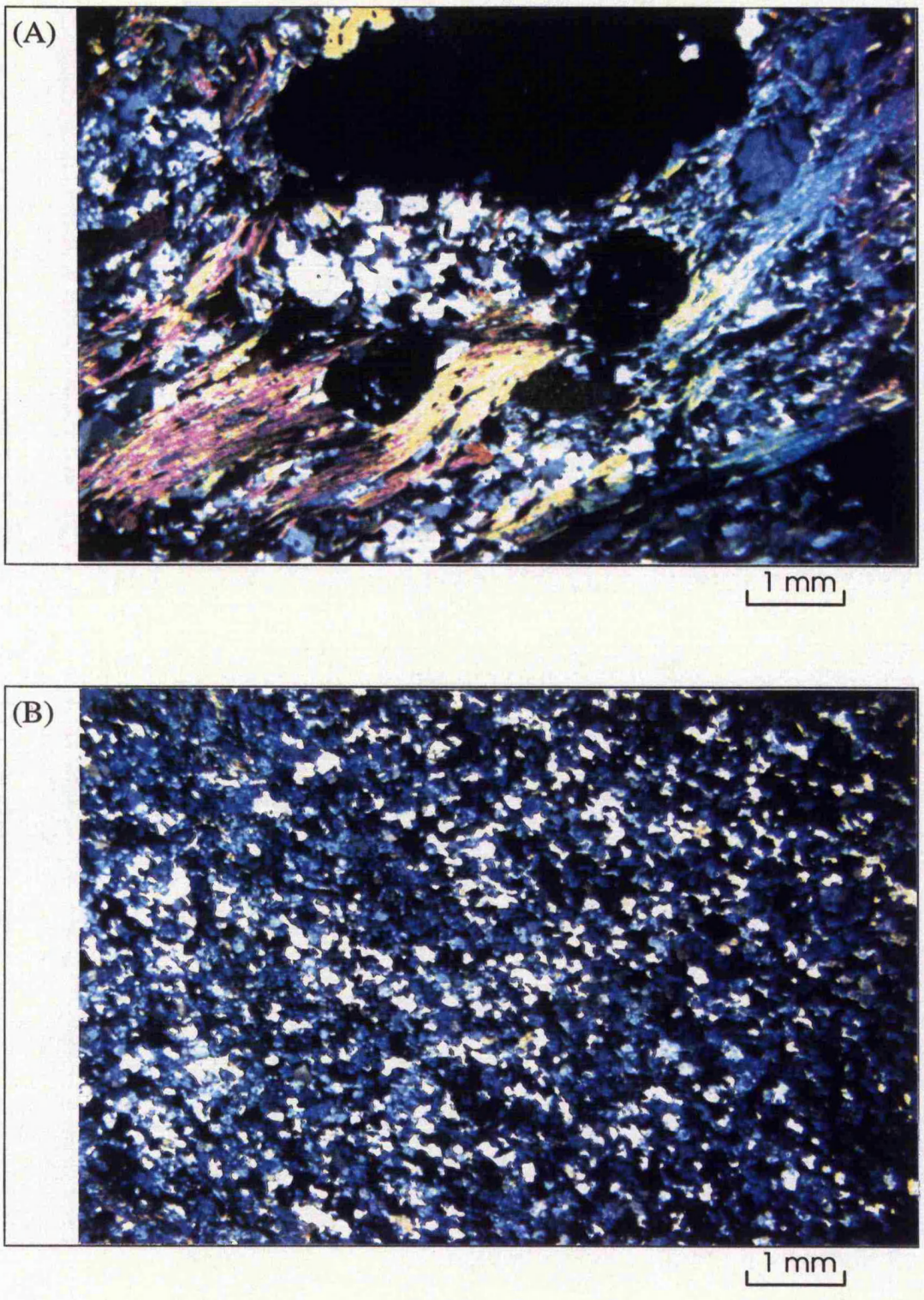

Fig. 4.2: Photomicrographs (crossed nicols): **(A)** Garnet and staurolite porphyroblasts wrapped in muscovite bands. **(B)** Granular clinozoisite (blue) associated with quartz grains (white). The quartz crystals show clear grain boundaries, indicating annealing.

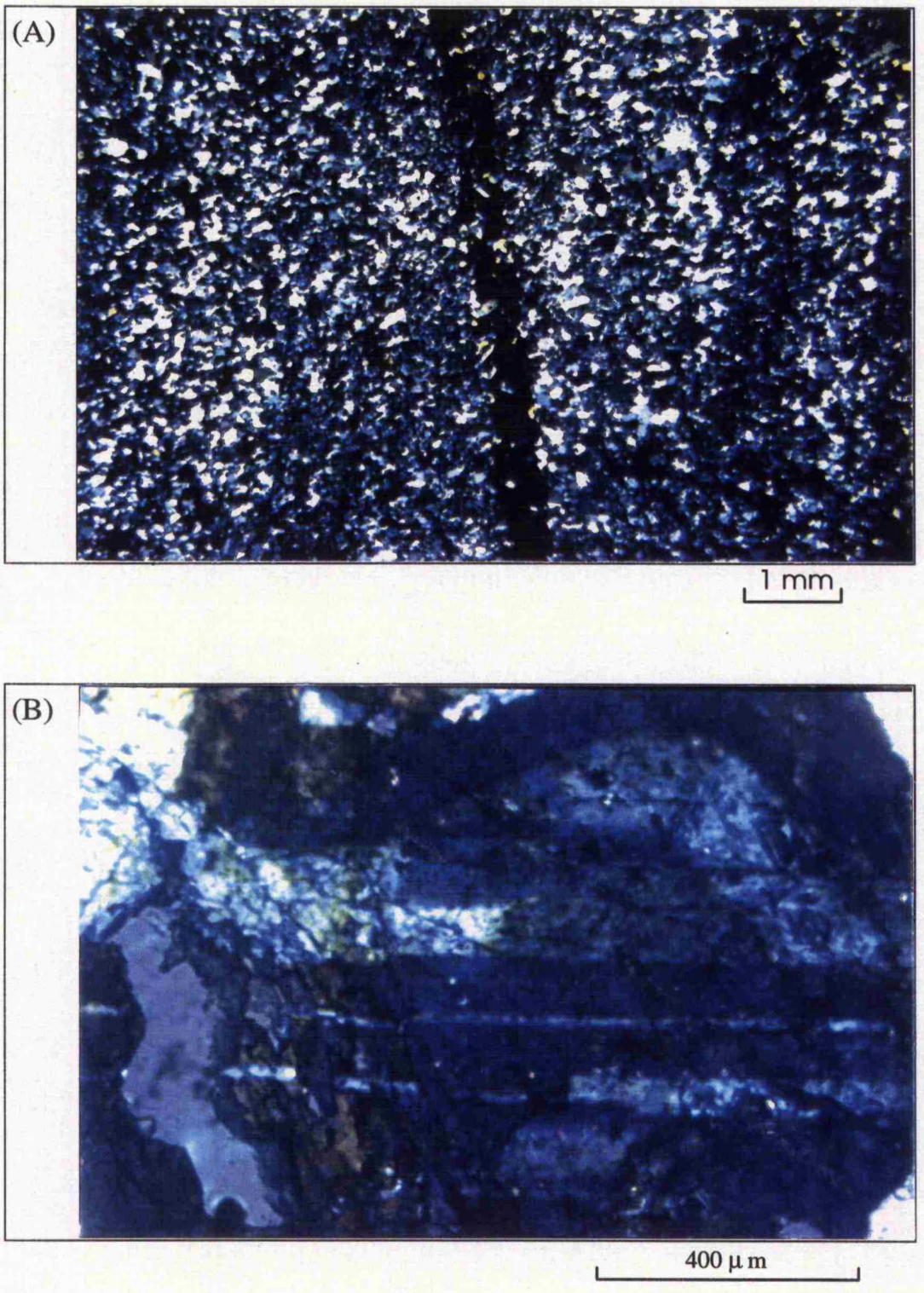

Fig. 4.3: Photomicrographs (crossed nicols): **(A)** Cross-cutting chlorite-rich vein in the calc-silicate quartzite. **(B)** Plagioclase grain replaced partially by clinozoisite.

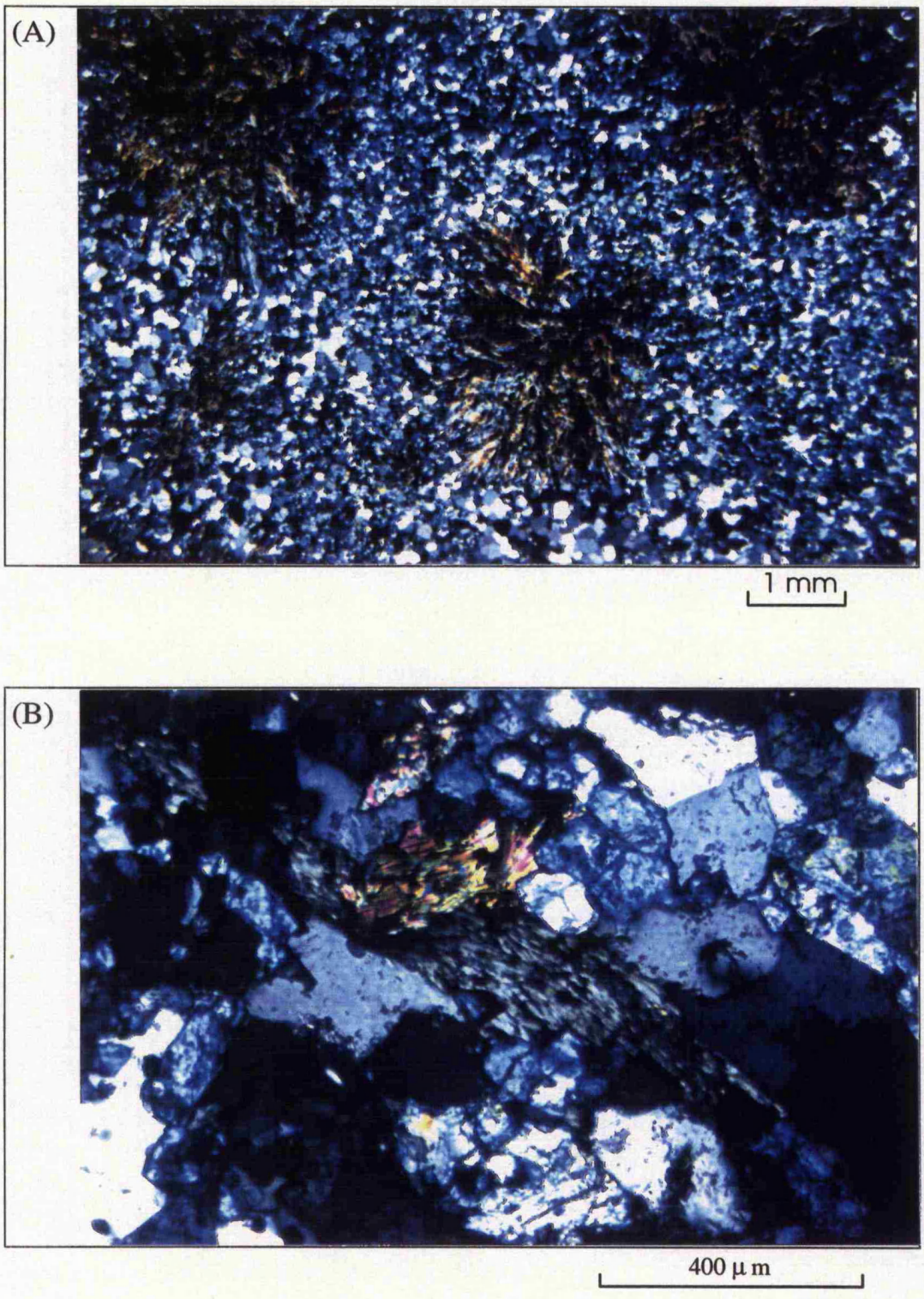

Fig. 4.4: Photomicrographs (crossed nicols): **(A)** Spherulitic actinolite and hornblende in the ground mass of clinozoisite. **(B)** Secondary biotite associated with secondary chlorite (grey).

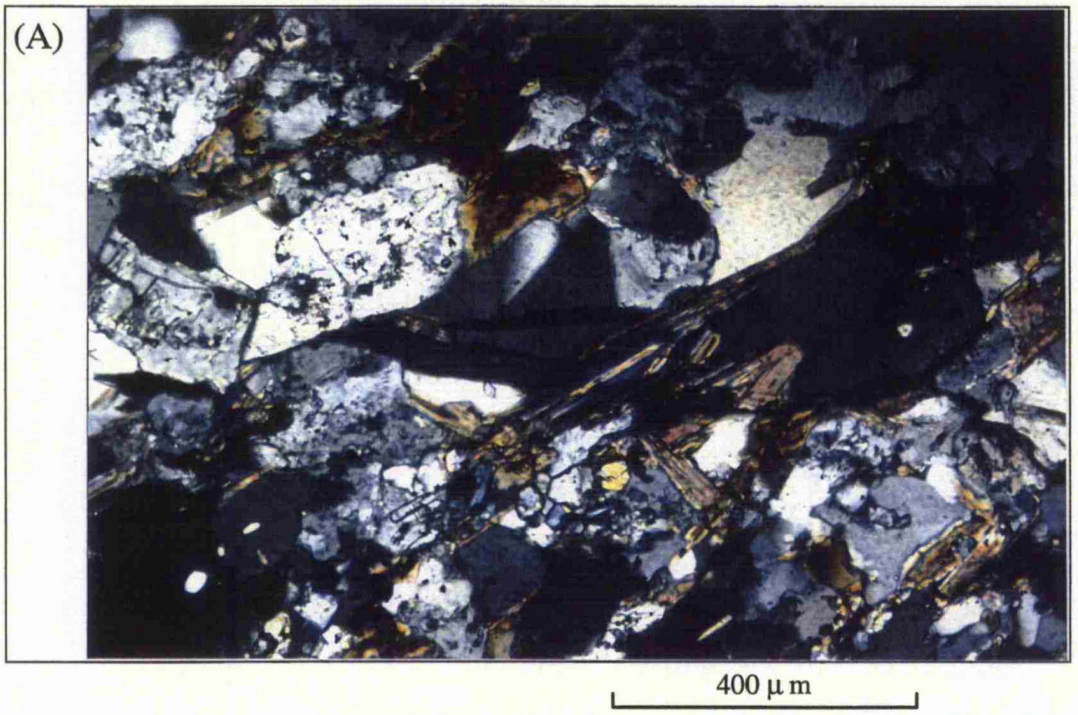

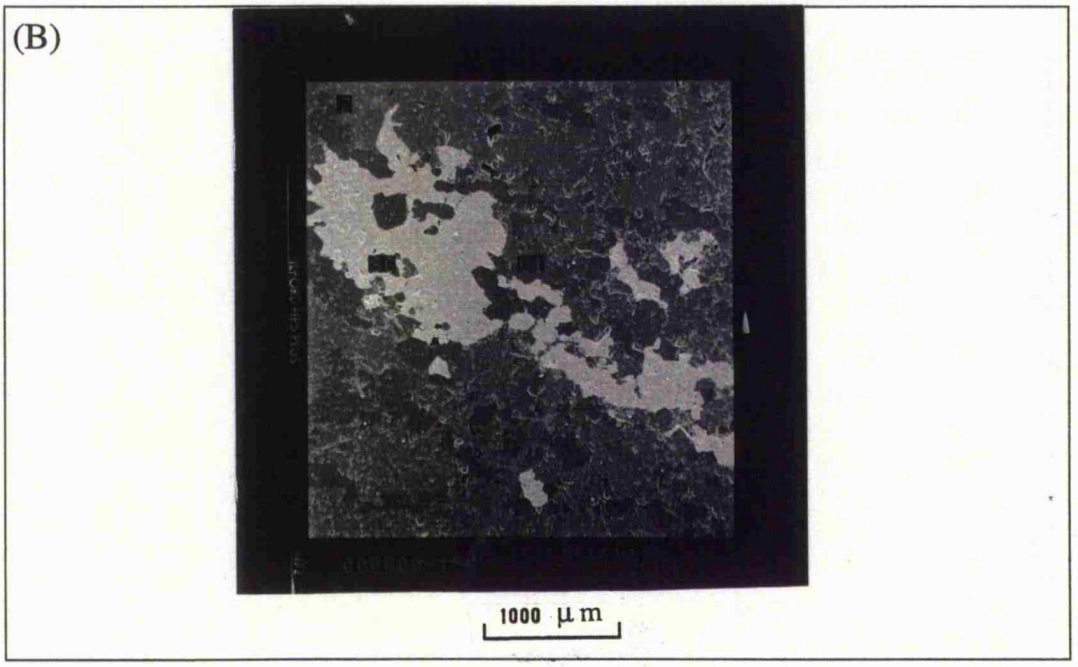

Fig. 4.5: Photomicrograph (crossed nicols): **(A)** Biotite needle (pinkish) is replaced at margin by chlorite. SEM photograph: **(B)** Scheelite (SC) patches (white) associated with clinozoisite (Cl).

The color of scheelite crystals varies from greyish-white through yellow to pinkish red in transmitted light. Most of the scheelite grains are intergrown with clinozoisite (Fig. 4.6 A). Although some small scheelite veins cross-cut clinozoisite grains (Fig. 4.6 B), which postdate the main clinozoisite phase.

4.3.5 Tourmalinite

Leake et al. (1989) have recognised three varieties of tourmaline-rich rocks. The first type occurs in lensoid masses which are spatially associated with discordant quartz veins. The second and most widespread type is the tourmaline-bearing schist, interlayered with mica schist. The third variety, a layered tourmaline-quartz gneiss or tourmalinite is much less common and has been identified at three locations within the mica schist. Scheelite has been found in this variety, where tourmaline reaches up to 80 % by volume (Fig 4.7 A). These scheelite-bearing tourmalinites are composed of tourmaline, spessartine-rich garnet (over 40 % by volume, Fig. 4.7 B), quartz, scheelite and manganifeous ilmenite together with traces of magnetite, pyrite and pyrrhotite.

Schistosity is well developed in the tourmaline-bearing schist and as well as tourmalinites, and is defined by tourmaline and quartz. Tourmaline needles and blades occur within the foliation but without alignment of long axes, whereas garnet occur as almost subhedral crystals. Both garnet and tourmaline contain numerous inclusions, which according to Leake et al. (1989) may define a planar fabric. Scheelite occurs as fine-grained disseminated grains as well as lenses (Fig. 3.4 B).

4.3.6 Marble

Marble in the study area consist of coarse-grained mosaics of calcite, muscovite and isolated quartz with accessory chlorite and phlogopite. Triple junctions, a typical metamorphic texture, has been noticed in these calcite crystals. The marble in the Miniki Gol is generally unmineralised. However, Leake et al. (1989) have reported the skarn assemblage at the eastern margin of the marble at Miniki Gol to be composed of actinolite, clinozoisite, muscovite, titanite and accessory zircon. Scheelite was observed in association with quartz in one sample.

In contrast to Miniki Gol area, marble at Besti Gol area contain Pb-Zn mineralisation, including a substantial amount of sphalerite together with subordinate galena and pyrite. Coarse-grained sphalerite occurs as layers concordant with the enclosing calcite, and appears to be elongated and flattened along grain boundaries during the metamorphism.

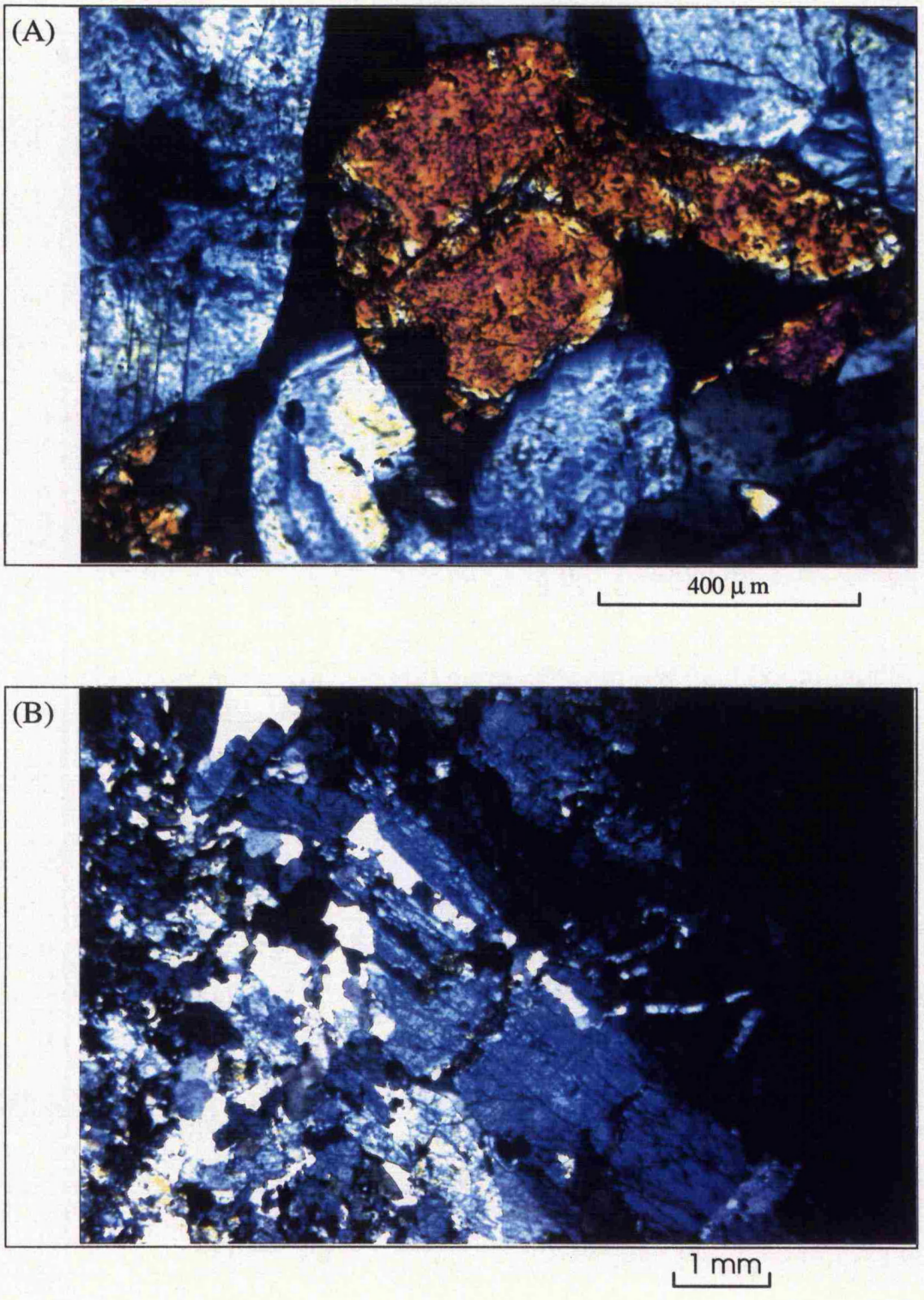

Fig. 4.6: Photomicrographs (crossed nicols): **(A)** Scheelite crystals (pinkish) intergrown with clinozoisite (blue). **(B)** Scheelite veinlets (yellowish) cross-cut the clinozoisite (blue) grains.

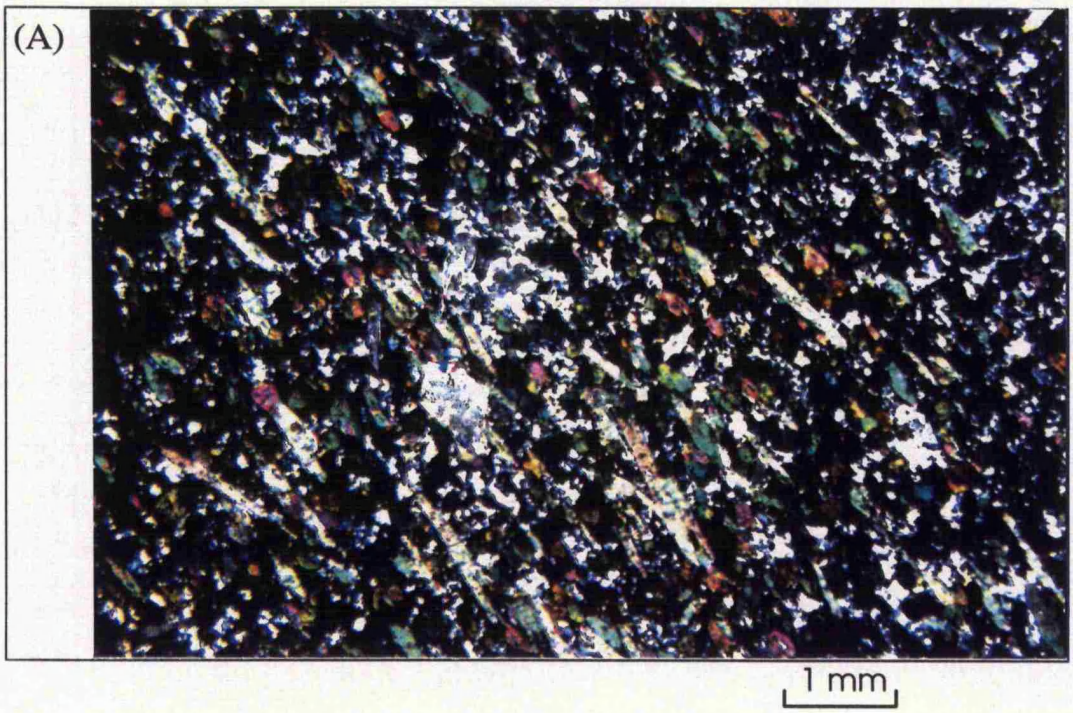

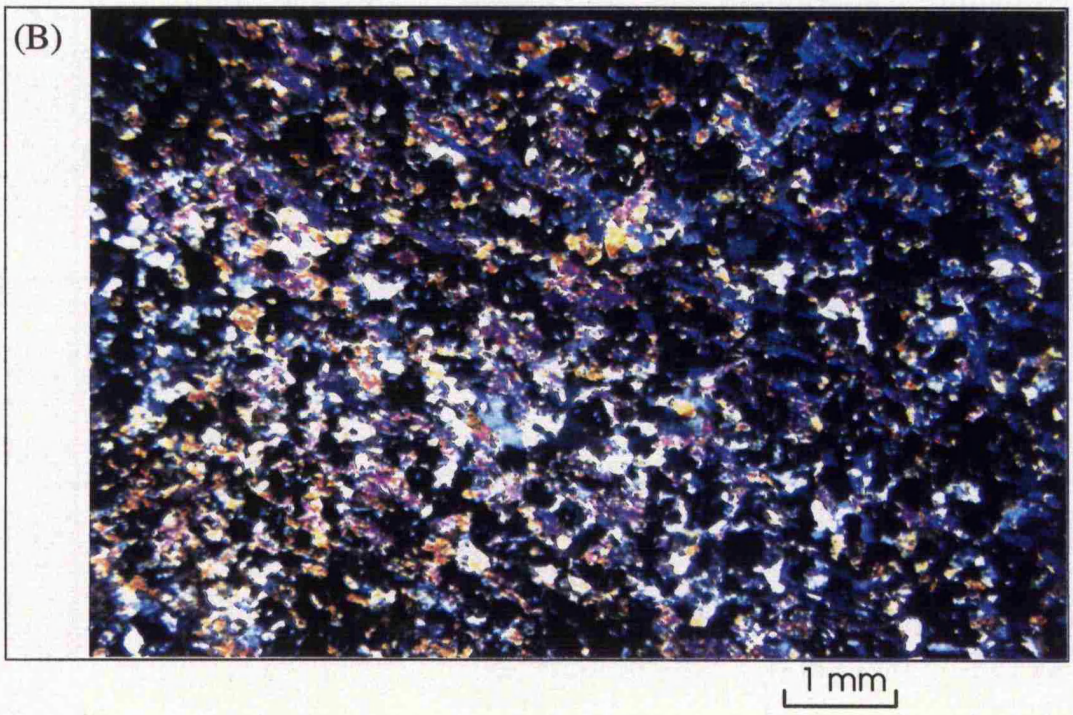

Fig. 4.7: Photomicrographs (crossed nicols): **(A)** Tourmaline blades associated with garnet in the tourmalinites. **(B)** Granular garnet (black) associated with tourmaline.

Triple junction texture can also be observed in these sphalerite grains (Fig. 4.8 A). Both sphalerite and galena appear to be recrystallised and coarsened during the course of metamorphism. Owing the brittleness of sphalerite and ductile behaviour of galena (Stanton 1972), these grains are foliated, displaying a knotty appearance (Fig. 4.8 B). This highly irregular and embayed form of sphalerite is typical of carbonate mineralisation in which sedimentary layering has been obliterated by recrystallisation during metamorphism (Stanton 1972).

Sphalerite and galena, at their margin are altered to probable hydrozincite and plattnerite respectively (Fig. 4.8 A, 4.9 A). Pyrite seems to be altered to zinc-bearing magnetite (Fig. 4.9 B).

4.3.7 Porphyritic granodiorites

Tirich Mir and Kafiristan granodiorites are essentially composed of plagioclase phenocrysts, biotite, hornblende, quartz and orthoclase together with minor muscovite. These granodiorites are strongly foliated giving a gneissic appearance in hand specimens.

4.3.8 Leucogranite and pegmatite

Miniki Gol homogenous leucogranite is characterised by coarse-grained aggregates of quartz, albite, orthoclase, muscovite and garnet together with subordinate biotite, tourmaline and apatite. In one sample ZS 10 the biotite is replaced by chlorite (Fig. 4.10 A). The garnet in the leucogranite is cracked indicating deformation within the granite. In addition coarse muscovite flakes also define penetrative foliation (see Leake et al. 1989).

Pegmatite is composed of large grains of quartz, albite, tourmaline and muscovite together with subordinate biotite. In one sample ZS 11 kaolin has been found associated with muscovite (Fig 4.10 B). The kaolin grain contains relicts of biotite flakes, probably indicating that kaolin was formed at the expense of biotite.

4.4 Mineral chemistry

Almost all major and minor phases (such as tourmaline, biotite, plagioclase and garnet) of granite, (tourmaline, garnet and plagioclase) of tourmalinites and (tourmaline, epidote, garnet, chlorite, plagioclase and biotite) of the schist were analysed through Jeol Superprobe. Pegmatite includes plagioclase and tourmaline. Similarly, mineral compositions of most of the phases (e.g. clinozoisite, garnet, amphibole, chlorite, biotite, sphene, plagioclase and scheelite) of calc-silicate quartzite and (biotite, plagioclase and chlorite) of mica quartzite and psammite were analysed.

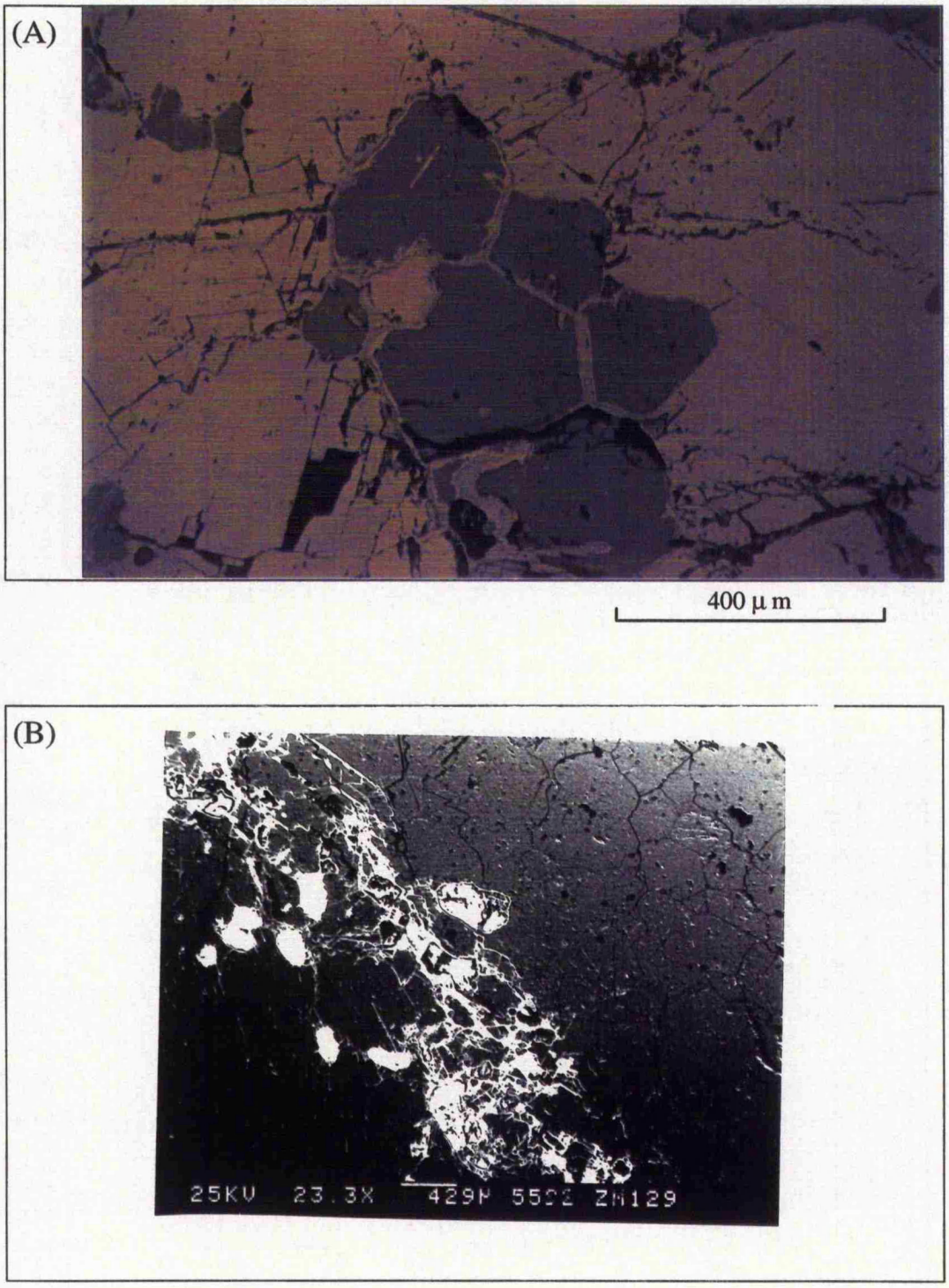

Fig. 4.8: Photomicrograph (plane polarised reflected light): **(A)** Sphalerite grains changing to hydrozincite at margin and also showing triple junction. SEM photograph: **(B)** Sphalerite grains (foliated) displaying knotty appearance.

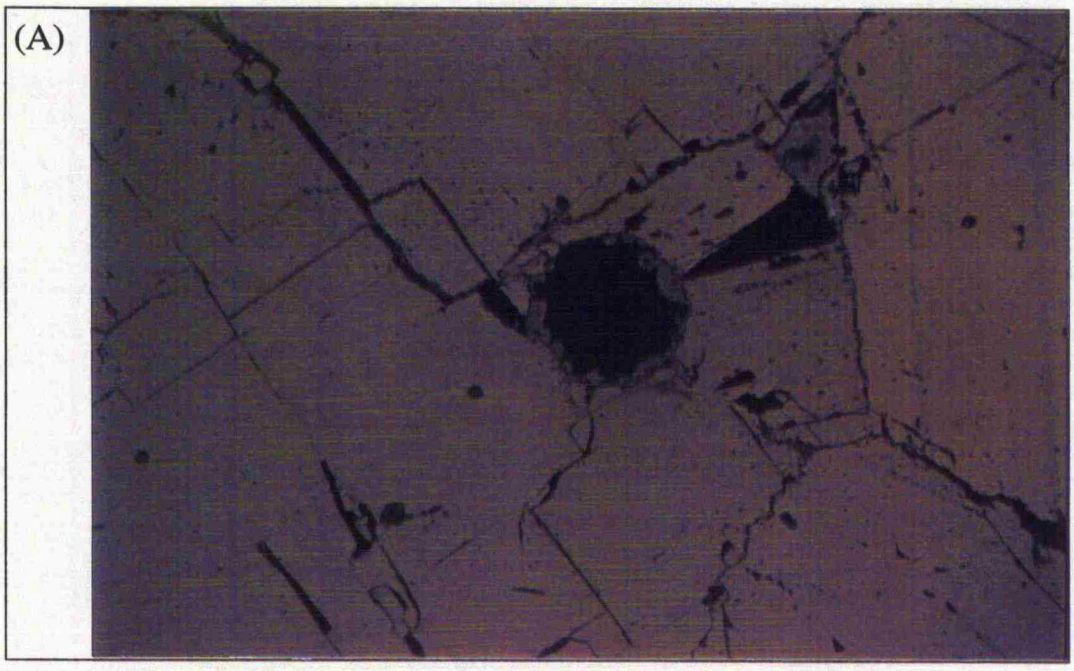

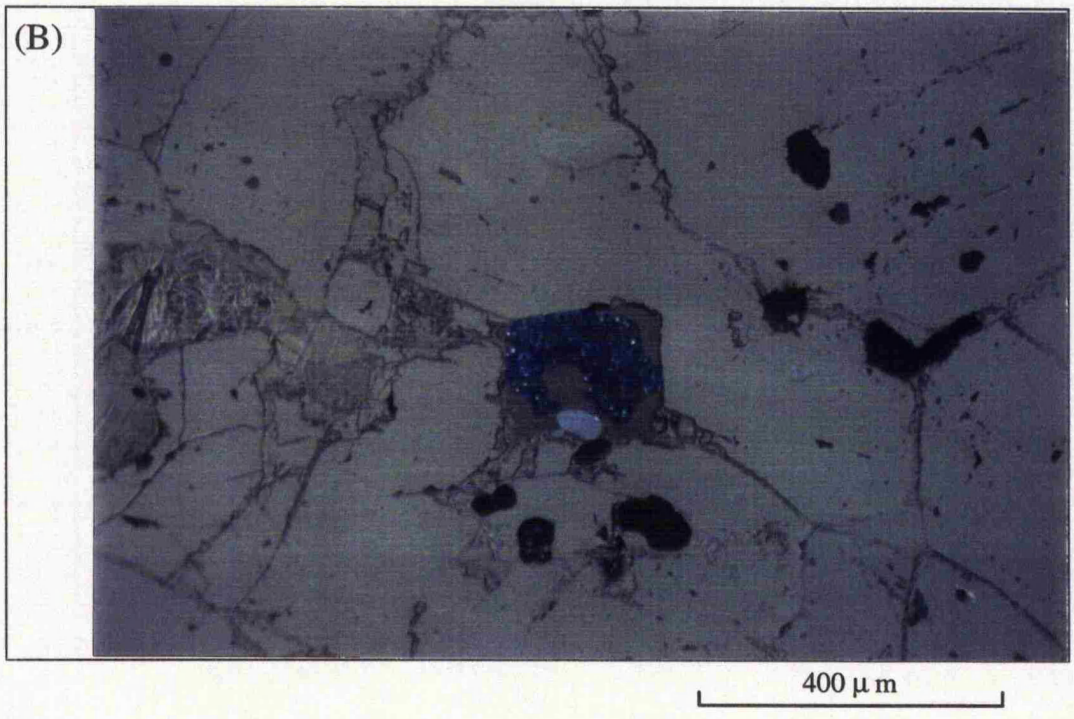

Fig. 4.9: Photomicrographs (plane polarised reflected light): **(A)** Galena (blue) is replaced by Pb-oxide at margin. **(B)** Pyrite (blue) is replaced by zinc-bearing magnetite or Fe-hydroxide. (Sections are carbon-coated due to which sulphide shows blue color).

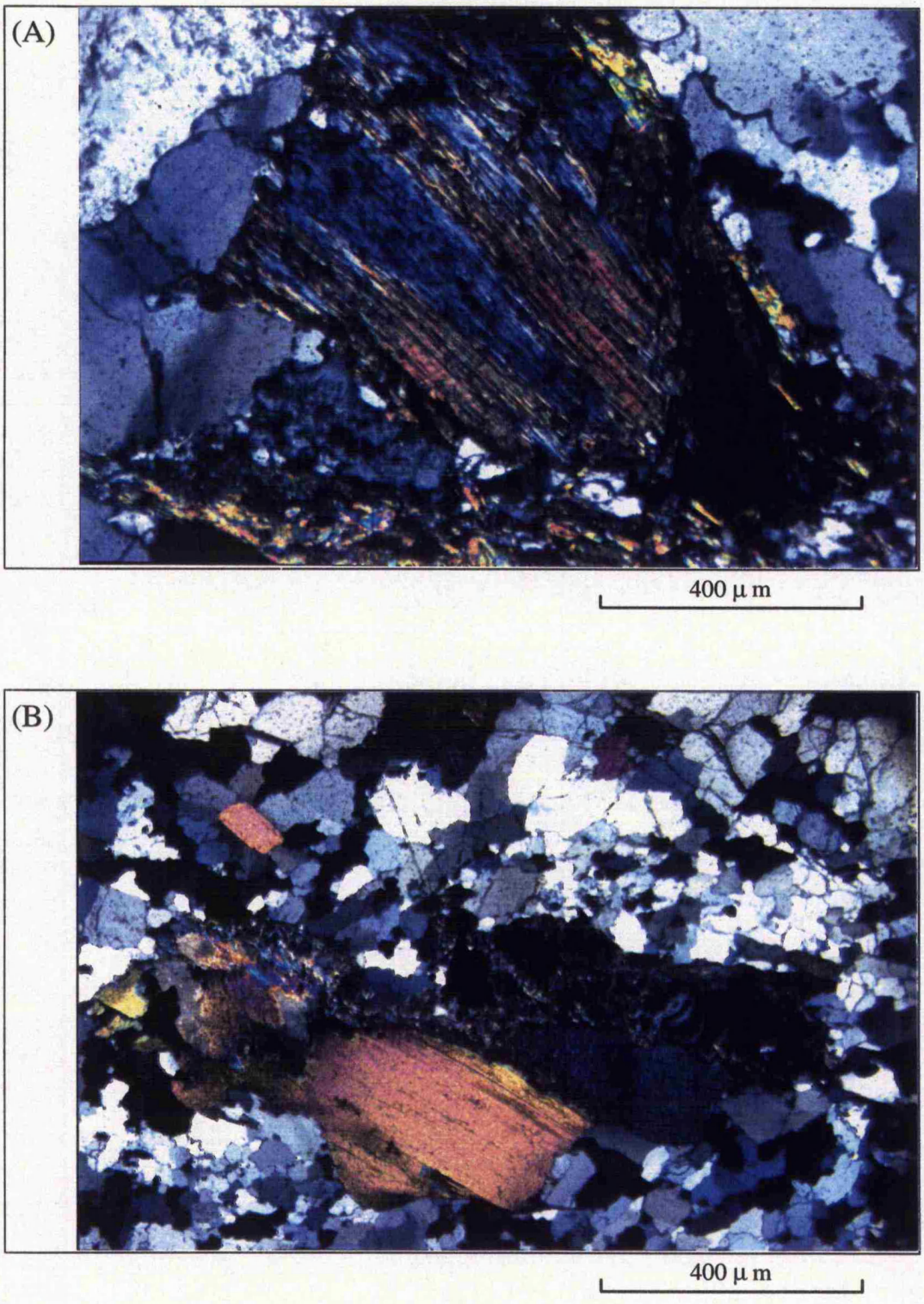

Fig. 4.10: Photomicrographs (crossed nicols): **(A)** Biotite is replaced by chlorite in leucogranite **(B)** Kaolin grain (black) having relics of biotite.

Sulphide phases include sphalerite, pyrite, arsenopyrite and galena. These silicate phases and oxides were analysed in each of the studied polished thin sections for major and minor oxides such as SiO_2, TiO_2, Al_2O_3, FeO (total), MnO, MgO, CaO, Na_2O, K_2O, Cr_2O_3 and NiO. Scheelite was analysed by a program, consisting of CaO, WO_3, MoO_2, SnO_2, FeO (total), MnO, MgO, Y_2O_3, TiO_2, ZrO_2, Nb_2O_5 and Ta_2O_5. Sulphide were analysed for S, Fe, Zn, Pb, Cd, Ge, Ag and As. Details about the method employed for microprobe analysis are presented in Appendix 4.2.

4.4.1 Tourmaline

The statistical data of 278 representative microprobe analyses from 11 samples of the Miniki Gol tourmaline are presented in Table 4.1. Cations per formula unit were calculated on the basis of 31 oxygen atoms and 3B and 4(OH) group assumed so that the actual factor used is 24.5 oxygen atoms. The Si deficiencies in the tetrahedral site are compensated by excessive Al, whereas Al_6 is placed in the Z site. The remaining unassigned Al is accommodated in the Y site.

The tourmalines analysed show a broad range of chemical composition and fall along the schorl-dravite solid solution join (Fig. 4.11 A), covering nearly the entire Fe-Mg range (Table 4.1). The negative correlation between the FeO and MgO corresponds to the schorl-dravite solid solution series (Fig. 4.12 A). TiO_2 in these tourmalines range from 0.01 to 1.69%, reflecting colour variation, with a brown colouration correlating with high Ti content (cf. Deer et al. 1986). High content of Na_2O is noted in the tourmaline of the tourmalinite and leucogranite, whereas tourmaline from schist is relatively alkali-deficient (Table 4.1). Low levels of CaO are recorded both in leucogranite and pegmatite whereas the Al_2O_3 content in the tourmaline of the pegmatite is generally higher than that of the leucogranite. An inverse relationship exist between these two oxides (see Fig. 4.12 B).

All the studied tourmalines contain excess alumina in the Y-site (Table 4.1). The relatively low alumina (Aly) in the tourmaline of the tourmalinites, probably, suggests that some Al may have been utilised in the formation of intergrown spessartine-rich garnet. A negative correlation exist between Fe^{2+} and Aly in the tourmaline of granite, whereas a positive correlation exist between these cations in xenoliths (within the pegmatite) and pegmatite (Fig. 4.12 C, D). A weak positive correlation can also be observed between these two cations in the tourmalinites (Fig. 4.12 E). No relationship is found in the tourmaline of schist (Fig. 4.12 F), suggesting that excessive alumina in the tourmaline of schist is the result of high Al activity in the pelitic rocks. High concentrations of FeO (average 8.54 %) can be noted in the tourmaline of tourmalinites compared with tourmaline in schists (average 7.89 %).

Table 4.1: Microprobe analyses of tourmaline from pegmatite, (ZS 12), leucogranite (ZS 10), xenolith (ZC 23), tourmalinite (ZC 39, ZC 69, ZM 63, ZM 64) and schist (ZC 47, ZC 61, ZC 68 and ZM 27).

Sample	**ZS12**				**ZS10**				**ZC23**			
Analy. Numb.	Mean (51)[2]	Sd[1]	Min	Max	Mean (29)	Sd	Min	Max	Mean (7)	Sd	Min	Max
SiO_2	36.12	0.19	35.51	36.47	36.20	0.16	35.83	36.59	36.21	0.43	35.71	36.77
TiO_2	0.34	0.10	0.12	0.59	0.75	0.14	0.48	1.09	0.31	0.37	0.01	0.75
Al_2O_3	34.01	0.25	33.30	34.54	32.32	1.12	30.86	33.64	33.51	1.25	31.65	34.57
Cr_2O_3	0.02	0.02	0.00	0.04	0.02	0.01	0.00	0.05	0.03	0.01	0.01	0.04
FeO^{tt}	10.54	0.64	9.85	11.87	7.75	0.83	6.64	9.29	11.49	3.07	6.97	13.89
MnO	0.11	0.03	0.05	0.16	0.06	0.02	0.01	0.11	0.31	0.21	0.02	0.51
MgO	3.25	0.50	2.21	3.76	5.89	0.24	5.58	6.49	2.61	3.18	0.07	7.19
CaO	0.15	0.04	0.05	0.21	0.61	0.18	0.39	0.94	0.18	0.24	0.03	0.61
Na_2O	2.02	0.12	1.72	2.19	2.12	0.06	2.04	2.26	1.82	0.31	1.49	2.23
K_2O	0.04	0.01	0.02	0.06	0.06	0.03	0.02	0.15	0.03	0.02	0.01	0.05
Total	86.60	0.27	85.99	87.14	85.78	0.31	85.06	86.41	86.50	0.29	86.03	86.88
Cations per 24.5 oxygen atoms												
Si	5.947	0.016	5.907	5.981	5.961	0.035	5.900	6.051	5.998	0.013	5.972	6.009
Alt	0.053	0.016	0.019	0.094	0.041	0.031	0.000	0.100	0.006	0.010	0.000	0.028
Alz	6.000	0.000	6.000	6.000	6.000	0.000	6.000	6.000	6.000	0.000	6.000	6.000
Aly	0.546	0.053	0.451	0.672	0.233	0.156	0.011	0.430	0.539	0.314	0.101	0.788
Ti	0.043	0.013	0.015	0.074	0.093	0.017	0.060	0.136	0.038	0.045	0.001	0.092
Cr	0.002	0.002	0.000	0.005	0.002	0.002	0.000	0.007	0.004	0.001	0.001	0.005
Fe^{2+}	1.451	0.092	1.354	1.642	1.068	0.120	0.910	1.288	1.595	0.440	0.954	1.944
Mn	0.015	0.004	0.007	0.023	0.008	0.003	0.001	0.016	0.044	0.030	0.003	0.073
Mg	0.798	0.120	0.545	0.921	1.447	0.064	1.371	1.595	0.637	0.774	0.018	1.753
Ca	0.026	0.007	0.009	0.037	0.107	0.032	0.069	0.167	0.032	0.041	0.005	0.107
Na	0.645	0.037	0.552	0.705	0.678	0.023	0.647	0.724	0.584	0.092	0.481	0.708
K	0.009	0.002	0.004	0.013	0.012	0.006	0.004	0.031	0.007	0.004	0.002	0.011
Total	15.534	0.040	15.442	15.629	15.651	0.068	15.564	15.758	15.482	0.158	15.352	15.700
Feo#	0.764	0.038	0.725	0.843	0.567	0.022	0.538	0.614	0.816	0.224	0.492	0.995

Sample	**ZC39**				**ZC69**				**ZM63**			
Analy. Numb.	Mean (26)	Sd	Min	Max	Mean (8)	Sd	Min	Max	Mean (29)	Sd	Min	Max
SiO_2	36.28	0.36	35.64	37.02	36.52	0.63	35.35	37.36	36.75	0.68	36.09	39.84
TiO_2	0.70	0.19	0.31	1.13	0.65	0.36	0.23	1.14	0.53	0.33	0.10	1.69
Al_2O_3	32.75	0.78	29.83	34.00	31.96	0.32	31.61	32.55	31.78	0.77	29.59	33.16
Cr_2O_3	0.03	0.02	0.01	0.09	0.04	0.02	0.00	0.07	0.06	0.05	0.00	0.24
FeO	9.25	0.60	8.40	10.77	8.47	0.96	6.81	9.41	8.90	1.26	6.39	10.88
MnO	0.04	0.02	0.01	0.08	0.14	0.07	0.06	0.25	0.12	0.06	0.01	0.24
MgO	5.06	0.53	3.20	5.60	5.42	1.07	3.55	7.01	5.47	0.76	4.23	6.65
CaO	0.91	0.18	0.39	1.13	0.63	0.35	0.29	1.20	0.49	0.43	0.10	2.08
Na_2O	1.73	0.14	1.43	1.90	2.16	0.29	1.67	2.43	2.23	0.40	1.60	3.87
K_2O	0.02	0.01	0.00	0.04	0.03	0.01	0.01	0.04	0.02	0.01	0.00	0.04
Total	86.77	0.56	84.51	87.53	86.01	0.26	85.65	86.39	86.35	0.37	85.33	87.01
Cations per 24.5 oxygen atoms												
Si	5.944	0.044	5.872	6.074	6.019	0.083	5.880	6.152	6.044	0.090	5.938	6.464
Alt	0.060	0.035	0.000	0.128	0.023	0.044	0.000	0.120	0.008	0.018	0.000	0.062
Alz	5.998	0.012	5.941	6.000	6.000	0.000	6.000	6.000	5.986	0.064	5.659	6.000
Aly	0.266	0.116	0.000	0.553	0.187	0.067	0.083	0.301	0.167	0.110	0.000	0.381
Ti	0.086	0.024	0.038	0.144	0.080	0.045	0.028	0.143	0.065	0.041	0.013	0.210
Cr	0.004	0.002	0.001	0.012	0.005	0.003	0.000	0.009	0.008	0.006	0.000	0.030
Fe^{2+}	1.268	0.087	1.146	1.486	1.168	0.136	0.935	1.296	1.225	0.180	0.867	1.510
Mn	0.005	0.003	0.001	0.011	0.020	0.009	0.009	0.034	0.016	0.009	0.001	0.033
Mg	1.236	0.128	0.782	1.363	1.331	0.260	0.871	1.715	1.341	0.183	1.049	1.628
Ca	0.160	0.032	0.068	0.199	0.111	0.062	0.051	0.214	0.086	0.074	0.018	0.362
Na	0.550	0.044	0.455	0.602	0.690	0.088	0.537	0.774	0.709	0.126	0.516	1.217
K	0.004	0.003	0.000	0.009	0.005	0.002	0.002	0.009	0.004	0.002	0.000	0.009
Total	15.581	0.069	15.404	15.653	15.638	0.078	15.524	15.736	15.660	0.080	15.467	15.755
Feo#	0.646	0.036	0.602	0.769	0.611	0.073	0.493	0.726	0.617	0.060	0.523	0.692

Table 4.1 (Contd.)

smaple	ZM64				ZC61C[3]				ZC61R[4]			
Analy.	Mean	Sd	Min	Max	Mean	Sd	Min	Max	Mean	SD	Min	Max
Numb.	(54)				(3)				(6)			
SiO_2	36.93	0.43	35.62	38.25	36.35	0.33	36.08	36.71	36.71	1.31	35.66	38.82
TiO_2	0.47	0.23	0.11	1.09	0.49	0.04	0.45	0.52	1.03	0.17	0.74	1.17
Al_2O_3	31.60	0.74	29.69	32.80	32.48	0.73	31.96	33.31	30.39	1.01	29.01	31.65
Cr_2O_3	0.03	0.02	0.00	0.07	0.05	0.02	0.03	0.07	0.05	0.02	0.03	0.08
FeO	7.55	0.93	5.57	9.57	7.14	0.83	6.40	8.04	7.19	0.53	6.73	8.24
MnO	0.07	0.03	0.00	0.15	0.02	0.01	0.02	0.03	0.04	0.02	0.02	0.07
MgO	6.73	0.93	4.88	9.35	5.72	0.16	5.54	5.83	6.70	0.25	6.48	7.09
CaO	0.50	0.37	0.19	2.28	0.36	0.15	0.19	0.47	1.07	0.33	0.51	1.51
Na_2O	2.27	0.26	1.60	2.60	1.98	0.09	1.88	2.06	1.75	0.21	1.40	2.05
K_2O	0.02	0.01	0.00	0.04	0.03	0.01	0.02	0.04	0.07	0.08	0.01	0.22
Total	86.17	0.55	84.25	87.43	84.62	0.37	84.37	85.04	84.99	0.57	84.43	85.98
Cations per 24.5 oxygen atoms												
Si	6.047	0.036	5.970	6.205	6.025	0.056	5.968	6.080	6.088	0.176	5.949	6.372
Alt	0.001	0.005	0.000	0.030	0.011	0.018	0.000	0.032	0.016	0.023	0.000	0.051
Alz	5.978	0.063	5.706	6.000	6.000	0.000	6.000	6.000	5.876	0.161	5.639	6.000
Aly	0.118	0.094	0.000	0.352	0.336	0.115	0.239	0.463	0.052	0.081	0.000	0.172
Ti	0.058	0.029	0.014	0.134	0.060	0.004	0.056	0.065	0.128	0.021	0.093	0.146
Cr	0.004	0.003	0.000	0.009	0.007	0.003	0.004	0.009	0.006	0.003	0.004	0.011
Fe^{2+}	1.034	0.133	0.760	1.334	0.990	0.115	0.885	1.113	0.998	0.072	0.924	1.137
Mn	0.010	0.004	0.000	0.021	0.003	0.001	0.003	0.004	0.006	0.002	0.003	0.010
Mg	1.643	0.220	1.194	2.273	1.414	0.041	1.368	1.446	1.658	0.065	1.586	1.756
Ca	0.087	0.064	0.033	0.398	0.064	0.027	0.033	0.083	0.189	0.058	0.091	0.269
Na	0.722	0.081	0.506	0.823	0.635	0.031	0.603	0.664	0.563	0.071	0.446	0.664
K	0.004	0.002	0.000	0.008	0.006	0.002	0.004	0.009	0.014	0.016	0.002	0.046
Total	15.705	0.071	15.500	15.819	15.551	0.024	15.528	15.575	15.593	0.116	15.364	15.686
Feo#	0.529	0.063	0.373	0.654	0.554	0.034	0.525	0.592	0.517	0.019	0.499	0.553

sample	ZC47C				ZC47R				ZM27			
Analy.	Mean	Sd	Min	Max	Mean	Sd	Min	Max	Mean	Sd	Min	Max
Numb.	(11)				(6)				(20)			
SiO_2	36.15	0.44	35.57	36.78	36.34	0.48	35.81	36.97	36.47	0.41	35.95	37.20
TiO_2	0.83	0.21	0.48	1.15	0.75	0.13	0.54	0.89	0.71	0.27	0.32	1.33
Al_2O_3	31.56	1.89	26.60	33.16	32.79	0.40	32.08	33.29	32.52	0.80	30.91	33.61
Cr_2O_3	0.08	0.10	0.02	0.37	0.05	0.01	0.03	0.06	0.05	0.03	0.00	0.12
FeO	9.10	1.26	7.50	10.93	7.90	0.81	6.92	9.04	8.05	0.33	7.61	8.98
MnO	0.08	0.09	0.02	0.27	0.02	0.01	0.00	0.03	0.03	0.01	0.01	0.06
MgO	5.54	1.34	4.42	9.23	5.65	0.48	5.02	6.31	5.60	0.29	5.12	6.05
CaO	0.73	0.77	0.10	2.79	0.73	0.42	0.14	1.20	0.57	0.19	0.29	0.87
Na_2O	1.90	0.41	1.41	2.53	1.66	0.14	1.50	1.89	1.80	0.13	1.57	1.98
K_2O	0.04	0.02	0.01	0.07	0.03	0.01	0.01	0.04	0.02	0.01	0.00	0.03
Total	85.99	0.31	85.50	86.41	85.91	0.34	85.48	86.44	85.82	0.42	85.08	86.59
Cations per 24.5 oxygen atoms												
Si	5.983	0.051	5.906	6.040	5.963	0.071	5.906	6.073	5.994	0.033	5.934	6.044
Alt	0.031	0.037	0.000	0.095	0.054	0.044	0.000	0.095	0.017	0.021	0.000	0.066
Alz	5.934	0.218	5.277	6.000	6.000	0.000	6.000	6.000	6.000	0.000	6.000	6.000
Aly	0.189	0.150	0.000	0.432	0.287	0.054	0.211	0.361	0.283	0.123	0.044	0.438
Ti	0.104	0.027	0.060	0.145	0.092	0.016	0.067	0.110	0.088	0.034	0.039	0.166
Cr	0.010	0.013	0.003	0.049	0.006	0.002	0.004	0.008	0.006	0.004	0.000	0.016
Fe^{2+}	1.260	0.183	1.034	1.524	1.084	0.109	0.948	1.237	1.107	0.050	1.055	1.246
Mn	0.011	0.013	0.003	0.038	0.003	0.002	0.000	0.004	0.004	0.002	0.001	0.009
Mg	1.368	0.340	1.084	2.316	1.383	0.119	1.224	1.540	1.372	0.078	1.248	1.489
Ca	0.129	0.139	0.018	0.503	0.129	0.075	0.025	0.212	0.100	0.035	0.050	0.154
Na	0.611	0.134	0.461	0.822	0.529	0.045	0.479	0.602	0.575	0.044	0.496	0.631
K	0.008	0.005	0.002	0.015	0.005	0.002	0.002	0.009	0.004	0.002	0.000	0.006
Total	15.637	0.153	15.447	15.954	15.533	0.031	15.496	15.576	15.551	0.068	15.438	15.636
Feo#	0.622	0.070	0.484	0.702	0.582	0.045	0.523	0.643	0.590	0.018	0.566	0.619

Table 4.1 (Contd.)

Sample	ZC68			
Analy.	Mean	Sd	Min	Max
Numb.	(31)			
SiO_2	36.22	0.28	35.76	36.67
TiO_2	0.62	0.24	0.18	1.14
Al_2O_3	33.05	0.95	30.44	34.65
Cr_2O_3	0.04	0.03	0.00	0.10
FeO	8.01	1.01	5.13	9.19
MnO	0.03	0.02	0.00	0.07
MgO	5.20	1.06	3.92	9.15
CaO	0.56	0.29	0.08	1.40
Na_2O	1.61	0.20	1.26	2.01
K_2O	0.02	0.01	0.00	0.06
Total	85.35	0.26	84.73	85.76
Cations per 24.5 oxygen atoms				
Si	5.975	0.030	5.930	6.042
Alt	0.029	0.025	0.000	0.070
Alz	5.996	0.022	5.878	6.000
Aly	0.401	0.168	0.000	0.692
Ti	0.078	0.031	0.023	0.142
Cr	0.005	0.003	0.000	0.013
Fe^{2+}	1.105	0.141	0.705	1.271
Mn	0.005	0.003	0.000	0.010
Mg	1.277	0.259	0.966	2.239
Ca	0.099	0.051	0.014	0.246
Na	0.515	0.065	0.401	0.645
K	0.004	0.003	0.000	0.013
Total	15.488	0.108	15.318	15.800
Feo#	0.607	0.075	0.359	0.701

*Total iron as FeO; [1]Standard deviation; [2] Number of analyses; [3]Core; [4]Rim; FeO# = FeO / (FeO + MgO).
Detection limits for the analysed oxides are tabulated in Appendix 4.2.

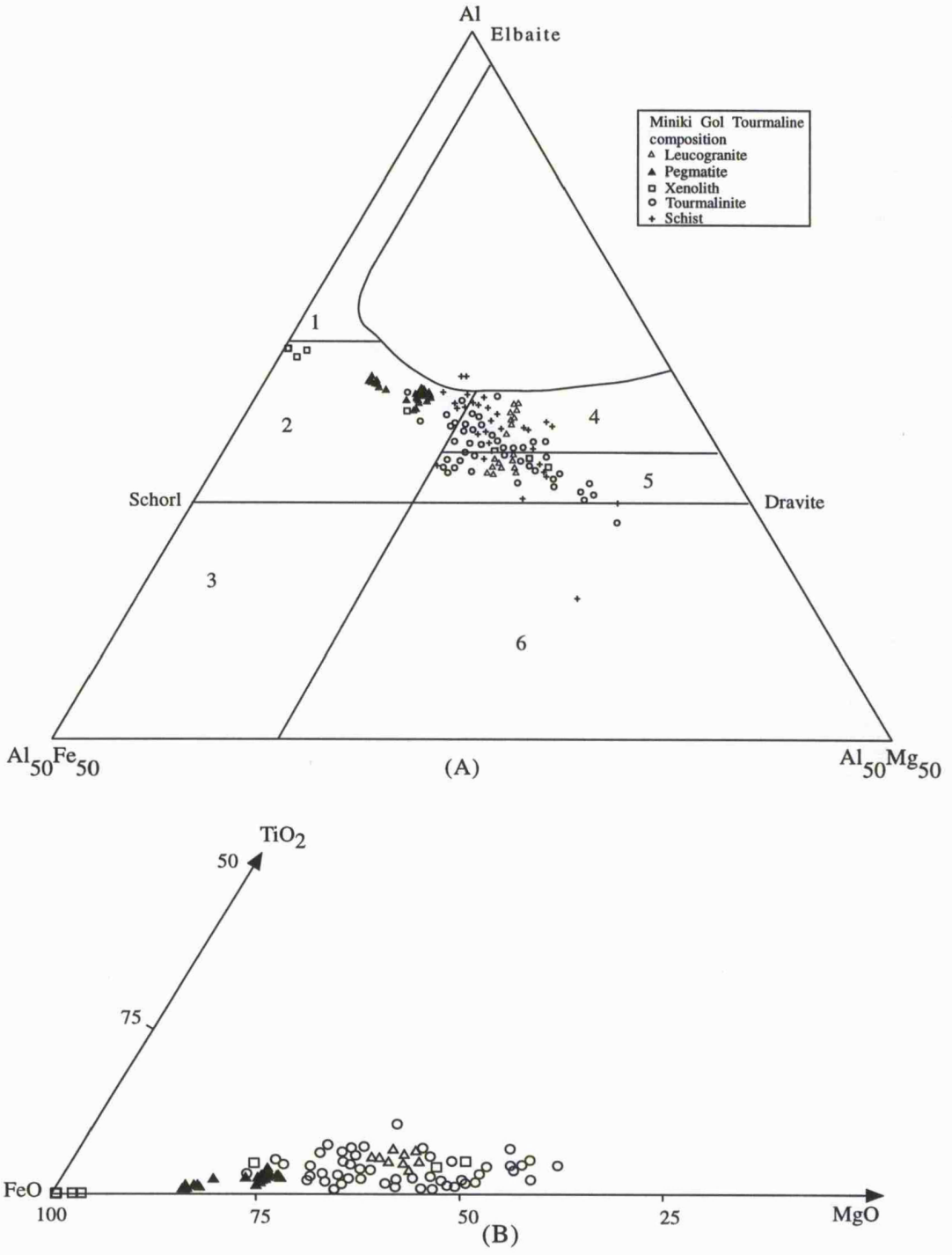

Fig. 4.11: Miniki Gol tourmaline compositions in terms of oxides and cations: **(A)** Cations proportions of Al, Fe (total) and Mg superimposed on the compositional fields (1-6) of Henry & Guidotti (1985); (1) Li-rich granitoid pegmatites and aplites (2) Li-poor granitoids and their associated pegmatites and aplites (3) Fe^{3+}-rich quartz-tourmaline rocks (Hydrothermally altered granites) (4) Metapelites coexisting with Al-saturating phase (5) Metapelites not coexisting with Al-saturating phase (6) Fe^{3+}-rich quartz-tourmaline rocks, calc-silicate rocks and metapelites. **(B)** TiO_2-MgO-FeO plot of tourmaline indicating iron enrichment trend. Symbols as shown in **(Fig. A)**. (Data from Table 4.1).

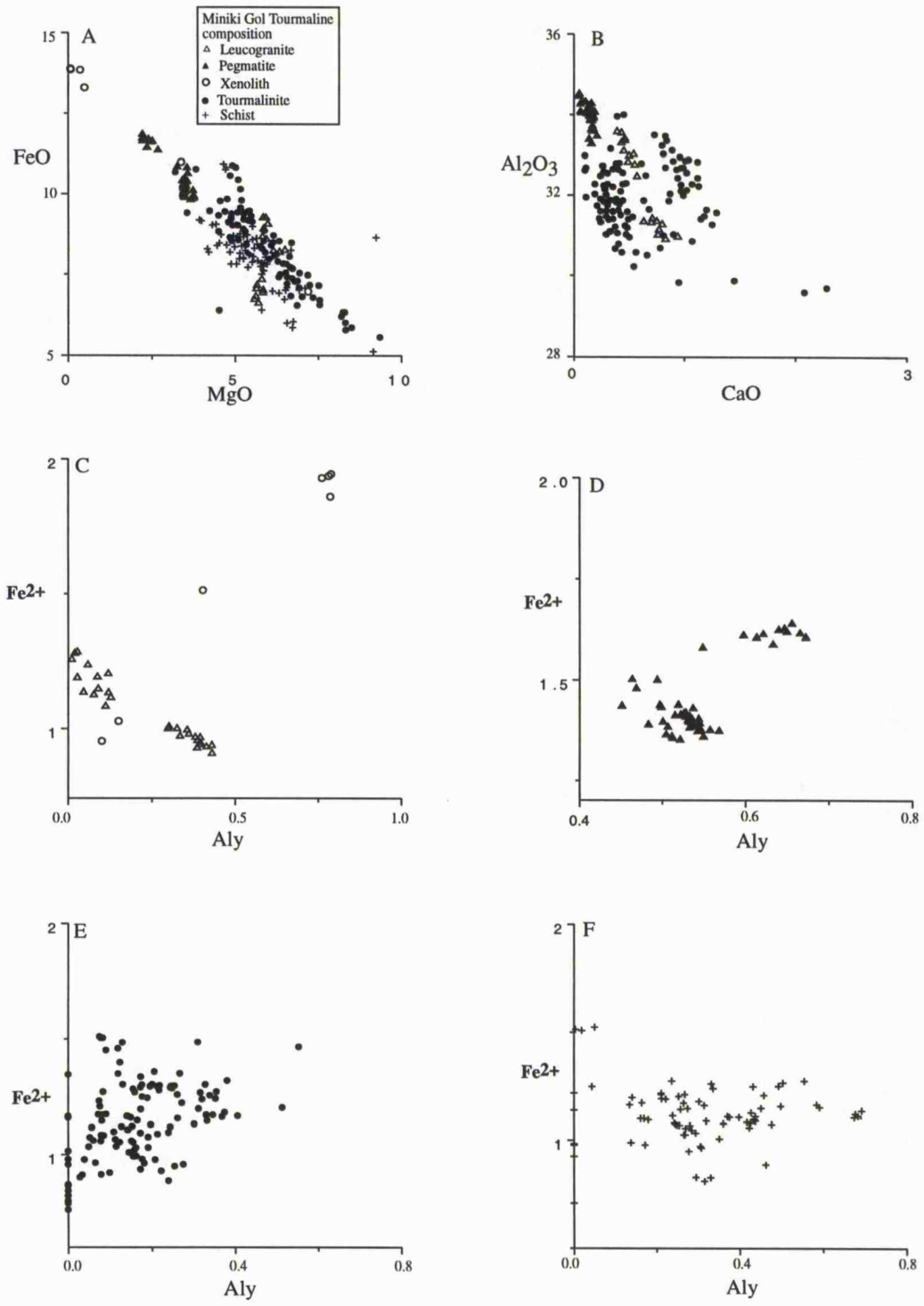

Fig. 4.12: Miniki Gol tourmaline compositions expressed as oxides and cations **(A)** FeO versus MgO **(B)** CaO versus Al_2O_3 **(C, D, E and F)** Fe^{2+} versus Aly. Symbols shown as in **(Fig. A)**. Data are taken from (Table 4.1).

Tourmaline in the schist, located further away from granite intrusion, contains even lower FeO (average 7.16 e.g. ZC 61, Table 4.1).

Irregular zoning is observed in the tourmaline of the garnet mica schist with marginal depletion of FeO and marginal enrichment of Al_2O_3 (see ZC 47, Table 4.1). Whereas enrichment of Al_2O_3 and depletion of MgO at the core are also noticed (ZC61). Plotting the data on the Al-Fe-Mg diagram of Henry and Guidotti (1985), tourmaline analyses from schist, leucogranite and tourmalinites fall in the field of metapelites. Some analyses from schist and tourmalinites plot (Fig. 4.11 A) in the field defined for granite by Henry and Guidotti (1985). Tourmalines in the study area clearly show an iron-enrichment trend from leucogranite to pegmatite on the TiO_2-FeO-MgO triangular diagram (Fig. 4.11 B). This trend is also observed in the tourmaline of xenolith and tourmalinite (Fig. 4.11 B).

It is worth mentioning that the tourmaline from Miniki Gol leucogranite plot within the field of metapelites coexisting and not-coexisting with Al-saturating phase (field 4 and 5, Fig. 4.11 A) of the Al-Fe-Mg diagram of the Henry and Guidotti (1985). This composition is markedly different from the Fe-rich schorl, which is considered as typical tourmaline related to felsic plutonic rocks (see Slack 1982). The composition (schorl-dravite) of the tourmaline from leucogranite could be considered as xenocrysts contaminated from wall rock or alternatively indicates the pelitic character of leucogranite. The plotting of the tourmaline from Miniki Gol leucogranite within the field of metapelites has also straddled the limits of fields drawn by Henry and Guidotti (1985). On the basis of these fields drawn by Henry and Guidotti (1985), it is difficult to differentiate among granitic, metapelitic and hydrothermal tourmalines.

4.4.2 Clinozoisite

Epidote and clinozoisite are the Fe-rich and Fe-poor members respectively of the epidote group. Clinozoisite in the study area occurs mainly in the calc-silicate quartzite and is very rare in mica quartzite. In addition, clinozoisite is totally absent in the mica schist at Miniki Gol area, although few grains of epidote were identified in the chlorite-rich schist at Besti Gol area (e.g. ZM 105, ZM 106, Table 4.2). Few grains of epidote are also found in the calc-silicate quartzite within and adjacent the cross-cutting-chlorite vein (ZC 27, Table 4.2), but these epidote grains clearly postdate the early-formed clinozoisite.

Representative microprobe analyses of the clinozoisite and epidote are presented in Table 4.2 considering total Fe as Fe_2O_3. Clinozoisite from the investigated area can be grouped into Fe-poor (1.1 to 3 wt % Fe_2O_3), intermediate-Fe (4 to 5 wt %) and Fe-rich (6 to 7.6 wt %). Clinozoisite grains, which are intergrown with the scheelite, are mostly Fe-

Table 4.2: Representative chemical compositions of studied clinozoisite and epidote from scheelite-bearing calc-silicate quartzite (ZC 43, ZC 65 A-B, ZC 67), **barren calc-silicate quartzite** (ZC 27 and ZC 49) **and Besti Gol greenschist** (ZM 105 and ZM 106).

Sample	ZC43	ZC43	ZC43	ZC43	ZC43	ZC43	ZC43	ZC43	ZC49	ZC49	ZC65	ZC65
Posit.	C	R	C	R	C	R	C	R	C	R	C	M
SiO_2	40.07	39.49	39.63	39.33	39.06	39.14	38.99	38.48	39.53	39.26	39.68	39.42
TiO_2	0.05	0.07	0.02	0.02	0.33	0.30	0.05	0.08	0.14	0.14	0.17	0.14
Al_2O_3	31.66	32.26	32.37	31.97	29.71	29.58	30.00	29.75	28.99	28.47	29.14	28.4
Cr_2O_3	0.01	0.04	0.03	0.01	0.01	0.01	0.01	0.04	0.06	0.04	0.02	0.04
Fe_2O_3*	1.49	1.30	1.12	1.37	3.63	3.79	3.68	3.45	5.66	5.88	5.11	6.19
MnO	0.02	0.03	0.03	0.02	0.10	0.13	0.23	0.32	0.17	0.13	0.23	0.11
MgO	0.02	0.01	0.01	0.01	0.05	0.06	0.05	0.09	0.03	0.02	0.06	0.02
CaO	24.79	24.9	24.91	24.94	24.52	24.2	23.97	23.86	24.34	24.13	24.07	24.09
Na_2O	0.01	0.01	0.02	0.01	0.02	0.02	0.02	0.01	0.01	0.13	0.03	0.02
K_2O	0.01	0.01	0.01	0.01	0.01	0.02	0.01	0.01	0.00	0.02	0.01	0.01
NiO	0.02	0.02	0.01	0.02	0.03	0.02	0.02	0.02	0.02	0.00	0.02	0.02
Total	98.15	98.14	98.16	97.71	97.47	97.27	97.03	96.11	98.95	98.22	98.54	98.46
Cations per 25 oxygen atoms												
Si	6.161	6.019	6.032	6.026	6.077	6.101	6.085	6.065	6.114	6.128	6.140	6.142
Ti	0.006	0.008	0.002	0.002	0.039	0.035	0.006	0.009	0.016	0.016	0.020	0.016
Al	5.668	5.796	5.807	5.774	5.449	5.435	5.519	5.527	5.285	5.238	5.315	5.215
Cr	0.001	0.005	0.004	0.001	0.001	0.001	0.001	0.005	0.007	0.005	0.002	0.005
Fe^{3+}	0.187	0.166	0.143	0.176	0.472	0.494	0.480	0.455	0.732	0.768	0.661	0.807
Mn	0.003	0.004	0.004	0.003	0.013	0.017	0.030	0.043	0.022	0.017	0.030	0.015
Mg	0.004	0.002	0.002	0.002	0.012	0.014	0.012	0.021	0.007	0.005	0.014	0.005
Ca	4.063	4.067	4.062	4.095	4.088	4.042	4.009	4.030	4.034	4.036	3.991	4.022
Na	0.003	0.003	0.006	0.003	0.006	0.006	0.006	0.003	0.003	0.039	0.009	0.006
K	0.002	0.002	0.002	0.002	0.002	0.004	0.002	0.002	0.000	0.004	0.002	0.002
Ni	0.002	0.002	0.001	0.002	0.004	0.003	0.003	0.003	0.002	0.000	0.002	0.003
Total	16.103	16.074	16.065	16.086	16.163	16.152	16.153	16.163	16.222	16.256	16.186	16.238
Ps	3.19	2.78	2.40	2.96	7.97	8.33	8.00	7.61	12.17	12.79	11.06	13.40

Sample	ZC65	ZC65	ZC65	ZC65	ZC65	ZC65	ZC65A	ZC65A	ZC65A	ZC65A	ZC65A	ZC65A
Posit.	C	R	C	R	C	R	C	R	C	R	M	R
SiO_2	39.79	39.18	39.22	39.06	39.43	39.62	39.25	39.00	39.34	39.11	38.84	39.08
TiO_2	0.20	0.17	0.16	0.17	0.19	0.09	0.08	0.09	0.13	0.13	0.04	0.01
Al_2O_3	29.34	28.67	28.06	29.04	29.16	29.35	28.3	28.48	28.33	28.05	28.45	28.16
Cr_2O_3	0.03	0.04	0.03	0.04	0.04	0.01	0.02	0.04	0.01	0.00	0.03	0.01
Fe_2O_3*	5.22	5.46	6.50	5.28	5.21	4.93	5.38	5.17	5.49	5.53	5.26	5.44
MnO	0.26	0.24	0.08	0.27	0.26	0.23	0.14	0.09	0.14	0.06	0.14	0.13
MgO	0.05	0.08	0.03	0.02	0.06	0.06	0.04	0.03	0.06	0.04	0.06	0.04
CaO	24.24	24.05	24.15	24.27	24.3	24.37	23.77	23.95	23.64	23.62	23.88	23.67
Na_2O	0.01	0.32	0.04	0.05	0.03	0.00	0.01	0.01	0.00	0.03	0.02	0.01
K_2O	0.02	0.03	0.02	0.01	0.00	0.00	0.00	0.03	0.02	0.01	0.03	0.02
NiO	0.00	0.02	0.00	0.01	0.02	0.02	0.00	0.02	0.04	0.03	0.01	0.01
Total	99.16	98.26	98.29	98.22	98.70	98.68	96.99	96.91	97.20	96.61	96.76	96.58
Cations per 25 oxygen atoms												
Si	6.124	6.108	6.136	6.084	6.104	6.121	6.178	6.144	6.180	6.184	6.133	6.180
Ti	0.023	0.020	0.019	0.020	0.022	0.010	0.009	0.011	0.015	0.015	0.005	0.001
Al	5.322	5.268	5.174	5.331	5.321	5.345	5.250	5.289	5.245	5.228	5.295	5.249
Cr	0.004	0.005	0.004	0.005	0.005	0.001	0.002	0.005	0.001	0.000	0.004	0.001
Fe^{3+}	0.672	0.712	0.850	0.688	0.675	0.637	0.708	0.681	0.721	0.731	0.695	0.719
Mn	0.034	0.032	0.011	0.036	0.034	0.030	0.019	0.012	0.019	0.008	0.019	0.017
Mg	0.011	0.019	0.007	0.005	0.014	0.014	0.009	0.007	0.014	0.009	0.014	0.009
Ca	3.997	4.018	4.048	4.050	4.031	4.034	4.009	4.043	3.979	4.002	4.041	4.011
Na	0.003	0.097	0.012	0.015	0.009	0.000	0.003	0.003	0.000	0.009	0.006	0.003
K	0.004	0.006	0.004	0.002	0.000	0.000	0.000	0.006	0.004	0.002	0.006	0.004
Ni	0.000	0.003	0.000	0.001	0.002	0.002	0.000	0.003	0.005	0.004	0.001	0.001
Total	16.194	16.288	16.265	16.237	16.217	16.194	16.187	16.204	16.183	16.192	16.219	16.195
Ps	11.21	11.91	14.11	11.43	11.26	10.65	11.88	11.41	12.09	12.27	11.6	12.05

Table 4.2 (contd.)

Sample	ZC65B	ZC65B	ZC65B	ZC65B	ZC67	ZC67	ZC67	ZC67	ZC67	ZC67	ZC27	ZC27
Posit.	C	R	C	R	C	R	C	R	C	R	C	R
SiO_2	39.32	39.69	39.70	39.29	40.17	39.73	39.65	39.85	40.39	39.52	39.38	39.42
TiO_2	0.06	0.06	0.10	0.11	0.06	0.13	0.05	0.00	0.31	0.04	0.16	0.21
Al_2O_3	28.22	29.2	28.91	28.76	29.49	29.50	29.87	30.54	29.27	29.37	27.5	27.17
Cr_2O_3	0.01	0.03	0.02	0.04	0.00	0.03	0.03	0.02	0.04	0.01	0.05	0.02
Fe_2O_3*	6.67	5.83	5.44	6.05	5.05	5.58	4.95	4.30	5.25	5.12	7.43	7.61
MnO	0.05	0.10	0.12	0.14	0.10	0.12	0.13	0.13	0.18	0.15	0.16	0.10
MgO	0.01	0.02	0.02	0.03	0.01	0.02	0.02	0.02	0.04	0.01	0.03	0.03
CaO	24.29	24.47	24.12	24.39	24.65	24.44	24.37	24.64	23.49	24.02	23.95	23.93
Na_2O	0.01	0.01	0.00	0.00	0.00	0.01	0.02	0.02	0.35	0.00	0.00	0.00
K_2O	0.01	0.00	0.01	0.01	0.01	0.01	0.01	0.02	0.01	0.01	0.01	0.01
NiO	0.04	0.02	0.05	0.03	0.05	0.05	0.04	0.01	0.02	0.03	0.02	0.02
Total	98.69	99.43	98.49	98.85	99.59	99.62	99.14	99.55	99.35	98.28	98.69	98.52
Cations per 25 oxygen atoms												
Si	6.130	6.111	6.155	6.100	6.148	6.098	6.094	6.078	6.188	6.128	6.162	6.184
Ti	0.007	0.007	0.012	0.013	0.007	0.015	0.006	0.000	0.036	0.005	0.019	0.025
Al	5.186	5.299	5.283	5.263	5.32	5.337	5.411	5.491	5.286	5.368	5.072	5.024
Cr	0.001	0.004	0.002	0.005	0.000	0.004	0.004	0.002	0.005	0.001	0.006	0.002
Fe^{3+}	0.870	0.751	0.705	0.786	0.646	0.716	0.636	0.549	0.673	0.664	0.972	0.998
Mn	0.007	0.013	0.016	0.018	0.013	0.016	0.017	0.017	0.023	0.02	0.021	0.013
Mg	0.002	0.005	0.005	0.007	0.002	0.005	0.005	0.005	0.009	0.002	0.007	0.007
Ca	4.058	4.037	4.007	4.057	4.042	4.019	4.013	4.027	3.856	3.991	4.016	4.022
Na	0.003	0.003	0.000	0.000	0.000	0.003	0.006	0.006	0.104	0.000	0.000	0.000
K	0.002	0.000	0.002	0.002	0.002	0.002	0.002	0.004	0.002	0.002	0.002	0.002
Ni	0.005	0.002	0.006	0.004	0.006	0.006	0.005	0.001	0.002	0.004	0.003	0.003
Total	16.271	16.232	16.193	16.255	16.186	16.221	16.199	16.180	16.184	16.185	16.28	16.28
Ps	14.37	12.41	11.77	12.99	10.83	11.83	10.52	9.09	11.29	11.01	16.08	16.57

Sample	ZC27	ZC27	ZC27	ZC27	ZC27[e]	ZC27[e]	ZM105[e]	ZM105[e]	ZM105[e]	ZM106[e]	ZM106[e]	ZM106[e]
Posit.	V	V	C	R	M	R	C	C	C	C	C	C
SiO_2	39.52	39.45	39.12	38.73	37.98	38.59	37.52	37.77	37.77	37.67	37.69	37.80
TiO_2	0.23	0.26	0.06	0.10	0.13	0.20	0.35	0.56	0.20	0.08	0.10	0.10
Al_2O_3	27.59	27.4	28.72	27.85	26.79	27.17	22.95	22.59	23.26	23.5	23.35	23.57
Cr_2O_3	0.01	0.08	0.04	0.02	0.02	0.04	0.05	0.04	0.07	0.01	0.00	0.04
Fe_2O_3*	7.33	7.56	5.80	6.73	10.64	9.27	10.13	11.95	11.45	11.79	11.93	11.7
MnO	0.18	0.08	0.15	0.25	0.14	0.12	0.15	0.23	0.24	0.32	0.39	0.35
MgO	0.02	0.04	0.01	0.02	1.14	0.52	1.41	0.01	1.93	0.02	0.02	0.04
CaO	23.79	24.02	24.38	23.66	21.16	22.79	20.38	23.77	20.65	23.48	23.27	23.29
Na_2O	0.01	0.00	0.00	0.01	0.00	0.01	1.31	0.00	0.05	0.01	0.01	0.02
K_2O	0.01	0.02	0.01	0.01	0.00	0.00	1.98	0.03	1.49	0.01	0.00	0.01
NiO	0.02	0.02	0.03	0.02	0.02	0.02	0.01	0.01	0.02	0.02	0.04	0.02
Total	98.71	98.93	98.32	97.4	98.02	98.73	96.24	96.96	97.13	96.91	96.8	96.94
Cations per 25 oxygen atoms												
Si	6.174	6.162	6.101	6.123	6.050	6.081	6.175	6.209	6.178	6.181	6.194	6.192
Ti	0.027	0.031	0.007	0.012	0.016	0.024	0.042	0.069	0.025	0.010	0.012	0.012
Al	5.081	5.045	5.279	5.190	5.030	5.047	4.450	4.377	4.484	4.545	4.523	4.551
Cr	0.001	0.01	0.005	0.003	0.003	0.005	0.006	0.005	0.009	0.001	0.000	0.005
Fe^{3+}	0.958	0.988	0.756	0.890	1.417	1.222	1.346	1.643	1.566	1.618	1.64	1.603
Mn	0.024	0.011	0.020	0.033	0.019	0.016	0.020	0.032	0.033	0.044	0.054	0.049
Mg	0.005	0.009	0.002	0.005	0.271	0.122	0.334	0.002	0.471	0.005	0.005	0.010
Ca	3.983	4.02	4.074	4.008	3.611	3.848	3.551	4.187	3.619	4.128	4.098	4.088
Na	0.003	0.000	0.000	0.003	0.000	0.003	0.404	0.000	0.016	0.003	0.003	0.006
K	0.002	0.004	0.002	0.002	0.000	0.000	0.401	0.006	0.311	0.002	0.000	0.002
Ni	0.003	0.003	0.004	0.003	0.003	0.003	0.001	0.001	0.003	0.003	0.005	0.003
Total	16.261	16.283	16.250	16.272	16.420	16.371	16.730	16.531	16.715	16.540	16.534	16.521
Ps	15.86	16.38	12.53	14.64	21.98	19.49	23.22	27.29	25.88	26.25	26.61	26.05

C = Core; M = Middle; R = Rim; V = Vein; Ps = (100 Fe^{3+}/ (Fe^{3+} + Al); * = Total iron as Fe_2O_3; e = Epidote
N. B. The underline indicates the various positions within the single grain. Detection limits for the analysed oxides are tabulated in Appendix 4.2.

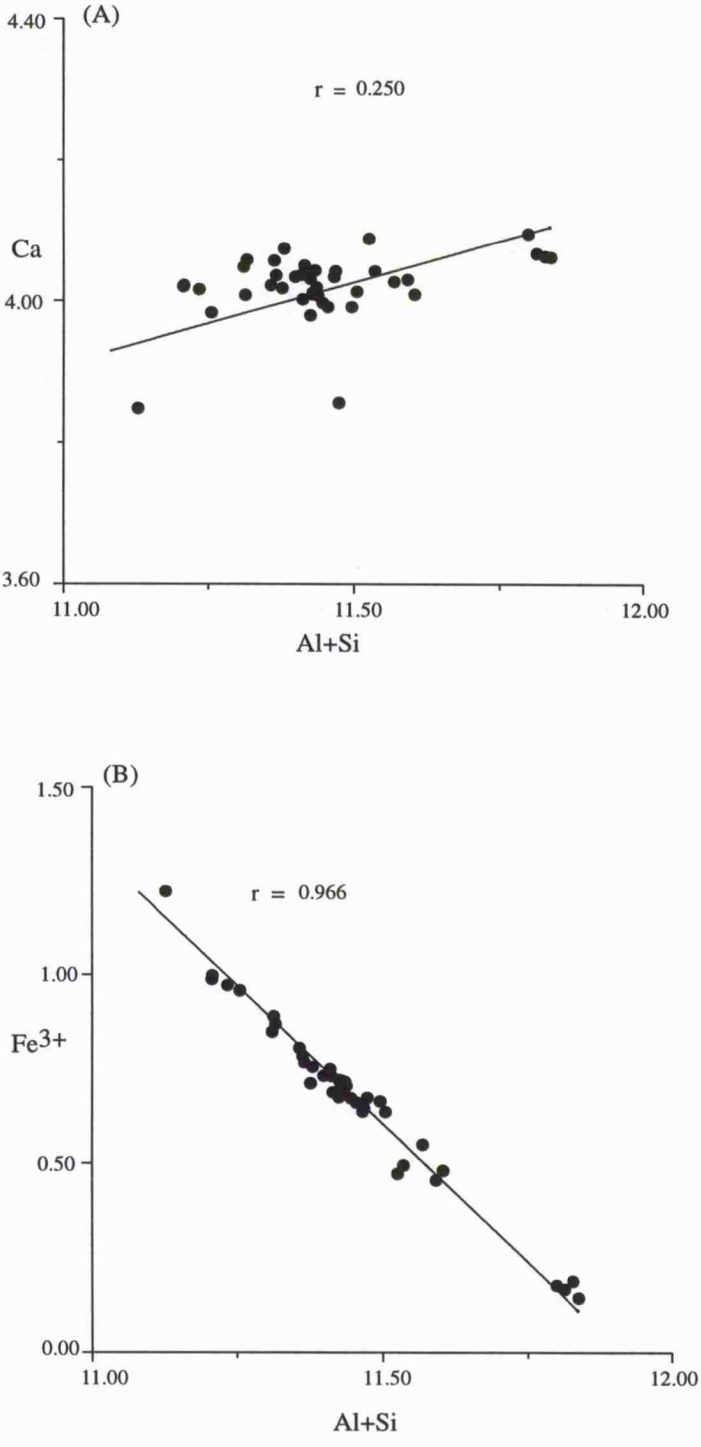

Fig. 4.13: Relationship of cations Si+Al with **(A)** Ca and **(B)** Fe^{3+} in the analysed clinozoisite (Data from Table 4.2)

poor and intermediate-Fe, containing 1.1 to 5 wt % Fe_2O_3 (ZC 65A-B, ZC 67, ZC 43). Cations, such as Si and Al show an inverse relationship with Fe^{3+} and a positive correlation with Ca in the clinozoisite (Fig. 4.13 A-B). Almost 40 % of the grains of clinozoisite show marginal enrichment of Fe_2O_3 within the single crystal, however, most of them exhibit an opposite relationship (Table 4.2). The marginal enrichment of Fe_2O_3 within the clinozoisite grains represent a later phase of retrogressive metamorphism (Miyashiro 1973). Such a compositional zoning is also reported from the epidote of the ancient geothermal systems (Shikazono 1984), from magmatic epidote and many skarns (Farrow and Barr 1992; Deer et al. 1986). The conversion of low-Fe clinozoisite to high-Fe clinozoisite (i.e. increase in Fe content) also correlates with the retrogressive environment (see Chalokwu and Kuehner 1992; Deer et al. 1986).

The pistacite content (100 Fe^{3+} / (Fe^{3+} + Al) of the clinozoisite ranges from 2.95 to 16 (Table 4.2), and is compatible with the epidote formed by alteration of plagioclase (Tulloch 1979). In contrast, the pistacite content (Ps) of epidote from chlorite-rich schist at Besti Gol ranges from 23.22 to 27.29 (see ZM 105-106, Table 4.2), and is considered as typical Ps for a schist (Deer et al. 1986).

4.4.3 Garnet

Garnet occurs in the mica schist as almandine whereas in leucogranite, pegmatite and tourmalinite it is spessartine-rich almandine. Garnet is rare in the calc-silicate quartzite, although grossular garnet was found in one sample. About 400 microprobe spot analyses of garnet from 16 samples (garnet mica schist, calc-silicate quartzite, tourmalinite and leucogranite) were made, from which 120 representative analyses are presented in the Table 4.3.

All the Fe is recorded as FeO so that the andradite end member does not appear. The MnO content in the almandine garnet from the studied schist ranges from 1.2 to 11.81 wt % with an average of 6.31 wt % (standard deviation 3.35). Almandine garnet in the Miniki Gol granite and tourmalinite is relatively rich in spessartine with up to 38.7 mole % and 36 mole % respectively.

Compositional zoning is observed in the garnet of both mica schist and tourmalinite in contrast to the lack of specific zoning pattern in the garnet from leucogranite. CaO, generally decreases from core to margin in the schist (except ZM 27, ZC 46), whereas it, significantly increases from core to margin in the garnet of tourmalinite (see Table 4.3). Samples ZM 27, ZC 46 are located within the Miniki Gol valley near the marble unit and seem to be affected by the calcium metasomatism. The grossular content in the garnet of the leucogranite and, to a certain extent, in the schist is very low.

Table 4.3: Representative compositions of garnets from Miniki Gol area.

sample	ZC9	ZC9	ZC9	ZC9	ZC9	ZC9	ZC9	ZC9	ZC11	ZC11	ZC11	ZC11
Posit.	C	C	C	C	C	R	R	R	C	R	C	R
SiO_2	37.98	37.64	37.57	37.84	37.47	37.66	37.94	37.66	37.40	37.69	37.83	37.88
TiO_2	0.03	0.00	0.00	0.01	0.01	0.01	0.00	0.01	0.03	0.01	0.11	0.03
Al_2O_3	21.57	21.61	21.60	21.56	21.66	21.41	21.44	21.44	21.20	21.58	21.35	21.54
Cr_2O_3	0.03	0.03	0.01	0.03	0.03	0.03	0.05	0.03	0.00	0.05	0.04	0.00
FeO*	36.09	36.56	36.69	36.57	36.25	36.93	36.74	36.83	27.69	29.01	23.19	29.00
MnO	1.21	1.32	1.27	1.20	1.28	1.22	1.28	1.38	6.88	7.03	11.81	7.36
MgO	2.09	1.96	2.11	1.97	2.03	2.04	2.14	2.16	2.75	2.45	1.92	2.35
CaO	1.85	1.40	1.27	1.71	1.70	1.42	1.33	1.78	3.78	2.75	4.43	2.67
Na_2O	0.00	0.01	0.00	0.03	0.01	0.02	0.02	0.02	0.01	0.02	0.02	0.01
K_2O	0.00	0.02	0.01	0.00	0.01	0.04	0.00	0.01	0.01	0.01	0.01	0.01
Total	100.87	100.55	100.55	100.93	100.46	100.81	100.96	101.34	99.75	100.62	100.72	100.85
Cations per 24 oxygen atoms												
Si	6.057	6.036	6.026	6.044	6.012	6.035	6.058	6.009	6.005	6.012	6.026	6.030
Ti	0.004	0.000	0.000	0.001	0.001	0.001	0.000	0.001	0.004	0.001	0.013	0.004
Al	4.054	4.085	4.084	4.059	4.097	4.044	4.035	4.032	4.012	4.057	4.009	4.042
Cr	0.004	0.004	0.001	0.004	0.004	0.004	0.007	0.004	0.000	0.006	0.005	0.000
Fe^{2+}	4.813	4.904	4.922	4.885	4.865	4.949	4.907	4.914	3.718	3.870	3.089	3.861
Mn	0.163	0.180	0.173	0.162	0.174	0.165	0.173	0.186	0.936	0.950	1.594	0.992
Mg	0.497	0.468	0.505	0.469	0.486	0.488	0.510	0.514	0.658	0.583	0.456	0.558
Ca	0.316	0.241	0.218	0.293	0.292	0.244	0.228	0.304	0.650	0.470	0.756	0.455
Na	0.000	0.003	0.000	0.010	0.003	0.006	0.006	0.006	0.003	0.006	0.006	0.003
K	0.000	0.004	0.002	0.000	0.002	0.009	0.000	0.002	0.002	0.002	0.002	0.002
Total	15.911	15.924	15.933	15.928	15.937	15.947	15.924	15.974	15.988	15.96	15.957	15.947
End-member compositions												
Alm	83.14	84.65	84.60	84.09	83.64	84.66	84.35	83.03	62.36	65.89	52.40	65.82
Pyr	8.59	8.09	8.68	8.08	8.35	8.34	8.76	8.68	11.04	9.93	7.74	9.51
Gross	5.46	4.16	3.75	5.04	5.02	4.17	3.91	5.14	10.90	8.00	12.82	7.76
Spess	2.82	3.10	2.97	2.79	2.99	2.82	2.97	3.15	15.70	16.18	27.04	16.91

sample	ZC11	ZC11	ZC11	ZC11	ZC37	ZC37	ZC46	ZC46	ZC52	ZC52	ZC52	ZC52
Posit.	C	R	C	R	C	R	C	R	C	R	C	R
SiO_2	37.88	38.07	37.60	37.80	37.10	37.22	37.78	37.91	37.03	37.01	37.03	37.14
TiO_2	0.10	0.03	0.08	0.04	0.07	0.04	0.00	0.04	0.03	0.00	0.06	0.01
Al_2O_3	21.32	21.37	21.24	21.57	20.60	20.78	21.49	21.40	20.88	20.90	21.09	20.92
Cr_2O3	0.04	0.04	0.02	0.04	0.04	0.01	0.02	0.01	0.00	0.02	0.03	0.03
FeO*	24.07	28.29	24.89	26.94	25.01	31.35	34.20	29.87	26.12	30.51	26.85	28.15
MnO	11.07	6.82	9.93	7.23	9.16	2.98	2.62	5.23	9.61	4.95	9.26	7.70
MgO	2.22	2.47	2.13	2.17	1.16	1.96	1.81	1.14	1.50	2.14	1.52	1.72
CaO	4.13	3.15	4.23	4.42	5.22	3.59	3.22	5.85	3.01	2.45	3.01	3.07
Na_2O	0.00	0.02	0.05	0.03	0.02	0.01	0.02	0.03	0.04	0.02	0.03	0.03
K_2O	0.01	0.00	0.00	0.02	0.00	0.01	0.00	0.03	0.01	0.01	0.01	0.01
Total	100.85	100.28	100.20	100.28	98.41	97.99	101.18	101.53	98.26	98.01	98.91	98.80
Cations per 24 oxygen atoms												
Si	6.024	6.069	6.020	6.027	6.064	6.084	6.021	6.018	6.064	6.061	6.033	6.052
Ti	0.012	0.004	0.010	0.005	0.009	0.005	0.000	0.005	0.004	0.000	0.008	0.001
Al	3.997	4.016	4.008	4.054	3.970	4.004	4.037	4.004	4.031	4.035	4.050	4.018
Cr	0.005	0.005	0.003	0.005	0.005	0.001	0.003	0.001	0.000	0.003	0.004	0.004
Fe^{2+}	3.201	3.772	3.333	3.592	3.420	4.286	4.559	3.966	3.578	4.179	3.659	3.836
Mn	1.491	0.921	1.347	0.976	1.268	0.413	0.353	0.704	1.333	0.686	1.278	1.063
Mg	0.526	0.587	0.508	0.516	0.282	0.478	0.430	0.270	0.366	0.522	0.370	0.418
Ca	0.704	0.538	0.726	0.755	0.914	0.629	0.550	0.996	0.528	0.430	0.525	0.536
Na	0.000	0.006	0.016	0.009	0.007	0.003	0.006	0.010	0.012	0.007	0.010	0.010
K	0.002	0.000	0.000	0.004	0.000	0.002	0.000	0.006	0.002	0.002	0.002	0.002
Total	15.963	15.921	15.975	15.946	15.942	15.910	15.962	15.981	15.923	15.925	15.940	15.941
End-member compositions												
Alm	54.05	64.83	56.36	61.52	58.12	73.83	77.37	66.82	61.63	71.83	62.74	65.55
Pyr	8.88	10.09	8.59	8.84	4.80	8.23	7.30	4.55	6.30	8.98	6.34	7.14
Gross	11.89	9.25	12.28	12.93	15.53	10.83	9.34	16.77	9.10	7.39	9.01	9.15
Spess	25.18	15.83	22.78	16.72	21.55	7.11	6.00	11.86	22.97	11.80	21.91	18.16

Table 4.3 (Contd.)

sample	ZC52	ZC52	ZC55	ZC55	ZC55	ZC55	ZC55	ZC55	ZM27	ZM27	ZM27	ZM27
Posit.	C	R	C	R	C	R	C	R	C	R	C	R
SiO_2	37.15	37.13	37.10	37.08	37.07	37.48	37.26	37.58	37.72	37.90	37.76	37.75
TiO_2	0.05	0.01	0.09	0.02	0.07	0.00	0.06	0.02	0.01	0.10	0.04	0.06
Al_2O_3	20.86	21.02	20.64	20.67	21.05	21.11	21.11	20.94	21.24	21.36	21.30	21.25
Cr_2O_3	0.03	0.04	0.03	0.00	0.02	0.01	0.02	0.03	0.03	0.03	0.00	0.02
FeO*	25.37	28.38	26.68	28.09	26.92	28.25	26.48	28.48	29.34	29.44	30.00	29.98
MnO	10.58	6.43	9.32	7.34	9.16	7.01	9.53	6.94	9.09	6.88	9.06	6.89
MgO	1.43	1.80	1.51	1.42	1.37	1.65	1.43	1.60	1.22	1.12	1.13	1.17
CaO	2.98	3.26	3.65	3.77	3.16	3.57	3.63	3.67	2.62	4.27	1.93	3.71
Na_2O	0.02	0.02	0.03	0.00	0.04	0.05	0.02	0.03	0.01	0.01	0.03	0.01
K_2O	0.00	0.01	0.00	0.01	0.00	0.02	0.00	0.01	0.01	0.02	0.01	0.02
Total	98.49	98.12	99.07	98.41	98.87	99.16	99.58	99.31	101.31	101.16	101.28	100.88
Cations per 24 oxygen atoms												
Si	6.072	6.067	6.046	6.070	6.042	6.069	6.032	6.082	6.037	6.044	6.049	6.046
Ti	0.006	0.001	0.011	0.003	0.009	0.000	0.008	0.003	0.001	0.012	0.005	0.008
Al	4.019	4.048	3.965	3.988	4.044	4.029	4.028	3.995	4.007	4.015	4.022	4.012
Cr	0.004	0.005	0.004	0.000	0.003	0.001	0.003	0.004	0.004	0.004	0.000	0.003
Fe^{2+}	3.468	3.878	3.636	3.846	3.670	3.826	3.586	3.854	3.927	3.926	4.020	4.016
Mn	1.465	0.890	1.286	1.018	1.264	0.962	1.307	0.951	1.233	0.929	1.230	0.935
Mg	0.348	0.439	0.367	0.347	0.333	0.398	0.345	0.386	0.291	0.266	0.270	0.279
Ca	0.522	0.571	0.637	0.661	0.552	0.619	0.630	0.636	0.449	0.730	0.331	0.636
Na	0.007	0.007	0.010	0.000	0.012	0.015	0.007	0.010	0.003	0.003	0.010	0.003
K	0.000	0.002	0.000	0.002	0.000	0.004	0.000	0.002	0.002	0.004	0.002	0.004
Total	15.914	15.911	15.965	15.935	15.931	15.924	15.948	15.924	15.957	15.936	15.941	15.945
End-member compositions												
Alm	59.76	67.12	61.35	65.50	63.06	65.90	61.12	66.13	66.56	67.10	68.71	68.45
Pyr	6.00	7.59	6.19	5.90	5.72	6.86	5.87	6.62	4.93	4.54	4.61	4.76
Gross	9.00	9.89	10.75	11.27	9.49	10.67	10.73	10.92	7.61	12.47	5.66	10.85
Spess	25.24	15.40	21.70	17.33	21.73	16.57	22.27	16.32	20.89	15.88	21.02	15.94

sample	ZM27	ZM27	ZC69	ZC69	ZC69	ZC69	ZC69	ZC69	ZM63	ZM63	ZM64	ZM64
Posit.	C	R	C	R	C	R	C	R	C	C	C	R
SiO_2	37.61	37.89	37.83	37.94	37.85	38.08	37.80	37.66	37.86	37.95	37.72	38.35
TiO_2	0.06	0.02	0.08	0.07	0.07	0.15	0.15	0.14	0.13	0.12	0.16	0.11
Al_2O_3	21.15	21.25	21.21	21.31	21.29	21.19	21.05	21.19	21.06	21.27	21.11	21.25
Cr_2O_3	0.03	0.00	0.02	0.02	0.03	0.00	0.01	0.04	0.01	0.06	0.06	0.04
FeO*	30.09	28.48	25.80	18.32	19.97	18.65	18.73	19.45	21.98	21.73	24.47	20.67
MnO	8.91	7.95	10.77	12.38	14.25	13.74	16.04	14.96	13.37	14.18	11.69	13.77
MgO	1.25	0.97	1.26	0.42	0.44	0.30	0.44	0.48	0.70	0.67	0.99	0.79
CaO	2.00	4.34	4.15	10.85	7.89	8.96	7.23	7.36	5.16	5.17	5.10	6.25
Na_2O	0.04	0.01	0.04	0.01	0.01	0.00	0.01	0.01	0.01	0.03	0.02	0.02
K_2O	0.01	0.01	0.01	0.00	0.01	0.01	0.02	0.02	0.01	0.01	0.01	0.01
Total	101.17	100.92	101.18	101.35	101.83	101.10	101.50	101.36	100.33	101.20	101.35	101.26
Cations per 24 oxygen atoms												
Si	6.036	6.060	6.037	5.999	6.000	6.046	6.018	6.000	6.078	6.051	6.018	6.082
Ti	0.008	0.003	0.010	0.009	0.009	0.018	0.018	0.016	0.015	0.014	0.019	0.013
Al	4.001	4.006	3.990	3.972	3.978	3.966	3.950	3.979	3.985	3.997	3.970	3.972
Cr	0.004	0.000	0.003	0.003	0.004	0.000	0.001	0.005	0.001	0.008	0.008	0.005
Fe^{2+}	4.040	3.810	3.444	2.423	2.648	2.477	2.494	2.591	2.951	2.897	3.265	2.741
Mn	1.212	1.077	1.456	1.658	1.913	1.848	2.163	2.019	1.818	1.915	1.580	1.850
Mg	0.300	0.231	0.300	0.099	0.104	0.071	0.105	0.114	0.168	0.159	0.235	0.187
Ca	0.344	0.744	0.709	1.838	1.340	1.524	1.234	1.257	0.888	0.883	0.872	1.062
Na	0.012	0.003	0.012	0.003	0.003	0.000	0.003	0.003	0.003	0.010	0.006	0.006
K	0.002	0.002	0.002	0.000	0.002	0.002	0.004	0.004	0.002	0.002	0.002	0.002
Total	15.961	15.937	15.964	16.007	16.003	15.955	15.993	15.995	15.914	15.938	15.978	15.920
End-member compositions												
Alm	68.53	64.99	58.28	40.26	44.09	41.84	41.60	43.32	50.66	49.48	54.86	46.93
Pyr	5.08	3.95	5.07	1.64	1.73	1.20	1.75	1.91	2.88	2.72	3.95	3.20
Gross	5.83	12.69	12.01	30.55	22.32	25.75	20.58	21.01	15.24	15.08	14.65	18.18
Spess	20.55	18.37	24.65	27.55	31.86	31.21	36.08	33.76	31.21	32.71	26.55	31.68

Table 4.3 (Contd.)

sample	ZM64	ZM64	ZM64	ZM64	ZM64	ZM64	ZM64	ZM64	ZM64	ZM64	ZM64
Posit.	C	R	C	R	C	R	C	R	C	R	C
SiO_2	37.86	37.80	38.03	38.04	38.18	37.84	37.32	37.82	37.91	38.05	37.58
TiO_2	0.13	0.11	0.02	0.01	0.03	0.05	0.01	0.01	0.13	0.07	0.21
Al_2O_3	20.94	20.90	21.23	21.54	21.53	21.26	20.82	21.36	21.07	21.46	21.05
Cr_2O_3	0.02	0.02	0.01	0.03	0.02	0.01	0.04	0.02	0.02	0.04	0.01
FeO*	24.68	20.05	26.91	26.56	26.53	26.42	25.72	27.16	25.71	20.37	25.55
MnO	10.73	12.87	8.84	8.04	8.10	9.92	8.94	9.39	9.75	10.29	9.69
MgO	0.99	0.76	1.06	1.06	3.02	1.12	1.03	1.23	1.00	0.62	0.98
CaO	5.57	7.25	5.19	5.12	3.25	3.74	5.01	3.24	5.55	9.32	5.49
Na_2O	0.03	0.02	0.00	0.01	0.01	0.01	0.02	0.01	0.03	0.04	0.00
K_2O	0.01	0.00	0.01	0.01	0.01	0.01	0.01	0.01	0.01	0.01	0.01
Total	101.00	99.80	101.30	100.42	100.70	100.40	98.93	100.27	101.22	100.29	100.60
Cations per 24 oxygen atoms											
Si	6.049	6.074	6.053	6.073	6.046	6.072	6.071	6.073	6.043	6.051	6.027
Ti	0.016	0.013	0.002	0.001	0.004	0.006	0.001	0.001	0.016	0.008	0.025
Al	3.944	3.959	3.983	4.054	4.019	4.021	3.992	4.043	3.959	4.023	3.979
Cr	0.003	0.003	0.001	0.004	0.003	0.001	0.005	0.003	0.003	0.005	0.001
Fe^{2+}	3.298	2.695	3.582	3.546	3.513	3.546	3.499	3.648	3.428	2.709	3.427
Mn	1.452	1.752	1.192	1.087	1.086	1.348	1.232	1.277	1.317	1.386	1.316
Mg	0.236	0.182	0.252	0.252	0.713	0.268	0.250	0.294	0.238	0.147	0.234
Ca	0.954	1.248	0.885	0.876	0.551	0.643	0.873	0.558	0.948	1.588	0.943
Na	0.009	0.006	0.000	0.003	0.003	0.003	0.006	0.003	0.009	0.012	0.000
K	0.002	0.000	0.002	0.002	0.002	0.002	0.002	0.002	0.002	0.002	0.002
Total	15.968	15.935	15.952	15.898	15.943	15.913	15.932	15.905	15.968	15.934	15.958
End-member compositions											
Alm	55.52	45.86	60.60	61.55	59.92	61.09	59.77	63.15	57.80	46.47	57.89
Pyr	3.97	3.10	4.26	4.37	12.16	4.62	4.27	5.09	4.01	2.52	3.95
Gross	16.06	21.24	14.97	15.21	9.40	11.08	14.91	9.66	15.98	27.24	15.93
Spess	24.44	29.81	20.17	18.87	18.52	23.22	21.05	22.10	22.21	23.77	22.23

sample	ZM64	ZM64	ZM64	ZM64	ZM64	ZM64	ZS17	ZS17	ZS17	ZS17	ZS17	ZS17
Posit.	C	R	C	R	C	R	C	C	R	R	R	R
SiO_2	37.67	37.89	37.85	38.22	38.03	37.94	37.26	37.11	37.23	37.29	37.35	37.34
TiO_2	0.03	0.08	0.11	0.03	0.07	0.20	0.01	0.01	0.00	0.01	0.01	0.03
Al_2O_3	21.03	21.28	21.15	21.46	21.20	21.22	21.31	21.48	21.48	21.40	21.35	21.29
Cr_2O_3	0.03	0.03	0.04	0.04	0.03	0.04	0.05	0.03	0.04	0.03	0.04	0.03
FeO	22.30	20.57	21.66	24.36	24.27	18.99	31.85	31.27	31.20	31.45	31.35	29.72
MnO	14.89	10.71	14.30	8.83	9.63	14.59	9.15	9.68	9.70	9.72	9.94	10.02
MgO	1.19	0.82	1.08	0.89	1.07	0.96	1.01	0.95	0.91	0.93	0.88	0.73
CaO	3.38	9.00	4.66	7.00	6.14	6.45	0.46	0.54	0.45	0.39	0.38	1.85
Na_2O	0.01	0.01	0.02	0.01	0.00	0.01	0.04	0.02	0.02	0.02	0.02	0.01
K_2O	0.01	0.03	0.00	0.02	0.01	0.01	0.00	0.01	0.01	0.01	0.01	0.01
Total	100.55	100.44	100.89	100.87	100.46	100.43	101.15	101.13	101.06	101.26	101.35	101.05
Cations per 24 oxygen atoms												
Si	6.056	6.032	6.049	6.067	6.072	6.056	6.014	5.992	6.010	6.013	6.020	6.021
Ti	0.004	0.010	0.013	0.004	0.008	0.024	0.001	0.001	0.000	0.001	0.001	0.004
Al	3.985	3.993	3.984	4.015	3.989	3.992	4.054	4.088	4.087	4.067	4.056	4.046
Cr	0.004	0.004	0.005	0.005	0.004	0.005	0.006	0.004	0.005	0.004	0.005	0.004
Fe^{2+}	2.998	2.739	2.895	3.234	3.241	2.535	4.299	4.222	4.212	4.241	4.226	4.008
Mn	2.028	1.444	1.936	1.187	1.302	1.973	1.251	1.324	1.326	1.328	1.357	1.369
Mg	0.285	0.195	0.257	0.211	0.255	0.228	0.243	0.229	0.219	0.224	0.211	0.175
Ca	0.582	1.535	0.798	1.191	1.050	1.103	0.080	0.093	0.078	0.067	0.066	0.320
Na	0.003	0.003	0.006	0.003	0.000	0.003	0.013	0.006	0.006	0.006	0.006	0.003
K	0.002	0.006	0.000	0.004	0.002	0.002	0.000	0.002	0.002	0.002	0.002	0.002
Total	15.948	15.964	15.946	15.922	15.924	15.924	15.962	15.965	15.948	15.954	15.953	15.955
End-member compositions												
Alm	50.87	46.32	49.18	55.54	55.42	43.41	73.20	71.95	72.19	72.37	72.12	68.26
Pyr	4.84	3.30	4.37	3.62	4.36	3.90	4.14	3.90	3.75	3.82	3.60	2.98
Gross	9.88	25.96	13.56	20.45	17.95	18.89	1.36	1.58	1.34	1.14	1.13	5.45
Spess	34.41	24.42	32.89	20.38	22.26	33.79	21.30	22.56	22.72	22.66	23.16	23.31

Table 4.3 (Contd.)

sample	ZS17	ZS17	ZC20	ZC20	ZC20	ZC20	ZC20	ZC20	ZC20	ZC20	ZC20	ZC20
Posit.	R	R	C	C	C	C	C	C	C	C	C	R
SiO_2	37.45	37.48	37.20	37.10	37.09	37.10	37.26	37.46	37.07	37.14	37.07	37.05
TiO_2	0.01	0.00	0.08	0.07	0.09	0.08	0.08	0.08	0.02	0.06	0.03	0.00
Al_2O_3	21.49	21.39	20.83	20.91	20.81	20.81	20.94	20.91	20.90	20.98	20.88	21.05
Cr_2O_3	0.00	0.01	0.03	0.04	0.01	0.04	0.00	0.03	0.05	0.01	0.04	0.04
FeO*	29.57	29.58	22.25	22.12	22.31	22.66	21.53	21.42	21.68	23.18	23.94	25.34
MnO	9.73	9.79	15.92	15.79	15.52	15.93	16.65	16.62	16.49	15.55	15.05	14.69
MgO	0.80	0.77	0.39	0.41	0.42	0.42	0.40	0.40	0.35	0.43	0.45	0.50
CaO	2.13	2.05	3.40	3.43	3.31	3.14	3.53	3.56	3.51	2.77	2.78	1.27
Na_2O	0.03	0.04	0.02	0.06	0.02	0.07	0.06	0.05	0.05	0.04	0.02	0.39
K_2O	0.01	0.01	0.00	0.01	0.00	0.01	0.01	0.01	0.02	0.01	0.00	0.04
Total	101.25	101.13	100.14	99.97	99.60	100.26	100.49	100.55	100.16	100.19	100.26	100.40
Cations per 24 oxygen atoms												
Si	6.015	6.028	6.043	6.034	6.050	6.030	6.032	6.054	6.026	6.035	6.028	6.027
Ti	0.001	0.000	0.010	0.009	0.011	0.010	0.010	0.010	0.002	0.007	0.004	0.000
Al	4.069	4.055	3.989	4.008	4.001	3.987	3.996	3.983	4.005	4.018	4.002	4.036
Cr	0.000	0.001	0.004	0.005	0.001	0.005	0.000	0.004	0.006	0.001	0.005	0.005
Fe^{2+}	3.972	3.979	3.023	3.009	3.044	3.080	2.915	2.895	2.947	3.150	3.256	3.447
Mn	1.324	1.334	2.191	2.175	2.144	2.193	2.283	2.275	2.271	2.140	2.073	2.024
Mg	0.192	0.185	0.094	0.099	0.102	0.102	0.097	0.096	0.085	0.104	0.109	0.121
Ca	0.367	0.353	0.592	0.598	0.579	0.547	0.612	0.616	0.611	0.482	0.484	0.221
Na	0.009	0.012	0.006	0.019	0.006	0.022	0.019	0.016	0.016	0.013	0.006	0.123
K	0.002	0.002	0.000	0.002	0.000	0.002	0.002	0.002	0.004	0.002	0.000	0.008
Total	15.955	15.950	15.955	15.962	15.941	15.978	15.970	15.952	15.976	15.955	15.967	16.016
End-member compositions												
Alm	67.84	68.01	51.24	51.16	51.87	52.01	49.35	49.22	49.83	53.61	54.98	59.30
Pyr	3.28	3.16	1.59	1.68	1.74	1.72	1.64	1.63	1.44	1.77	1.84	2.08
Gross	6.27	6.03	10.03	10.17	9.87	9.24	10.36	10.47	10.33	8.20	8.17	3.80
Spess	22.61	22.80	37.14	36.98	36.53	37.03	38.65	38.68	38.40	36.42	35.01	34.82

sample	ZC20	ZC20	ZM70	ZM70	ZM70	NMG1	NMG1	NMG1	NMG1	NMG1	NMG1	ZC8
Posit.	R	R	C	C	C	C	C	R	R	R	R	M
SiO_2	36.95	36.79	37.16	37.24	37.01	37.14	37.31	37.24	37.28	37.18	37.01	38.07
TiO_2	0.04	0.01	0.04	0.02	0.01	0.06	0.01	0.01	0.00	0.00	0.04	0.07
Al_2O_3	21.11	20.94	21.05	20.94	21.00	21.37	21.37	21.36	21.29	21.34	21.36	20.58
Cr_2O_3	0.01	0.00	0.01	0.00	0.04	0.03	0.03	0.01	0.03	0.03	0.03	0.15
FeO*	25.40	25.07	28.01	27.77	27.92	31.50	30.84	31.64	31.58	31.14	31.24	15.42
MnO	15.31	15.11	13.43	13.08	13.17	9.07	10.14	9.67	9.82	9.69	9.71	5.62
MgO	0.54	0.51	0.83	0.82	0.83	1.08	0.85	0.95	0.94	0.92	0.89	0.51
CaO	1.88	1.90	0.76	0.77	0.79	0.55	0.54	0.50	0.50	0.56	0.53	18.89
Na_2O	0.05	0.03	0.01	0.01	0.00	0.05	0.04	0.03	0.03	0.05	0.04	0.09
K_2O	0.00	0.01	0.01	0.01	0.01	0.02	0.01	0.00	0.01	0.01	0.01	0.05
Total	101.30	100.41	101.32	100.68	100.80	100.90	101.16	101.41	101.49	100.92	100.91	99.46
Cations per 24 oxygen atoms												
Si	5.976	5.996	6.006	6.042	6.009	6.002	6.020	6.002	6.007	6.013	5.993	6.027
Ti	0.005	0.001	0.005	0.002	0.002	0.007	0.001	0.001	0.000	0.000	0.005	0.009
Al	4.025	4.023	4.010	4.005	4.019	4.071	4.064	4.058	4.043	4.068	4.077	3.840
Cr	0.001	0.000	0.002	0.000	0.005	0.004	0.004	0.001	0.004	0.004	0.004	0.019
Fe^{2+}	3.436	3.417	3.786	3.768	3.791	4.258	4.162	4.265	4.256	4.212	4.231	2.042
Mn	2.098	2.086	1.839	1.798	1.811	1.242	1.386	1.320	1.340	1.327	1.332	0.754
Mg	0.130	0.124	0.200	0.198	0.201	0.260	0.204	0.228	0.226	0.222	0.215	0.120
Ca	0.326	0.332	0.131	0.134	0.137	0.095	0.093	0.086	0.086	0.097	0.092	3.204
Na	0.016	0.009	0.003	0.003	0.000	0.016	0.013	0.009	0.009	0.016	0.013	0.028
K	0.000	0.002	0.002	0.002	0.002	0.004	0.002	0.000	0.002	0.002	0.002	0.011
Total	16.014	15.995	15.986	15.954	15.980	15.963	15.952	15.970	15.974	15.961	15.971	16.054
End-member compositions												
Alm	57.36	57.34	63.56	63.89	63.82	72.72	71.21	72.30	72.04	71.90	72.08	33.36
Pyr	2.17	2.08	3.36	3.36	3.38	4.44	3.49	3.87	3.83	3.79	3.66	1.96
Gross	5.44	5.57	2.20	2.26	2.31	1.62	1.59	1.46	1.46	1.66	1.57	52.36
Spess	35.03	35.01	30.87	30.48	30.49	21.21	23.71	22.38	22.68	22.65	22.69	12.31

Table 4.3 (Contd.)

sample	ZC8	ZC8	ZC8	ZC8	ZC8	ZC8	ZC8	ZC8	ZC8	ZC8	ZC8
Posit.	M	C	C	C	C	C	C	R	R	R	C
SiO_2	38.78	39.56	39.12	38.82	39.36	39.43	39.33	39.55	37.23	38.05	39.50
TiO_2	0.04	0.22	0.20	0.17	0.20	0.19	0.21	0.20	0.19	0.13	0.72
Al_2O_3	20.92	20.58	20.03	19.56	20.25	19.95	20.11	20.27	19.39	19.70	19.98
Cr_2O_3	0.12	0.02	0.00	0.01	0.01	0.01	0.02	0.02	0.04	0.04	0.15
FeO*	15.73	5.26	5.41	6.84	5.15	5.10	5.24	6.00	7.54	7.22	4.67
MnO	5.64	1.21	1.31	1.53	1.50	1.52	1.39	1.59	1.83	1.65	1.26
MgO	0.48	0.07	0.07	0.03	0.06	0.06	0.06	0.12	0.12	0.10	0.08
CaO	18.74	33.92	33.56	32.65	34.04	33.89	33.70	32.58	30.67	31.30	34.15
Na_2O	0.05	0.04	0.06	0.03	0.04	0.04	0.03	0.04	0.18	0.23	0.02
K_2O	0.01	0.01	0.01	0.03	0.02	0.03	0.01	0.01	0.03	0.03	0.01
Total	100.53	100.89	99.77	99.67	100.63	100.24	100.13	100.42	97.23	98.47	100.57
Cations per 24 oxygen atoms											
Si	6.061	6.017	6.029	6.027	6.016	6.048	6.036	6.054	5.950	5.986	6.026
Ti	0.005	0.025	0.023	0.020	0.023	0.022	0.024	0.023	0.023	0.015	0.083
Al	3.854	3.690	3.639	3.579	3.648	3.607	3.638	3.657	3.653	3.653	3.593
Cr	0.014	0.002	0.000	0.001	0.001	0.001	0.002	0.002	0.005	0.005	0.018
Fe^{2+}	2.056	0.669	0.697	0.888	0.658	0.654	0.673	0.768	1.008	0.950	0.596
Mn	0.747	0.156	0.171	0.201	0.194	0.197	0.181	0.206	0.248	0.220	0.163
Mg	0.111	0.016	0.016	0.007	0.014	0.014	0.014	0.027	0.029	0.023	0.018
Ca	3.138	5.529	5.542	5.432	5.575	5.570	5.542	5.344	5.252	5.276	5.582
Na	0.015	0.012	0.018	0.009	0.012	0.012	0.009	0.012	0.056	0.070	0.006
K	0.002	0.002	0.002	0.006	0.004	0.006	0.002	0.002	0.006	0.006	0.002
Total	16.008	16.118	16.137	16.170	16.145	16.133	16.125	16.100	16.231	16.207	16.091
End-member compositions											
Alm	33.97	10.50	10.85	13.60	10.22	10.16	10.50	12.10	15.42	14.69	9.37
Pyr	1.84	0.25	0.25	0.11	0.22	0.22	0.22	0.43	0.44	0.36	0.28
Gross	51.85	86.80	86.24	83.21	86.55	86.56	86.46	84.22	80.34	81.56	87.78
Spess	12.34	2.45	2.66	3.08	3.01	3.06	2.82	3.25	3.79	3.40	2.56

sample	ZC8	ZC8	ZC8	ZC8	ZC8	ZC8	ZC8	ZC8	ZC8	ZC41	ZC41
Posit.	C	C	M	R	R	C	C	R	R	C	R
SiO_2	39.51	39.58	39.42	38.69	37.64	39.26	39.45	39.19	39.83	42.50	39.09
TiO_2	0.58	0.29	0.08	0.18	0.21	0.10	0.07	0.11	0.09	0.02	0.05
Al_2O_3	20.14	20.19	20.33	19.83	19.17	20.76	20.75	21.03	20.14	20.57	21.37
Cr_2O_3	0.13	0.14	0.10	0.05	0.06	0.04	0.02	0.04	0.04	0.02	0.01
FeO*	4.78	5.15	7.66	7.40	7.11	7.38	7.71	9.67	8.40	19.00	19.60
MnO	1.30	1.23	2.99	1.79	2.02	1.92	1.78	2.14	1.97	6.17	6.33
MgO	0.08	0.07	0.07	0.07	0.09	0.10	0.11	0.15	0.16	0.84	0.97
CaO	34.11	33.72	29.94	30.96	30.85	30.82	30.98	28.13	28.92	12.39	12.78
Na_2O	0.01	0.01	0.02	0.04	0.02	0.04	0.04	0.03	0.03	0.02	0.01
K_2O	0.02	0.01	0.04	0.05	0.05	0.01	0.03	0.02	0.01	0.01	0.01
Total	100.67	100.41	100.66	99.08	97.23	100.45	100.95	100.53	99.60	101.56	100.25
Cations per 24 oxygen atoms											
Si	6.022	6.048	6.057	6.036	6.004	6.022	6.027	6.025	6.151	6.492	6.132
Ti	0.066	0.033	0.009	0.021	0.025	0.012	0.008	0.013	0.010	0.002	0.006
Al	3.618	3.636	3.682	3.646	3.604	3.754	3.736	3.811	3.666	3.704	3.951
Cr	0.016	0.017	0.012	0.006	0.008	0.005	0.002	0.005	0.005	0.003	0.001
Fe^{2+}	0.609	0.658	0.984	0.965	0.948	0.947	0.985	1.243	1.085	2.428	2.572
Mn	0.168	0.159	0.389	0.237	0.273	0.249	0.230	0.279	0.258	0.799	0.841
Mg	0.018	0.016	0.016	0.016	0.021	0.023	0.025	0.034	0.037	0.191	0.227
Ca	5.571	5.521	4.929	5.175	5.273	5.066	5.071	4.634	4.785	2.028	2.148
Na	0.003	0.003	0.006	0.012	0.006	0.012	0.012	0.009	0.009	0.006	0.003
K	0.004	0.002	0.008	0.010	0.010	0.002	0.006	0.004	0.002	0.002	0.002
Total	16.096	16.095	16.093	16.127	16.173	16.094	16.103	16.059	16.009	15.658	15.887
End-member compositions											
Alm	9.57	10.36	15.57	15.09	14.55	15.07	15.61	20.08	17.60	44.58	44.44
Pyr	0.28	0.25	0.25	0.25	0.32	0.37	0.40	0.55	0.60	3.51	3.91
Gross	87.51	86.89	78.02	80.95	80.94	80.60	80.35	74.86	77.62	37.25	37.12
Spess	2.64	2.50	6.16	3.71	4.19	3.96	3.64	4.51	4.18	14.67	14.53

Schist: ZC 9, ZC 11, ZC 37, ZC 46, ZC52, ZC55, ZM 27; Tourmalinite: ZC 69, ZM 63, ZM 64; Leucogranite: ZS 17, ZC 20, ZM 70, NMG1; Calc-silicate quartzite: ZC 8, ZC 41; C = Core; M = Middle; R = Rim; * = Total iron as FeO; Alm = almandine ; Pyr = pyrope; Gross = grossular; Spess = spessartine. N. B. The underline indicates the various positions within the single grain. Detection limits for the analysed oxides are tabulated in Appendix 4.2.

In contrast, it is very high in garnet of tourmalinite and scheelite-bearing calc-silicate quartzite (Table 4.3). Similarly, the almandine content is high in the garnet from schist and leucogranite, whereas it is low in the garnet of tourmalinite and calc-silicate quartzite (Table 4.3).

MnO decreases significantly, from core to margin with marginal enrichment of FeO in most of the analyses from the schist (Fig. 4.14 B, Table 4.3; ZC 46, ZC 52, ZC 55). This zoning profile is considered as a characteristic feature of the staurolite grade pelitic schist (Woodsworth 1977). In contrast, MnO in the garnet of tourmalinite generally increases from core to margin with marginal depletion of FeO (Fig. 4.14 B, Table 4.3). The occurrence of compositional zoning (Mn-rich core and Fe-rich margin) in the garnet of studied schist, suggest that prograde regional metamorphism is still preserved with in the garnet porphyroblast due its large volume.

Plotting the Miniki Gol garnet data on an Mn-Mg-Fe triangular diagram (Fig. 4.14 A) shows that most analyses of garnet from all the rocks in the studied area fall within the compositional field of the igneous garnets defined by Miller and Stoddard (1981). In contrast, garnet analyses from two-mica granites at Miniki Gol, plot above the line of 20 mol % spessartine (Fig. 4.14 A) described for two-mica granites by Miller and Stoddard (1981). Except for the Ca content which is higher in tourmalinite, garnets from Miniki Gol leucogranite and tourmalinite, are similar in composition (Table 4.4). In contrast, the garnet from schist is different in composition from that of granite.

4.4.4 Amphibole

Amphibole is one of the dominant constituents of both the scheelite-bearing calc-silicate and barren calc-silicate rocks. Most calc-silicates (such as TR 132, ZC 65, ADIT 3, ZC 41, ZC 43, Table 4.4), contain scheelite grains that are in places, associated with amphibole grains, allowing pressure-temperature estimates to be made. About 300 microprobe analyses from calc-silicate quartzite were performed on different grains, from which 92 representative analyses are presented in the Table 4.4. Mineral formulae were calculated on the basis of 23 oxygen atoms following the procedure of Leake (1978) and Robinson (1982). Ferrous and ferric iron were computed following the method of Robinson et al. (1982), making the total numbers of cations 13 excluding K, Na, and Ca. This gives a maximum estimates of Fe^{3+} when balanced to 23 (O).

The analysed amphibole is calcic as defined by Leake (1978) with $(Ca + Na_B)$ greater than 1.34 and Na_B is less than 0.67 and $(Na + K)_A$ is less than 0.5 (Table 4.4). Al_4 represents tetrahedral site whereas the remaining Al is adjusted in C-site (Al_6). Almost all the Ca is accommodated in B-site (Table 4.4).

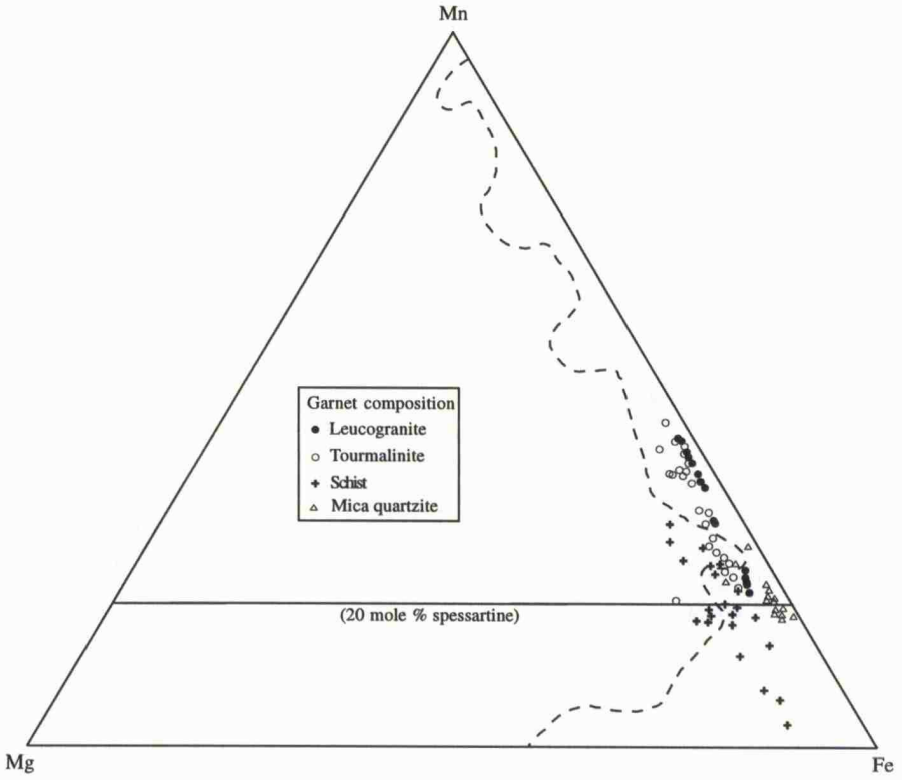

(A)

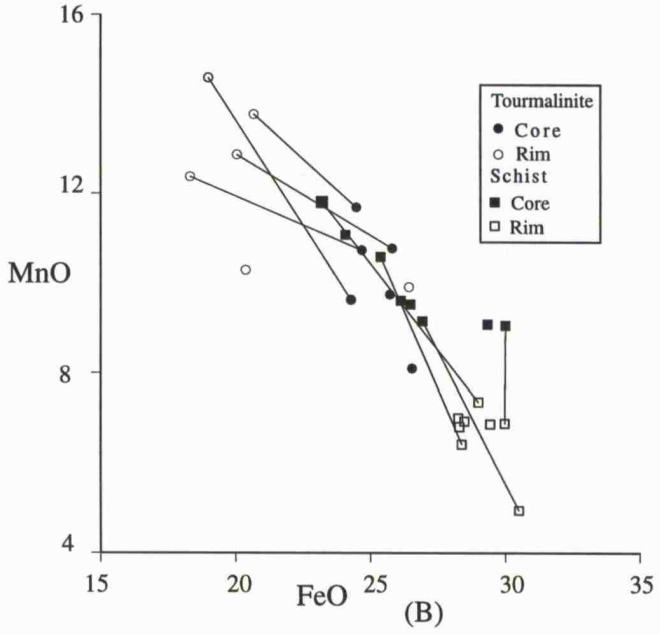

(B)

Fig. 4.14: **(A)** Composition of Miniki Gol garnet in terms of Mn, Mg and Fe (atomic proportions), showing the compositional field of igneous garnets defined by Miller and Stoddard (1981). **(B)** Relationship of wt % FeO with MnO indicating core and rim compositions of Miniki Gol garnet. Tie lines connect core and rim compositions within a single grains. Some of the tie lines were omitted for the sake of clarity. Data taken from Table 4.3.

Table 4.4: Chemical variation in the Miniki Gol amphibole from scheelite-bearing calc-silicate quartzite, except ZC 4, ZC 32 and ZC 49 **(barren calc-silicate quartzite).**

Sample	TR132*	TR132*	TR132*	TR132*	TR132*	TR132*	TR132*	TR132*	TR132*	TR132	TR132*	TR132*
Posit.	C	C	C	C	M	M	M	M	R	R	R	R
SiO_2	47.23	50.28	50.69	49.10	50.83	51.29	50.80	44.50	45.22	49.62	49.26	49.31
TiO_2	0.10	0.08	0.06	0.11	0.09	0.04	0.04	0.25	0.17	0.13	0.10	0.11
Al_2O_3	8.51	6.21	5.76	8.27	5.66	5.03	5.54	14.08	12.69	7.37	7.74	7.53
Fe_2O_3	13.76	4.83	3.56	3.50	2.89	2.97	2.50	3.04	3.14	3.80	2.98	1.48
FeO	6.19	13.17	13.91	14.68	13.87	13.74	14.08	15.96	15.38	14.02	13.49	14.55
MnO	0.35	0.35	0.37	0.35	0.33	0.34	0.31	0.31	0.39	0.30	0.33	0.36
MgO	11.03	11.40	11.55	10.26	11.95	12.38	12.21	7.52	8.06	11.11	11.59	11.60
CaO	10.18	11.75	11.90	11.83	12.05	12.21	12.25	11.89	11.66	11.98	12.07	12.35
Na_2O	0.37	0.34	0.32	0.55	0.36	0.29	0.39	0.86	0.71	0.47	0.53	0.54
K_2O	0.27	0.30	0.34	0.33	0.35	0.40	0.46	0.47	0.64	0.47	0.65	0.68
Total	98.00	98.70	98.47	98.98	98.38	98.69	98.58	98.89	98.05	99.27	98.74	98.51
Cations per 23 oxygen atoms												
Si	6.850	7.293	7.373	7.137	7.386	7.429	7.380	6.542	6.689	7.183	7.151	7.190
Ti	0.011	0.009	0.007	0.012	0.010	0.004	0.004	0.028	0.019	0.014	0.011	0.012
Al4	1.150	0.707	0.627	0.863	0.614	0.571	0.620	1.458	1.311	0.817	0.849	0.810
Al6	0.304	0.355	0.361	0.554	0.356	0.288	0.329	0.982	0.901	0.440	0.475	0.484
Fe^{3+}	1.501	0.527	0.390	0.383	0.316	0.324	0.273	0.337	0.349	0.413	0.326	0.162
Fe^{2+}	0.751	1.597	1.693	1.784	1.686	1.664	1.711	1.962	1.902	1.698	1.637	1.775
Mn	0.043	0.043	0.046	0.043	0.041	0.042	0.038	0.039	0.049	0.037	0.041	0.044
Mg	2.385	2.465	2.504	2.223	2.589	2.673	2.644	1.648	1.777	2.397	2.508	2.521
Ca	1.582	1.826	1.855	1.843	1.876	1.895	1.907	1.873	1.848	1.858	1.877	1.930
Ca_B	1.582	1.826	1.855	1.843	1.876	1.895	1.907	1.873	1.848	1.858	1.877	1.930
Na	0.104	0.096	0.090	0.155	0.101	0.081	0.110	0.245	0.204	0.132	0.149	0.153
Na_B	0.104	0.096	0.090	0.155	0.101	0.081	0.093	0.127	0.152	0.132	0.123	0.070
Na_A	0.000	0.000	0.000	0.000	0.000	0.000	0.017	0.118	0.052	0.000	0.027	0.082
K	0.050	0.056	0.063	0.061	0.065	0.074	0.085	0.088	0.121	0.087	0.120	0.127
Mg#	0.761	0.607	0.597	0.555	0.606	0.616	0.607	0.457	0.483	0.585	0.605	0.587
$(Ca+Na_B)$	1.686	1.922	1.945	1.998	1.977	1.976	2.000	2.000	2.000	1.990	2.000	2.000
$(Na+K)_A$	0.050	0.056	0.063	0.061	0.065	0.074	0.102	0.206	0.173	0.087	0.1470	0.209

Sample	TR132	TR132	TR132	TR132	TR132	TR132	ADIT 3	ADIT 3	ADIT 3	ADIT 3	ADIT 3	ADIT 3
Posit.	C	R	M	R	C	R	C	R	C	R	C	R
SiO_2	42.55	52.43	45.30	43.01	42.35	44.91	46.19	41.41	42.57	45.16	41.66	41.41
TiO_2	0.25	0.14	0.22	0.22	0.16	0.16	0.30	0.31	0.21	0.32	0.30	0.28
Al_2O_3	16.45	11.72	11.93	14.92	15.87	12.83	15.15	17.81	16.45	15.04	17.57	16.92
Fe_2O_3	1.77	0.00	2.06	1.63	1.46	1.27	0.00	0.93	1.70	0.00	1.03	0.58
FeO	16.18	14.32	15.75	16.68	16.83	15.78	15.79	15.89	15.04	15.88	15.73	15.85
MnO	0.32	0.24	0.37	0.37	0.35	0.29	0.34	0.34	0.38	0.29	0.39	0.32
MgO	6.67	5.59	8.21	6.60	6.39	8.35	6.71	6.47	7.15	7.25	6.55	6.85
CaO	11.85	9.93	11.77	11.66	11.84	11.98	11.11	11.91	11.74	11.45	11.84	11.93
Na_2O	0.93	0.73	0.69	0.81	0.85	0.76	0.94	1.03	1.00	0.95	1.04	0.99
K_2O	0.60	0.56	0.36	0.57	0.65	0.45	0.50	0.54	0.45	0.43	0.50	0.63
Total	97.57	95.66	96.67	96.47	96.76	96.78	97.03	96.64	96.69	96.77	96.61	95.76
Cations per 23 oxygen atoms												
Si	6.343	7.844	6.782	6.494	6.386	6.709	6.840	6.216	6.361	6.712	6.250	6.278
Ti	0.028	0.016	0.025	0.025	0.018	0.018	0.033	0.035	0.024	0.036	0.034	0.032
Al4	1.657	0.156	1.218	1.506	1.614	1.291	1.160	1.784	1.639	1.288	1.750	1.722
Al6	1.233	1.911	0.887	1.150	1.207	0.967	1.484	1.368	1.259	1.346	1.357	1.301
Fe^{3+}	0.199	0.000	0.233	0.185	0.166	0.142	0.000	0.105	0.192	0.000	0.116	0.066
Fe^{2+}	2.016	1.792	1.972	2.107	2.123	1.971	1.955	1.995	1.879	1.974	1.974	2.009
Mn	0.040	0.030	0.047	0.047	0.045	0.037	0.043	0.043	0.048	0.037	0.050	0.041
Mg	1.482	1.247	1.832	1.486	1.436	1.859	1.481	1.448	1.593	1.606	1.465	1.548
Ca	1.893	1.592	1.888	1.887	1.913	1.917	1.763	1.916	1.880	1.823	1.903	1.938
Ca_B	1.893	1.592	1.888	1.887	1.913	1.917	1.763	1.916	1.880	1.823	1.903	1.938
Na	0.269	0.212	0.200	0.237	0.249	0.220	0.270	0.300	0.290	0.274	0.303	0.291
Na_B	0.107	0.212	0.112	0.113	0.087	0.083	0.237	0.084	0.120	0.177	0.097	0.062
Na_A	0.162	0.000	0.088	0.124	0.162	0.138	0.033	0.216	0.170	0.097	0.206	0.229
K	0.114	0.107	0.069	0.110	0.125	0.086	0.094	0.103	0.086	0.082	0.096	0.122
Mg#	0.424	0.410	0.482	0.414	0.403	0.485	0.431	0.421	0.459	0.449	0.426	0.435
$(Ca+Na_B)$	2.000	1.804	2.000	2.000	2.000	2.000	2.000	2.000	2.000	2.000	2.000	2.000
$(Na+K)_A$	0.276	0.107	0.157	0.234	0.287	0.224	0.127	0.319	0.256	0.179	0.302	0.351

Table 4.4 (contd.)

Sample	ADIT 3	ADIT 3	ZC41	ZC41	ZC41	ZC41	ZC41	ZC41	ZC41	ZC41	ZC41	ZC41
Posit.	C	R	C	R	C	R	C	R	C	R	C	R
SiO_2	42.38	49.23	47.33	46.17	44.84	43.65	43.77	43.76	54.61	54.64	55.12	53.65
TiO_2	0.31	0.22	0.28	0.28	0.21	0.27	0.23	0.31	0.03	0.01	0.04	0.04
Al_2O_3	16.48	14.34	11.46	16.34	13.93	16.08	15.89	16.44	2.98	2.48	2.06	3.85
Fe_2O_3	0.79	0.00	3.52	0.00	1.54	1.25	0.99	0.00	1.28	1.25	0.58	1.10
FeO	15.68	14.69	13.06	16.00	14.76	15.35	15.80	16.92	10.17	10.01	10.50	10.46
MnO	0.37	0.28	0.37	0.33	0.42	0.35	0.35	0.40	0.46	0.49	0.39	0.47
MgO	7.16	6.22	10.22	6.75	8.53	7.51	7.38	6.40	15.96	16.26	16.38	15.54
CaO	11.93	10.55	11.98	11.29	11.98	11.89	11.91	11.76	12.60	12.74	12.75	12.67
Na_2O	1.02	0.84	0.75	0.90	0.87	0.94	0.93	0.99	0.23	0.18	0.14	0.29
K_2O	0.52	0.43	0.28	0.46	0.36	0.48	0.47	0.49	0.03	0.03	0.07	0.09
Total	96.64	96.80	99.24	98.52	97.43	97.78	97.72	97.47	98.35	98.13	98.04	98.16
Cations per 23 oxygen atoms												
Si	6.350	7.265	6.823	6.714	6.622	6.441	6.470	6.508	7.733	7.757	7.826	7.633
Ti	0.035	0.024	0.030	0.031	0.023	0.030	0.026	0.035	0.003	0.001	0.004	0.004
Al4	1.650	0.735	1.177	1.286	1.378	1.559	1.530	1.492	0.267	0.243	0.174	0.367
Al6	1.260	1.759	0.770	1.514	1.046	1.238	1.238	1.390	0.230	0.172	0.171	0.279
Fe^{3+}	0.089	0.000	0.381	0.000	0.171	0.139	0.110	0.000	0.137	0.134	0.062	0.118
Fe^{2+}	1.965	1.813	1.574	1.946	1.823	1.895	1.953	2.105	1.204	1.189	1.247	1.244
Mn	0.047	0.035	0.045	0.041	0.053	0.044	0.044	0.050	0.055	0.059	0.047	0.057
Mg	1.599	1.368	2.196	1.463	1.878	1.652	1.626	1.419	3.369	3.441	3.467	3.296
Ca	1.915	1.668	1.851	1.759	1.896	1.880	1.886	1.874	1.912	1.938	1.940	1.931
Ca_B	1.915	1.668	1.851	1.759	1.896	1.880	1.886	1.874	1.912	1.938	1.940	1.931
Na	0.296	0.240	0.210	0.254	0.249	0.269	0.267	0.285	0.063	0.050	0.039	0.080
Na_B	0.085	0.240	0.149	0.241	0.104	0.120	0.114	0.126	0.063	0.050	0.039	0.069
Na_A	0.212	0.000	0.060	0.013	0.145	0.149	0.153	0.160	0.000	0.000	0.000	0.012
K	0.099	0.081	0.051	0.085	0.068	0.090	0.089	0.093	0.005	0.005	0.013	0.016
Mg#	0.449	0.430	0.582	0.429	0.507	0.466	0.454	0.403	0.737	0.743	0.735	0.726
$(Ca+Na_B)$	2.000	1.908	2.000	2.000	2.000	2.000	2.000	2.000	1.975	1.988	1.979	2.000
$(Na+K)_A$	0.311	0.081	0.111	0.098	0.213	0.239	0.242	0.253	0.005	0.005	0.013	0.028

Sample	ZC41	ZC41	ZC41	ZC41	ZC41	ZC41	ZC43	ZC43	ZC43	ZC43	ZC43	ZC43
Posit.	M	R	C	R	M	R						
SiO_2	44.01	43.48	45.54	43.75	43.98	58.15	50.23	50.65	54.01	53.78	53.63	54.05
TiO_2	0.25	0.32	0.24	0.26	0.25	0.23	0.13	0.13	0.04	0.03	0.07	0.03
Al_2O_3	18.04	16.32	13.77	16.43	15.75	12.86	6.79	7.09	2.47	2.77	2.69	2.63
Fe_2O_3	0.00	1.37	1.13	0.91	1.52	0.00	1.56	2.09	0.08	1.23	1.22	1.14
FeO	13.28	13.03	13.70	14.23	14.61	11.77	10.00	9.63	9.55	8.42	8.83	8.72
MnO	0.40	0.40	0.46	0.43	0.43	0.33	0.62	0.62	0.59	0.72	0.64	0.69
MgO	7.58	8.85	9.57	8.41	8.14	6.02	14.56	14.55	16.87	17.10	16.85	16.97
CaO	11.93	11.98	12.15	12.21	12.07	9.20	12.67	12.48	13.00	12.96	12.90	12.84
Na_2O	1.34	1.08	0.90	1.00	0.95	0.75	0.64	0.70	0.23	0.26	0.24	0.28
K_2O	0.56	0.44	0.38	0.45	0.44	0.40	0.31	0.31	0.09	0.11	0.12	0.13
Total	97.39	97.27	97.83	98.08	98.14	99.71	97.51	98.25	96.93	97.38	97.19	97.48
Cations per 23 oxygen atoms												
Si	6.485	6.391	6.658	6.404	6.452	8.163	7.246	7.239	7.743	7.671	7.677	7.702
Ti	0.028	0.035	0.026	0.029	0.028	0.024	0.014	0.014	0.004	0.003	0.008	0.003
Al4	1.515	1.609	1.342	1.596	1.548	0.000	0.754	0.761	0.257	0.329	0.323	0.298
Al6	1.618	1.219	1.031	1.238	1.175	2.128	0.400	0.434	0.161	0.137	0.131	0.144
Fe^{3+}	0.000	0.151	0.124	0.100	0.168	0.000	0.169	0.224	0.008	0.132	0.132	0.122
Fe^{2+}	1.636	1.602	1.675	1.742	1.793	1.382	1.206	1.151	1.145	1.005	1.057	1.040
Mn	0.050	0.050	0.057	0.053	0.053	0.039	0.076	0.075	0.072	0.087	0.078	0.083
Mg	1.665	1.939	2.086	1.835	1.780	1.260	3.131	3.100	3.605	3.636	3.595	3.605
Ca	1.883	1.887	1.903	1.915	1.897	1.384	1.958	1.911	1.997	1.981	1.979	1.961
Ca_B	1.883	1.887	1.903	1.915	1.897	1.220	1.958	1.911	1.997	1.981	1.979	1.961
Na	0.383	0.308	0.255	0.284	0.270	0.204	0.179	0.194	0.064	0.072	0.067	0.077
Na_B	0.117	0.113	0.097	0.085	0.103	0.204	0.042	0.089	0.003	0.019	0.021	0.039
Na_A	0.266	0.195	0.159	0.199	0.167	0.000	0.137	0.105	0.061	0.053	0.045	0.038
K	0.105	0.083	0.071	0.084	0.082	0.072	0.057	0.057	0.016	0.020	0.022	0.024
Mg#	0.504	0.548	0.555	0.513	0.498	0.477	0.722	0.729	0.759	0.783	0.773	0.776
$(Ca+Na_B)$	2.000	2.000	2.000	2.000	2.000	1.588	2.000	2.000	2.000	2.000	2.000	2.000
$(Na+K)_A$	0.371	0.278	0.230	0.283	0.249	0.072	0.194	0.162	0.077	0.073	0.067	0.062

Table 4.4 (contd.)

Sample	ZC65*	ZC65*	ZC65*	ZC65*	ZC65*	ZC65*	ZC65*	ZC65*	ZC65*	ZC4♤	ZC4♤	ZC4♤
Posit.	C	C	C	R	R	C	C	R	R	C	C	C
SiO_2	42.94	43.02	43.03	42.38	41.88	42.79	42.79	42.06	42.13	53.93	53.50	47.42
TiO_2	0.19	0.25	0.20	0.22	0.18	0.15	0.22	0.22	0.15	0.04	0.07	0.28
Al_2O_3	16.39	16.52	15.85	16.82	17.19	16.34	16.23	16.81	17.59	2.02	3.36	9.43
Fe_2O_3	3.78	3.43	3.24	4.21	7.74	3.43	3.20	3.47	8.68	2.79	1.99	0.96
FeO	15.33	15.34	15.67	14.39	11.32	15.24	15.29	15.10	10.25	9.36	10.85	14.03
MnO	0.28	0.37	0.41	0.37	0.36	0.39	0.35	0.36	0.32	0.55	0.61	0.58
MgO	6.72	6.89	6.63	6.93	7.02	6.83	7.00	6.73	6.92	15.97	15.28	11.21
CaO	11.64	11.79	11.56	11.60	10.60	11.68	11.75	11.78	10.09	12.40	12.74	12.43
Na_2O	0.98	0.99	0.94	1.04	1.10	0.99	1.04	1.01	1.10	0.13	0.28	0.79
K_2O	0.57	0.60	0.60	0.59	0.74	0.63	0.61	0.56	0.73	0.06	0.15	0.60
Total	98.82	99.19	98.13	98.54	98.14	98.47	98.48	98.10	97.96	97.25	98.83	97.76
Cations per 23 oxygen atoms												
Si	6.318	6.307	6.381	6.246	6.163	6.320	6.318	6.240	6.174	7.742	7.609	6.970
Ti	0.021	0.028	0.022	0.024	0.020	0.017	0.024	0.025	0.017	0.004	0.007	0.031
Al4	1.682	1.693	1.619	1.754	1.837	1.680	1.682	1.760	1.826	0.258	0.391	1.030
Al6	1.160	1.161	1.151	1.167	1.144	1.164	1.143	1.180	1.212	0.084	0.172	0.603
Fe^{3+}	0.418	0.378	0.362	0.466	0.857	0.381	0.355	0.388	0.957	0.301	0.213	0.106
Fe^{2+}	1.886	1.880	1.944	1.773	1.393	1.883	1.889	1.873	1.256	1.124	1.290	1.725
Mn	0.035	0.046	0.052	0.046	0.045	0.049	0.044	0.045	0.040	0.067	0.073	0.072
Mg	1.474	1.506	1.466	1.522	1.540	1.504	1.541	1.488	1.512	3.418	3.239	2.456
Ca	1.835	1.852	1.837	1.832	1.671	1.848	1.859	1.873	1.584	1.907	1.941	1.958
Ca_B	1.835	1.852	1.837	1.832	1.671	1.848	1.859	1.873	1.584	1.907	1.941	1.958
Na	0.280	0.281	0.270	0.297	0.314	0.284	0.298	0.291	0.313	0.036	0.077	0.225
Na_B	0.165	0.148	0.163	0.168	0.314	0.152	0.141	0.127	0.313	0.036	0.059	0.042
Na_A	0.115	0.133	0.107	0.129	0.000	0.132	0.157	0.163	0.000	0.000	0.019	0.183
K	0.107	0.112	0.114	0.111	0.139	0.119	0.115	0.106	0.136	0.011	0.027	0.113
Mg#	0.439	0.445	0.430	0.462	0.525	0.444	0.449	0.443	0.546	0.753	0.715	0.587
$(Ca+Na_B)$	2.000	2.000	2.000	2.000	1.985	2.000	2.000	2.000	1.897	1.943	2.000	2.000
$(Na+K)_A$	0.222	0.245	0.221	0.240	0.139	0.251	0.272	0.269	0.136	0.011	0.046	0.296

Sample	ZC4♤	ZC4♤	ZC4♤	ZC32	ZC32	ZC32	ZC32	ZC32	ZC32	ZC32	ZC32	ZC32
Posit.	M	M	R	C	R	C	R	C	R	C	M	R
SiO_2	47.39	47.34	47.10	43.94	45.38	44.16	45.06	43.76	50.39	43.29	43.70	42.92
TiO_2	0.29	0.27	0.30	0.27	0.25	0.28	0.26	0.27	0.18	0.28	0.26	0.28
$Al2O_3$	9.85	10.11	9.42	14.89	13.03	14.03	13.03	15.33	7.30	15.78	15.62	16.45
Fe_2O_3	0.72	2.18	0.65	2.58	2.69	2.88	3.27	2.64	4.11	2.64	2.94	1.99
FeO	13.43	12.37	13.98	12.95	12.50	12.73	12.52	13.35	10.09	13.56	12.82	13.92
MnO	0.63	0.61	0.53	0.36	0.39	0.36	0.35	0.37	0.38	0.41	0.37	0.36
MgO	11.57	11.67	11.26	8.88	9.88	9.31	9.82	8.70	13.27	8.19	8.65	8.16
CaO	12.46	12.33	12.32	11.81	11.94	11.98	12.02	12.04	12.01	11.84	11.80	12.14
Na_2O	0.89	0.85	0.89	0.98	0.85	0.89	0.87	0.98	0.54	0.98	0.94	0.93
K_2O	0.62	0.61	0.61	0.34	0.27	0.31	0.27	0.35	0.09	0.43	0.43	0.49
Total	97.85	98.34	97.05	97.01	97.18	96.93	97.47	97.78	98.35	97.38	97.52	97.64
Cations per 23 oxygen atoms												
Si	6.938	6.885	6.969	6.488	6.669	6.530	6.621	6.426	7.215	6.389	6.423	6.330
Ti	0.032	0.030	0.033	0.030	0.028	0.031	0.029	0.030	0.019	0.031	0.029	0.031
Al4	1.062	1.115	1.031	1.512	1.331	1.470	1.379	1.574	0.785	1.611	1.577	1.670
Al6	0.638	0.618	0.612	1.079	0.926	0.976	0.877	1.080	0.447	1.134	1.129	1.189
Fe3	0.080	0.238	0.072	0.287	0.297	0.321	0.362	0.292	0.442	0.293	0.325	0.221
Fe2	1.644	1.505	1.730	1.600	1.537	1.574	1.538	1.639	1.208	1.673	1.575	1.717
Mn	0.078	0.075	0.066	0.045	0.049	0.045	0.044	0.046	0.046	0.051	0.046	0.045
Mg	2.525	2.530	2.484	1.954	2.164	2.052	2.151	1.905	2.832	1.802	1.895	1.794
Ca	1.955	1.921	1.953	1.868	1.880	1.898	1.892	1.895	1.843	1.872	1.858	1.918
Ca_B	1.955	1.921	1.953	1.868	1.880	1.898	1.892	1.895	1.843	1.872	1.858	1.918
Na	0.253	0.240	0.255	0.281	0.242	0.255	0.248	0.279	0.150	0.280	0.268	0.266
Na_B	0.045	0.079	0.047	0.132	0.120	0.102	0.108	0.105	0.150	0.128	0.142	0.082
Na_A	0.207	0.161	0.209	0.149	0.122	0.153	0.140	0.174	0.000	0.153	0.126	0.184
K	0.116	0.113	0.115	0.064	0.051	0.058	0.051	0.066	0.016	0.081	0.081	0.092
Mg#	0.606	0.627	0.589	0.550	0.585	0.566	0.583	0.538	0.701	0.519	0.546	0.511
$(Ca+Na_B)$	2.000	2.000	2.000	2.000	2.000	2.000	2.000	2.000	1.993	2.000	2.000	2.000
$(Na+K)_A$	0.323	0.274	0.324	0.213	0.173	0.211	0.191	0.240	0.016	0.234	0.207	0.276

Table 4.4 (contd.)

Sample	ZC32	ZC32	ZC49	ZC49	ZC49	ZC49	ZC49	ZC49	ZC49	ZC49
Posit.	C	R	C	R	C	R	C	R	C	R
SiO_2	44.18	46.15	50.80	51.85	47.48	49.64	52.04	51.50	49.72	50.39
TiO_2	0.28	0.28	0.06	0.07	0.17	0.09	0.10	0.12	0.14	0.10
Al_2O_3	15.75	12.21	5.91	4.60	9.99	7.61	4.78	4.89	8.12	7.37
Fe_2O_3	1.53	2.44	0.42	0.77	2.01	1.37	1.01	0.00	0.48	0.26
FeO	13.81	12.07	13.21	12.78	12.82	13.07	12.21	12.99	13.61	13.88
MnO	0.31	0.36	0.48	0.48	0.46	0.48	0.50	0.52	0.56	0.58
MgO	8.58	10.35	12.89	13.55	10.89	12.27	13.78	13.44	12.18	12.43
CaO	11.99	11.78	12.33	12.38	11.71	12.34	12.32	12.44	12.56	12.68
Na_2O	0.94	0.78	0.46	0.34	0.75	0.57	0.36	0.45	0.60	0.55
K_2O	0.37	0.26	0.27	0.20	0.56	0.38	0.20	0.22	0.36	0.31
Total	97.73	96.67	96.83	97.03	96.84	97.82	97.30	96.57	98.33	98.56
Cations per 23 oxygen atoms										
Si	6.473	6.783	7.434	7.554	6.994	7.222	7.543	7.547	7.198	7.277
Ti	0.031	0.031	0.007	0.008	0.019	0.010	0.011	0.013	0.015	0.011
Al4	1.527	1.217	0.566	0.446	1.006	0.778	0.457	0.453	0.802	0.723
Al6	1.192	0.899	0.454	0.343	0.728	0.527	0.360	0.392	0.584	0.532
Fe3	0.168	0.270	0.046	0.085	0.223	0.150	0.110	0.000	0.052	0.029
Fe2	1.692	1.483	1.617	1.558	1.580	1.590	1.480	1.592	1.648	1.677
Mn	0.038	0.045	0.060	0.059	0.057	0.059	0.061	0.065	0.069	0.071
Mg	1.874	2.268	2.812	2.943	2.391	2.661	2.977	2.936	2.629	2.676
Ca	1.882	1.855	1.933	1.933	1.848	1.924	1.913	1.953	1.948	1.962
Ca_B	1.882	1.855	1.933	1.933	1.848	1.924	1.913	1.953	1.948	1.962
Na	0.267	0.222	0.131	0.096	0.214	0.161	0.101	0.128	0.168	0.154
Na_B	0.118	0.145	0.067	0.067	0.152	0.076	0.087	0.047	0.052	0.038
Na_A	0.149	0.078	0.064	0.029	0.062	0.084	0.015	0.081	0.117	0.116
K	0.069	0.049	0.050	0.037	0.105	0.071	0.037	0.041	0.066	0.057
Mg#	0.526	0.605	0.635	0.654	0.602	0.626	0.668	0.648	0.615	0.615
$(Ca+Na_B)$	2.000	2.000	2.000	2.000	2.000	2.000	2.000	2.000	2.000	2.000
$(Na+K)_A$	0.218	0.127	0.114	0.066	0.167	0.155	0.052	0.122	0.183	0.173

Sample	ZC49	ZC49	ZC49	ZC49	ZC49	ZC49	ZC66	ZC66	ZC66	ZC66
Posit.	C	R	C	R	C	R	M	R	C	R
SiO_2	50.58	62.13	47.41	57.70	52.68	51.40	42.99	41.22	46.39	44.38
TiO_2	0.10	0.06	0.18	0.08	0.09	0.10	0.26	0.27	0.18	0.27
Al_2O_3	5.83	4.03	10.69	7.35	4.69	5.43	14.42	17.59	10.57	13.30
Fe_2O_3	0.79	0.00	0.70	0.00	0.00	0.00	2.84	1.77	2.76	2.47
FeO	12.53	10.79	14.33	11.54	13.00	12.97	15.54	16.14	14.37	14.89
MnO	0.60	0.39	0.50	0.46	0.50	0.51	0.38	0.37	0.38	0.32
MgO	13.21	11.31	10.75	8.54	13.58	12.98	7.57	6.24	9.91	8.60
CaO	12.38	10.45	12.47	9.99	12.38	12.47	12.07	11.96	12.21	12.16
Na_2O	0.48	0.33	0.78	0.59	0.34	0.42	0.91	1.01	0.76	0.87
K_2O	0.31	0.18	0.51	0.39	0.20	0.24	0.47	0.58	0.34	0.33
Total	96.81	99.67	98.32	96.64	97.46	96.52	97.44	97.15	97.87	97.59
Cations per 23 oxygen atoms										
Si	7.402	8.670	6.914	8.408	7.624	7.549	6.428	6.187	6.838	6.580
Ti	0.011	0.006	0.020	0.009	0.010	0.011	0.029	0.030	0.020	0.030
Al4	0.598	0.000	1.086	0.000	0.376	0.451	1.572	1.813	1.162	1.420
Al6	0.408	0.663	0.752	1.262	0.424	0.489	0.970	1.298	0.674	0.905
Fe^{3+}	0.087	0.000	0.077	0.000	0.000	0.000	0.319	0.200	0.306	0.276
Fe^{2+}	1.534	1.259	1.748	1.406	1.573	1.593	1.943	2.026	1.771	1.846
Mn	0.074	0.046	0.062	0.057	0.061	0.063	0.048	0.047	0.047	0.040
Mg	2.882	2.353	2.337	1.855	2.930	2.842	1.687	1.396	2.178	1.901
Ca	1.941	1.562	1.949	1.560	1.920	1.962	1.934	1.923	1.928	1.932
Ca_B	1.941	0.893	1.949	1.152	1.920	1.962	1.934	1.923	1.928	1.932
Na	0.136	0.089	0.221	0.167	0.095	0.120	0.264	0.294	0.217	0.250
Na_B	0.059	0.089	0.051	0.167	0.080	0.038	0.066	0.077	0.072	0.068
Na_A	0.077	0.000	0.169	0.000	0.015	0.082	0.198	0.217	0.146	0.182
K	0.058	0.032	0.095	0.073	0.037	0.045	0.090	0.111	0.064	0.062
Mg#	0.653	0.651	0.572	0.569	0.651	0.641	0.465	0.408	0.552	0.507
$(Ca+Na_B)$	2.000	1.651	2.000	1.727	2.000	2.000	2.000	2.000	2.000	2.000
$(Na+K)_A$	0.135	0.032	0.264	0.073	0.052	0.127	0.288	0.328	0.210	0.244

Mg# = Mg / (Mg + Fe^{2+}); C = Core; M = Middle; R = Rim; * = Amphibole associated with scheelite grains;°Amphibole co-existing with plagioclase (used in Fig. 4.6C); ♤ Amphibole containing plagioclase inclusion (used in Fig. 4.6C).N. B. The underline indicates the various positions within the single grain. Detection limits for the analysed oxides are tabulated in Appendix 4.2.

The calcic amphiboles in the area of under consideration range in composition from tschermakite to actinolite (end members) and are classified as ferro-tschermakite, ferro-tschermakitic and tschermakitic hornblende, ferro and magnesio-hornblende, actinolitic hornblende and actinolite after the Leake (1978) nomenclature (Fig. 4.15).

Compositional variation was noticed within the single grain of the calcic amphibole. Marginal depletion of Al_2O_3 as compare to the core in the studied amphibole is dominant. However, an opposite relationship (marginal enrichment of Al_2O_3) is also noticed, suggesting that prograde metamorphism is still preserved in these rocks (Table 4.4, Fig. 4.16 A).

Co-existing amphibole and plagioclase are widely used for pressure-temperature estimation in the metamorphic rocks (see Spear 1980; Plyusnina 1982). Where the systematic partitioning of X_{An} / X_{Ab} in plagioclase and Ca, M_4/ Na, M_4) in amphibole is generally accounted for geothermometry (Spear 1980; Perchuk 1966). These pairs appear to have been developed under equilibrium condition and systematic partitioning of Na and Ca has occurred between plagioclase and M_4 site of the co-existing amphibole with Ca enriched in the plagioclase. In order to assess the temperature estimation in the Miniki Gol calc-silicate rocks, two pairs of coexisting ferro-tschermakitic hornblende and anorthite in scheelite-bearing calc-silicate quartzite (Fig. 4.16 C, Table 4.4, ZC 65) and coexisting andesine and magnesio-hornblende in barren calc-silicate quartzite were selected (ZC 4, Table 4.4). From the Spear (1980) diagram $\ln(X_{An} / X_{Ab})$ vs. $\ln(Ca, M_4/ Na, M_4)$ the tschermakitic-hornblende and anorthite data plot between the contours 650 ± 25°C and 725 ± 25°C, whereas the andesine and magnesio-hornblende composition gives a temperature between 530 ± 20°C and 490 ± 20°C (Fig. 4.16 C).

A general agreement was also observed, when these estimates were checked with the criteria described for the correlation of temperature with increase in TiO_2, Na_2O Al_2O_3 from actinolite to tschermakite (Ernst 1972; Raase 1974; Plyusnina 1982). Spear (1980) model is used with the understanding that the temperature obtained is probably not accurate to more than ± 50°C. Thus the tschermakite-anorthite pairs probably developed between 600-650°C. This temperature estimate is compatible with the upper amphibolite facies deduced by Leake et al. (1989) on the basis of mineral assemblages. The tschermakitic amphiboles in the studied area are aluminous with Al_2O_3 reaching up to 18.04 wt % (Table 4.4). The high alumina appear to be regional in N. Pakistan as maintained by Jan and Howie (1982).

The high tschermakitic content reflects high pressure conditions and the Al-content, particularly Al_6 is generally considered as an indication of increasing pressure (Raase 1974; Leake 1965; cf. Doolan et al. 1978). On Al_6 vs. Si diagram (Fig. 4.16 B) of the

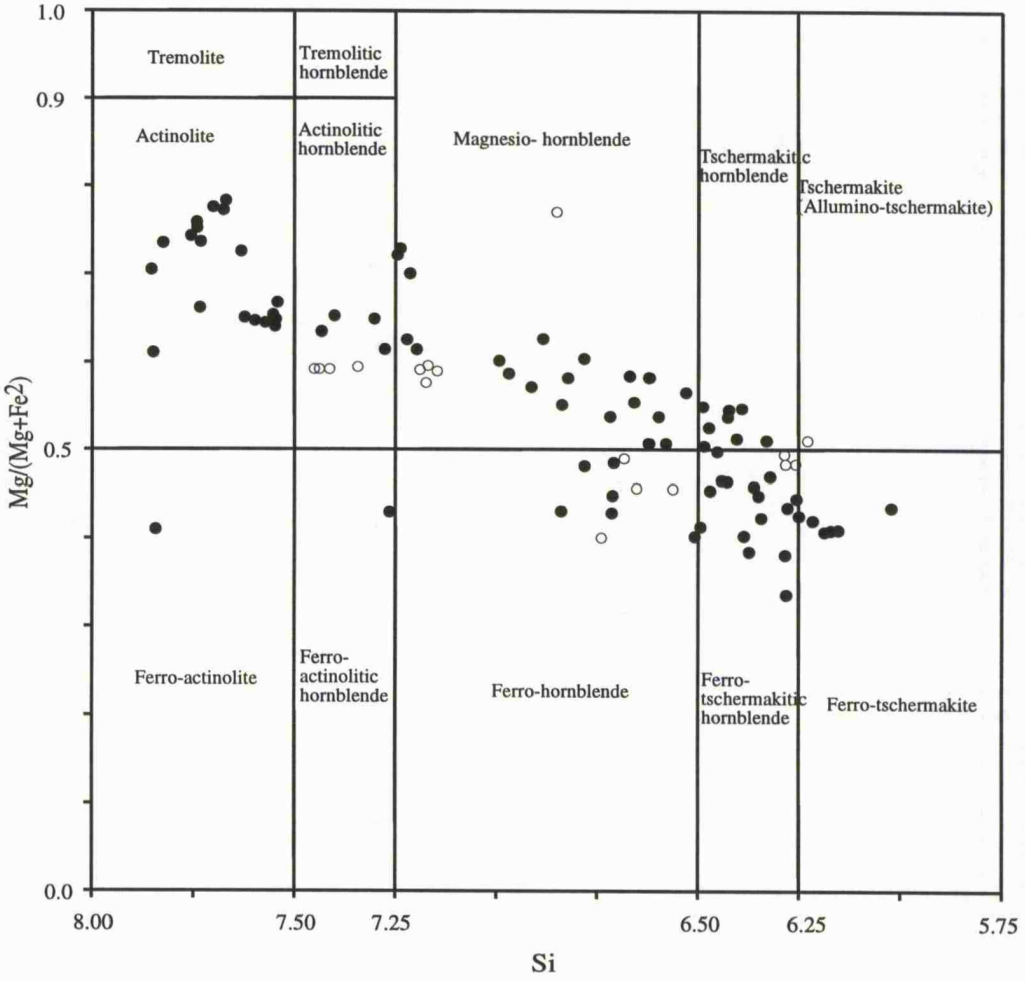

Fig. 4.15: Compositions of Miniki Gol amphiboles on the classification diagram of Leake (1978). The open circles indicate amphibole associated with scheelite grains whereas the filled circles show amphibole not directly associated with scheelite grains in the calc-silicate quartzite. Data taken from Table 4.4.

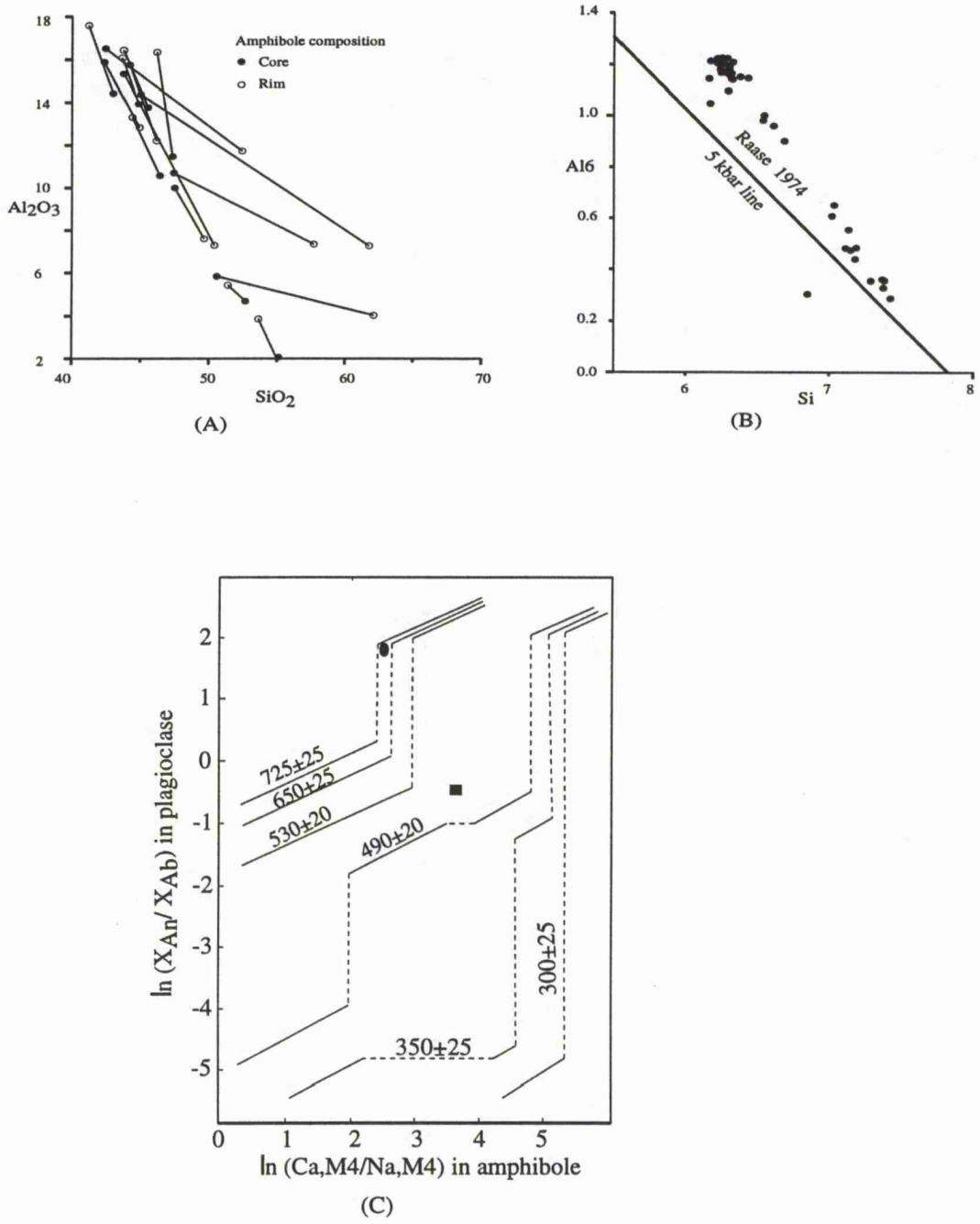

Fig. 4.16: **(A)** Relationship of wt % Al_2O_3 with SiO_2 indicating core and rim compositions of studied amphiboles. Tie lines show core and rim compositions within a single grain. **(B)** Plot of Al6 vs. Si of Miniki Gol amphiboles, the line indicates an assumed pressure of 5 kbar after (Raase 1974). **(C)** Plot of (Ca/Na) vs. (X_{An}/X_{Ab}) of studied amphibole and plagioclase superimposed on the Spear (1980) contours. The ellipse indicates the Miniki Gol anorthite-tschermakite composition of scheelite-bearing quartzite and square shows the andesine-magnesio-hornblende composition of barren calc-silicate quartzite. M4 = B-site; (X_{An}/X_{Ab})= Ca / Na. Data taken from Table 4.4 and 4.8.

calcic-amphibole from the scheelite-bearing calc-silicate quartzites at Miniki Gol, plot above the 5 kbar line of Raase (1974). However, this should be treated with caution because according to Engel and Engel (1962) the mere Al content of the amphibole can not be used as pressure parameter. Excessive alumina in these amphiboles might be influenced by bulk rock composition, fO_2 and the nature of the hydrothermal fluid.

4.4.5 Chlorite

Microprobe data for chlorite are listed in Table 4.5, summarising the result of 46 representative points analysed within ten samples. The number of cations in the unit cell were calculated on the basis of 28 oxygen, assuming the total iron as Fe^{+2}. The Si deficiency in the tetrahedral coordination is compensated by Alz (tetrahedral alumina), whereas the unassigned alumina is placed in the octahedral site (Aly) see (Table 4.5).

Chlorite in schist of the area under consideration is different clearly from the calc-silicate quartzite (Table 4.5). The composition of the former falls in the field of ripidolite, whereas the later plots between the field of ripidolite and brunsvigite (Fig. 4.17 A) of Foster (1962). Chlorite of the Miniki Gol calc-silicate quartzite is relatively rich in silica, ranging from 25.86 to 30.62 wt %, whereas in the schist, it ranges from 23.78 to 25.99 wt % see (Table 4.5). Low values of Al_2O_3 of chlorite are noted in the calc-silicate quartzite, ranging from 18.34 to 22.47 wt % and in schist from 21.92 to 24.36 wt %. Similarly, the level of FeO in chlorite is higher in the schist than in scheelite-bearing calc-silicate quartzite. In contrast, MgO values in chlorite are low in the schist compared with those of scheelite-bearing calc silicate quartzite see (Table 4.5).

Chlorite, from the calc-silicate quartzite, exhibits low Alz values compared with those of the schist (Table 4.5). This level of Alz is compatible with the chlorite from igneous rocks (Bailey 1988; Abdel-Rahman 1995). The chlorites in the investigated area occupy two different positions on the diagram {Alz vs. $Fe^{2+}/(Fe^{2+} + Mg)$} but plot within the compositional field of metamorphic rocks (Fig. 4.17 B) after Bailey (1988). Most of the analyses of chlorites from Miniki Gol calc-silicates quartzite fall within the field of Pan-African Nubian igneous chlorites (Fig. 4.17 B) of Abdel-Rahman (1995).

4.4.6 Biotite

Biotite is one of the dominant constituents in the schist and mica quartzite but also has been found in the leucogranite and calc-silicate quartzite at Miniki Gol. A summary of microprobe data of 178 analyses from 12 sample in the studied biotite is given in the (Table 4.6). Structural formula were calculated on the basis of 22 oxygen, assuming total Fe as Fe^{+2}. The following are the main characteristics of the biotite at Miniki Gol.

Table 4.5: Microprobe analyses of chlorite from schist (ZC 1, ZC 9, ZC 25 and ZC 45)**, mica quartzite** (ZC 4A)**, barren calc-silicate quartzite** (ZC 27, ZC 32 and ZC 50) **and scheelite-bearing calc-silicate quartzite** (ZC 65A) **at Miniki Gol.**

Sample	ZC1	ZC1	ZC1	ZC1	ZC2	ZC2	ZC	ZC9	ZC9	ZC9	ZC9	ZC9
SiO_2	24.06	24.09	24.22	24.23	24.48	24.41	24.43	24.27	24.56	23.85	24.35	24.22
TiO_2	0.05	0.04	0.09	0.06	0.08	0.08	0.05	0.07	0.04	0.10	0.09	0.09
Al_2O_3	24.29	24.30	24.33	24.36	23.21	23.37	22.98	23.71	23.44	23.14	23.78	23.84
Cr_2O_3	0.04	0.02	0.03	0.04	0.05	0.03	0.06	0.07	0.03	0.02	0.05	0.05
FeO*	27.72	27.70	28.00	27.95	26.16	25.99	26.24	27.66	27.46	27.16	27.49	27.35
MnO	0.10	0.09	0.09	0.12	0.14	0.14	0.10	0.01	0.01	0.03	0.01	0.02
MgO	11.97	11.73	11.86	11.83	13.55	13.64	13.69	12.41	12.71	12.10	12.47	12.56
CaO	0.01	0.01	0.00	0.01	0.02	0.02	0.01	0.01	0.02	0.01	0.01	0.01
Na_2O	0.07	0.04	0.03	0.02	0.02	0.01	0.01	0.01	0.02	0.01	0.00	0.00
K_2O	0.02	0.01	0.01	0.01	0.01	0.00	0.02	0.01	0.01	0.00	0.05	0.02
Total	88.33	88.03	88.66	88.63	87.72	87.69	87.59	88.23	88.30	86.42	88.30	88.16
Cations per 28 oxygen atoms												
Si	5.088	5.107	5.105	5.106	5.177	5.158	5.177	5.134	5.183	5.153	5.142	5.121
Ti	0.008	0.007	0.015	0.009	0.012	0.012	0.008	0.011	0.007	0.017	0.015	0.015
Alz	2.912	2.893	2.895	2.894	2.823	2.842	2.823	2.866	2.817	2.847	2.858	2.879
Aly	3.143	3.180	3.150	3.157	2.961	2.978	2.917	3.047	3.014	3.045	3.061	3.061
Cr	0.007	0.003	0.004	0.007	0.008	0.004	0.010	0.011	0.004	0.003	0.008	0.008
Fe^{2+}	4.902	4.912	4.936	4.927	4.627	4.592	4.650	4.894	4.847	4.908	4.855	4.836
Mn	0.018	0.016	0.016	0.021	0.025	0.025	0.018	0.002	0.002	0.006	0.002	0.003
Mg	3.773	3.707	3.726	3.716	4.271	4.296	4.324	3.913	3.998	3.896	3.926	3.958
Ca	0.002	0.002	0.000	0.002	0.004	0.004	0.002	0.002	0.004	0.002	0.002	0.002
Na	0.029	0.017	0.012	0.008	0.008	0.004	0.004	0.004	0.008	0.004	0.000	0.000
K	0.006	0.002	0.002	0.002	0.002	0.000	0.006	0.002	0.002	0.000	0.013	0.006
Fe#	0.565	0.570	0.570	0.570	0.520	0.517	0.518	0.556	0.548	0.557	0.553	0.550
Sample	ZC9	ZC9	ZC9	ZC25	ZC25	ZC25	ZC25	ZC27	ZC27	ZC27	ZC27	ZC46
SiO_2	24.50	24.16	24.05	24.60	25.19	23.78	24.21	25.97	25.86	27.27	27.03	24.23
TiO_2	0.06	0.06	0.10	0.08	0.07	0.07	0.03	0.04	0.01	0.03	0.03	0.07
Al_2O_2	23.44	23.77	23.13	23.71	22.54	23.67	23.02	21.97	21.98	22.47	22.33	23.10
Cr_2O_3	0.05	0.07	0.03	0.01	0.02	0.03	0.03	0.00	0.01	0.01	0.00	0.03
FeO*	27.35	27.63	26.75	26.70	26.50	27.24	27.22	28.61	29.13	26.33	26.57	28.76
MnO	0.05	0.02	0.02	0.02	0.11	0.04	0.10	0.38	0.35	0.36	0.34	0.20
MgO	12.53	12.28	12.44	12.90	13.17	12.46	12.49	11.59	11.76	10.22	10.64	11.24
CaO	0.01	0.02	0.02	0.02	0.00	0.01	0.01	0.04	0.05	2.72	2.28	0.04
Na_2O	0.00	0.01	0.00	0.13	0.00	0.01	0.01	0.06	0.05	0.03	0.03	0.01
K_2O	0.02	0.02	0.00	0.13	0.03	0.01	0.00	0.05	0.01	0.01	0.01	0.02
Total	88.01	88.04	86.54	88.30	87.63	87.32	87.12	88.71	89.21	89.45	89.26	87.70
Cations per 28 oxygen atoms												
Si	5.187	5.124	5.174	5.176	5.331	5.083	5.187	5.487	5.447	5.663	5.628	5.198
Ti	0.010	0.010	0.016	0.012	0.011	0.011	0.004	0.007	0.001	0.004	0.004	0.011
Alz	2.813	2.876	2.826	2.824	2.669	2.917	2.813	2.513	2.553	2.337	2.372	2.802
Aly	3.035	3.067	3.040	3.056	2.955	3.045	3.000	2.958	2.903	3.162	3.108	3.039
Cr	0.008	0.011	0.006	0.001	0.003	0.006	0.006	0.000	0.001	0.001	0.000	0.006
Fe^{2+}	4.842	4.901	4.813	4.698	4.691	4.869	4.876	5.056	5.132	4.573	4.627	5.160
Mn	0.009	0.003	0.003	0.003	0.020	0.007	0.018	0.068	0.063	0.064	0.060	0.036
Mg	3.954	3.883	3.989	4.047	4.155	3.969	3.988	3.650	3.693	3.164	3.303	3.594
Ca	0.002	0.004	0.004	0.004	0.000	0.002	0.002	0.009	0.011	0.605	0.508	0.009
Na	0.000	0.004	0.000	0.053	0.000	0.004	0.004	0.025	0.020	0.012	0.012	0.004
K	0.006	0.006	0.000	0.035	0.008	0.002	0.000	0.013	0.002	0.002	0.002	0.006
Fe#	0.550	0.558	0.547	0.537	0.530	0.551	0.550	0.581	0.582	0.591	0.583	0.589

Table 4.5 (contd.)

Sample	ZC46	ZC46	ZC4A	ZC4A	ZC4A	ZC4A	ZC32	ZC32	ZC50	ZC50	ZC50
SiO_2	24.51	25.99	28.26	26.57	26.02	29.28	25.94	26.05	29.01	29.27	30.62
TiO_2	0.06	0.06	0.09	0.10	0.02	0.05	0.09	0.07	0.01	0.01	0.02
Al_2O_3	22.85	21.92	21.47	21.57	21.12	20.65	22.10	22.23	19.55	19.33	18.34
Cr_2O_3	0.06	0.03	0.04	0.04	0.04	0.03	0.04	0.01	0.01	0.02	0.01
FeO*	29.09	27.98	26.43	27.74	28.15	27.03	21.58	21.70	21.75	21.81	20.87
MnO	0.21	0.22	0.52	0.59	0.63	0.50	0.29	0.38	0.42	0.39	0.40
MgO	11.03	10.50	10.82	11.22	11.66	10.21	16.99	17.16	16.78	16.82	16.15
CaO	0.01	0.04	0.02	0.02	0.03	0.05	0.04	0.09	0.06	0.09	0.11
Na_2O	0.02	0.17	0.02	0.03	0.02	0.16	0.01	0.02	0.03	0.03	0.04
K_2O	0.02	0.08	0.60	0.26	0.02	0.62	0.00	0.03	0.33	0.32	0.65
Total	87.86	86.99	88.27	88.14	87.71	88.58	87.08	87.74	87.95	88.09	87.21
Cations per 28 oxygen atoms											
Si	5.254	5.580	5.915	5.630	5.562	6.114	5.386	5.374	5.952	5.992	6.294
Ti	0.010	0.010	0.015	0.016	0.003	0.008	0.015	0.011	0.001	0.001	0.003
Alz	2.746	2.420	2.085	2.370	2.438	1.886	2.614	2.626	2.048	2.008	1.706
Aly	3.028	3.127	3.211	3.017	2.883	3.197	2.795	2.779	2.679	2.657	2.737
Cr	0.010	0.006	0.007	0.007	0.007	0.004	0.007	0.001	0.001	0.003	0.001
Fe^{2+}	5.215	5.024	4.627	4.916	5.032	4.721	3.748	3.744	3.732	3.734	3.587
Mn	0.038	0.040	0.092	0.106	0.114	0.088	0.052	0.066	0.073	0.067	0.069
Mg	3.525	3.361	3.376	3.545	3.715	3.179	5.258	5.277	5.132	5.133	4.948
Ca	0.002	0.009	0.004	0.004	0.007	0.011	0.009	0.020	0.013	0.020	0.025
Na	0.008	0.071	0.008	0.012	0.008	0.065	0.004	0.008	0.012	0.012	0.016
K	0.006	0.022	0.160	0.071	0.006	0.165	0.000	0.008	0.086	0.084	0.170
$Fe^{\#}$	0.597	0.599	0.578	0.581	0.575	0.598	0.416	0.415	0.421	0.421	0.420

Sample	ZC65A	ZC65A	ZC65A	ZC65A	ZC65A	ZC65A	ZC65A	ZC65A	ZC65A	ZC65A	ZC65A
SiO_2	26.43	26.63	26.69	26.36	26.38	26.60	26.16	26.40	25.95	26.04	25.88
TiO_2	0.07	0.09	0.03	0.01	0.00	0.05	0.03	0.04	0.08	0.08	0.06
Al_2O_3	21.54	21.52	21.65	21.68	21.69	21.17	21.07	21.93	21.67	21.60	21.58
Cr_2O_3	0.01	0.00	0.01	0.00	0.03	0.00	0.05	0.04	0.02	0.03	0.01
FeO*	21.38	21.51	21.04	21.23	21.35	21.09	21.56	21.64	21.64	21.61	21.87
MnO	0.38	0.39	0.41	0.37	0.41	0.39	0.43	0.40	0.37	0.38	0.44
MgO	16.62	16.73	17.05	16.77	17.02	16.88	16.67	16.81	16.60	16.58	16.70
CaO	0.07	0.10	0.06	0.08	0.01	0.15	0.03	0.01	0.12	0.24	0.14
Na_2O	0.07	0.07	0.02	0.06	0.04	0.04	0.11	0.02	0.06	0.13	0.13
K_2O	0.05	0.08	0.10	0.05	0.00	0.01	0.07	0.01	0.02	0.07	0.05
Total	86.62	87.12	87.06	86.61	86.93	86.38	86.18	87.30	86.53	86.76	86.86
Cations per 28 oxygen atoms											
Si	5.513	5.524	5.524	5.495	5.480	5.554	5.501	5.466	5.433	5.441	5.411
Ti	0.011	0.015	0.004	0.001	0.000	0.008	0.004	0.007	0.012	0.012	0.009
Alz	2.487	2.476	2.476	2.505	2.520	2.446	2.499	2.534	2.567	2.559	2.589
Aly	2.808	2.786	2.806	2.821	2.791	2.764	2.725	2.817	2.781	2.761	2.730
Cr	0.001	0.000	0.001	0.000	0.004	0.000	0.008	0.007	0.003	0.004	0.001
Fe^{2+}	3.730	3.732	3.642	3.702	3.709	3.683	3.792	3.746	3.789	3.777	3.825
Mn	0.067	0.068	0.072	0.065	0.072	0.069	0.076	0.071	0.066	0.067	0.078
Mg	5.168	5.173	5.261	5.211	5.271	5.254	5.226	5.188	5.181	5.164	5.205
Ca	0.016	0.022	0.013	0.018	0.002	0.034	0.007	0.002	0.027	0.054	0.031
Na	0.028	0.028	0.008	0.025	0.016	0.016	0.045	0.008	0.025	0.053	0.053
K	0.013	0.021	0.027	0.013	0.000	0.002	0.019	0.002	0.006	0.019	0.013
$Fe^{\#}$	0.419	0.419	0.409	0.415	0.413	0.412	0.421	0.419	0.422	0.422	0.424

*= Total Fe is considered as FeO; Fe# = Fe^{2+} / (Fe^{2+}+ Mg). Detection limits for the analysed oxides are tabulated in Appendix 4.2.

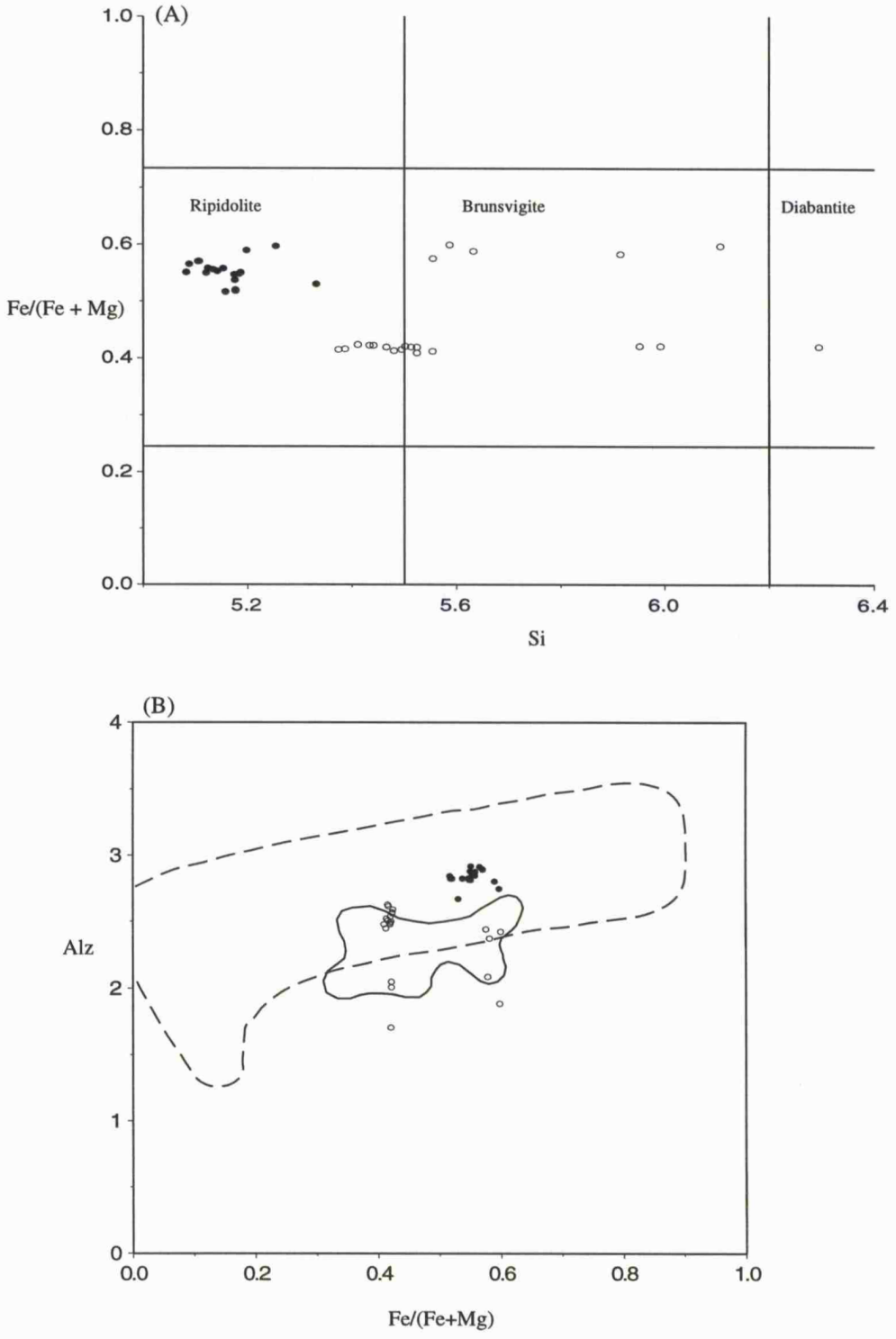

Fig. 4.17: **(A)** Compositional variations of the studied chlorites on the classification scheme of Foster (1962). Open circles = chlorites from calc-silicate quartzite; solid circles =chlorites from schist. **(B)** Plot of Alz vs. Fe/(Fe+Mg) of the Miniki Gol chlorites. The dashed line indicates the field of metamorphic chlorites after Bailey (1988), and the solid line shows the field of Nubian shield igneous chlorites after Abdel-Rahman (1995). Symbols as (Fig. A). Total Fe is considered as Fe^{+2}. Data taken from Table 4.5.

- Most of the mica analyses are compatible with biotite in the sense of Deer et al. (1962) (i.e. Fe / (Fe + Mg) ≥ 0.33), although, some analyses plot on the boundary of phlogopite and biotite (Fig. 4.18 A)
- Compositional variation exists within the biotite from schist and calc-silicate quartzite whereas biotites from leucogranite and granodiorite are homogenous in composition.
- The chemistry of biotite in the scheelite-bearing calc-silicate quartzite is different from that of the barren calc-silicate quartzite.
- Biotite in the scheelite-bearing quartzite contains relatively high levels of SiO_2 and MgO (mean 38.60 and 15.61 respectively) compared with those of barren calc-silicate quartzite (37.43 and 12.50), mica quartzite (37.05 and 8.37), schist (35.82 and 8.72) leucogranite (35.15 and 4.09) and biotite granodiorite (35.27 and 4.27) respectively.
- Low values of Al_2O_3, FeO and TiO_2 in the biotite of scheelite-bearing calc-silicate quartzite have been found compared with other investigated rocks. The average values are as follows; scheelite-bearing calc-silicate quartzite (15.25, 13.41 and 0.60), barren calc-silicate quartzite (17.20, 16.56 and 1.41), mica quartzite (17.55, 19.91 and 2.15), schist (19.31, 20.89 and 1.60), leucogranite (19.16, 24.05 and 1.78) and biotite granodiorite (16.53, 25.44 and 1.19) respectively.

The structure of biotite is flexible and can accept a large amount of cations and even anions, depending on the mineral assemblages (see Labotka 1983), providing some clues to the geochemical activities in the investigated area. According to Dymek (1983), hydrothermal biotite contains low TiO_2 content, which corresponds to the low concentration of TiO_2 in the Miniki Gol scheelite-bearing calc-silicate quartzite indicating hydrous activity in the study area. These Ti values are also consistent with the hydrothermal biotites of Butte, Montana (Brimhall 1977; Brimhall et al. 1985). The low total of the biotite from the scheelite-bearing quartzite also points to H_2O-rich phases in the investigated area (Table 4.6). The concentration of TiO_2 in the Miniki Gol biotite sampled from schist and mica quartzite generally corresponds with the grade of metamorphism (Dymek 1983). However, high grade does not correlate with the Ti-content in the low-grade metamorphosed rock and the phyllitic slate (ZC 61) has high TiO_2 (2.76 wt %, Table 4.6).

Biotite in the granodiorite contains low Al-content than the leucogranite and is noticeably low in the scheelite-bearing quartzite (Fig. 4.18 A, Table 4.6). This low Al_2O_3 has also been reported in many skarns (cf. Robert 1972). The low Al-content and high Si in the scheelite-bearing quartzite reflects high silica activity in these rocks. In contrast, the Al_2O_3 content in the Miniki Gol schist is high, typical of the Al-rich regionally

Table 4.6: Statistical microprobe analyses of the investigated biotite: Schist (ZC 2, ZC 9 and ZC 61), **scheelite-bearing calc-silicate quartzite** (ZC 65A), **barren calc-silicate quartzite** (ZC 4), **mica quartzite** (ZC 4A and ZC 6), **leucogranite** (ZM 3, ZM 52, ZM 70 and NMG1) **and biotite granodiorite** (ZM 86).

Sample	ZC2				ZC9				ZC61			
Analy. Numb·	Min (5)[a]	Max	Mean	Sd[1]	Min (24)[a]	Max	Mean	Sd[1]	Min (6)[a]	Max	Mean	Sd[1]
SiO_2	34.44	37.66	36.46	01.27	35.01	36.84	35.59	00.39	35.68	37.28	36.21	00.73
TiO_2	01.17	01.53	01.40	00.14	01.31	01.51	01.41	00.06	02.00	02.76	02.53	00.29
Al_2O_3	19.56	20.40	19.94	00.37	19.08	19.98	19.61	00.25	17.47	17.89	17.66	00.16
FeO*	19.29	20.69	20.01	00.62	20.70	22.12	21.54	00.36	17.67	19.97	19.01	00.82
MnO	00.03	00.06	00.04	00.01	00.00	00.07	00.03	00.02	00.25	00.36	00.28	00.04
MgO	09.10	11.01	10.07	00.68	07.94	08.87	08.31	00.22	09.00	09.98	09.27	00.37
CaO	00.00	00.02	00.01	00.01	00.00	00.02	00.01	00.01	00.00	00.32	00.06	00.13
Na_2O	00.21	00.28	00.26	00.03	00.22	00.33	00.26	00.03	00.06	00.55	00.16	00.19
K_2O	06.43	08.36	07.84	00.80	07.41	08.36	08.11	00.21	08.90	09.57	09.34	00.24
Total	94.33	98.12	96.03	01.66	93.26	96.81	94.87	00.71	93.80	96.19	94.53	00.87
Cations per 22 oxygen atom												
Si	5.231	5.512	5.442	0.118	5.386	5.494	5.441	0.028	5.506	5.650	5.545	0.057
Ti	0.134	0.168	0.157	0.014	0.150	0.173	0.163	0.006	0.232	0.320	0.292	0.034
Al	3.421	3.652	3.508	0.087	3.447	3.595	3.533	0.038	3.133	3.237	3.188	0.035
Fe^{+2}	2.396	2.629	2.498	0.089	2.690	2.826	2.754	0.040	2.240	2.517	2.435	0.107
Mn	0.004	0.008	0.005	0.002	0.000	0.009	0.003	0.002	0.032	0.047	0.037	0.005
Mg	2.066	2.493	2.241	0.155	1.814	2.008	1.893	0.046	2.056	2.295	2.117	0.089
Ca	0.000	0.004	0.002	0.001	0.000	0.004	0.002	0.001	0.000	0.052	0.010	0.021
Na	0.062	0.083	0.075	0.008	0.065	0.099	0.078	0.009	0.018	0.162	0.048	0.056
K	1.246	1.624	1.493	0.146	1.435	1.636	1.583	0.044	1.720	1.878	1.826	0.061
Total	15.39	15.45	15.42	00.02	15.36	15.49	15.45	00.03	15.40	15.58	15.50	0.062
Fe#	0.513	0.545	0.527	0.012	0.580	0.607	0.593	0.008	0.509	0.546	0.535	0.016
Sample	ZC65A				ZC4				ZC4A			
Analy. Numb·	Min (35)[a]	Max	Mean	Sd[1]	Min (4)[a]	Max	Mean	Sd[1]	Min (16)[a]	Max	Mean	Sd[1]
SiO_2	37.33	39.61	38.60	00.53	37.21	37.85	37.43	00.30	36.10	38.51	36.85	00.69
TiO_2	00.46	00.67	00.60	00.05	01.16	01.52	01.41	00.17	01.76	02.28	02.01	00.11
Al_2O_3	14.53	15.80	15.26	00.23	17.10	17.40	17.20	00.14	17.08	18.26	17.73	00.27
FeO*	12.66	14.13	13.41	00.27	16.13	17.27	16.56	00.49	19.73	20.86	20.29	00.39
MnO	00.14	00.25	00.20	00.02	00.33	00.38	00.36	00.02	00.34	00.44	00.39	00.03
MgO	14.61	16.21	15.62	00.38	12.28	12.79	12.50	00.22	07.94	08.32	08.17	00.13
CaO	00.00	01.52	00.12	00.27	00.00	00.19	00.08	00.08	00.00	00.33	00.05	00.08
Na_2O	00.09	00.43	00.19	00.07	00.08	00.11	00.10	00.01	00.05	00.48	00.13	00.10
K_2O	08.21	09.67	09.23	00.36	08.45	09.74	09.32	00.59	08.79	09.91	09.64	00.28
Total	90.52	94.59	93.22	01.14	94.12	96.06	94.95	00.81	94.33	96.36	95.25	00.55
Cations per 22 oxygen atom												
Si	5.754	5.898	5.816	0.032	5.613	5.639	5.628	0.013	5.575	5.806	5.632	0.074
Ti	0.053	0.075	0.068	0.006	0.132	0.172	0.160	0.019	0.203	0.261	0.231	0.013
Al	2.644	2.823	2.711	0.037	3.040	3.054	3.048	0.006	3.085	3.240	3.193	0.044
Fe^{+2}	1.610	1.762	1.690	0.034	2.030	2.189	2.082	0.073	2.479	2.673	2.594	0.063
Mn	0.018	0.032	0.025	0.003	0.042	0.048	0.045	0.003	0.044	0.057	0.051	0.004
Mg	3.302	3.608	3.508	0.058	2.774	2.832	2.800	0.024	1.785	1.907	1.862	0.035
Ca	0.000	0.247	0.019	0.044	0.000	0.031	0.012	0.013	0.000	0.054	0.008	0.013
Na	0.026	0.126	0.056	0.021	0.023	0.033	0.028	0.004	0.015	0.140	0.038	0.030
K	1.588	1.838	1.775	0.056	1.633	1.874	1.788	0.106	1.719	1.934	1.879	0.058
Total	15.44	15.73	15.67	00.05	15.53	15.64	15.59	00.05	15.32	15.56	15.49	0.073
Fe#	0.315	0.340	0.325	0.006	0.419	0.441	0.426	0.010	0.575	0.591	0.582	0.005

Table 4.6 (contd.)

Sample	ZC6				ZM3				ZM52			
Analy. Numb.	Min (9)[a]	Max	Mean	Sd[1]	Min (20)[a]	Max	Mean	Sd[1]	Min (17)[a]	Max	Mean	Sd[1]
SiO_2	34.98	39.78	37.39	01.48	34.65	36.04	35.20	00.30	34.89	36.22	35.30	00.29
TiO_2	02.14	02.77	02.42	00.19	01.65	01.98	01.81	00.07	01.68	01.96	01.83	00.08
Al_2O_3	16.34	17.74	17.26	00.47	18.81	19.79	19.22	00.27	18.68	19.57	19.19	00.21
FeO*	17.58	20.12	19.24	00.73	22.72	25.33	24.11	00.77	23.22	24.37	23.73	00.31
MnO	00.08	00.20	00.16	00.04	00.46	00.63	00.54	00.04	00.49	00.63	00.55	00.04
MgO	06.16	09.45	08.74	01.00	03.83	04.30	04.08	00.15	03.86	04.04	03.98	00.05
CaO	00.03	00.54	00.12	00.16	00.00	00.03	00.01	00.01	00.00	00.33	00.05	00.08
Na_2O	00.09	01.48	00.33	00.46	00.05	00.15	00.09	00.03	00.03	00.21	00.10	00.04
K_2O	08.27	09.57	09.21	00.40	08.92	09.56	09.28	00.21	08.57	09.51	09.21	00.26
Total	91.76	95.84	94.86	01.27	93.21	95.52	94.34	00.79	93.06	94.52	93.95	00.39
Cations per 22 oxygen atom												
Si	5.551	5.997	5.686	0.156	5.475	5.585	5.536	0.036	5.519	5.699	5.563	0.039
Ti	0.243	0.316	0.277	0.022	0.197	0.235	0.214	0.009	0.199	0.232	0.217	0.009
Al	2.933	3.152	3.095	0.067	3.494	3.678	3.563	0.048	3.464	3.627	3.565	0.036
Fe^{+2}	2.217	2.599	2.449	0.116	2.996	3.323	3.171	0.100	3.055	3.220	3.127	0.041
Mn	0.011	0.026	0.020	0.005	0.062	0.085	0.072	0.006	0.065	0.084	0.074	0.005
Mg	1.384	2.132	1.982	0.231	0.902	1.006	0.958	0.032	0.902	0.952	0.936	0.013
Ca	0.005	0.087	0.020	0.027	0.000	0.005	0.002	0.002	0.000	0.056	0.008	0.014
Na	0.026	0.433	0.096	0.133	0.015	0.045	0.027	0.008	0.009	0.064	0.030	0.013
K	1.590	1.946	1.788	0.099	1.794	1.933	1.863	0.039	1.719	1.915	1.851	0.053
Total	15.15	15.61	15.41	00.15	15.32	15.52	15.41	00.07	15.27	15.42	15.37	0.042
Fe#	0.536	0.616	0.554	0.024	0.758	0.775	0.768	0.004	0.764	0.776	0.770	0.003

Sample	ZM70				NMG1				ZM86			
Analy. Numb.	Min (21)[a]	Max	Mean	Sd[1]	Min (4)[a]	Max	Mean	Sd[1]	Min (17)[a]	Max	Mean	Sd[1]
SiO_2	34.62	35.64	35.05	00.28	34.01	35.29	34.82	00.56	34.54	36.00	35.27	00.38
TiO_2	01.52	01.96	01.78	00.14	01.24	01.78	01.52	00.29	01.04	01.30	01.19	00.07
Al_2O_3	18.43	19.33	19.02	00.29	19.15	19.92	19.55	00.38	16.25	16.82	16.53	00.17
FeO*	23.63	25.40	24.32	00.54	22.66	25.08	23.77	01.22	24.81	26.30	25.44	00.44
MnO	00.45	00.59	00.53	00.04	00.39	00.55	00.49	00.07	00.36	00.47	00.41	00.04
MgO	04.05	04.38	04.16	00.09	03.99	04.32	04.16	00.15	04.14	04.46	04.27	00.09
CaO	00.00	00.13	00.03	00.04	00.06	00.11	00.09	00.02	00.00	00.19	00.04	00.05
Na_2O	00.04	00.12	00.07	00.02	00.18	00.25	00.23	00.03	00.10	00.25	00.18	00.04
K_2O	08.58	09.48	09.10	00.29	08.31	09.20	08.84	00.39	08.87	09.84	09.58	00.22
Total	92.79	95.51	94.06	00.66	93.09	93.90	93.46	00.36	91.85	94.87	92.91	00.84
Cations per 22 oxygen atom												
Si	5.513	5.550	5.534	0.012	5.441	5.550	5.511	0.048	5.657	5.805	5.709	0.034
Ti	0.182	0.232	0.211	0.016	0.148	0.211	0.180	0.034	0.128	0.158	0.145	0.008
Al	3.456	3.581	3.539	0.036	3.570	3.705	3.648	0.059	3.099	3.206	3.154	0.025
Fe^{+2}	3.114	3.370	3.211	0.082	2.990	3.356	3.148	0.182	3.378	3.571	3.444	0.050
Mn	0.061	0.079	0.070	0.005	0.052	0.074	0.066	0.010	0.048	0.064	0.057	0.005
Mg	0.949	1.015	0.979	0.020	0.936	1.018	0.982	0.039	1.001	1.056	1.030	0.018
Ca	0.000	0.022	0.005	0.006	0.010	0.018	0.014	0.003	0.000	0.033	0.006	0.009
Na	0.012	0.036	0.023	0.006	0.055	0.078	0.069	0.011	0.032	0.079	0.055	0.013
K	1.745	1.895	1.833	0.049	1.697	1.846	1.785	0.066	1.831	2.028	1.978	0.044
Total	15.35	15.44	15.40	00.02	15.35	15.46	15.40	00.06	15.44	15.67	15.58	00.05
Fe#	0.760	0.777	0.766	0.005	0.756	0.768	0.762	0.005	0.764	0.775	0.770	0.004

*= Total Fe is considered as FeO; Fe# $=Fe^{2+}/(Fe^{2+}+Mg)$; [a] = Number of analyses in each sample; 1= standard deviation
Detection limits for the analysed oxides are tabulated in Appendix 4.2.

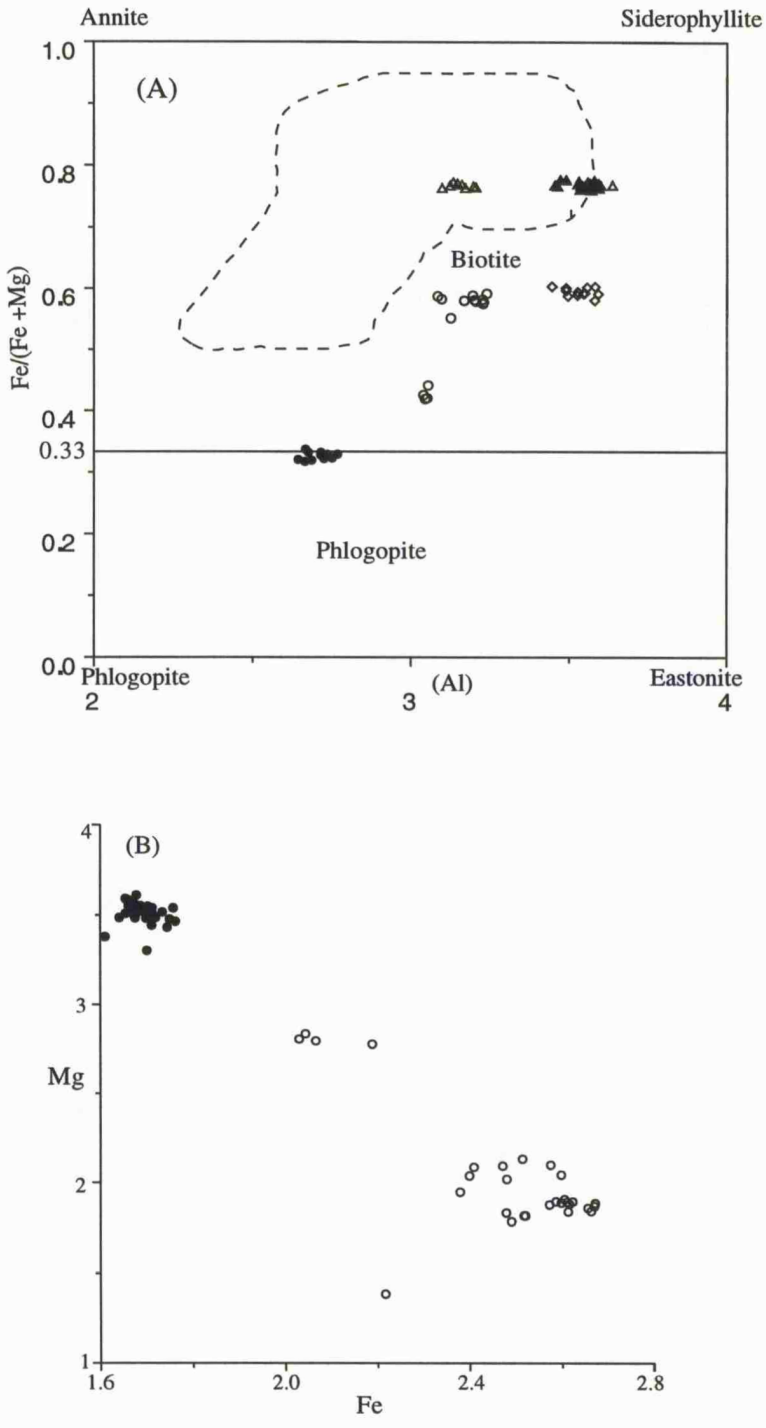

Fig. 4.18: (**A**) Miniki Gol biotite composition in terms of Fe /(Fe+Mg) vs. Al cation. The dashed line indicates the field of Japanese I-series granite, superimposed on the plot, after Lalonde & Bernard (1993). Solid circle = scheelite-bearing calc-silicate quartzite; Open circle = Barren quarzite; Solid triangle = Leucogranite; Open triangle = biotite granodiorite; Open rhomb = schist. Total Fe is considered as Fe^{+2}. (**B**). Cation Fe vs. Mg plot of studied biotite showing negative correlation. Symbols as in (Fig. **A**). Data taken from Table 4.6.

metamorphosed schist (Robert 1972).

When plotted on the diagram of $Fe^{2+}/ (Fe^{2+} + Mg)$ vs. total Al cation (see Fig. 4.18 A), the data falls in the field of ilmenite (I-series granite) of Lalonde and Bernard (1993). The Fe-depletion trend is noted in the biotite from leucogranite to the biotite of scheelite-bearing quartzite at study area (Fig. 4.18 A). The Fe deficiency in the biotite of W-bearing quartzite is compensated by Mg and the negative correlation between these two cations acknowledge the substitution (Fig. 4.18 B).

4.4.7 Titanite (sphene)

Sphene, mostly occurs in calc-silicate and tourmalinite sequence in the study area, however, a few grains have also been found in mica schist. The chemical analyses of sphene from 6 samples shown in Table 4.7 have been recalculated on the basis of 4 Si in the unit cell, rather than on the more usual oxygen atoms following Higgins and Ribbe (1976) and with total Fe considered as FeO. Unfortunately, no large enough sphene grain was found in the schist to compare with the calc-silicate rocks.

One of the striking feature of the sphene in the investigated area is the occurrence of high-Al titanite in one sample from barren calc-silicate quartzite (ZC 27, Table 4.7). Highly aluminous sphene with Al_2O_3 up to 9.31 % and 14.08 % is recorded from eclogite facies by Smith (1980) and in high-pressure schist of New Caledonia by Franz and Spear (1985) respectively. Aluminous sphene with Al_2O_3 up to 5.42 % has also been recorded from the pegmatite of the Strzegom-Sobótka granitic massif, Poland (Janeczek and Sachanbinski 1992). Tulloch (1979) noted that metamorphic sphene is richer in Al-content (6-7 wt % Al_2O_3) than magmatic sphene. However some of the metamorphic sphene analyses from Victoria Range, New Zealand, plot in the igneous field (Fig. 4.19 A), for which Tulloch (1979) argued that Al has preferentially partitioned into the coexisting Ca-Al silicate phase. On the basis of this criterion the Miniki Gol sphene from the both scheelite-bearing and barren calc-silicate rocks (with the exception of ZC 27), correlate with igneous and skarn sphene (Fig. 4.19 A-B). However, four analyses from ZC 65A are Al-rich (Fig. 4.19 B) and plot in the field of metamorphic sphene of Tulloch (1979) diagram. The TiO_2 content of sphene in the calc-silicate rocks (except ZC 27) ranges from 27.63 to 38.00 wt % (mean 34.93 wt %). The inverse relationship of the Ti and Al demonstrates the mutual substitution in the sphene (Fig 4.19 C). The TiO_2 content of studied sphene is also consistent with the sphene from skarn and granitoid rocks (Lee et al. 1969; Deer et al. 1982).

Table 4.7: Chemical analyses of studied sphene of scheelite-bearing calc-silicate quartzite except ZC 4 and ZC 27 (barren calc-silicate quartzite).

Sample	ZC4	ZC4	ZC4	ZC4	ZC4	ZC27	ZC27	ZC27	ZC27	ZC27	ZC27
SiO_2	30.91	30.72	30.68	30.65	30.66	32.32	32.11	31.81	31.90	31.81	31.47
TiO_2	37.75	38.00	37.81	37.42	37.85	27.40	27.78	29.46	29.92	31.25	28.58
Al_2O_3	01.89	01.85	01.75	02.14	01.87	09.44	09.06	08.03	07.73	06.98	08.22
FeO*	00.32	00.34	00.29	00.36	00.35	00.54	00.41	00.48	00.25	00.37	00.38
MnO	00.13	00.16	00.12	00.12	00.15	00.05	00.04	00.09	00.03	00.02	00.01
MgO	00.01	00.01	00.00	00.03	00.01	00.04	00.07	00.05	00.02	00.04	00.11
CaO	29.17	28.86	28.99	28.76	28.93	30.12	30.17	29.99	29.82	29.83	29.85
Na_2O	00.00	00.00	00.01	00.04	00.04	00.00	00.02	00.01	00.00	00.00	00.01
K_2O	00.01	00.01	00.01	00.00	00.00	00.00	00.00	00.00	00.01	00.01	00.00
Total	100.19	99.95	99.66	99.52	99.86	99.91	99.66	99.92	99.68	100.31	98.63
Numbers of ions on the basis of 4 Si											
Si	4.000	4.000	4.000	4.000	4.000	4.000	4.000	4.000	4.000	4.000	4.000
Ti	3.670	3.720	3.710	3.670	3.710	2.550	2.600	2.790	2.820	2.960	2.730
Al	0.290	0.280	0.270	0.330	0.290	1.380	1.330	1.190	1.140	1.030	1.230
Fe+2	0.030	0.040	0.030	0.040	0.040	0.060	0.040	0.050	0.030	0.040	0.040
Mn	0.010	0.020	0.010	0.010	0.020	0.010	0.000	0.010	0.000	0.000	0.000
Mg	0.000	0.000	0.000	0.010	0.000	0.010	0.010	0.010	0.000	0.010	0.020
Ca	4.040	4.030	4.050	4.020	4.040	3.990	4.030	4.040	4.010	4.020	4.070
Na	0.000	0.000	0.000	0.010	0.010	0.000	0.000	0.000	0.000	0.000	0.000
K	0.000	0.000	0.000	0.000	0.000	0.000	0.000	0.000	0.000	0.000	0.000
Total	12.06	12.09	12.08	12.09	12.11	11.99	12.02	12.09	12.01	12.06	12.09
O	19.88	19.96	19.93	19.93	19.97	19.24	19.3	19.47	19.4	19.54	19.44

Sample	ZC27	ZC27	ZC27	ZC27	ZC27	ZC65	ZC65	ZC65	ZC65	ZC65	ZC65
SiO_2	31.45	31.76	30.82	31.33	31.37	31.21	31.29	31.77	31.28	31.35	31.53
TiO_2	28.13	27.59	29.71	30.00	29.65	35.96	36.43	33.22	34.72	34.99	34.30
Al_2O_3	08.92	09.08	07.64	07.59	07.72	03.34	03.04	05.00	03.97	04.18	04.06
FeO*	00.55	00.65	00.55	00.49	00.38	00.20	00.24	00.28	00.18	00.21	00.19
MnO	00.01	00.05	00.03	00.00	00.03	00.06	00.04	00.07	00.04	00.07	00.04
MgO	00.07	00.07	00.05	00.03	00.02	00.01	00.01	00.02	00.02	00.00	00.01
CaO	29.86	29.73	29.78	29.81	29.79	29.29	29.04	29.56	29.57	29.57	29.18
Na_2O	00.02	00.01	00.01	00.00	00.00	00.03	00.03	00.04	00.05	00.02	00.02
K_2O	00.01	00.01	00.01	00.00	00.01	00.02	00.03	00.01	00.03	00.00	00.01
Total	99.02	98.95	98.60	99.25	98.97	100.12	100.15	99.97	99.86	100.39	99.34
Numbers of ions on the basis of 4 Si											
Si	4.000	4.000	4.000	4.000	4.000	4.000	4.000	4.000	4.000	4.000	4.000
Ti	2.690	2.610	2.900	2.880	2.840	3.470	3.500	3.150	3.340	3.360	3.270
Al	1.340	1.350	1.170	1.140	1.160	0.500	0.460	0.740	0.600	0.630	0.610
Fe+2	0.060	0.070	0.060	0.050	0.040	0.020	0.030	0.030	0.020	0.020	0.020
Mn	0.000	0.010	0.000	0.000	0.000	0.010	0.000	0.010	0.000	0.010	0.000
Mg	0.010	0.010	0.010	0.010	0.000	0.000	0.000	0.000	0.000	0.000	0.000
Ca	4.070	4.010	4.140	4.080	4.070	4.020	3.980	3.990	4.050	4.040	3.970
Na	0.000	0.000	0.000	0.000	0.000	0.010	0.010	0.010	0.010	0.000	0.000
K	0.000	0.000	0.000	0.000	0.000	0.000	0.000	0.000	0.000	0.000	0.000
Total	12.18	12.06	12.29	12.16	12.12	12.03	11.98	11.93	12.03	12.06	11.88
O	19.54	19.35	19.78	19.62	19.55	19.76	19.71	19.44	19.67	19.74	19.46

Table 4.7 (Contd.)

Sample	ZC65	ZC65A	ZC65A	ZC65A	ZC65A	ZC65A	ZC65A	ZC66	ZC66	ZC66	ZC66
SiO_2	31.38	31.42	31.35	31.56	31.71	31.25	31.12	30.18	30.10	29.75	28.98
TiO_2	36.40	30.56	31.64	27.63	30.83	34.79	34.01	35.99	35.86	36.11	35.15
Al_2O_3	03.10	06.89	06.13	07.96	05.98	04.11	04.45	02.74	02.73	02.60	03.74
FeO*	00.31	00.43	00.22	01.28	01.13	00.28	00.34	00.37	00.36	00.42	02.35
MnO	00.11	00.12	00.11	00.07	00.05	00.10	00.03	00.09	00.02	00.03	00.17
MgO	00.01	00.03	00.03	00.74	00.60	00.02	00.02	00.01	00.00	00.01	00.03
CaO	29.02	28.53	28.70	26.78	27.37	28.81	28.87	29.32	29.63	29.44	27.84
Na_2O	00.07	00.01	00.00	00.03	00.03	00.01	00.05	00.02	00.02	00.04	00.00
K_2O	00.04	00.08	00.02	00.72	00.46	00.04	00.01	00.00	00.01	00.02	00.02
Total	100.44	98.07	98.20	96.77	98.16	99.41	98.90	98.72	98.73	98.42	98.28
Numbers of ions on the basis of 4 Si											
Si	4.000	4.000	4.000	4.000	4.000	4.000	4.000	4.000	4.000	4.000	4.000
Ti	3.490	2.930	3.040	2.630	2.920	3.350	3.290	3.590	3.580	3.650	3.650
Al	0.470	1.030	0.920	1.190	0.890	0.620	0.670	0.430	0.430	0.410	0.610
Fe+2	0.030	0.050	0.020	0.140	0.120	0.030	0.040	0.040	0.040	0.050	0.270
Mn	0.010	0.010	0.010	0.010	0.010	0.010	0.000	0.010	0.000	0.000	0.020
Mg	0.000	0.010	0.010	0.140	0.110	0.000	0.000	0.000	0.000	0.000	0.010
Ca	3.960	3.890	3.920	3.640	3.700	3.950	3.980	4.160	4.220	4.240	4.120
Na	0.020	0.000	0.000	0.010	0.010	0.000	0.010	0.000	0.000	0.010	0.000
K	0.010	0.010	0.000	0.120	0.070	0.010	0.000	0.000	0.000	0.000	0.000
Total	11.99	11.93	11.93	11.87	11.83	11.97	12	12.24	12.28	12.37	12.67
O	19.71	19.38	19.43	19.04	19.16	19.63	19.62	20.04	20.08	20.23	20.64

Sample	ZC66	ZC66	ZC66	ZC66	ZC66	ZC66	ZC66	ZC66	ZC66	ZC67	ZC67
SiO_2	30.54	30.56	30.61	30.69	30.62	30.59	30.83	30.22	30.79	31.02	31.00
TiO_2	35.95	35.87	35.36	35.29	35.71	34.47	34.58	35.67	35.42	33.16	33.83
Al_2O_3	02.56	02.58	02.79	02.95	02.80	03.47	03.54	02.81	02.87	04.76	04.19
FeO*	00.26	00.24	00.28	00.28	00.31	00.38	00.42	00.40	00.40	00.54	00.58
MnO	00.07	00.07	00.08	00.06	00.10	00.00	00.06	00.03	00.05	00.02	00.01
MgO	00.00	00.01	00.00	00.00	00.01	00.00	00.01	00.02	00.01	00.02	00.02
CaO	28.93	29.50	29.36	29.32	29.77	29.04	29.18	29.09	29.09	28.07	28.03
Na_2O	00.01	00.01	00.02	00.02	00.02	00.02	00.02	00.02	00.02	00.02	00.04
K_2O	00.01	00.01	00.00	00.01	00.01	00.01	00.02	00.02	00.02	00.02	00.03
Total	98.33	98.85	98.50	98.62	99.35	97.98	98.66	98.28	98.67	97.63	97.73
Numbers of ions on the basis of 4 Si											
Si	4.000	4.000	4.000	4.000	4.000	4.000	4.000	4.000	4.000	4.000	4.000
Ti	3.540	3.530	3.480	3.460	3.510	3.390	3.370	3.550	3.460	3.220	3.280
Al	0.390	0.400	0.430	0.450	0.430	0.540	0.540	0.440	0.440	0.720	0.640
Fe+2	0.030	0.030	0.030	0.030	0.030	0.040	0.050	0.040	0.040	0.060	0.060
Mn	0.010	0.010	0.010	0.010	0.010	0.000	0.010	0.000	0.010	0.000	0.000
Mg	0.000	0.000	0.000	0.000	0.000	0.000	0.000	0.000	0.000	0.000	0.000
Ca	4.060	4.140	4.110	4.090	4.170	4.070	4.060	4.130	4.050	3.880	3.880
Na	0.000	0.000	0.000	0.000	0.000	0.000	0.000	0.000	0.000	0.000	0.010
K	0.000	0.000	0.000	0.000	0.000	0.000	0.000	0.000	0.000	0.000	0.000
Total	12.04	12.11	12.06	12.05	12.16	12.04	12.03	12.18	12.01	11.89	11.88
O	19.78	19.85	19.76	19.74	19.89	19.7	19.68	19.94	19.69	19.46	19.48

*= Total Fe is considered as FeO. Detection limits for the analysed oxides are tabulated in Appendix 4.2.

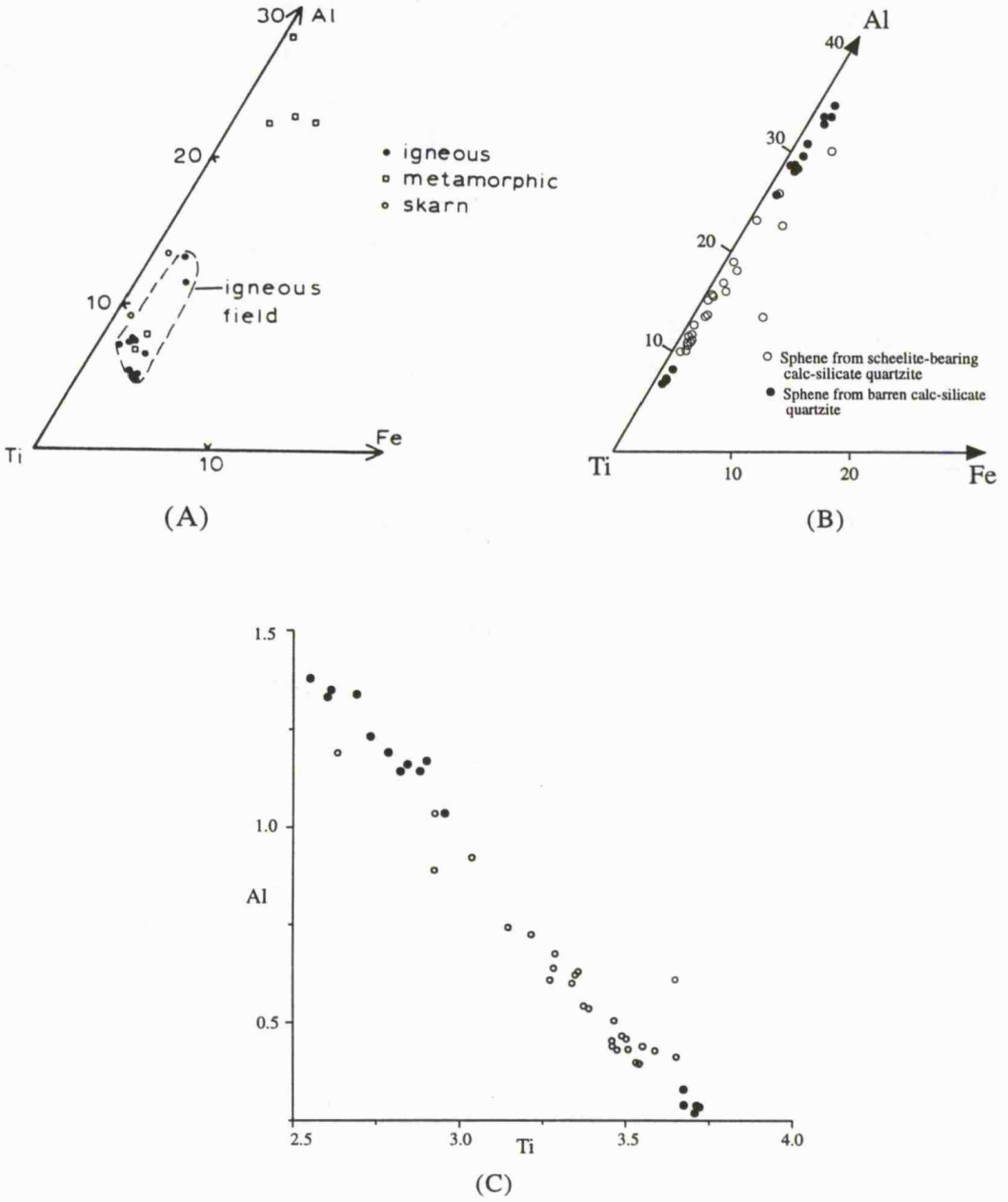

Fig. 4.19: (**A**) Composition of sphene in granitiod rocks, paragneisss skarn and metamorphic rocks from the Victoria Range, New Zealand, after Tulloch (1979). (**B**) Composition of Minki Gol sphene in terms of cations Al, Ti and Fe from calc-silicate rocks. (**C**) Plot of cations Ti vs. Al from the investigated sphene. Symbols as in (Fig. B). Data taken from Table 4.7

4.4.8 Plagioclase

Plagioclase occurs almost in every lithology of the Miniki Gol and surrounding rocks. Table 4.8 shows 72 representative microprobe analyses (selected out of 350 analyses) of plagioclase from 16 samples. Plagioclase in the scheelite-bearing rocks (ZC 65) and marble (ZC 56) is highly anorthitic ranging from An_{84-92} and An_{89-92} respectively, whereas plagioclase from leucogranite, pegmatite and Besti Gol schist is very albitic (Table 4.8). Anorthite content of the plagioclase from Miniki Gol schist and mica quartzite ranges from An_{19-31} and An_{20-34} respectively. Anorthite content of the plagioclase from tourmalinite and barren calc-silicate quartzite (ZC 27), is also high and reaches up to An_{49} and An_{88} respectively (see Table 4.8). However, the content in the barren calc-silicate quartzite (ZC 4, used in geothermometry, Fig. 4.16 C), is low and ranges from An_{29-43}.

The An content of plagioclase form Besti Gol green schist, is very low as compared to Miniki Gol garnet mica schist and scheelite-bearing calc-silicate quartzite (Table 4.8). This is compatible with the observation of Rambaldi (1973) and Goldsmith (1982), that the increase in anorthite content in the metamorphic rocks is correlated, generally, with increasing metamorphic grade. However Höy (1976) suggested that the anorthite content also greatly depends on the bulk rock chemistry, X_{CO_2} and temperature. This interpretation correlates with the high anorthite content of the plagioclase from the marble in the investigated area (ZC 56, Table 4.8). The composition of plagioclase from schist, mica quartzite, granite and pegmatite within a single grain is homogenous. However, compositional variation does exist within single grains of plagioclase from calc-silicate quartzite and tourmalinite. Positive zoning i.e. the marginal enrichment of CaO and negative zoning i.e. the marginal depletion of CaO have been observed within single grains of plagioclase from tourmalinite (ZC 40) and calc-silicate quartzite (ZC 4, ZC 27, ZC 65 Table 4.8). This normal and reverse zoning seems to be related to prograde and retrograde metamorphism respectively (Höy 1976). A partial marginal depletion of CaO is also noticed in the plagioclase of leucogranite and pegmatite, reflecting a cooling trend in these granites. The occurrence of pure albitic plagioclase in the Miniki Gol leucogranite and pegmatite is consistent with its classification as a peralumious granite (Schwartz 1992).

4.4.9 Scheelite

Microprobe analyses of scheelite are given in Table 4.9. Scheelite from both the rock types, is virtually Mo free; Y, Ti, Sn, Fe and Mn have also not been found. The outstanding feature of the scheelite in the investigated area is the occurrence of zirconium and to a lesser extent tantalum, of up to 0.46 and 0.35 wt % respectively (Table 4.9).

Table 4.8: Chemical composition of investigated plagioclase from schist (ZC 1, ZC 2, ZC 9, ZC 25 and ZM 105), **marble (ZC 56), mica quartzite** (ZC 4A and ZC 6), **tourmalinite** (ZC 40), **barren calc-silicate quartzite** (ZC 27 and ZC 4), **scheelite-bearing calc-silicate quartzite** (ZC 65), **leucogranite** (ZC 20 and ZM 70) **and pegmatite** (ZS 12).

Sample	ZC1	ZC1	ZC1	ZC1	ZC2	ZC2	ZC2	ZC2	ZC9	ZC9	ZC9	ZC9
Posit.	C	R	M	R	C	R	C	R	C	R	C	R
SiO_2	60.39	60.48	61.15	61.58	62.10	62.46	62.11	62.63	63.04	62.94	64.09	63.04
TiO_2	00.01	00.02	00.00	00.01	00.00	00.02	00.01	00.01	00.01	00.01	00.01	00.01
Al_2O_3	24.72	24.93	24.21	24.21	23.62	23.95	23.84	23.32	22.76	22.90	22.79	22.51
FeO	00.03	00.02	00.02	00.09	00.09	00.05	00.03	00.08	00.04	00.03	00.03	00.02
MnO	00.00	00.00	00.03	00.01	00.01	00.03	00.02	00.05	00.02	00.00	00.02	00.03
MgO	00.00	00.00	00.00	00.00	00.00	00.00	00.00	00.00	00.00	00.00	00.00	00.00
CaO	06.48	06.79	05.90	05.82	05.77	05.91	05.34	04.80	04.18	04.19	03.95	03.97
Na_2O	08.17	08.11	08.37	08.54	08.63	08.74	08.76	09.23	09.31	09.27	09.05	09.57
K_2O	00.04	00.05	00.06	00.04	00.10	00.08	00.10	00.11	00.07	00.06	00.06	00.05
Total	99.84	100.4	99.74	100.3	100.32	101.24	100.21	100.23	99.43	99.40	100	99.20
Cations per 32 oxygen atoms												
Si	10.770	10.734	10.894	10.908	10.998	10.967	10.996	11.084	11.208	11.192	11.292	11.237
Ti	0.001	0.003	0.000	0.001	0.000	0.003	0.001	0.001	0.001	0.001	0.001	0.001
Al	5.197	5.215	5.084	5.055	4.931	4.956	4.975	4.865	4.769	4.800	4.733	4.730
Fe^{2+}	0.004	0.003	0.003	0.013	0.013	0.008	0.004	0.012	0.006	0.004	0.004	0.003
Mn	0.000	0.000	0.005	0.001	0.001	0.004	0.003	0.008	0.003	0.000	0.003	0.005
Mg	0.000	0.000	0.000	0.000	0.000	0.000	0.000	0.000	0.000	0.000	0.000	0.000
Ca	1.238	1.292	1.126	1.105	1.094	1.112	1.012	0.910	0.796	0.799	0.746	0.758
Na	2.825	2.790	2.892	2.934	2.963	2.976	3.008	3.168	3.209	3.196	3.092	3.308
K	0.009	0.012	0.014	0.009	0.023	0.018	0.023	0.024	0.015	0.014	0.014	0.012
Total	20.044	20.047	20.018	20.026	20.023	20.044	20.023	20.072	20.008	20.006	19.886	20.052
Mol % An	30.4	31.55	27.94	27.29	26.82	27.09	25.04	22.18	19.8	19.92	19.37	18.59

Sample	ZC25	ZC25	ZC25	ZC25	ZM105	ZM105	ZM105	ZM105	ZC56	ZC56	ZC56	ZC56
Posit.	C	R	C	R	C	R	M	R	C	R	M	R
SiO_2	62.43	62.31	62.50	62.48	68.67	68.45	68.32	68.47	45.02	45.47	57.81	44.93
TiO_2	00.03	00.01	00.01	00.01	00.01	00.01	00.00	00.01	00.01	00.00	00.00	00.01
Al_2O_3	24.15	24.17	24.24	24.27	19.80	19.91	19.81	19.82	35.11	34.50	27.56	34.20
FeO	00.05	00.03	00.05	00.01	00.11	00.11	00.09	00.23	00.01	00.10	00.05	00.12
MnO	00.03	00.01	00.03	00.01	00.01	00.03	00.02	00.00	00.02	00.03	00.02	00.00
MgO	00.01	00.00	00.00	00.00	00.00	00.00	00.01	00.00	00.00	00.00	00.00	00.01
CaO	05.54	05.56	05.57	05.60	00.42	00.53	00.62	00.54	18.90	18.32	14.88	18.19
Na_2O	08.81	08.81	08.77	08.83	10.98	10.84	10.96	10.86	00.85	01.16	00.89	01.09
K_2O	00.08	00.07	00.10	00.09	00.06	00.08	00.07	00.08	00.01	00.02	00.05	00.04
Total	101.13	100.97	101.27	101.3	100.06	99.96	99.90	100.01	99.93	99.60	101.26	98.59
Cations per 32 oxygen atoms												
Si	10.961	10.956	10.959	10.950	11.967	11.944	11.939	11.949	8.314	8.416	10.207	8.403
Ti	0.004	0.001	0.001	0.001	0.001	0.001	0.000	0.001	0.001	0.000	0.000	0.001
Al	4.997	5.009	5.010	5.014	4.067	4.095	4.081	4.077	7.643	7.528	5.736	7.540
Fe^{2+}	0.008	0.004	0.008	0.001	0.017	0.017	0.013	0.033	0.001	0.015	0.008	0.019
Mn	0.004	0.001	0.004	0.001	0.001	0.004	0.003	0.000	0.003	0.005	0.003	0.000
Mg	0.003	0.000	0.000	0.000	0.000	0.000	0.003	0.000	0.000	0.000	0.000	0.003
Ca	1.042	1.047	1.047	1.052	0.078	0.099	0.116	0.101	3.740	3.634	2.815	3.645
Na	2.999	3.004	2.982	3.000	3.711	3.667	3.713	3.675	0.305	0.416	0.305	0.396
K	0.018	0.015	0.022	0.020	0.013	0.018	0.015	0.018	0.003	0.005	0.012	0.009
Total	20.035	20.037	20.033	20.041	19.854	19.844	19.882	19.854	20.009	20.019	19.084	20.017
Mol % An	25.67	25.75	25.85	25.83	2.05	2.6	3.03	2.67	92.41	89.61	89.9	90.01

Table 4.8. (Contd.)

Sample	ZC4A	ZC4A	ZC4A	ZC4A	ZC6	ZC6	ZC6	ZC6	ZC40	ZC40	ZC40	ZC40
Posit.	C	R	M	R	C	R	C	R	C	R	C	R
SiO_2	60.26	60.15	59.88	60.12	63.10	62.90	63.42	63.32	60.64	56.17	55.87	55.41
TiO_2	00.03	00.01	00.02	00.00	00.01	00.02	00.01	00.01	00.02	00.03	00.01	00.03
Al_2O_3	25.29	25.58	25.62	25.46	23.40	22.89	23.16	23.48	24.21	26.35	26.42	26.61
FeO	00.02	00.03	00.02	00.05	00.04	00.00	00.04	00.08	00.04	00.04	00.04	00.07
MnO	00.03	00.03	00.01	00.07	00.02	00.00	00.03	00.05	00.00	00.04	00.03	00.01
MgO	00.01	00.00	00.00	00.00	00.00	00.00	00.00	00.01	00.01	00.00	00.00	00.00
CaO	06.88	07.18	07.22	07.05	04.73	04.17	04.57	04.59	07.43	09.77	09.79	10.27
Na_2O	07.72	07.52	07.57	07.63	08.92	08.58	09.05	09.06	07.04	06.31	06.23	05.93
K_2O	00.19	00.16	00.16	00.18	00.15	01.08	00.14	00.19	00.06	00.07	00.07	00.04
Total	100.43	100.66	100.5	100.56	100.37	99.64	100.42	100.79	99.45	98.78	98.46	98.37
Cations per 32 oxygen atoms												
Si	10.694	10.648	10.627	10.660	11.124	11.192	11.171	11.122	10.839	10.228	10.209	10.141
Ti	0.004	0.001	0.003	0.000	0.001	0.003	0.001	0.001	0.003	0.004	0.001	0.004
Al	5.290	5.338	5.359	5.321	4.863	4.801	4.809	4.861	5.101	5.656	5.691	5.741
Fe^{2+}	0.003	0.004	0.003	0.008	0.006	0.000	0.006	0.012	0.006	0.006	0.006	0.010
Mn	0.005	0.005	0.001	0.010	0.003	0.000	0.004	0.008	0.000	0.006	0.005	0.001
Mg	0.003	0.000	0.000	0.000	0.000	0.000	0.000	0.003	0.003	0.000	0.000	0.000
Ca	1.308	1.362	1.373	1.339	0.893	0.795	0.863	0.864	1.423	1.906	1.917	2.015
Na	2.656	2.582	2.605	2.623	3.049	2.961	3.091	3.086	2.440	2.228	2.208	2.104
K	0.044	0.036	0.036	0.041	0.033	0.246	0.032	0.042	0.014	0.017	0.017	0.009
Total	20.006	19.976	20.006	20.001	19.973	19.997	19.977	19.999	19.828	20.052	20.055	20.026
Mol % An	32.64	34.22	34.22	33.45	22.47	19.87	21.64	21.64	36.71	45.91	46.29	48.81

Sample	ZC27	ZC27	ZC27	ZC27	ZC27	ZC27	ZC27	ZC27	ZC27	ZC27	ZC4	ZC4
Posit.	C	R	C	R	C	R	C	R	M	R	C	R
SiO_2	50.67	48.71	63.61	51.48	49.99	57.08	45.60	50.80	48.13	46.78	60.23	58.44
TiO_2	00.03	00.01	00.02	00.04	00.03	00.01	00.02	00.01	00.01	00.03	00.01	00.01
Al_2O_3	29.78	33.13	23.66	32.38	31.13	26.74	34.34	31.56	33.69	34.88	25.39	26.51
FeO	01.61	00.33	00.65	00.05	00.56	00.32	00.05	00.02	00.03	00.04	00.04	00.04
MnO	00.04	00.03	00.01	00.00	00.03	00.03	00.02	00.03	00.02	00.03	00.03	00.01
MgO	00.19	00.01	00.00	00.01	00.03	00.00	00.07	00.01	00.00	00.03	00.00	00.00
CaO	14.67	16.93	12.63	14.88	14.86	11.67	16.21	14.04	17.04	17.67	07.09	08.32
Na_2O	02.14	02.03	01.87	03.35	01.97	01.60	01.08	01.33	02.08	01.25	07.81	07.10
K_2O	00.71	00.08	00.07	00.04	01.75	03.99	00.59	02.95	00.07	00.17	00.19	00.17
Total	99.84	101.26	102.52	102.23	100.35	101.44	97.98	100.75	101.07	100.88	100.79	100.6
Cations per 32 oxygen atoms												
Si	9.320	8.829	10.999	9.174	9.164	10.240	8.534	9.249	8.740	8.521	10.664	10.404
Ti	0.004	0.001	0.003	0.005	0.004	0.001	0.003	0.001	0.001	0.004	0.001	0.001
Al	6.456	7.078	4.822	6.801	6.726	5.654	7.575	6.774	7.210	7.489	5.298	5.563
Fe^{2+}	0.247	0.050	0.093	0.008	0.086	0.049	0.008	0.003	0.005	0.006	0.006	0.006
Mn	0.006	0.005	0.001	0.000	0.005	0.005	0.003	0.005	0.003	0.005	0.005	0.001
Mg	0.052	0.003	0.000	0.003	0.008	0.000	0.019	0.003	0.000	0.008	0.000	0.000
Ca	2.892	3.288	2.340	2.842	2.918	2.244	3.251	2.739	3.315	3.448	1.345	1.587
Na	0.763	0.713	0.627	1.157	0.700	0.557	0.392	0.470	0.732	0.442	2.682	2.451
K	0.166	0.018	0.015	0.009	0.410	0.913	0.141	0.685	0.017	0.040	0.044	0.038
Total	19.907	19.986	18.900	19.997	20.020	19.662	19.924	19.928	20.023	19.963	20.045	20.052
Mol % An	75.68	81.82	78.45	70.90	72.45	60.43	85.93	70.35	81.57	87.75	33.05	38.93

Table 4.8. (Contd.)

Sample	ZC4	ZC4	ZC4*	ZC4*	ZC65*	ZC65*	ZC65*	ZC65*	ZC65*	ZC65*	ZC65*	ZC65*
Posit.	C	R	Inc	Inc	C	C	C	C	M	M	R	R
SiO_2	57.46	61.06	58.46	56.75	45.28	46.18	45.22	46.02	45.63	46.35	45.84	46.18
TiO_2	00.00	00.02	00.04	00.02	00.01	00.00	00.02	00.04	00.01	00.00	00.01	00.01
Al_2O_3	27.15	24.64	24.82	26.75	35.08	34.14	35.35	34.23	35.31	34.50	32.37	32.99
FeO	00.01	00.04	00.24	00.84	00.08	00.08	00.03	00.07	00.09	00.12	01.28	00.29
MnO	00.01	00.03	00.02	00.04	00.02	00.00	00.00	00.03	00.01	00.01	00.03	00.01
MgO	00.00	00.00	00.00	00.35	00.00	00.01	00.01	00.01	00.00	00.00	00.38	00.04
CaO	09.17	06.13	07.35	07.62	19.15	17.73	18.94	17.98	18.55	17.63	16.02	16.63
Na_2O	06.49	08.19	07.30	06.26	00.85	01.18	00.82	01.05	00.95	01.35	01.47	01.52
K_2O	00.13	00.23	00.17	01.00	00.02	00.43	00.02	00.57	00.03	00.03	00.38	00.10
Total	100.42	100.34	98.40	99.63	100.49	99.75	100.41	100	100.58	99.99	97.78	97.77
Cations per 32 oxygen atoms												
Si	10.264	10.828	10.618	10.262	8.324	8.529	8.307	8.493	8.361	8.521	8.655	8.672
Ti	0.000	0.003	0.005	0.003	0.001	0.000	0.003	0.005	0.001	0.000	0.001	0.001
Al	5.716	5.149	5.313	5.701	7.602	7.432	7.654	7.446	7.626	7.476	7.204	7.302
Fe^{2+}	0.001	0.006	0.036	0.127	0.013	0.013	0.005	0.010	0.014	0.018	0.202	0.046
Mn	0.001	0.005	0.003	0.006	0.003	0.000	0.000	0.005	0.001	0.001	0.005	0.001
Mg	0.000	0.000	0.000	0.095	0.000	0.003	0.003	0.003	0.000	0.000	0.108	0.012
Ca	1.755	1.165	1.431	1.476	3.772	3.508	3.729	3.556	3.642	3.473	3.241	3.346
Na	2.248	2.816	2.572	2.195	0.303	0.422	0.292	0.376	0.338	0.481	0.538	0.553
K	0.029	0.052	0.040	0.230	0.005	0.101	0.005	0.134	0.006	0.006	0.092	0.024
Total	20.015	20.024	20.017	20.095	20.023	20.008	19.997	20.028	19.990	19.977	20.046	19.958
Mol % An	43.52	28.88	35.40	37.83	92.44	87.02	92.62	87.44	91.36	87.69	83.73	85.29

Sample	ZC20	ZC20	ZC20	ZC20	ZM70	ZM70	ZM70	ZM70	ZS12	ZS12	ZS12	ZS12
Posit.	C	R	C	R	C	R	M	R	C	R	C	R
SiO_2	66.22	68.13	66.91	67.79	65.95	66.00	66.69	66.62	66.25	67.82	66.88	67.28
TiO_2	00.00	00.00	00.01	00.02	00.02	00.01	00.01	00.00	00.01	00.01	00.00	00.00
Al_2O_3	20.66	19.86	20.46	19.96	20.53	20.65	19.97	20.43	20.24	19.62	19.96	20.16
FeO	00.02	00.01	00.02	00.02	00.01	00.03	00.02	00.02	00.01	00.00	00.01	00.03
MnO	00.01	00.01	00.03	00.01	00.03	00.01	00.01	00.00	00.03	00.03	00.02	00.00
MgO	00.00	00.00	00.00	00.00	00.01	00.00	00.00	00.01	00.00	00.00	00.00	00.01
CaO	01.78	00.69	01.46	00.88	01.74	01.71	01.23	01.47	01.24	00.53	00.37	00.37
Na_2O	10.74	11.48	10.97	11.23	10.53	10.42	10.98	10.71	11.10	11.62	11.27	11.15
K_2O	00.13	00.12	00.18	00.17	00.16	00.14	00.17	00.16	00.15	00.16	00.40	00.65
Total	99.56	100.3	100.04	100.08	98.98	98.97	99.08	99.42	99.03	99.79	98.91	99.65
Cations per 32 oxygen atoms												
Si	11.677	11.889	11.740	11.859	11.691	11.692	11.800	11.746	11.741	11.901	11.845	11.833
Ti	0.000	0.000	0.001	0.003	0.003	0.001	0.001	0.000	0.001	0.001	0.000	0.000
Al	4.295	4.085	4.231	4.116	4.290	4.312	4.165	4.246	4.228	4.059	4.167	4.180
Fe^{2+}	0.003	0.001	0.003	0.003	0.001	0.004	0.003	0.003	0.001	0.000	0.001	0.004
Mn	0.001	0.001	0.004	0.001	0.005	0.002	0.001	0.000	0.004	0.004	0.003	0.000
Mg	0.000	0.000	0.000	0.000	0.003	0.000	0.000	0.003	0.000	0.000	0.000	0.003
Ca	0.336	0.129	0.275	0.165	0.331	0.325	0.233	0.278	0.236	0.100	0.071	0.069
Na	3.672	3.884	3.732	3.809	3.620	3.579	3.767	3.662	3.815	3.953	3.871	3.803
K	0.029	0.027	0.040	0.037	0.036	0.032	0.038	0.036	0.033	0.036	0.091	0.145
Total	20.013	20.017	20.025	19.993	19.980	19.947	20.008	19.974	20.060	20.055	20.048	20.037
Mol % An	8.32	3.20	6.79	4.12	8.30	8.26	5.77	6.99	5.78	2.45	1.75	1.73

Mol % An = 100 Ca / (Ca + Na + K); * = Used in geothermometry in Fig. 4.6 (C); Inc = Inclusion in amphibole; C= Core; M= Middle; R= Rim; The underline indicates the different positions within the single grain. Detection limits for the analysed oxides are tabulated in Appendix 4.2.

Similar values of Ta_2O_5 have also been reported from the wolframite within a pegmatite from Thailand (Linnen and Williams-Jones 1993). As for as the author is aware significant amounts of ZrO_2 and Ta_2O_5 in the scheelite have not been previously reported, and it is of considerable interest, therefore, to consider the petrogenetic implications. Significant concentrations of zirconium and tantalum are usually related to igneous activity and the concentration of these elements, is noted very high in plutonic rocks relatively rich in soda or alkaline igneous rocks (Deer et al. 1982; Tukiainen 1988). The Ta concentration also increases with the differentiation of granitoid magmatism (Boissavy-Vinau and Roger 1980). Taylor (1965) argued that Ta is concentrated in those minerals which contain Zr in the post-magmatic environment and both these elements (i.e. Zr^{4+} and Ta^{5+}) replaces W^{4+} and W^{6+} respectively.

The cogenesis of W and Zr and their association poses some problems as Zr is compatible element and its mobility is limited particularly in igneous melts (Taylor 1965). In contrast, W and Ta, being incompatible, are usually concentrated in the volatile-rich phase (Imeokparia 1985). In addition, Zr is also immobile during the low to medium-temperature metasomatism and metamorphic rocks such as metamorphosed basalt (Ball et al. 1985; Pearce and Norry 1979). However, Rubin et al. (1993) pointed out that Zr can be highly mobile element in the fluorine-rich, peralkaline and peralumious hydrothermal system.

4.4.10 Sphalerite

Sphalerite is the dominant constituent of sulphide mineralisation and occurs with in the marble horizon at Besti Gol. Table 4.10 shows the chemistry of this sphalerite, which shows a consistent chemical composition from core to margin of the grain. However, two apparently distinct generations, Fe-poor sphalerite (2.85 to 3.65 wt % FeS) and relatively Fe-rich sphalerite (6 - 7 wt % FeS) have been found in different grains (Table 4.10). The yellow and dark red color the sphalerite corresponds to generally low-Fe and high-Fe content respectively. The Besti Gol sphalerite is extensively altered to hydrozincite. The ideal hydrozincite contain ZnO ranging from 69.7 up to 76.13 wt % along with CO_2 + H_2O (approximately 16 and 11 wt % respectively) see (Jambor 1964). Whereas the zincite composed of 91.47 to 99.63 wt % ZnO with PbO 5.3 wt % and CO_2 2.85 % (Palache et al. 1944). The analysed hydrozincite composed of ZnO (59.6 to 80 wt %) and FeO 4.5 to 16.9 wt % with total 73.8 to 91.10. In one analysis ZnO reaches up to 85.3 wt % with FeO 7.08 wt % (total 94.30).

The chemistry of the analysed mineral is very close to hydrozincite. ZnO can easily be replaced by FeO and hence effect the concentration of CO_2 + H_2O.

Table 4.9: Composition of scheelite from investigated calc-silicate quartzite, except ZM 64 from tourmalinite.

Analy.	ZC43	ZC43	ZC43	ZC43	ZC43	ZC43	ZC43	ZC43	ZC43	ZC43	ZC70	ZC70
CaO	20.80	20.76	20.15	20.55	20.59	20.62	20.24	20.67	20.62	20.90	20.80	20.64
WO_3	79.24	77.16	79.24	79.54	78.45	78.70	77.40	79.01	79.69	78.19	77.29	77.24
MoO_2	0.08	0.06	0.15	0.06	0.06	0.05	0.03	0.06	0.06	0.03	0.06	0.06
SnO_2	0.02	0.02	0.02	0.00	0.02	0.02	0.02	0.02	0.00	0.00	0.02	0.02
FeO	0.02	0.06	0.03	0.00	0.00	0.03	0.04	0.03	0.01	0.02	0.05	0.02
MgO	0.01	0.01	0.00	0.01	0.00	0.03	0.05	0.00	0.01	0.01	0.00	0.00
MnO	0.02	0.02	0.02	0.01	0.02	0.00	0.02	0.01	0.01	0.01	0.02	0.01
Y_2O_3	0.06	0.00	0.06	0.06	0.06	0.06	0.06	0.06	0.06	0.06	0.06	0.06
TiO_2	0.03	0.09	0.09	0.09	0.05	0.09	0.10	0.02	0.04	0.02	0.00	0.12
ZrO_2	0.01	0.26	0.28	0.12	0.14	0.28	0.05	0.17	0.17	0.44	0.18	0.09
Nb_2O_5	0.05	0.08	0.09	0.07	0.12	0.04	0.07	0.07	0.07	0.11	0.04	0.07
Ta_2O_5	0.05	0.16	0.11	0.18	0.05	0.21	0.19	0.28	0.26	0.21	0.16	0.05
Total	100.39	98.68	100.24	100.69	99.56	100.13	98.27	100.4	101	100	98.68	98.38

Analy.	ZC70	ZC70	ZC70	ZC70	ZC70	ZC70	ZC70	ZC70	ZC67	ZC67	ZC67	ZC67
CaO	20.58	20.74	20.50	20.45	20.61	20.74	20.78	20.63	20.80	20.63	20.37	20.28
WO_3	78.25	78.18	77.60	78.33	77.96	78.32	78.78	78.01	79.39	76.88	78.15	78.31
MoO_2	0.06	0.10	0.06	0.06	0.02	0.09	0.02	0.06	0.01	0.04	0.04	0.06
SnO_2	0.02	0.02	0.00	0.02	0.02	0.02	0.01	0.02	0.05	0.02	0.02	0.02
FeO	0.03	0.00	0.02	0.01	0.04	0.00	0.02	0.02	0.01	0.02	0.01	0.02
MgO	0.00	0.00	0.02	0.00	0.01	0.00	0.00	0.00	0.01	0.00	0.00	0.00
MnO	0.02	0.02	0.03	0.02	0.02	0.02	0.01	0.01	0.02	0.02	0.01	0.03
Y_2O_3	0.06	0.04	0.06	0.06	0.06	0.06	0.06	0.06	0.06	0.06	0.06	0.04
TiO_2	0.03	0.03	0.06	0.08	0.09	0.05	0.03	0.03	0.09	0.03	0.06	0.05
ZrO_2	0.24	0.30	0.10	0.33	0.41	0.35	0.28	0.37	0.46	0.39	0.24	0.18
Nb_2O_5	0.01	0.07	0.08	0.01	0.06	0.07	0.01	0.07	0.09	0.04	0.07	0.02
Ta_2O_5	0.05	0.05	0.12	0.16	0.19	0.26	0.19	0.18	0.18	0.25	0.18	0.05
Total	99.35	99.55	98.65	99.53	99.49	99.98	100.19	99.46	101.17	98.38	99.21	99.06

Table 4.9 (Contd.)

Analy.	ZC67	ZC67	ZC67	ZC67	ZC67	ZC67	TR132	TR132	TR132	TR132	TR132	TR132
CaO	20.52	20.74	20.57	20.42	20.74	20.77	20.33	20.34	20.63	20.31	20.44	20.62
WO_3	77.63	77.94	78.28	77.56	77.67	77.50	78.75	78.18	77.33	77.97	77.62	77.77
MoO_2	0.01	0.06	0.06	0.00	0.06	0.09	0.08	0.02	0.05	0.04	0.06	0.07
SnO_2	0.02	0.02	0.02	0.02	0.02	0.02	0.02	0.02	0.02	0.02	0.02	0.02
FeO	0.02	0.01	0.02	0.00	0.04	0.02	0.04	0.02	0.02	0.03	0.02	0.02
MgO	0.00	0.00	0.02	0.00	0.00	0.00	0.00	0.00	0.00	0.01	0.00	0.00
MnO	0.08	0.02	0.01	0.02	0.02	0.01	0.01	0.03	0.02	0.02	0.01	0.01
Y_2O_3	0.06	0.06	0.06	0.06	0.06	0.06	0.06	0.06	0.06	0.06	0.06	0.06
TiO_2	0.09	0.02	0.09	0.01	0.13	0.07	0.07	0.05	0.09	0.10	0.09	0.03
ZrO_2	0.39	0.26	0.06	0.28	0.35	0.15	0.39	0.31	0.18	0.23	0.15	0.28
Nb_2O_5	0.08	0.07	0.09	0.06	0.07	0.00	0.04	0.07	0.07	0.05	0.07	0.01
Ta_2O_5	0.21	0.05	0.25	0.09	0.11	0.35	0.24	0.13	0.09	0.11	0.19	0.02
Total	99.11	99.25	99.53	98.52	99.27	99.04	100.03	99.23	98.56	98.95	98.73	98.91

Analy.	TR132	TR132	TR132	TR132	ZC65	ZC65	ZC65	ZC65	ZC65	ZC65	ZC65	ZC65
CaO	20.53	20.76	20.59	20.58	20.75	20.76	20.97	20.79	20.51	20.86	20.68	20.95
WO_3	78.13	77.85	77.75	77.86	79.02	78.97	78.51	78.31	79.17	79.21	79.35	78.94
MoO_2	0.08	0.07	0.08	0.03	0.01	0.02	0.04	0.08	0.07	0.06	0.00	0.01
SnO_2	0.02	0.02	0.01	0.02	0.02	0.02	0.02	0.02	0.02	0.02	0.01	0.02
FeO	0.03	0.03	0.01	0.02	0.02	0.02	0.00	0.04	0.04	0.03	0.02	0.02
MgO	0.00	0.01	0.00	0.00	0.00	0.01	0.01	0.00	0.01	0.01	0.00	0.00
MnO	0.02	0.02	0.02	0.06	0.05	0.01	0.03	0.02	0.03	0.02	0.01	0.08
Y_2O_3	0.06	0.06	0.06	0.02	0.01	0.05	0.05	0.05	0.05	0.05	0.05	0.00
TiO_2	0.01	0.02	0.05	0.01	0.12	0.01	0.07	0.00	0.04	0.09	0.02	0.02
ZrO_2	0.19	0.05	0.35	0.23	0.28	0.30	0.29	0.29	0.22	0.19	0.22	0.12
Nb_2O_5	0.09	0.02	0.02	0.03	0.04	0.07	0.07	0.03	0.01	0.11	0.07	0.04
Ta_2O_5	0.05	0.03	0.02	0.06	0.05	0.04	0.11	0.07	0.01	0.05	0.05	0.27
Total	99.21	98.94	98.96	98.92	100.37	100.28	100.17	99.7	100.18	100.7	100.48	100.47

Table 4.9 (Contd.)

Analy.	ZC65	ZC65	ZC41	ZC41	ZC41	ZC41	ZC41	ZC41	ZC41	ZC41	ZC41	ZC41
CaO	21.04	21.00	20.94	20.96	21.32	20.18	20.86	20.83	20.81	20.87	20.51	21.02
WO_3	78.01	77.98	79.15	79.47	78.25	79.56	78.59	78.79	79.79	77.71	80.05	77.06
MoO_2	0.04	0.06	0.05	0.12	0.12	0.17	0.06	0.06	0.02	0.06	0.02	0.06
SnO_2	0.02	0.05	0.02	0.02	0.02	0.02	0.02	0.02	0.01	0.02	0.02	0.01
FeO	0.11	0.06	0.05	0.25	0.05	0.06	0.08	0.07	0.03	0.02	0.07	0.01
MgO	0.00	0.01	0.00	0.00	0.00	0.00	0.00	0.00	0.01	0.00	0.00	0.01
MnO	0.00	0.02	0.00	0.00	0.03	0.01	0.02	0.01	0.01	0.05	0.02	0.01
Y_2O_3	0.05	0.05	0.06	0.06	0.06	0.06	0.06	0.06	0.00	0.06	0.01	0.06
TiO_2	0.09	0.09	0.05	0.09	0.03	0.05	0.03	0.05	0.09	0.09	0.09	0.11
ZrO_2	0.15	0.24	0.21	0.29	0.16	0.34	0.33	0.18	0.37	0.31	0.25	0.42
Nb_2O_5	0.07	0.07	0.07	0.07	0.08	0.07	0.13	0.07	0.12	0.07	0.07	0.07
Ta_2O_5	0.05	0.09	n.a	n.a	n.a	n.a	n.a	n.a	n.a	n.a	n.a	n.a
Total	99.63	99.72	100.6	101.33	100.12	100.52	100.18	100.14	101.26	99.26	101.11	98.84

Analy.	ZM64	ZM64	ZM64	ZM64	ZM64	ZM64	ZM64	ZM64	ZM64	ZM64	ZM64	ZM64
CaO	20.73	20.58	20.01	20.72	20.72	20.51	20.78	21.00	20.84	20.83	20.43	20.65
WO_3	78.97	78.32	77.96	78.60	77.84	78.41	78.91	78.72	79.60	78.18	79.42	79.19
MoO_2	0.10	0.02	0.06	0.09	0.06	0.06	0.02	0.04	0.06	0.00	0.06	0.06
SnO_2	0.02	0.01	0.02	0.02	0.02	0.04	0.02	0.02	0.02	0.00	0.02	0.02
FeO	0.01	0.04	0.02	0.04	0.02	0.02	0.07	0.01	0.03	0.10	0.02	0.00
MgO	0.00	0.00	0.00	0.00	0.02	0.01	0.00	0.00	0.00	0.00	0.01	0.00
MnO	0.01	0.02	0.04	0.05	0.07	0.02	0.04	0.04	0.01	0.02	0.04	0.05
Y_2O_3	0.06	0.06	0.06	0.06	0.00	0.01	0.06	0.06	0.06	0.06	0.06	0.00
TiO_2	0.05	0.09	0.02	0.09	0.00	0.10	0.01	0.09	0.03	0.08	0.13	0.09
ZrO_2	0.00	0.27	0.30	0.15	0.14	0.21	0.26	0.19	0.32	0.43	0.17	0.28
Nb_2O_5	0.06	0.05	0.12	0.01	0.07	0.07	0.07	0.12	0.08	0.07	0.07	0.13
Ta_2O_5	n.a	n.a	n.a	n.a	n.a	n.a	n.a	n.a	n.a	n.a	n.a	n.a
Total	100.01	99.46	98.61	99.83	98.96	99.46	100.24	100.29	101.05	99.77	100.43	100.47

n.a = Not analysed. Detection limits for the analysed oxides are tabulated in Appendix 4.2.

Moreover, the banded or blade like crystal and its pale blue fluorescence in ultraviolet light corresponds to hydrozincite rather than zincite, which occurs as granular masses and is non-fluorescent (Palache et al. 1944, 1951). Similarly zincite is rare except unusual zinc deposit at Franklin, New Jersey (Frondel and Baum 1974; Palache et al. 1944). Hydrozincite is often found as alteration product of sphalerite at many places (Palache et al. 1951).

Galena is a minor phase in the sulphide mineralisation and only few grains of galena have been located. The microprobe analyses of galena are presented in Table 4.10. Co, Ni and Ag have not been found in these analyses. Galena, at places, appears to be probably altered to plattnerite (PbO_2). Plattnerite is mainly composed of PbO (91 wt %) with some SiO_2, Al_2O_3 and Fe_2O_3, the analysed mineral contains PbO 94 wt % with FeO .05 Wt %, whereas SiO_2 and Al_2O_3 have not been analysed. In other grains PbO ranges from 60 to 70 %, suggesting a probable lead carbonate phase such as hydrated cerussite.

Pyrite has also been found in association with sphalerite. Pyrite is composed of 47 atomic % Fe and 52 atomic % S. Most of the pyrite grains are replaced by zinc bearing magnetite. Arsenopyrite occur in the associated quartz veins of the study area. Chemical composition of the analysed arsenopyrite is given in Table 4.10. Arsenopyrite has been replaced by secondary arsenate complex compounds which normally contain (Fe, Al, Si, PO_4^{-3}, AsO_4^{-3}) (see Boyle and Jonasson 1973).

4.5 Discussion

4.5.1 Calc-silicate rocks

The evolution of calc-silicate mineralogy at Miniki Gol, consisting of calcic-amphibole, clinozoisite, calcite, sphene, calcite, anorthite, grossular garnet, diopside and scheelite signify a metasomatic skarn mineral assemblages.

The occurrence of euhedral to subhedral grains of clinozoisite without proper orientation along the general fabric; lack of reaction rims such as development of clinozoisite at the margin of plagioclase and amphibole in these clinozoisite-rich-scheelite-bearing rocks, suggest that these clinozoisite grains were developed from high temperature hydrothermal fluids. It is noted that epidote often develops under metamorphism by saussuritization of plagioclase but the formation of granular clinozoisite at the expense of anorthite, indicates an extensive hydrothermal activity. In addition, the presence of abundant plagioclase in the mica quartzite and garnet mica schist and the complete absence of clinozoisite in the garnet mica schist also imply that the clinozoisite has developed as a separate hydrothermal phase in the calc-silicate rocks.

Table 4.10: Chemistry (atomic percent) of sphalerite (analyses 1-20), arsenopyrite (analyses 21-30) and galena (analyses 31-40).

Analy.	**ZM128**	**ZM128**	**ZM128**	**ZM128**	**ZM128**	**ZM128**	**ZM128**	**ZM128**	**ZM128**	**ZM128**
Numb.	1	2	3	4	5	6	7	8	9	10
S	33.39	32.90	32.91	33.45	33.20	33.18	32.90	32.99	32.55	32.58
Zn	59.81	59.22	59.58	59.26	59.80	59.01	59.07	59.77	59.32	59.42
Fe	06.33	06.16	06.33	06.23	06.32	07.06	06.28	06.51	06.31	06.41
Cd	00.04	00.04	00.04	00.04	00.04	00.04	00.04	n.a	n.a	n.a
Ge	00.01	00.01	00.01	00.01	00.01	00.01	00.00	n.a	n.a	n.a
Total	99.58	98.33	98.87	98.99	99.37	99.3	98.29	99.27	98.18	98.41
mol % Fes	11.04	10.74	11.04	10.86	11.02	12.31	10.95	11.35	11.00	11.18

Analy.	**ZM129**	**ZM129**	**ZM129**	**ZM129**	**ZM129**	**ZM129**	**ZM129**	**ZM129**	**ZM129**	**ZM129**
Numb.	11	12	13	14	15	16	17	18	19	20
S	32.83	32.60	32.78	32.40	32.86	33.05	33.37	33.00	33.16	32.94
Zn	62.35	61.11	61.68	62.57	62.48	62.61	61.83	61.50	61.73	61.97
Fe	03.47	03.37	03.65	03.47	03.32	03.17	02.85	03.36	03.10	02.88
Cd	00.04	00.04	00.04	00.04	00.04	00.04	n.a	n.a	n.a	n.a
Ge	00.04	00.01	00.01	00.01	00.01	00.01	n.a	n.a	n.a	n.a
Total	98.73	97.13	98.16	98.49	98.71	98.88	98.05	97.86	97.99	97.79
mol % Fes	6.05	5.88	6.36	6.05	5.79	5.53	4.97	5.86	5.41	5.02

Analy.	**ZM121**	**ZM121**	**ZM121**	**ZM121**	**ZM121**	**ZM121**	**ZM121**	**ZM121**	**ZM121**	**ZM121**
Numb.	21	22	23	24	25	26	27	28	29	30
S	19.80	19.81	19.60	19.85	20.40	20.08	19.97	19.62	19.72	19.58
Fe	35.21	35.82	35.52	34.90	36.17	35.44	35.19	35.78	35.86	35.11
Zn	00.00	00.01	00.04	00.02	00.01	00.04	00.02	00.06	00.08	00.05
As	43.00	42.88	43.39	42.46	42.68	42.75	42.93	43.40	42.82	42.73
Ag	00.05	00.05	00.05	00.07	00.00	00.07	00.02	00.05	00.06	00.08
Pb	00.12	00.07	00.07	00.09	00.12	00.01	00.06	00.10	00.08	00.19
Total	98.18	98.64	98.67	97.39	99.38	98.39	98.19	99.01	98.62	97.74

Analy.	**ZM129**	**ZM129**	**ZM129**	**ZM129**	**ZM129**	**ZM129**	**ZM129**	**ZM129**	**ZM128**	**ZM128**
Numb.	31	32	33	34	35	36	37	38	39	40
S	12.33	12.27	12.34	11.93	12.17	12.19	12.26	12.01	11.16	12.29
Fe	00.01	00.01	00.02	00.01	00.01	00.05	00.01	00.03	00.55	01.40
Zn	00.10	00.08	00.02	00.00	00.07	00.07	00.04	00.28	00.34	00.02
As	00.00	00.00	00.00	00.00	00.00	00.00	00.00	00.01	00.01	00.01
Ag	00.04	00.04	00.04	00.06	00.17	00.04	00.09	00.04	00.04	00.04
Pb	86.86	87.46	88.10	87.32	88.32	88.74	89.21	87.91	87.13	88.15
Total	99.34	99.86	100.52	99.32	100.74	101.09	101.61	100.28	99.229	101.905

However, the presence of 11.95 wt % Fe_2O_3 in epidote from the chlorite-rich schist at Besti Gol suggest that epidote may have formed at the expense of plagioclase and ferromagnesian minerals such as biotite and actinolite during metamorphism. The association of low-Fe clinozoisite with scheelite probably indicates that the low-Fe clinozoisite precipitated first from hydrothermal fluid at high temperature followed by lower temperature Fe-rich clinozoisite. A very similar composition of clinozoisite has been reported from calc-silicate veins (skarns) associated with the Land's End granite, Cornwall (Alderton and Jackson 1978) and from pegmatite (Rao and Rao 1971).

The positive correlation between Si + Al and Ca and a negative correlation with Fe^{3+} indicate that Ca, Al and Si were the dominant constituents of Fe-poor hydrothermal solutions. Epidote in the calc-silicate rocks did not develop as at first, the ore-forming solution was Fe-poor, corresponding to a high temperature hydrothermal fluid (Chalokwu and Kuehner 1992; Deer et al. 1986).

The stability of clinozoisite is discussed by Moody et al. (1985), who experimentally concluded that clinozoisite grows between 450°C and 575°C. Fyfe (1960) also maintained that clinozoisite is stable under hydrothermal condition at 2 kbar and up to 605°C.

These lines of evidence all suggest that a high temperature hydrothermal fluid broke down the pre-existing plagioclase and calcite in these quartzites. The break down of the calcic-plagioclase and calcite in the quartzitic rocks could have provided the required amount of Ca and Al for the growth of clinozoisite and intergrown scheelite. The Na released during breakdown of plagioclase may have been accommodated in sodic-rich plagioclase (see ZC 9 and ZC 6) or albite-rich quartzite reported in the study area by Leake et al. (1989). The presence of high calcic plagioclase in the scheelite-bearing calc-silicate quartzite suggest high calcic activity in hydrothermal solution. The anorthite content of skarn calc-silicate assemblages of Var, France (Sonnet et al. 1985) is also similar to the plagioclase of Miniki Gol scheelite-bearing calc-silicate quartzite.

The sphene analysed from the scheelite-bearing calc-silicate quartzite is similar to the skarn and igneous sphene from the Victoria Range, New Zealand, (Tulloch 1979). Titanite along with orthoclase has also been found in the skarn calc-silicate assemblages of Var, France (Sonnet et al. 1985).

The unusual concentration of Al in the titanite (ranges from 6.98 up to 9.44 wt %) is hard to explain in the sense, that it occurs in a hydrothermal cross-cutting vein (ZC 27, Table 4.7) and clearly postdates the main Ca-Al silicate phase in these rocks.

According to the Itaya et al. (1985), sphene mostly forms by replacement process during retrograde metamorphism, indicating that not all the titaniferous phases form in

equilibrium. Furthermore some sphene analyses from high pressure schist in New Caledonia and eclogite zone, Tauern Window, Austria are also characterised by a low Al-content, 1.08 and 0.99 wt % Al_2O_3 respectively (Itaya et al. 1985; Franz and Spear 1985). This would, probably, indicate that the chemistry of the sphene also greatly depends on the availability of Al_2O_3 in the host rocks, P-T condition, fluorine and oxygen fugacities (see also Franz and Spear 1985).

The composition of the chlorite and biotite from the studied scheelite-bearing calc-silicate quartzite is quite different from the other lithologies in the area. The composition of these minerals seem to be markedly effected by metasomatic activity. The high level of Mg in the biotite and chlorite (specially in the scheelite-bearing quartzite), seems to be the function of hydrothermal activity in these rocks. In general, hydrothermal biotite is more Mg-rich than igneous biotite (Brimhall et al. 1977). The present data in terms of Fe^{2+}/ (Fe^{2+} + Mg) ratio in the scheelite-bearing quartzite is compatible with the biotite of the Var (France) calc-silicate quartzite-hosted tungsten mineralisation that is suggested to be of metasomatic origin (Sonnet et al. 1985) and consistent with the Morocco skarn-related stratiform-scheelite-biotite mineralisation of Cheilletz (1985).

The presence of grossular garnet in the calc-silicate quartzite and high grossular content (up to 87.8 mol %) of this garnet (Table 4.3, ZC 8, ZC 41) clearly signifies a calcium metasomatism in the Miniki Gol area. Grossular garnet is a typical garnet found in skarns or occurs in rocks that have undergone calcium metasomatism (Deer et al. 1982). Pure grossular garnet did not develop in the Miniki Gol tourmalinite, because Mn was also part of the hydrothermal fluid and the element is strongly partitioned into garnet in preference to other silicate minerals (Woodsworth 1977). However, the occurrence of a high grossular content in the garnet of tourmalinite (up to 30.5 mol %) indicates a solid solution series between grossular and spessartine, where Mn is replaced by Ca. Such a solid solution series with relatively high spessartine content has also reported from a scheelite-bearing skarn in Japan (Shimazaki, 1977). The lack of grossular garnet and spessartine rich garnet in the calc-silicate quartzite imply that Ca was mainly utilised by clinozoisite in the calc-silicate quartzite and Mn was accommodated by garnet in the associated tourmalinites.

The generation of five members of the calcic amphiboles in the calc-silicate quartzite and the occurrence of three members of amphiboles (tschermakitic hornblende, magnesio-hornblende and actinolitic hornblende) within a single grains (Fig. 4.15, Table 4.4) signify that equilibrium has not been attained during metamorphism. The growth of fibrous and spherulitic actinolite over the hornblende and the occurrence of secondary amphibole (actinolite) in these rocks depicts a retrogressive environment. Such

retrogression is generally attributed to the late stage igneous-hydrothermal solutions or metasomatic metamorphism (Deer et al. 1992). The variation in the chemical composition in amphibole also reflects a wide range of pressures and temperatures in the study area. It is very difficult to propose an exact temperature for the partitioning of the scheelite from the ore-bearing fluid. However, keeping in view the variation of chemical composition (Al_2O_3 content) in calcic-amphibole associated with scheelite grains (Table 4.4, TR 132), it can be suggested tentatively that scheelite fractionated during a temperature range of (550^oC-400^oC). This is compatible with the observation of the Foster (1977) that scheelite is stable between 400-560^oC. On the basis of Al6 vs. Si diagram (Fig. 4.16 B), it can also be tentatively concluded that the pressure of the calc-silicate quartzite has not exceeded 5-6 kbar.

As far as the genesis of the W mineralisation is considered, it appears that W, Zr and possibly Ta were part of the post-magmatic solution or may have been leached from the silicate phase. Zircon, being a resistant mineral to chemical attack, seems to be not a possible source of Zr. Zirconium and tantalum are usually related to igneous activity and the concentration of these elements is very high in plutonic rocks relatively rich in soda or alkaline igneous rocks (Deer et al. 1982; Tukiainen 1988).

The lack of cinnabar-stibnite mineralisation with the Miniki Gol scheelite deposits, also rules out the possibility of volcano-sedimentary origin for these rocks (see Maucher 1976).

4.5.2 Tourmalinites

The genesis of the Miniki Gol tourmalinite, its protolith and environment of deposition is very difficult to assess as the study area has suffered multiple episodes of deformation and metamorphism. The interpretation of these rocks is further complicated by the intrusion of leucogranite near the tourmalinite, which is a potential source of boron-rich fluids.

The presence of graphitic schist, carbonaceous material and a thick unit of calcite overlying the pelitic schist, apparently without structural discontinuity (Leake et al. 1989), suggest a marine depositional environment. However, the lack of sedimentary structures in the these metamorphosed rocks does not support exhalative activity at Miniki Gol area.

The availability of Al for the formation of tourmaline on the sea floor near the vicinity and within the submarine hydrothermal fluids has been discussed by Boström et al. (1969), Von Damm et al. (1985) and Slack et al. (1993). These authors argued that exhalative fluid precipitating tourmaline would consume so much alumina initially that the fluids would be undersaturated with respect to the tourmaline away from the submarine

vents. Similarly the co-genetic relationship of W and B and the simultaneous precipitation of scheelite and tourmaline during exhalation is hard to explain, as B occurs as $B(OH)^-_4$, BF^-_4, ions and undissociated $B(OH)_3$ in natural water whereas W is normally transported as tungstic acid, hydro- and simple tungstate ions (Willner 1992). These lines of evidences manifest that the direct precipitation of tourmaline would not be possible during exhalation on the sea floor. The absence of associated Sb and Hg (see Chapter 5) in the study area are also inconsistent with exhalative activities (James and Ineson 1993).

An evaporitic-sabkha model for the Miniki Gol tourmalinite is unlikely as there is a lack of evaporites (such as secondary halides) and the schists are not compatible with the lacustrine environment. The absence of metamorphosed products of the evaporites, such as Cl-rich scapolite, abundant magnetite, sillimanite and andalusite-corundum (metamorphosed bauxite or laterites) (Slack et al. 1993), rule out the possibility of coastal sabkha environment.

A boron-rich clay is also an inadequate precursor as clay minerals are not known to contain more than 2000 ppm of boron (cf. Slack et al. 1984). This amount of boron would only be sufficient for 9 % tourmaline by volume (Plimer 1986), whereas the Miniki Gol tourmalinite constitute up to 80 % tourmaline by volume. As deduced by Leake et al. (1989) and this petrographic study, the Miniki Gol tourmalinite crystallised after the first deformation. This would suggest that sufficient B was not available at the time of diagenesis and low-grade metamorphism for the growth of these tourmalinites. However, isolated, relatively zoned and sparsely distributed grains of tourmaline in the studied pelitic schist may be formed during diagenesis and recrystallised during subsequent regional metamorphism. The concentration of tourmaline at one particular site of deposition (tourmalinite) by regional metamorphism would not be possible, particularly when sufficient B was not available at its protolith.

The high concentration of FeO and Na_2O in the tourmaline of tourmalinites also correlate with a pegmatitic origin (see Table 4.1). Moreover the FeO # (FeO / FeO + MgO) of the studied tourmaline (0.6) corresponds to the tourmaline from hydrothermal (greisen-related) Sn-W deposits, Witkop and Van Rooi localities, South Africa (Pirajno and Smithies 1992) and Kirwana Hill and Doctor Hill, New Zealand (Mackenzie 1983).

The widespread occurrence of spessartine-rich garnet and its concentration in the tourmalinites (up to 50 % in some section) also reflect extensive Mn-rich hydrothermal activity in the Miniki Gol area. The reverse trend with rims richer in MnO than the core in the garnet of the tourmalinites reflects falling temperature during retrograde metamorphism, and correspond to a metasomatic origin (Deer et al. 1982).

4.5.3 Leucogranite

The Miniki Gol leucogranite can be considered as a potential source of boron for these tourmalinites. The mineral chemistry of tourmaline can provide some, although not conclusive, constraints on the genetic relationship between the leucogranite and tourmalinisation. The FeO content of the tourmaline increases from leucogranite to pegmatite, indicating an iron-enrichment trend (Fig. 4.11 B). The iron-enrichment trend can also be noticed in tourmalines of pegmatite-hosted xenoliths and as well as tourmalinite, suggesting that excessive Fe in these tourmalinites may have been introduced from pegmatite (Fig 4.11 B, Table 4.1). This iron-enrichment trend in tourmaline is regarded as the function of a late-stage magmatic differentiation (Benard et al. 1985; Taylor et al. 1992). The Miniki Gol tourmaline iron-enrichment trend is also consistent with the granite and pegmatitic tourmalines from SW England (Lister 1979), northern Portugal (Neiva 1974), the Hub Kapong batholith of Thailand (Manning 1982) and the Karagwe-Ankolean belt, Tanzania (Taylor et al. 1992). The positive correlation between the Fe and Aly in the tourmaline of pegmatite, xenolith and tourmalinites (Fig. 4.12 C, D and E), probably demonstrates similar geochemical behaviour during post-magmatic hydrothermal activity. In addition, excessive Al is considered as a common feature of pegmatites and occasionally correlated with magmatic evolution (Jolliff et al. 1986; Linnen and Williams-Jones 1993).

The most prominent compositional characteristic of the biotite from Miniki Gol leucogranite and Kafiristan biotite granodiorite, in terms of $Fe^{2+}/(Fe^{2+} + Mg)$ vs. total Al cation (see Fig. 4.18 A) is that it plots in the field of ilmenite (I-series granite) of Lalonde and Bernard (1993). The increasing Al-content (Fig. 4.18 A), from biotite of the granodiorite to leucogranite, also reflects directly the peraluminosity of the host magma (Lalonde and Bernard 1993). Peraluminous magma has been ascribed to the fractional crystallisation (Ringwood 1974), metasomatic loss of alkalis (Martin and Bowden 1981) and anatexis or assimilation of pelitic metasediments (Chapell and White 1974).

Garnet in the granite has been considered as xenocrysts contaminated from wall rock (Green 1977; Stone 1988) or as a product of primary but late stage magmatic crystallisation by Miller and Stoddard (1981) and Stone (1988). The garnet of the Miniki Gol leucogranite is spessartine-rich (Table 4.3), and such composition is generally regarded as post-magmatic garnet (Puziewicz 1990; Deer et al. 1982). The level of MnO in the garnet of the country rocks (garnet mica schist) is lower than the garnet of leucogranite, suggesting that the garnet analysed from the leucogranite is magmatic and not xenocrystic in origin (Crawford and Searle 1993). The homogenous composition of these garnets and their large size are also compatible with a magmatic origin.

Green (1977) demonstrated that increasing MnO content in the garnet increases the stability of the phase with regard to pressure and has also shown that garnet with >10 mol % spessartine is stable in silicic liquid at 5 kbar or less. Green (1977) also noted that garnet with 20-25 mol % spessartine may crystallise in equilibrium with granitic liquid at depths as shallow as 12 km (3 kbar). The Miniki Gol garnet in the leucogranite contain up to 38.7 mol % spessartine (mean 29 %) and that of tourmalinites contain up to 36 mol % spessartine (mean 26 %), indicating that leucogranite has crystallised at 3 to 4 kbar pressure. As the garnet is intergrown with scheelite grains in the tourmalinite, assuming that both these minerals may have experienced 3-4 kbar pressure.

4.5.4 Pb-Zn mineralisation

The conformability of the sulphide mineralisation with the host marble probably indicates that the mineralisation (sphalerite and galena and pyrite) was precipitated earlier in a synsedimentary environment. The subsequent metamorphism has induced distinct textural changes in sphalerite during recrytallisation as the original sedimentary layering has been obliterated. The coarse grain size, the euhedral crystal and triple junction in the calcite also indicate metamorphism. However, variation of FeS content in sphalerite has been found in both stratiform primary carbonate-hosted Pb-Zn mineralisation and metamorphosed sphalerite (Moles 1983; Koh et al. 1992). Many authors have speculated on the mechanism of ore formation, nature of ore-forming fluid and physico-chemical environment of deposition of sphalerite within the submarine exhalative deposits. Fe-rich sphalerite is considered to precipitate at high temperature, low sulphur and oxygen fugacity during exhalation. This is followed by Fe-poor sphalerite at lower temperature and higher sulphur activity (Moles 1983).

The amount of FeS in sphalerite, in the metamorphic rocks, is regarded as a function of pressure, temperature and sulphur activity when buffered by pyrite (Scott and Barnes 1971; Scott 1983; Moles 1983). Unfortunately, no sphalerite co-existing with pyrite grain was found. However, the FeS content in the Besti Gol sphalerite might indicate a wide pressure and temperature range (Scott and Barnes 1971; Deer et al. 1992). Further more the contrasting composition of the Besti Gol sphalerite also suggest that equilibrium was not attained during the regional metamorphism. The lack of any sedimentary structure, the presence of irregular and embayed form of the sphalerite and its coarse grain size, indicate that metamorphism has changed the sphalerite composition. The occurrence of hydrozincite indicate pervasive alteration and extensive supergene activity in the Besti Gol area.

The pale blue fluorescence could be related to hydrozincite or sphalerite itself. The formation of zincite can easily be explained as during high temperature CO_2 and H_2O are lost, leaving ZnO as zincite (Frondel and Baum 1974; Palache et al. 1951).

As only five samples were collected from the Pb-Zn mineralised zone at Besti Gol, these investigations are preliminary and more detailed work needs to be done to draw firm conclusion.

4.6 Summary

The association of the scheelite with clinozoisite, sphene and chlorite, in calc-silicate rocks and their chemistry suggest that these minerals have been significantly affected by the hydrothermal activity under the retrogressive environment. The excessive tourmaline (tourmalinisation) and the abundant spessartine-rich garnet in the scheelite-bearing tourmalinites appears to be the product of post-magmatic hydrothermal solution. The conversion of tschermakitic hornblende into actinolitic hornblende, calcic-plagioclase into sodic-plagioclase and extensive epidotization (development of clinozoisite) along with titanite could be related to the calcic metasomatism. The kaolinisation within the pegmatite also demonstrates hydrothermal activity within the granite itself. The extensive tourmalinisation, epidotization and kaolinisation might be related to post-magmatic activity in the study area. The Miniki Gol mineral assemblage (with the exception of sillimanite and wollastonite) fairly consistent with many scheelite-bearing skarns such as Sierra Nevada, California (Newberry 1982), and calc-silicate rocks, Var, France (Sonnet et al. 1985).

The Pb-Zn mineralisation seems to be synsedimentry and subsequent metamorphism has brought about changes in sphalerite texture and possibly composition. The metasomatic activity has led to the growth of hydrozincite after sphalerite.

Chapter Five

GEOCHEMISTRY

5.1 Introduction

In order to understand the geochemical signature of the leucogranite, to evaluate its source of melt, the geochemical behaviour and association of ore elements with the other trace elements during the metamorphism, anatexis and hydrothermal alteration; the geochemistry of rocks in the study area is discussed in this chapter. The rock units include leucogranite, granodiorite, schist, psammite (mica quartzite), calc-silicate quartzite, tourmalinites and marble. The emphasis has been focused mainly on the leucogranite and scheelite-bearing calc-silicate rocks. Little attention has been given to the Besti Gol mineralised-marble as few samples were collected from this rock unit.

The chemistry of the leucogranite, metasediments and tourmalinites is compared with specialised granites and low-Ca granites (Tischendorf 1977; Turekian and Wedepohl 1961), average shale (Turekian and Wedepohl 1961) and Broken Hill tourmalinites (Slack et al. 1993) respectively.

The background levels of trace elements (such as Li, W and Sn) from the rocks surrounding Miniki Gol have been discussed and compared with the background levels of tin-tungsten mineralisation, SW England. Around 40 trace elements including REE from the study rocks were analysed by X-ray Fluorescence Spectrometry (XRF), Instrumental Neutron Activation Analysis (INAA), Inductively Coupled Plasma Emission Spectrometry (ICPES). Be and Li were analysed by ICP-ES, B, Cs, U, Hf, Ta, Sb and REE by INAA and all the other elements were analysed by XRF.
See (Appendix 5.1) for detail.

5.2 Geochemistry of Miniki Gol granite

5.2.1 Petrographic and mineralogical features of the Miniki Gol two-mica leucogranite

As discussed earlier, the Miniki Gol leucogranite is essentially composed of two-feldspar, quartz, muscovite and subordinate biotite, garnet, tourmaline and apatite. Muscovite is more abundant than biotite in these leucogranites. Such a mineralogy is considered as the characteristic feature of the felsic variety of S-type granite or two-mica leucogranite (see Barbarin 1990).

Biotite in the leucogranite of the area under investigation is brownish red in color and suggesting that it is a magmatic biotite (Anderson and Rowley 1981). The high alumina content and high Fe / (Fe + Mg) ratio of the biotite (see Table 4.6, Fig. 4.18 A) of the Miniki Gol leucogranite is consistent with the biotite of peraluminous S-type granite (Clarke 1981; Chappell and White 1992). The high Fe / (Fe + Mg) ratio is also ascribed to the highly differentiated magmatic rocks (Clarke 1981) .

Muscovite in the investigated leucogranite has well-developed crystal boundaries and appears to be primary. However, many grains have been found as an alteration product of plagioclase and seem to be secondary. The average composition "SiO_2 content (45.81 %), high Al_2O_3 (32.52 %), low MgO (0.73 %) and FeO (2.55 %)" of muscovite from the Miniki Gol leucogranite is compatible with the primary muscovite (see Miller et al. 1981). However, TiO_2 content (mean 0.26 %), which is considered as a sensitive parameter in distinguishing primary and secondary muscovite (Miller et al. 1981), correlates with the secondary muscovite. Moreover, the studied muscovite chemistry in terms of Na / (Na + K+ Ca) vs. Fe + Mg / (Fe + Mg + Mn + Ti + Al_6) plots in the field of peraluminous two-mica granite (Fig. 5.1 A) defined by Clarke (1981).

The garnet of the studied leucogranite is relatively spessartine-rich than the garnet of the schist (Table 4.3, Fig. 4.14 A) and fairly coordinates with the felsic variety of peraluminous granite (Chappell and White 1992).

Tourmaline composition in peraluminous granites is generally close to the schorl end-member (Clarke 1981). However, the studied tourmaline in the leucogranite has intermediate composition in the dravite-schorl solid solution series (Fig. 4.11 A).

5.2.2 Major element geochemistry

Geochemical data of the Miniki Gol leucogranite, Kafiristan and Tirich Mir granodiorites are presented in the Table 5.1 and 5.2. These granites are compared with the average low Ca granite of Turekian and Wedepohl (1961) and the Tischendorf (1977) specialised granite. Based on the aluminium saturation index (molar Al_2O_3 / Na_2O + K_2O + CaO), the Miniki Gol leucogranite and granodiorites are characterised as peraluminous granite (Chappell and White 1974). The aluminium saturation index (ASI) of the Miniki Gol leucogranite is markedly higher (mean 1.85) than the Kafiristan granodiorite (mean 1.46) and Tirich Mir granodiorite mean 1.50 (see Table 5.1, Fig. 5.1 B).

Higher levels of wt % SiO_2 (mean 75) Na_2O (mean 3.44) and P_2O_5 (mean 0.24) and low values of total iron, Fe_2O_3 (mean 0.94) and TiO_2 (mean 0.09) are recorded in the Miniki Gol leucogranite compare to the typical S-type granite of Lachlan Fold Belt (White and Chappell 1988).

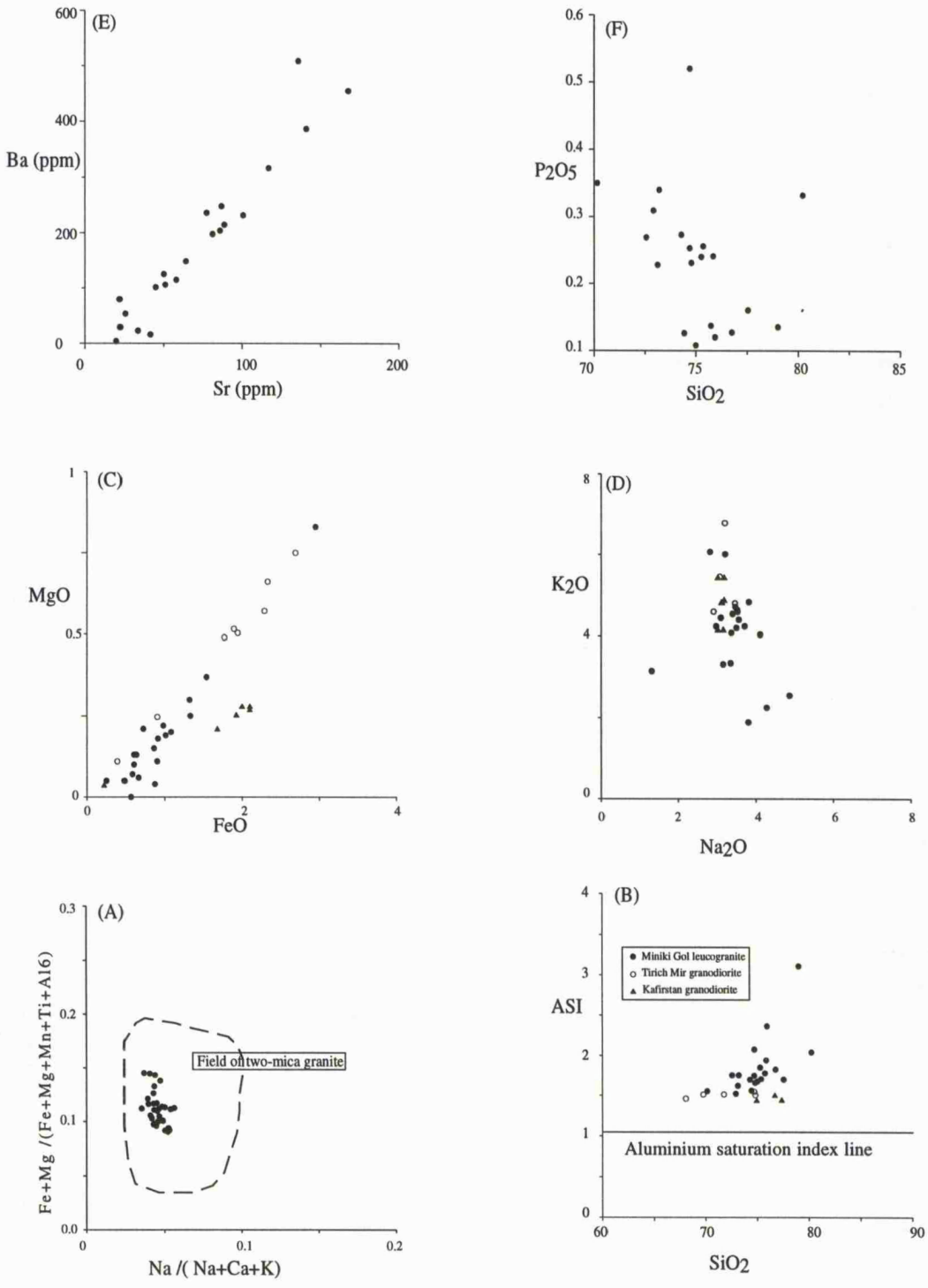

Fig. 5.1: **(A)** Fe+Mg/(Fe+Mg+Mn+Ti+Al_6) vs. Na/(Na+Ca+K) cations plot of muscovite from Miniki Gol leucogranite, field of peraluminous two-mica granite of (Clarke 1981) is superimposed. Plots of geochemical relationship of Miniki Gol leucogranite, Kafirstan and Tirich Mir granodiorites in terms of oxides and trace elements: **(B)** SiO_2 vs. ASI (Al_2O_3 / (CaO+Na_2O+K_2O) **(C)** FeO vs. MgO and **(D)** Na_2O vs. K_2O. **(E)** Relationship of Ba with Sr in the studied leucogranite and **(F)** Correlation between P_2O_5 and SiO_2 in the Miniki Gol leucogranite. Data taken from Table 5.2 and Appendix 5.2. Symbols as in **Fig. B.**

Table 5.1: Major and trace element geochemistry of the Miniki Gol leucogranite.

	Min	max	Mean	Std[1]	n[2]	Average low-Ca granite Turekian & Wedepohl (1961)	Specialised granite of Tischendorf (1977)
SiO_2	70.2	80.2	75.1	2.3	20		73.4 ± 1.4
TiO_2	0	0.5	0.1	0.1	20		0.16 ± 0.1
Al_2O_3	12.6	16	14.8	0.7	20		14 ± 1.1
*Fe_2O_3	0.3	3	0.9	0.6	20		1.9 ± 0.5
MnO	0	0.2	0	0	20		0.05± 0.04
MgO	0	0.8	0.2	0.2	20		0.5 ± 0.5
CaO	0.2	1.8	0.7	0.3	20		0.75 ± 0.4
Na_2O	1.3	4.9	3.4	0.7	20		3.2± 0.6
K_2O	1.9	6.1	4.1	1.1	20		4.7 ± 0.7
P_2O_5	0.1	0.5	0.2	0.1	20		
Total	97.8	100.6	99.6	0.7	20		
ASI	1.5	3.1	1.8	0.4	20		
Trace elements (ppm)							
B	8	23	15.1	4.1	14	10	
F	170	1370	807	309	13	850	3700 ± 1500
Cl	50	270	171	76.3	13	200	
S	0	60	30.8	19.3	13	300	
As	1.1	5.6	2.4	1.1	11	1.5	
Li	24	453	159	121	21	40	400 ± 200
Be	1.2	172	20.1	39.2	21	3	13 ± 6
Cs	5	29	15.6	6.9	13	4	
Ba	4	508	180	142	21	840	
Rb	135	326	242	56.6	21	170	580 ± 200
Sr	19.9	167	72	42.3	21	100	
Th	0.6	5.4	3	1.4	13	17	
U	1.2	46	9.5	11.6	13	3	
Zr	2.9	185	43.4	38.3	21	175	
Hf	1	3	1.9	0.5	12	3.9	
Ta	3.1	21	7.3	6.4	11	4.2	
Nb	2.8	32.3	15	7.1	21	21	
Y	2.1	27.8	14.9	6.2	20	40	
Sc	0.8	10.3	5.1	2.3	21	7	
V	0.1	39.6	8.6	8.1	21	44	
Cr	1.6	22.3	7.1	6.1	13	4.1	
Co	0	8.2	1.3	2.5	10	1	
Ni	0.1	10	2.8	2.7	15	4.5	
Cu	0	2	0.9	0.8	6	10	
Zn	1.3	67.1	26.7	17.1	20	39	
Ga	10.6	24	17.3	3.5	21	17	

Table 5.1: (Contd.)

	Min	max	Mean	Std[1]	n[2]	Average low-Ca granite Turekian & Wedepohl (1961)	Specialised granite of Tischendorf (1977)
Pb	9.8	78	38	15.4	21	19	
W	2	10	5.3	2.9	10	2.2	7 ±3
Sn[3]	18	77	33.3	19	12	3	40 ± 20
Mo	1.6	1.7	1.7	0.1	2	1.3	3.5 ± 2
Sb	0.2	0.6	0.4	0.1	10	0.2	
La	0.6	11	6.8	3.5	13	55	
Ce	7	29	16.6	6	11	92	
Nd	5	15	7.7	3.7	6	37	
Sm	0.1	2.5	1.6	0.7	12	10	
Eu	0.2	0.7	0.4	0.2	12	1.6	
Gd	1	3	1.8	0.7	9	10	
Tb	0.6	0.9	0.7	0.2	3	1.6	
Yb	0.5	1.6	1.1	0.3	11	4	
Lu	0.1	0.2	0.1	0	11	1.2	
La/Y	4.58	12.2					
Eu / Eu*	.29	1.16					
Mg/Li			0.7		20		
Rb/Ba			1.3		21		
Rb/Sr			3.4		21		
Sr/Ba			0.4		21		
Ba/Rb			0.7		21		
K/Rb			60		20		
TiO_2/ Ta			126		10		

[1]= Standard Deviation; [2] = Number of samples; [3]= Statistics of Sn values excluding leucogranite at Garam Chashma; * Total iron considered as Fe_2O_3; ASI= Al_2O_3 / (CaO +K_2O + Na_2O); Eu / Eu* (i.e. Eu_N/ $[(Sm_N)\ (Gd_N)]^{1/2}$; N= chondrite normalised value. Be and Li were analysed by ICP-ES and B, Cs, U, Hf, Ta, W, Sb and REE by INAA. All the other elements were analysed by XRF.

Table 5.2: Geochemical data for the Kafiristan granodiorite (ZM 85, ZM 86 and ZM 87) and Tirich Mir granodiorite (ZM 92, ZM 93, ZM 94 and ZM 95).

	ZM 85	ZM 86	ZM 87	ZM 92	ZM 93	ZM 94	ZM 95
SiO_2	77.4	76.7	74.9	71.8	69.8	68.1	74.7
TiO_2	0.2	0.2	0.3	0.3	0.4	0.4	0.3
Al_2O_3	12.5	12.7	13.6	14.5	15.2	16.6	13.6
Fe_2O_3*	1.7	2.1	2.0	2.3	2.7	2.3	1.8
MnO	0.0	0.0	0.0	0.1	0.0	0.0	0.1
MgO	0.2	0.3	0.3	0.6	0.8	0.7	0.5
CaO	0.6	1.1	1.0	1.4	1.5	1.4	1.2
Na_2O	3.2	3.2	3.0	3.5	3.1	3.2	2.9
K_2O	4.9	4.2	5.4	4.8	5.4	6.8	4.7
P_2O_5	0.0	0.1	0.1	0.2	0.3	0.2	0.3
Total	100.7	100.5	100.5	99.3	99.2	99.6	100.0
ASI	1.4	1.5	1.4	1.5	1.5	1.5	1.5
Trace elements (ppm)							
B	7.0	2.0	n.a	n.a	n.a	9	n.a
F	940	1220	n.a	630	860	590	n.a
Cl	170	190	n.a	50	70	60	n.a
S	0.0	0.0	n.a	0.0	0.0	0.0	n.a
As	3	1.5	1.1	n.a	n.a	n.a	n.a
Li	48	65	57	158	154	139	117
Be	4.1	2.9	2.1	5.8	4.2	3.6	6
Cs	8	12	n.a	n.a	n.a	8	n.a
Ba	146	163	375	317	379	481	236
Rb	289	291	314	265	281	310	262
Sr	34	58	61	107	116	134	86
Th	45.0	50.0	n.a	n.a	n.a	22.0	n.a
U	9.6	11.0	n.a	n.a	n.a	6.2	n.a
Zr	87	174	162	145	163	148	100
Hf	6	9	n.a	n.a	n.a	6	n.a
Ta	2.6	2.8	n.a	n.a	n.a	< 0.5	n.a
Nb	14.8	17.5	17.7	17.8	17.8	16.6	15.7
Y	100.1	60.8	54.8	19.4	16.6	13.7	16.9
Sc	12.0	8.4	8.5	11.4	11.0	7.6	7.8
V	11	15.7	24	25.2	30.5	25.0	11.9
Cr	25.8	6.3	3.0	5.6	40	10.5	14.6
Co	2.3	1	0.9	5.6	4.3	4.8	2.7
Ni	0.6	1.3	0.6	1.2	3.9	2.6	1.6
Cu	3	3.5	0.8	1	16.6	4	< 0.2
Zn	22.6	23	29	55.6	64.4	53.4	43
Ga	16.4	17.5	17.4	18	19	19	16
Pb	27.7	18.2	24	40	43	51	35
W	6	10	n.a	n.a	n.a	< 1	n.a
Sn	3.5	2.2	2.5	12.1	14	10.8	7.3
Mo	0.2	< 0.1	0.2	< 0.6	0.1	< 0.6	< 0.8
Sb	0.3	< 0.1	n.a	n.a	n.a	< 0.1	n.a
La	60	52	n.a	n.a	n.a	38	n.a
Ce	150	120	n.a	n.a	n.a	77	n.a
Nd	37	42	n.a	n.a	n.a	22	n.a
Sm	13	10	n.a	n.a	n.a	7	n.a
Eu	0.5	0.8	n.a	n.a	n.a	1.2	n.a
Gd	11	8	n.a	n.a	n.a	3	n.a
Tb	3.1	2.0	n.a	n.a	n.a	< 0.5	n.a
Yb	18	8.7	n.a	n.a	n.a	2	n.a
Lu	2.5	1.4	n.a	n.a	n.a	0.3	n.a

* = Total iron considered as Fe_2O_3; ASI= $(Al_2O_3/(CaO + K_2O + Na_2O)$. ASI= $Al_2O_3 / (CaO + K_2O + Na_2O)$. Be and Li were analysed by ICP-ES and B, Cs, U, Hf, Ta, W, Sb and REE by INAA. All the other elements were analysed by XRF.

The Lachlan Fold Belt granites comprise monzogranite, quartz diorite, granodiorite and tonalite, which contain minerals such as cordierite, andalusite, sillimanite, almandine garnet, rare pyroxene and are rich in biotite. In contrast, the Miniki Gol leucogranite contains less than 5 % biotite and spessartine-almandine garnet. The major element chemistry is fairly similar to the Himalayan (Manaslu) leucogranite of France-Lanord and Le Fort (1988) and Le Fort et al. (1987). The FeO and MgO values of the Kafiristan and Tirich Mir granodiorite are slightly higher than the Miniki Gol leucogranite and both these oxides show a positive correlation (Fig. 5.1 C, Table 5.2). These two elements are mainly accommodated in the biotite and garnet of the Miniki Gol granite. High Na_2O and K_2O contents are noted in the Miniki Gol albite-rich leucogranite and granodiorite respectively (see Fig. 5.1 D, Table 5.1, 5.2). The P_2O_5 content in the Miniki Gol leucogranite and Tirich Mir granodiorite is higher than the Kafiristan granodiorite (Table 5.1, 5.2).

A general similarity exists in the major element chemistry in terms of SiO_2, Al_2O_3, Na_2O and K_2O of the metasediments with the Miniki Gol leucogranite. When plotting these major elements of the metasediments and leucogranite against total FeO, it is seen that leucogranite overlaps in composition with the low-FeO range calc-silicate quartzite, and psammite (Fig. 5.2 A-D, 5.3 A). This overlapping can also be observed between FeO and trace elements Sc and Ni (Fig. 5.3 B-C). White and Chappell (1988) have argued that the ability of the metasediments to produce magma is basically dependent on the SiO_2, Na_2O and K_2O in the country rocks and termed it as a fertile window. This fertile window in the Miniki Gol metasediments is defined by the major and trace elements corresponding to a total FeO value of about (1-3 %).

5.2.3 Trace element geochemistry

The trace element geochemistry of the Miniki Gol two mica leucogranite is summarised in Table 5.1. The leucogranite is characterised by high values of Rb, Li, Be, Sn, W, Pb, Ta, U and low concentrations of Zn, Zr, Hf, Y, Th, Sr, Ba, V and Ni compared with the average low Ca granite of Turekian and Wedepohl (1961). The Miniki Gol leucogranite is also depleted in ratios Ba / Rb, TiO_2 / Ta, K / Rb, Mg / Li and enriched in Rb / Sr and Rb / Ba. Comparing the chemical composition of Miniki Gol leucogranite with the Tirich Mir and Kafiristan gneissic granodiorite, it is noted that the leucogranite is generally low in Ba, Th, Zr, Y, Sc, V, Cr, Ni and high in Be, Li, Ta, Sn and Cs (Table 5.1, 5.2, Appendix 5.2). The tungsten content is relatively high (mean 8 ppm) in the Kafiristan granodiorite, however, it is very low in the Tirich Mir granodiorite. The low levels of Zr, Y, Ba, Sr and high levels of Be, Li, Ta, Sn, Cs and Rb in the leucogranite indicate a very evolved magmatic signature for these leucogranites

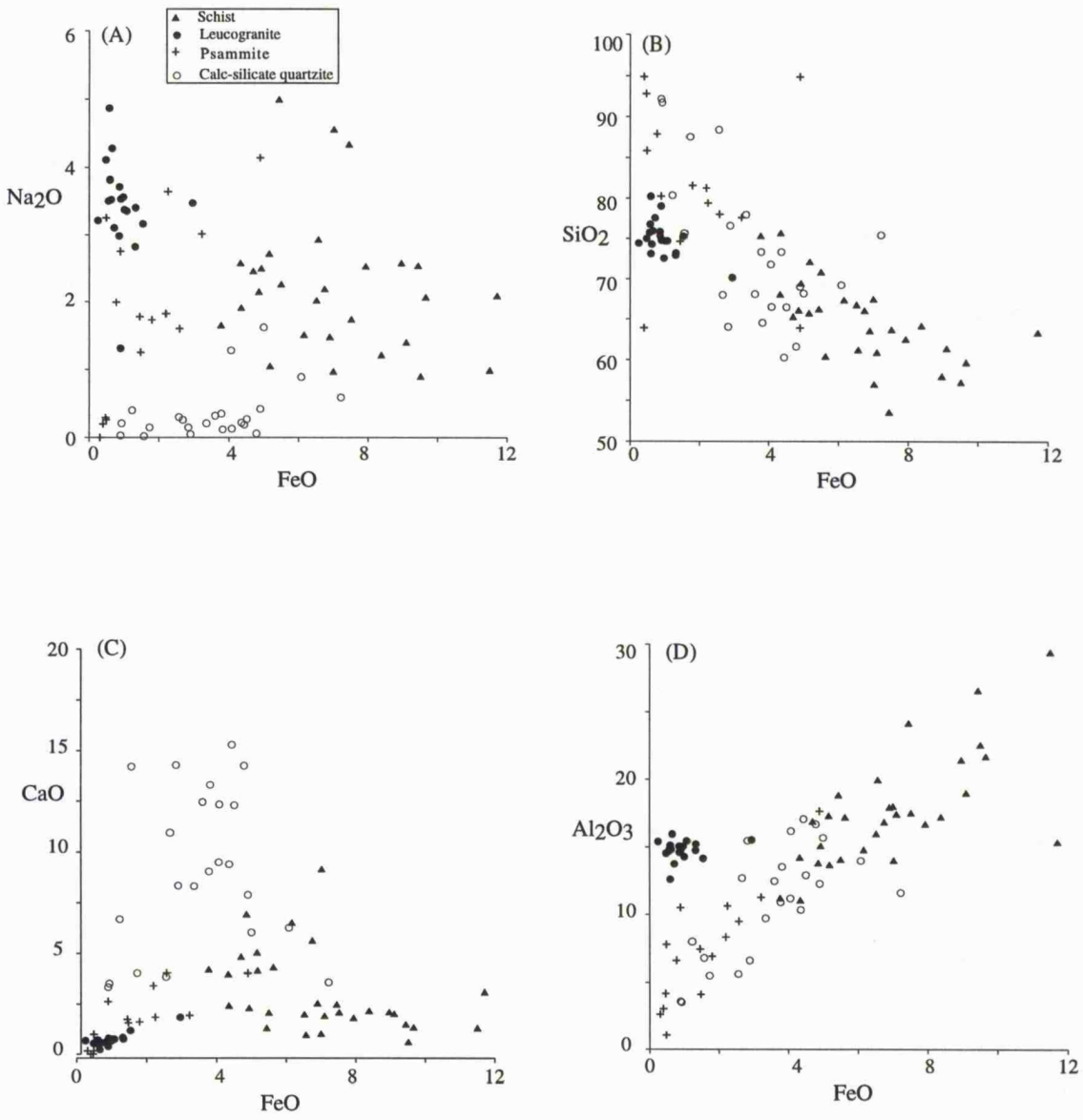

Fig. 5.2: (A-D) Relationship of FeO with the oxides such as Na_2O, SiO_2, CaO and Al_2O_3 of Miniki Gol leucogranite, psammite, calc-silicate quartzite and schist. Overlapping can be seen among leucogranite, psammite and calc-silicate quartzite analyses. Data taken from Appendix (5.2-4). Symbols as in (**Fig. A**).

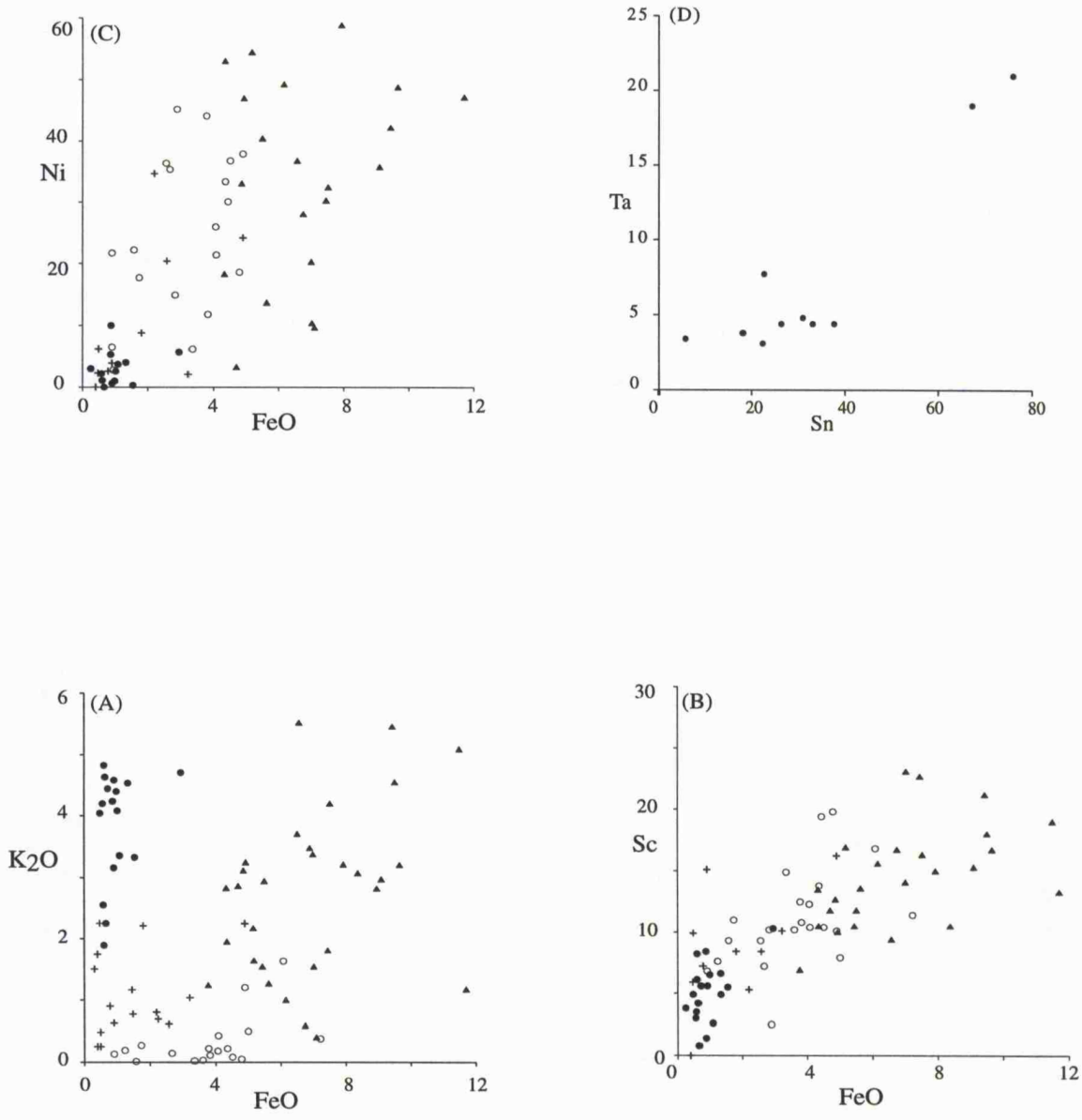

Fig. 5.3: Relationship of FeO **(A)** with the oxide K_2O and **(B-C)** trace elements Ni and Sc (ppm) of Miniki Gol leucogranite, psammite, calc-silicate quartzite and schist. Overlapping can be noticed among leucogranite, psammite and calc-silicate quartzite data. **(D)** Linear relationship between Sn and Ta (ppm) from Miniki Gol leucogranite. Data taken from Appendix (5.2-4). Symbols as in (**Fig. 5.2 A**).

(e.g. Vidal et al. 1982; Chappell et al. 1987). This is similar to the chemistry of the Miniki Gol pegmatites and these are also very rich in Be, Rb and very low in Sr, Ba, Zr, Y, Th, Sc, V, Cr, and Ni. Very similar enrichment and depletion trend has been observed in the most evolved granites (type E and F) relatively to less differentiated granite (type B) from the Cornubian batholith, SW England (Stone and Exley 1986). According to Chappell et al. (1987) the depleted elements (Sr, Ba and Eu) strongly partition into the solid phase and Rb increases in abundance in the melt relative to the feldspars. The low TiO_2 (ppm) / Ta ratio (126) of the Miniki Gol leucogranite also shows its differentiated behaviour (Boissavy-Vinau and Roger 1980). Similarly the positive correlation between Sr and Ba, and a linear relationship between FeO and MgO (Fig. 5.1 C and E) also signify a fractional crystallisation. The lack of zircon and low content of Zr (mean 43 ppm) suggest a low magmatic temperature (see Crawford and Searle 1993).

An alternate explanation is that of Harris and Inger (1992), who have argued that the high Rb / Sr and low Sr / Ba ratios in the Himalayan leucogranite indicate an unfractionated melt. Keeping in view the above criteria, the Miniki Gol leucogranite is represented by a high Rb / Sr ratio 3.4 and low Sr / Ba ratio 0.4 together with negative Eu anomalies. This signify a unfractionated eutectic melt derived from pelitic protolith. The high Rb and low Sr and Ba contents in the leucogranite relative to the psammo-pelites and their overlap are consistent with this pelitic source. The Rb value of the Miniki Gol leucogranite is also consistent with the pelite-derived granite as Miller (1985) has demonstrated that the pelite-derived magma contains approximately as much as 200 ppm Rb.

It is not clear whether the melt in the Miniki Gol leucogranite is vapour-saturated or unsaturated. In case of vapour-present melting, an external source of fluid is proposed by Le Fort (1981) and Le Fort et al. (1987) for the Himalayan leucogranite. These fluids have been generated by decorbonation metamorphic reactions and dehydration of underthrust of the Kohistan crust during the collision along the MMT. However, it is unlikely that the water is abundant in the lower crust due to the P-T conditions and low porosities (Clemens and Vielzeuf 1987) and alternatively a vapour-absent melting model should be invoked. High Rb / Sr and low Sr / Ba ratios are indication of vapour-absent melting (Harris and Inger 1992). The presence of abundant muscovite in the pelites could be a possible source of water as muscovite break down during the upper amphibolite facies metamorphism.

Based on the positive correlation between MgO and SiO_2 and a general linear trend for P_2O_5 (Fig. 5.1 F), which intersects the SiO_2-axis > 75 per cent SiO_2, a minimum melt composition is proposed for the Miniki Gol leucogranite. Chappell et al. (1987) have

argued that the minimum melt contains small amount of P_2O_5 and MgO and its composition will lie above 75 % SiO_2. Most of the trace elements from the Miniki Gol leucogranite show no consistent variation against the silica, indicating a minimum melt composition for these leucogranites. The high content of Na_2O in the Miniki Gol leucogranite and granodiorite also correlates with a minimum melt (Miller 1985). Minimum melt composition and low crystallisation temperature and a possible water-saturated nature also suggest melting of a pelitic source (see Crawford and Searle 1993).

5.2.4 Specialised granite

Many authors such as Tischendorf (1977), Shaw and Flood (1981), Plant et al. (1985) and MacLellan and Taylor (1989) have set geochemical criteria for the recognition of specialised granites associated with tin-tungsten deposits. According to these authors specialised granites are enriched generally in elements such as Si, Na, K, F, Li, B, Be, Rb, Cs, Ga, Sn, W, Ta, Nb, Y, U, Th, Pb, and light REE and impoverished in Ti, Mg, Ca, Fe, P, Zr, Hf, Sr, Ba, V, Co, Cr, Ni and Eu. These granites are also characterised by high Al_2O_3 / (Na_2O + K_2O + CaO), Rb / Sr and Rb /Ba ratios and low TiO_2 / Ta, K / Rb and Mg / Li (Boissavy-Vinau and Roger 1980; Plimer 1987b). The concentration of these elements varies within the ore-bearing granites and has been found to be higher in the upper contacts of the granites and in the vicinity of the mineralised veins and lodes (Plimer 1987b).

It should be noted however, that the concentration of the trace elements in the ore-bearing granites depend mainly upon the nature of magma, source and its fractional crystallisation history. For example Sn-W-bearing alkaline-biotite granites of Nigeria (Imeokparia 1985), are significantly enriched in Nb, Zr, Y, Th and U whereas S-type mineralised granites from Cornubian batholith, SW England (Stone and Exley 1986), are depleted in Zr and Y. Similarly the Grey River W-bearing K-feldspar granites, Canada (Higgins 1985) are enriched in Zr and depleted in Li and Nb, whilst the most evolved tin granites of Eastern Marche (France) and Viseu, Portugal, (Boissavy-Vinau and Roger 1980) are depleted in U and Th.

As mentioned earlier the Miniki Gol leucogranite is represented by high levels of Rb, Li, Be, Sn, W, Pb, Ta, U and Rb / Sr ratio (3.4) and low concentration of Zr, Hf, Y, Th, Sr, Ba, Zn, V, Co, Cr, Ni, TiO_2 / Ta (126), K / Rb (59.64) and Mg / Li (0.7). The concentration of these elements in the Miniki Gol leucogranites, is more or less the same as compared to the ore bearing granite of the Tischendorf (1977), Plant et al. (1985), and Boissavy-Vinau and Roger 1980). High levels of certain elements particularly Li (mean 160 ppm) Be (mean 20 ppm) Sn (mean 33.4 ppm) W (mean 5.3 ppm) and Ta (mean 7.3

ppm) in the Miniki Gol granite highlight its geochemical signature. Using the criteria of the specialised granites of Tischendorf (1977) the Miniki Gol leucogranite can be considered as potential specialised granite.

It should also be noted, however, that most of the unmineralised S-type or leucogranite and ore-bearing granites have a number of geochemical features in common. Similarly the concentration of many of the trace elements of the Miniki Gol leucogranite are similar to those of barren S-type (leucogranite) such as Himalayan leucogranite (France-Lanord and Le Fort 1988).

However, the Miniki Gol leucogranite can be differentiated from the Himalayan (Manaslu) leucogranite (France-Lanord and Le Fort 1988; Le Fort et al. 1987) by containing low levels of Cs, Co, B, and Th and high values of Mo, W, Sn, Ta and Be. The enriched elements, such as Sn and Ta in the Miniki Gol leucogranite are regarded as an essential parameter for the Sn-W bearing granites (see Schwartz 1992; Boissavy-Vinau and Roger 1980). According to these authors Sn and Ta increase with the increasing degree of magmatic differentiation. This evolution trend is evident from the strong positive correlation between these two elements in the leucogranite of the study area (Fig. 5.3 D). According to Lehmann (1990) concentration of Sn increases from least evolved to highly fractionated granite (e.g. Bolivian tin granites). The enrichment trend of the incompatible elements in the Miniki Gol pegmatite such as Sn (up to 99 ppm) Rb (up to 766 ppm) B (1433 ppm) Be (up to 275 ppm) and Na_2O (up to 6.43 wt %) indicate the metallogenic character of these pegmatites.

Beryl deposits have also been located in the granite-pegmatite about 15 km south of Miniki Gol. Mineralised pegmatite throughout the Hindu Kush and Pamirs belts have been reported by Rossovskiy (1991). These pegmatite outcrops are spatially and genetically related to Li-Ta-Be-Sn deposits in the Hindu Kush and Pamirs metallogenic province.

Specialised granites normally contain higher Sn values and this enrichment is generally lower for W than for Sn. The W content of the investigated leucogranite is relatively low compared to the specialised granite (mean 5. 3 ppm), although slightly higher than Manaslu leucogranite (mean 4.4 ppm) see (France-Lanord and Le Fort 1988). Similarly, the investigated pegmatite also contains low values of W up to 2.2 ppm. It should also be noted that the level of tungsten varies from one specialised granite to another. For example the W content in the W-Sn-bearing Burnthill granite Canada (MacLellan and Taylor 1989) generally ranges from 1.5 to 4 ppm, whereas in Grey River W-bearing K-feldspar granites, Canada (Higgins 1985) contains low levels of W (mean 5 ppm). In contrast, the SW England granite such as Hemerdon (Beer and Ball 1987),

contains high levels of W (mean 70 ppm). This is due the fact that the enrichment and depletion of W within the ore-bearing granite varies from place to place. Plimer (1987b) has argued that the concentration of W within the granite is related to the proximity to tungsten deposits. That is the main reason for the occurrence of high level of tungsten in the cupolas and ridges at the top of the pluton and decreases further away from the mineralised zone. This could be the reason that the Miniki Gol leucogranite contains low levels of W as these granites are not spatially related, at least on the surface, to the Miniki Gol tungsten deposits.

5.3 Schists

The summary of the major elements chemistry together with the trace elements of the schist from the Miniki Gol, Besti Gol and Garam Chashma area is given in the Table 5.3. The major element chemistry of the studied metasediments is compared with the average post-Archean shale after Krauskopf (1967), whereas the trace element geochemistry is compared with the average shale (Turekian and Wedepohl 1961). Compared with the post-Archean shale, the Miniki Gol schistose rocks are rich in Na and poor in Ca (Table 5.3). The CaO content of the calcareous schist reaches up to 9.15 wt % (ZM 105), whereas those rocks rich in FeO such as ZC 11 (FeO 11.71 Wt % and MnO 2.09 Wt %, contain substantial amount of garnet (Appendix 5.3). The schist from Besti Gol area is characterised by a high level of Na and low level of K (see Appendix 5.3).

Comparing the present data with the average shale of Turekian and Wedepohl (1961), the Miniki Gol schist is highly enriched in F, Li, Cs, and to a lesser extent Be, W, Pb, Th, Zr, Y, Hf and Nb (Table 5.3). Barium is very high in some of the calcareous and mica schist, reflecting its occurrence in calcite or plagioclase (Appendix 5.3). Leake et al. (1989) have also reported high levels of B (minimum 201 ppm), W (mean 11 ppm) and As (up to 26 ppm) in the schist. The schists at Miniki Gol, are also significantly depleted in S and to a lesser extent, Cl, Ni, Cu and Mo (Table 5.3). The enrichment of many of these elements provide clearest expression of metasomatic activity (see Christensen et al. 1983; Leake et al. 1989; Van de Haar et al. 1993), in the Miniki Gol schist.

5.4 Background level of W at Miniki Gol

In order to know the pre-granitic concentration of the tungsten, the background levels of Sn and W both in Miniki Gol, Chitral and SW England have been analysed. In the Miniki Gol area the samples have been taken along a section from Garam Chashma to Shoghor (see Fig. 5.4). These background metapelites (slate and schist) are located up to 15 km away from the mineralised zone (Fig. 5.4). It can be seen from Table 5.3 that the

Table 5.3: Major and trace element geochemistry of the schist from Miniki Gol and surrounding area.

	Min	Max	Mean	Std[1]	N[2]	-	-	Krauskopf (1967) average post-Archean shale
SiO_2	47.3	75.7	63.2	6.7	31	-	-	61.6
TiO_2	0.4	1.2	0.8	0.2	31	-	-	1
Al_2O_3	11.1	29.4	17.9	4.2	31	-	-	18.3
Fe_2O_3	3.8	12.2	7.1	2.3	31	-	-	7.4
MnO	0.0	2.1	0.2	0.4	31	-	-	0.13
MgO	1.2	4.4	2.4	0.7	31	-	-	2.7
CaO	0.6	9.2	3.0	2.0	31	-	-	4.2
Na_2O	0.9	7.1	2.5	1.6	31	-	-	1.1
K_2O	0.4	5.5	2.8	1.4	31	-	-	3.4
P_2O_5	0.1	0.3	0.2	0.1	31	-	-	0.22
Total	98.7	102.1	100.1	0.9	-	-	-	100.1
Trace elements (ppm)								
						Mean*	N[2]	Turekian & Wedepohl (1961) average shale
B	17	184	75	60.5	6	100	2	100
F	270	3210	1135	522	29	1150	2	740
Cl	40	230	115	75	29	215	2	180
S	0	1390	130	279	29	85	2	2400
Li	27.5	469	190	110	43	102	8	66
Be	1	20.9	4.4	3.2	43	2.7	8	3
Cs	9	83	33	34.5	4	n.a	-	5
Ba	55.1	949.7	485.1	220.9	43	567	8	580
Rb	14	420	180	84	43	151	8	140
Sr	40	712	256	138	43	137	8	300
Th	4.8	31.6	20	6.2	43	12.8	5	12
U	1.8	6.4	4.7	2.2	4	n.a	-	3.7
Zr	110	658	210	103	43	212	8	160
Hf	3	8	6.3	2.2	4	n.a	-	2.8
Ta	2	3.1	1.9	0.6	3	n.a	-	0.8
Nb	6.9	31.1	18.8	4.5	43	13.4	8	11
Y	19.9	57.7	35.9	7.5	43	33.2	8	26
Sc	9.4	23.3	16.7	3.5	43	13.2	8	13
V	53.3	153	106	23	43	87	8	130
Cr	31.3	173	110	32.7	43	66	8	90
Co	9.6	41.3	20.2	7	43	13.8	8	19
Ni	8.5	74.4	37.8	18.4	43	28.4	8	68
Cu	1.2	74.2	21.8	13.6	41	14.6	8	45
Zn	50.5	256	100	37.4	43	88	8	95
Ga	11.3	39.4	24.8	5.8	43	19.8	8	19
Pb	6.7	60	31.2	11.6	43	19	8	20
W	0.4	8	3.2	2	36	2.6	8	1.8
Sn	1.3	16.5	5.03	3.55	43	3.08	8	6
Mo	0.1	3.4	0.8	0.9	37	0.7	5	2.6
Sb	2.2	2.9	2.6	0.4	3	n.a	-	1.5
La	17	92	65.3	34.5	4	n.a	-	92
Ce	42	180	128	63	4	n.a	-	59
Nd	14	59	43.3	21	4	n.a	-	24
Sm	2.9	14	9.5	5.1	4	n.a	-	6.4
Eu	0.8	2.8	2	1	4	n.a	-	1
Gd	2	11	5.5	4	6	n.a	-	6.4
Tb	2	2.4	2.2	0.3	2	n.a	-	1
Yb	1.9	6.3	4.6	2	4	n.a	-	2.6
Lu	0.3	1	0.7	0.3	4	n.a	-	0.7
(La/Y)cn	8.7	10.8						
Eu/Eu*	0.7	0.9						

*= Garam Chashma back ground schist; 1 = Standard deviation; Fe_2O_3 is regarded as total iron; n.a = Not analysed
2 = Numbers of samples; Eu / Eu* (i.e. $Eu_N / [(Sm_N)\ (Gd_N)]^{1/2}$; cn= chondrite normalised value. Be and Li were analysed by ICP-ES and B, Cs, U, Hf, Ta, Sb and REE by INAA. All the other elements were analysed by XRF.

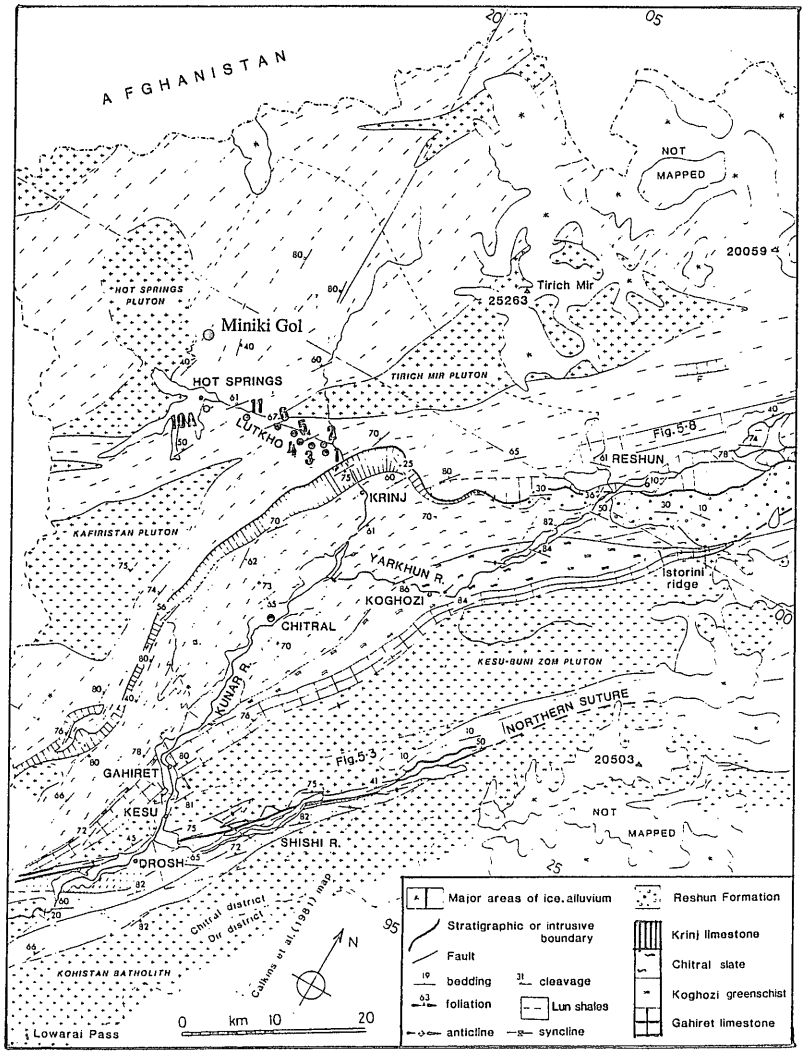

Fig. 5.4: Sample locations of the background pelites (prefix ZS) at Garam Chashma-Shoghor section superimposed on geological map (after Calkins et. al. 1981; Pudsey et al. 1985).

background metapelite's levels of Sn (mean 3.08 ppm) are lower than average shale (mean 6 ppm) of Turekian and Wedepohl (1961). However, level of tungsten (mean 2.6 ppm) are slightly higher than the average shale 1.8 ppm and reaches up to 7 ppm (Appendix 5.3).

Plotting the background Sn and W against the distance (Fig. 5.5 A-B) it is noted that Sn progressively increase from Shoghor to Garam Chashma. The tungsten levels against the distance are erratic and not conclusive, however the levels of W at Garam Chashma metasediments are higher than the Shoghor. Tungsten against the distance are also plotted from Miniki Gol mineralised zone to Garam Chashma area (Fig. 5.5 C). It is seen that W levels progressively increase from Garam Chashma towards the Miniki Gol mineralised zone. The levels of W (4.1 ppm) and Sn (5 ppm) around Miniki Gol mineralised zone are also higher from the background metapelites (2.6 ppm and 3 ppm) respectively. The tungsten data within the alteration zone, appear to define a positive gradient towards the Miniki Gol rich zone and also show distinct dispersion around the mineralised zone (Fig. 5.5 C).

Both fluorine and lithium are also high (1150 ppm and 102 ppm) in Miniki Gol background metapelites compared to the average shale (740 ppm and 66 ppm respectively) of Turekian and Wedepohl (1961). F and Li are also noted high in the Miniki Gol schist around the mineralised zone (Table 5.3).

5.4.1 Background level of W at SW England

As a comparison to the study in Chitral, Northern Pakistan, background levels of tungsten in the pelites and volcanic rocks surrounding granite and greisen related mineralisation, have also been analysed. About 40 specimens were collected from different locations, mainly quarries away from granites (see Fig. 5.6, Appendix 5.6). These samples were collected from Whympston, Wadham, Jennyclift Bay, Bigbury, Bridestowe, Brentor, Burley Wood, Tintagel Castle, Cansford quarry, Egloskerry, Polyphant, Michaelstow, Tregildrans, Waderidge, Pentire, Trevose and Pendeen.

The rocks include slates, shale, black shale, sandstone and siltstones. Some of these pelites are metamorphosed up to greenschist facies, developing schistosity. These pelites and metapelites are highly fractured and weathered and most of them exhibit iron leaching. Deformational activities such as kink folds are also noticed in some of the schist.

5.4.2 Levels of Li, W and Sn

The statistics of the geochemical data in terms of Li, W and Sn and its comparison with the corresponding average rocks is given in the Table 5.4 and Appendix 5.7.

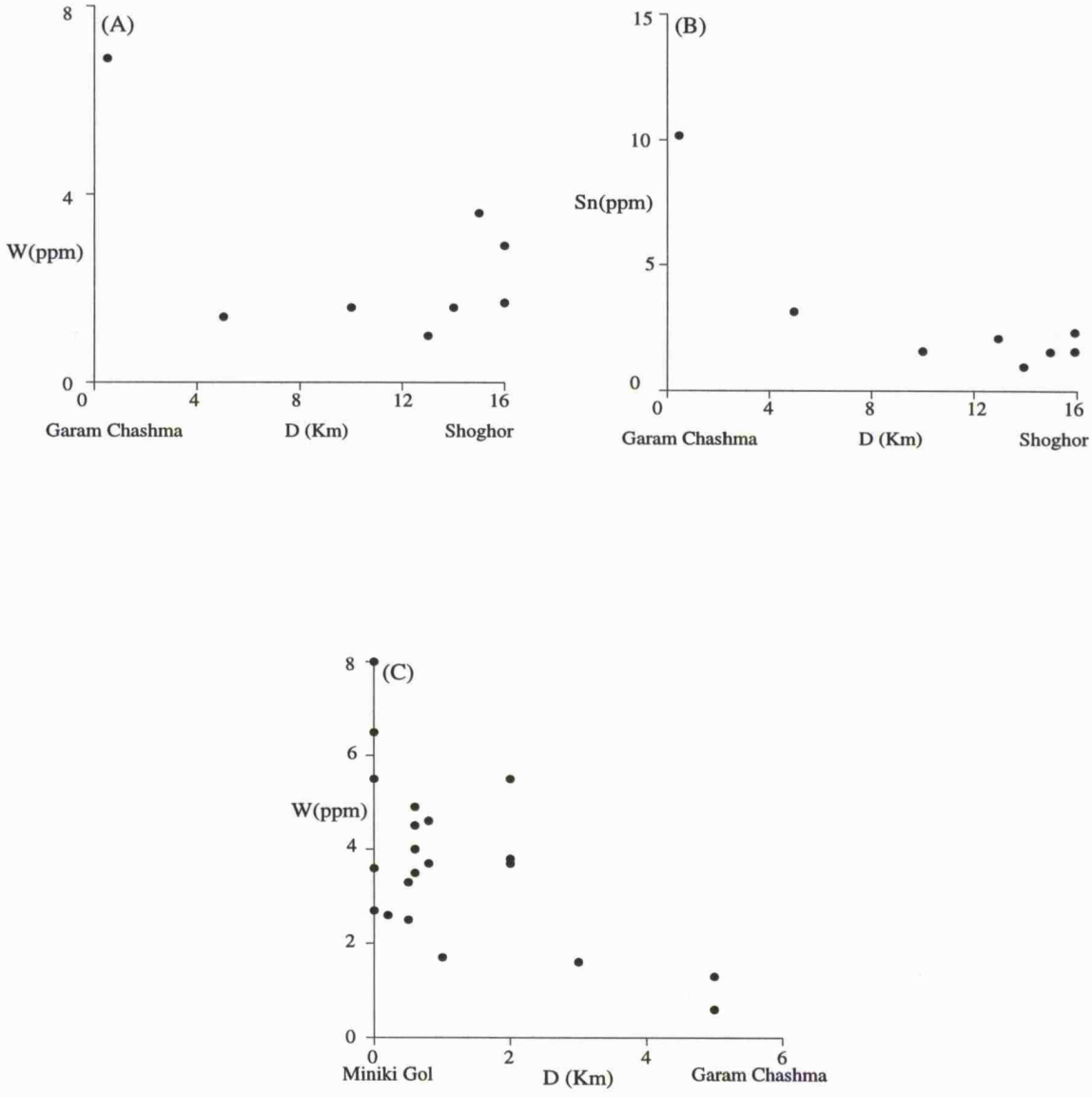

Fig. 5.5: Concentrations of W and Sn against distance (D) in the background schist: **(A-B)** From Shoghor to Garam Chashma. **(C)** From Garam Chashma to Miniki Gol.

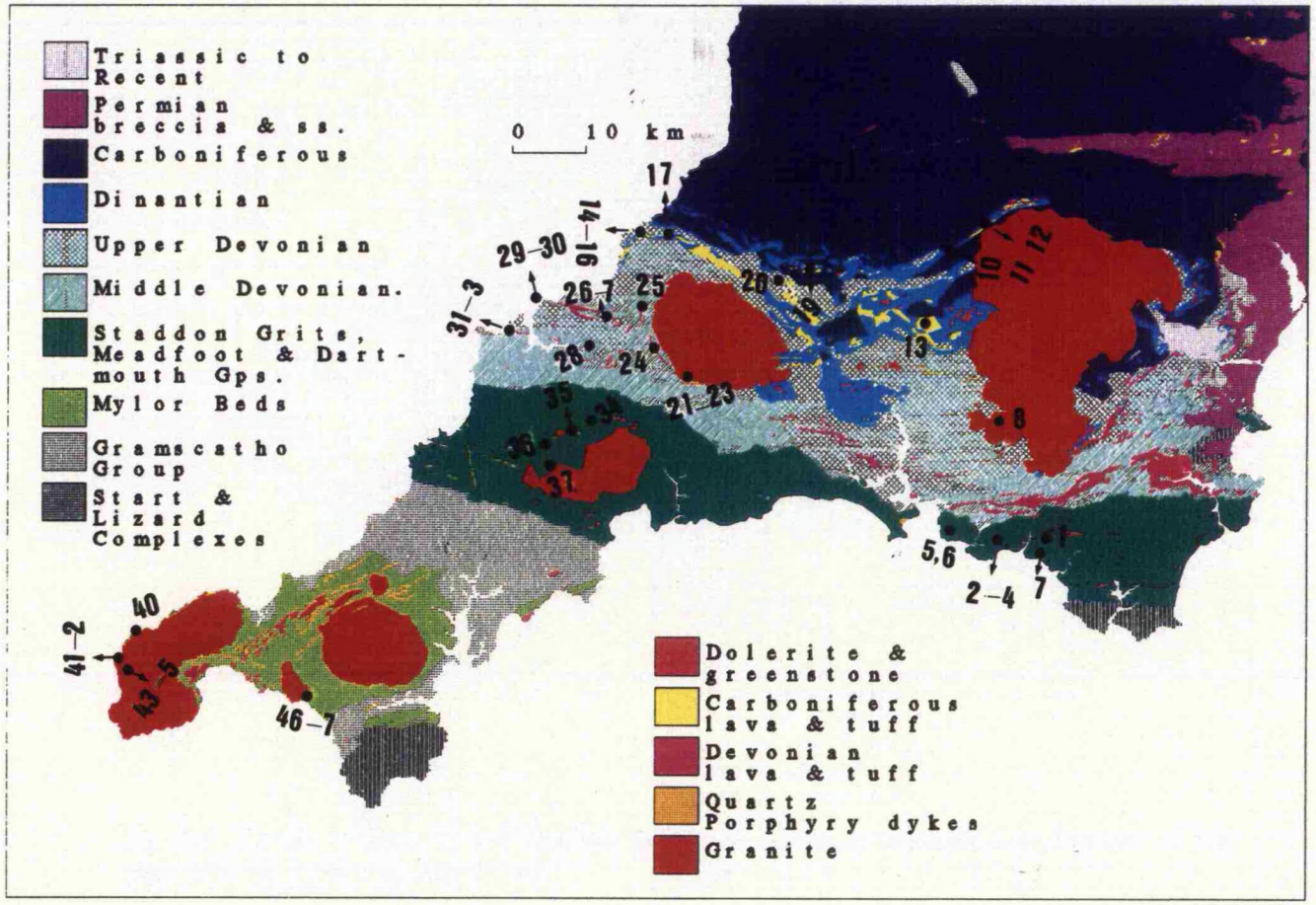

Fig. 5.6: Sample locations of SW England background pelites (prefix SW) superimposed on the generalised geological map (after B. G. S).

Table 5.4: Li, W and Sn concentrations in pelites and volcanic rocks of SW England.

	This work	Beer & Ball	Hall (1990)	Turekian and Wedepohl (1961)	(Jeffery 1959)
Pelites	(n= 14)	(1986)		**(Avg. shale)**	**(Avg. shale)**
Li	118	-	102	66	
W	2.9	4.6	-	1.8	3.9
Sn	2.2	3.3	9	6	
Volcanics	(n=12)			**(Avg. basic rocks)**	**(Avg. volcanic)**
Li	137	-	102	17	-
W	2.3	-	-	0.7	5.2
Sn	3	-	9	1.5	-

High level of Li (118 ppm) and low level of tin (2.2 ppm) have been recorded from the background pelites of the Cornubian province, SW England (Table 5.4), compared with the average shale of Turekian and Wedepohl (1961). Although, Hall (1990) has recorded high concentration of Sn (9 ppm) in the Cornubian shales and slate. Like Miniki Gol, the background level of tungsten (2.9 ppm) from the pelites of SW England, is relatively higher than the average shale (1.8 ppm, Table 5.4).

The background volcanic rocks of the Cornubian province, SW England, also contain high levels of lithium, tin and tungsten compared with the average values of basic rocks reported by Turekian and Wedepohl (1961). However, the level of W in these volcanic rock, is low compared with the basic rocks (dolerite and amphibolite, mean 5.2 ppm, Table 5.4), associated with the tungsten mineralisation of the Uganda Protectorate, after Jeffery (1959). High concentration of tin has been recorded, particularly in dolerite during the present study (see Appendix 5.7). Similarly, Hall (1990) has also reported high concentration of Sn (9 ppm) in the Cornubian volcanic rocks.

It is of great interest to compare the background geochemical data (in term of Li, W and Sn) of Cornubian province, SW England with the Miniki Gol, Chitral background metapelites. The concentration trend of these elements in both the areas are more or less similar. These elements are also enriched in the leucogranites of both the areas of under investigation. Levels of W in both the Miniki Gol, Chitral, Northern Pakistan and Cornubian province SW England are slightly higher than the average shale but are not anomalous. This rules out the possibility of pre-granitic concentration of tungsten in both these areas and also inconsistent with the enrichment of W during exhalation. The post-granitic enrichment of the tungsten probably suggest that the emplacement of the leucogranite has played a significant role in the concentration of W at Miniki Gol.

Whereas tungsten mineralisation at Cornubian province SW England, is spatially and genetically related to greisenation.

The enrichment of fluorine, lithium, tungsten and tin both in the Cornubian province and Miniki Gol schist around the mineralising zone, reflect the evidence of dispersion. According to Beer and Ball (1986) the dispersion of Sn-W progressively decreases from the contact aureoles or the mineralisation zone towards the background levels at Cornubian province. High values of fluorine, lithium and particularly tin (mean 64 ppm) are noted in the Miniki Gol calc-silicate rocks compared with the schist and these elements could be described as pathfinder elements towards the Miniki Gol W mineralisation, particularly in the dispersion zone. Van de Haar et al. (1993) have also considered these elements as mineralisation factor. Moreover, Oosterom et al. (1984) have expressed that the anomalous dispersed tin values in the Panasqueira schist could be considered as a 'pathfinder' to the tungsten mineralisation in Portugal.

5.5 Calc-silicate quartzite and psammite

The geochemical data for the Miniki Gol calc-silicate quartzite and psammite are summarised in the Table 5.5. The chemistry of the Miniki Gol calc-silicate quartzites differs significantly from the post-Archean shale after Krauskopf (1967), by high levels of CaO (mean 9.08 wt %) and SiO_2 (mean 73.5 wt %) and low levels of FeO (mean 3.53 wt %), K_2O (mean 0.26 wt %) and Na_2O (mean 0.36 wt %). Compared with the schist from the study area, they are also enriched in Ca, Si and depleted in K, Al and Na (Table 5.3, 5.5).

There is a positive correlation between CaO and Al_2O_3 in the calc-silicate quartzite and both these elements probably concentrated in the clinozoisite as plagioclase is very rare in the calc-silicate quartzites (Fig. 5.7 A). This contrasts with the general negative relationship (r = -0.02) between these two elements in the schist. The CaO content of the calc-silicate quartzite reaches up to 15.27 wt %, which amount is very high compared to the quartz-rich Phanerozoic greywacke (sandstone), Australia or even quartz-poor greywacke where the maximum CaO is recorded as 5.52 wt % (see Taylor and McLennan 1985). This probably suggest the occurrence of calcium-rich rocks such as calcite and calcic-plagioclase (as pure anorthite, reported in one sample) in the protoliths of the calc-silicate rocks. It is also possible that some additional Ca was introduced to these rocks by metasomatic fluids.

A positive correlation also exist between Fe and Mg in the calc-silicate quartzite (Fig. 5.7 B).

Table 5.5: Summary of the geochemical data of the Miniki Gol psammite and calc-silicate quartzites.

	Psammite					Calc-silicate quartzite				
	Min	Max	Mean	Std[1]	N[2]	min	Max	Mean	Std[1]	N[2]
SiO_2	63.9	94.9	74.7	11.4	10	60.3	92.2	73.5	9.3	23
TiO_2	0.2	0.8	0.4	0.2	10	0.1	1.3	0.6	0.3	23
Al_2O_3	3.0	17.7	7.5	5.4	10	3.5	17.1	11.0	4.2	23
*Fe_2O_3	0.4	4.9	1.5	1.8	10	0.9	7.2	3.5	1.6	23
MnO	0.0	0.1	0.0	0.0	10	0.0	0.5	0.1	0.1	23
MgO	0.2	1.5	0.5	0.5	10	0.2	1.8	0.8	0.4	23
CaO	0.0	4.0	1.7	1.6	10	3.3	15.3	9.1	4.0	23
Na_2O	0.2	4.1	1.8	1.5	10	0.0	1.6	0.4	0.4	23
K_2O	0.3	2.3	1.2	0.9	10	0.0	1.6	0.3	0.4	23
P_2O_5	0.0	0.3	0.1	0.1	10	0.0	1.2	0.3	0.3	23
Total	96.9	100.8	89.3	1.4	10	96.9	101.7	99.5	1.5	23
Trace elements in ppm										
B	5.0	6.0	5.5	0.7	2	2.0	14.0	4.9	3.2	13
F	70	920	313	290	10	130	1430	770	325	31
Cl	40	80	53	14.9	10	30	220	86	65	31
S	0.0	80	15	31	10	0.0	550	100	158	31
AS	1.3	1.4	1.4	0.1	2	0.5	3.8	1.6	0.8	20
Li	12	225	65	50	19	5.2	204	55	50	44
Be	0.5	8.5	2.4	2.0	19	0.5	51.5	4.3	9.2	44
Cs	3.0	9.0	6.0	4.2	2	1.0	11.0	3.9	3.4	16
Ba	21	1295	326	282	19	0.8	452	98	112	43
Rb	5.2	130	51.3	33.9	19	0.1	167	41.2	42.4	39
Sr	28.3	1148	280	258	19	47	420	212	87	44
Th	1.0	25.0	12.8	5.7	19	3.6	81.0	17.1	14.8	44
U	3.3	6.5	4.9	2.3	2	1.7	17.0	5.3	3.7	20
Zr	6.0	562	325	127	19	70	1567	350	242	44
Hf	11.0	16.0	13.5	3.5	2	3.0	46.0	12.4	10.2	21
Ta	2.3		2.3		1	0.7	4.0	1.5	0.9	13
Nb	1.1	18.1	9.0	4.0	19	3.4	24.6	12.5	5.5	44
Y	3.0	37.6	21.4	9.6	19	12.3	75.7	31.5	12.9	44
Sc	0.5	16.2	8.0	4.3	17	0.2	20.9	10.3	4.6	42
V	4.2	77.2	33.4	18.5	19	11.8	93	49.6	22.3	44
Cr	10.6	78	37	22.2	18	2.9	166	47	30	44
Co	0.5	13.0	4.2	3.5	18	1.8	27.9	10.6	5.1	43
Ni	2.1	34.7	11.9	10.3	16	2.8	90	28.3	20.0	43
Cu	1.2	18.3	7.7	5.5	10	0.4	49.2	11.4	11.3	39
Zn	1.4	193	30.0	44.6	18	6.7	93.3	37	22	40
Hg	< 1	< 1			2	< 1	< 1			21
Ag	< 5	< 5			2	< 5	< 5			21
Ga	3.0	20.4	8.7	4.0	19	3.8	70.5	19.9	12.9	42
Pb	2.5	206	27	45	19	2.0	48.7	20.3	10.1	44
W	0.1	21.0	2.7	5.5	14	0.4	30550	3090	7290	39
Sn	1.0	39.6	6.4	10.16	17	1.2	452	64.2	114	43
Mo	0.1	3.2	1.7	0.9	19	0.0	5.0	1.2	1.2	36
Sb	0.3	0.9	0.6	0.4	2	0.2	2.0	0.7	0.6	14
La	39	44	41.5	3.5	2	8.4	130	43	29.4	21
Ce	83	86	84.5	2.1	2	20	280	89	59.7	21
Nd	24	30	27	4.2	2	10	100	35	20	20
Sm	5.5	5.8	5.7	0.2	2	1.6	19.0	6.9	3.8	21
Eu	1.1	1.6	1.4	0.4	2	0.6	2.9	1.6	0.6	21
Gd	4.0	5.0	4.5	0.7	2	1.0	13	5.1	2.9	21
Tb	0.7		0.7		1	0.7	4.9	1.9	1.3	15
Yb	2.3	3.0	2.7	0.5	2	2.0	9.0	4.4	2.0	21
Lu	0.4	0.5	0.4	0.0	2	0.2	1.4	0.6	0.3	21
Eu/Eu*	0.7	0.9				0.6	1.6			
La/Yb	13	19				3.2	15.6			
(La/Lu)cn	8.6	10.8				2.5	9.7			

* = Total iron considered as Fe_2O_3; 1= Standard deviation; 2 = Number of samples; Eu / Eu* (i.e. Eu_N/ $[(Sm_N)(Gd_N)]^{1/2}$; cn= chondrite normalised value. Be and Li were analysed by ICP-ES and B, Cs, U, Hf, Ta, Sb, Hg, Ag and REE by INAA. All the other elements were analysed by XRF.

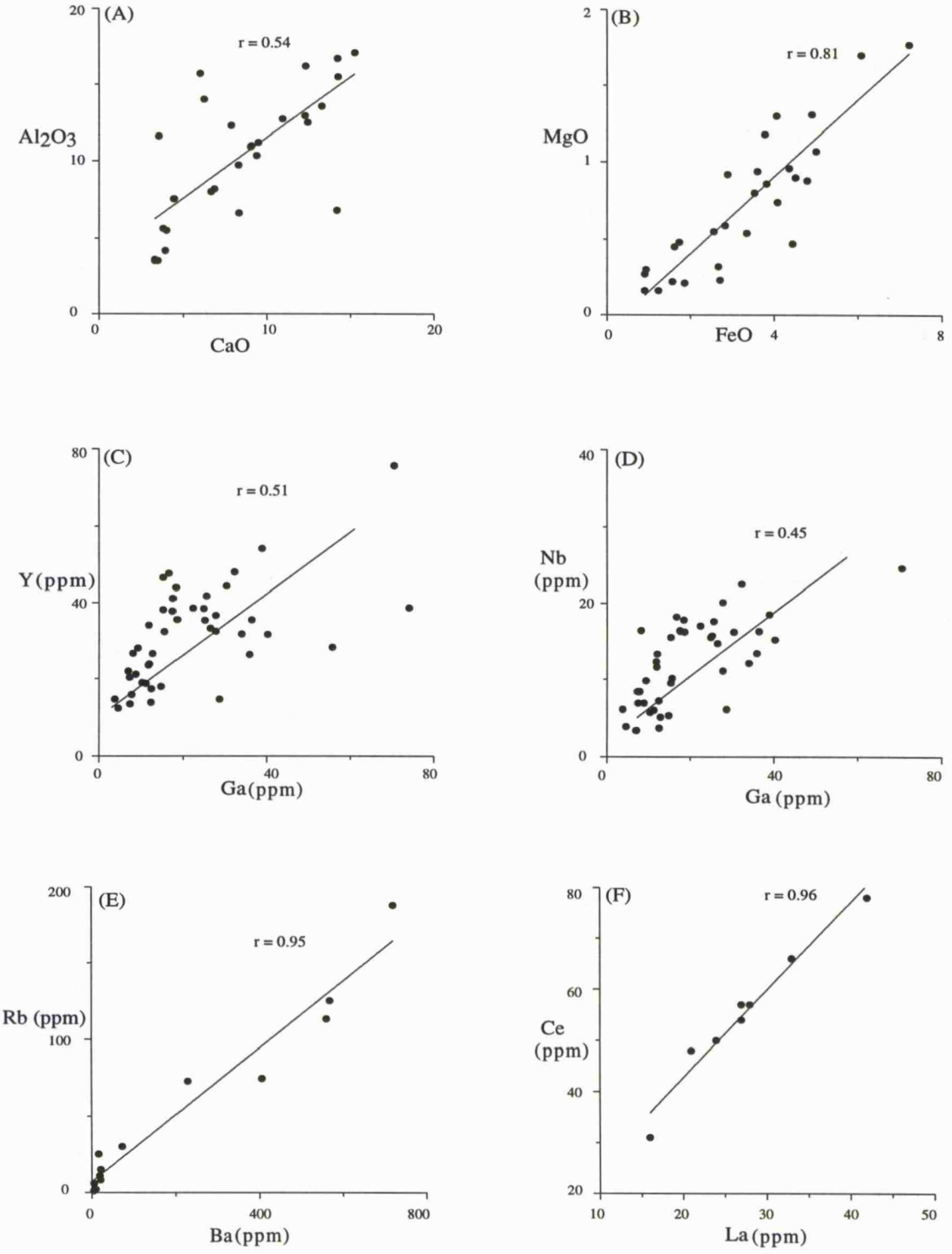

Fig. 5.7: **(A-B)** Relationship of the oxides, CaO vs. Al2O3 and FeO vs. MgO in the Miniki Gol calc-silicate quartzite. **(C-D)** Correlation of Ga vs. Y and Nb in the studied calc-silicate quartzite. **(E-F)** Linear relationship between trace elements (Rb-Ba) and (La-Ce) in the proposed tourmalinite. Data taken from **Appedix (5.4, 5.5).**

5.5.1 Trace element chemistry

The trace element geochemistry of the proposed calc-silicate quartzite and psammite is summarised in the Table 5.5. Compared with the mica schist, the calc-silicate rocks are richer in W, Sn, Zr and Hf and impoverished in B, F, Li, Ba, Rb, Cs, V, Cr and Zn (Table 5.3, 5.5). The scheelite-bearing calc-silicate quartzites are characterised by high value of Zr (mean 455 ppm), Hf (mean 16 ppm), Be (mean 8.4 ppm), Th (mean 24 ppm), U (mean 6.1 ppm) Ga (mean 31 ppm), Nb (mean 14.7 ppm) and Y (mean 35.3 ppm) compared to the unmineralised calc-silicate quartzite, psammite and schist (Table 5.5). The calc-silicate rocks also contain very low level of Ba (mean 43 ppm) and Rb (mean 16.4 ppm). The F content is notably high in the calc-silicate quartzite compared with psammite (Table 5.5).

Tungsten levels are highly variable in these rocks, reaching 3 %. A weak positive correlation exist between Sn and W ($r = 0.2$) in the calc-silicate quartzites. Ga has a linear relationship with the Zr ($r = 0.27$), Y and Nb in the calc-silicate quartzite (Fig. 5.7 C-D). This indicates that Ga, Nb, Y and Zr have similar geochemical behaviour in the scheelite-bearing calc-silicate quartzite. The enrichment of the elements such as Zr, Hf, Ga, Y, Nb, W, Be, U and Th in the scheelite-bearing calc-silicate quartzite clearly reflect that these elements have been introduced by hydrothermal fluids. This metasomatic activity is more prominent in the scheelite-bearing calc-silicate quartzite than the unmineralised psammite and schist.

Very low concentrations of B (mean 4.9 ppm) Hg (< 1 ppm), Sb (mean 0.7 ppm), MnO (mean 0.1 wt %), FeO (mean 3.5 wt %) and relatively low F (mean 770 ppm) are recorded in the scheelite-bearing calc-silicate quartzites. This may be considered as an indication of the negligible role of exhalative activity (see Sonnet et al. 1985; Plimer 1984; Maucher 1976) in the calc-silicate quartzites. The depletion of Ba in the scheelite-bearing calc-silicate quartzites is also consistent with this interpretation (see Plimer 1987a). The low concentration of Ba and Rb could be related to the absence of mica and plagioclase respectively in the proposed calc-silicate quartzite. Enrichment of the P_2O_5 (up to 1.2 wt %) in the scheelite-bearing calc-silicate quartzite could signify an exhalative activity, although it might also be ascribed to the formation of apatite, which is normally found in the skarn assemblage.

5.6 Tourmalinite

Major and trace elements analyses of the Miniki Gol tourmalinite are presented in the Table 5.6, and compared with the exhalative scheelite-bearing tourmalinite of Broken Hill, Australia, (Slack et al. 1993).

Table 5.6: Major and trace element chemistry of the studied tourmalinites.

Sample	Min	Max	Mean	Std[1]	N[2]	Broken Hill[3]
SiO_2	46.8	61.7	51.2	4.8	12	58
TiO_2	0.7	1.5	1.0	0.2	12	0.93
Al_2O_3	21.0	29.5	23.7	2.3	12	21.31
*Fe_2O_3	6.3	13.3	9.8	2.9	12	7.6
MnO	0.0	2.6	1.1	1.1	12	0.12
MgO	2.3	4.5	3.1	0.7	12	1.86
CaO	0.3	3.7	2.0	1.2	12	0.39
Na_2O	1.0	3.3	1.7	0.7	12	0.94
K_2O	0.1	3.1	0.9	1.1	12	1.23
P_2O_5	0.0	0.2	0.1	0.1	12	0.12
Total	90.9	96.0	94.5	1.5	12	
Trace elements in ppm						
B	9310	14800	11827	1810	10	7455
F	790	1350	1070	209	8	2800
Cl	40.0	70.0	50	10.7	8	335
S	0.0	280	110	113	8	---
As	0.7	2.4	1.4	0.5	9	73.15
Li	37.7	172	80	37	13	39.28
Be	2.8	13.7	6.5	3.2	13	1.92
Cs	4.0				1	10.46
Ba	4.9	720	204	264	13	330
Rb	1.1	187	51.8	59	13	148.7
Sr	200	520	300	90	13	71.7
Th	2.5	41.6	17.5	9.7	13	34.3
U	3.9	5.8	4.6	0.6	7	6.34
Zr	106	323	170	60	13	213.4
Hf	2.0	6.0	3.2	1.6	5	5.8
Ta	1.1	1.5	1.3	0.2	3	5.8
Nb	4.9	33.1	18.6	7.7	13	24.57
Y	6.3	44.9	31.4	12.1	13	44.14
Sc	11.5	26.2	18.3	3.8	13	18.24
V	80	170	114	24	13	107.7
Cr	102	200	142	28	13	89.8
Co	10.2	29.7	18.1	6.6	13	15.16
Ni	11.7	48.2	30.5	13.3	13	28.28
Cu	1.4	36.2	11.6	9.4	12	14.28
Zn	97	153	130	16	13	2048
Hg	< 1	< 1			8	---
Ag	< 5	< 5			8	---
Ga	21.7	42.2	27.6	5.7	13	30
Pb	16.7	39.0	24.8	7.1	13	53.33
W	0.3	7830	1760	2660	13	86
Sn	3.8	23.1	13.21	6.18	13	22.5
Mo	0.0	1.1	0.5	0.4	10	---
Sb	0.3	1.7	0.9	0.7	4	0.19
La	16.0	42.0	27.3	7.8	8	69.0
Ce	31.0	78	55	13.7	8	128.7
Nd	16.0	39.0	24.9	8.4	8	51.97
Sm	3.9	6.5	5.1	0.7	8	11.81
Eu	0.5	1.0	0.7	0.2	8	1.3
Gd	1.0	2.0	1.3	0.6	3	---
Tb	0.6	2.7	1.4	0.9	5	1.61
Yb	1.6	2.5	2.0	0.3	8	4.06
Lu	0.2	0.4	0.3	0.1	8	0.6
La/Yb	8.8	26.3				

* = Total iron considered as Fe_2O_3; [1]= Standard deviation; [2] = Number of samples; [3] = Mean analyses of Broken Hill tourmalinites (after Slack et al. 1993). Be and Li were analysed by ICP-ES and B, Cs, U, Hf, Ta, Sb and REE by INAA. All the other elements were analysed by XRF.

The chemistry of these tourmalinites shows high levels of Mn and Fe, and low K content compared with the schist and calc-silicate quartzite (Table 5.3, 5.5, 5.6). The Mn and Fe concentrations are high in those samples which contain abundant (relatively spessartine-rich) garnet (see ZC 69, ZM 62-64A, Appendix 5.5). High K_2O content is reported in the muscovite-bearing tourmalinite (ZM 28, Appendix 5.5). Tourmalinites in the area of under consideration, are also high in B, Be, Sn, in addition to W and low in Li, Ba, Rb and REE compared with Miniki Gol schist (Table 5.3, 5.6). Apart of these elements, the geochemistry of the Miniki Gol tourmalinites (including F) and schist are similar. The proposed tourmalinite is significantly different from the Broken Hill tourmalinite by high level of wt % Al_2O_3 (mean 23.7), FeO (mean 9.8), MnO (mean 1.1), MgO (mean 3.1), CaO (mean 2.0), Na_2O (mean 1.7) and low value of SiO_2 (mean 51.2). This difference can also be noticed in trace elements as the Miniki Gol tourmalinites are represented by high levels of W, Sn, B, Li, Be, Sr, Cr and low level of F, Cl, As, Ba, Rb, Th, Y, Zn and Pb (Table 5.6).

Tungsten level in the Miniki Gol tourmalinites is not consistent, ranging from few ppm up to 0.8 %. No positive or negative relationship has been found between W and elements of obvious hydrothermal origin such as Sn, Li and Be in the tourmalinites. Similarly, tungsten shows no relationship with the Zr and elements of possible exhalative character such as B and F. In contrast, F and B show some positive correlation with each other (r = 0.3). Rb and Ba show a strong positive correlation with each other (Fig. 5.7 E) and as in the calc-silicate rocks, both these elements are depleted in the tourmalinites. The Rb and Ba are probably, accommodated in the plagioclase and muscovite. It is interested to note that the concentrations of elements such as P and F which might indicate a exhalative activity (Sonnet et al. 1985; Plimer 1984, 1987a), are almost the same as found in the schist. All these evidences suggest strongly against the possibility of the precipitation of tungsten as scheelite during the exhalation in the Miniki Gol area. The high content of MnO is due the presence of abundant spessartine-rich garnet. However, the positive correlation between B and F may signify a pre-metamorphic cogenetic relationship.

5.7 Marble-hosted stratiform Pb-Zn mineralisation

The trace element geochemical data of the Miniki Gol unmineralised marble and Besti Gol mineralised marble are presented in Table 5.7. The following are the main characteritic geochemical features of these rocks.

Table 5.7: Trace elements analyses of the Miniki Gol marble and Besti Gol stratiform Pb-Zn bearing marble.

	ZC56B*	ZC57*	ZC57A*	ZC57B*	ZC60*	ZC60A*	ZM115°	ZM119°	ZM120°	ZM127°	ZM128°	ZM129°	ZM130°	ZM131°
B	n.a	n.a	n.a	n.a	n.a	n.a	n.a	n.a	n.a	2	3	< 2	< 2	< 2
F	n.a	n.a	n.a	n.a	n.a	n.a	80	630	130	50	70	60	40	30
Cl	n.a	n.a	n.a	n.a	n.a	n.a	40	50	40	60	80	100	70	80
S	n.a	n.a	n.a	n.a	n.a	n.a	450	140	100	1080	2460	80	2340	330
As	n.a	n.a	n.a	n.a	n.a	n.a	n.a	n.a	n.a	250	410	59	250	40
Li	6.7	16.8	7.1	7.5	8	7.6	4.9	108	26.2	7.5	2	11.7	1.5	2.4
Be	0.2	0.3	0.2	0.2	0.2	0.2	<0.3	1.6	0.2	<0.2	<0.15	<0.03	<0.3	<0.3
Cs	n.a	n.a	n.a	n.a	n.a	n.a	n.a	n.a	n.a	< 1	< 1	< 1	< 1	< 1
Ba	125	170	75	105	80	990	116	830	1355	874	2050	245	500	256
Rb	23.1	52.1	16.4	23.2	3.7	0.2	< 1.9	117	15.6	10.3	5.1	2	2.6	2.2
Sr	460	525	600	478	331	392	6850	329	749	1118	704	380	305	275
Th	3.2	5.3	< 1.8	0.9	0.7	< 1.1	< 1.3	7.2	0.9	0.6	0.5	0.3	3.8	0.7
U	n.a	n.a	n.a	n.a	n.a	n.a	n.a	n.a	n.a	<0.5	<0.5	<0.5	<0.5	<0.5
Zr	22.1	46.5	16	23.2	6.8	3.6	< 140	96.7	26.3	4.8	3.5	<4.7	0.3	< 3.8
Hf	n.a	n.a	n.a	n.a	n.a	n.a	n.a	n.a	n.a	< 1	< 1	< 1	< 1	< 1
Ta	n.a	n.a	n.a	n.a	n.a	n.a	n.a	n.a	n.a	< 0.5	< 0.5	< 0.5	< 0.5	< 0.5
Nb	2.3	6.6	1.6	2.7	2.5	0.7	< 0.7	9.7	2	0.7	0.6	0.5	0.8	< 0.2
Y	6.9	11.8	6.7	5.6	2.7	2	< 5.1	10.7	7.2	6.3	3.1	1.8	3.1	1.2
Sc	39.4	36.2	51.3	49.5	49.8	63.5	60.8	37	35.1	63.1	64.6	30.4	55.7	47.2
V	32.8	69.4	10.2	32	2.2	5.4	8.9	113	16.2	5.1	24.9	4.9	< 4	11.9
Cr	14.2	37.3	8.5	12.7	< 2.7	2.6	< 4.6	81.1	16.1	12.5	8.2	18.7	< 2.4	< 2
Co	5.4	6.9	3.5	2.4	3.5	2.6	2.6	14.9	4.1	5.2	0.5	< 0.9	3.1	< 0.5
Ni	7.8	29	2.7	9.4	10.3	< 5.7	0.5	34.5	5.4	4.7	6.2	< 0.3	2	0.3
Cu	10.5	17.5	15.2	10.6	9.9	10	16.3	11.3	75.2	117	43	12.9	26.1	13.3
Zn	3.5	32.2	9.2	9.9	21	16.5	30.9	55.4	29.4	10980	25000	592	15376	2172
Hg	n.a	n.a	n.a	n.a	n.a	n.a	n.a	n.a	n.a	77	110	3	48	5
Ag	n.a	n.a	n.a	n.a	n.a	n.a	n.a	n.a	n.a	15	< 5	< 5	< 5	< 5
Ga	5.7	6.8	3.5	4.4	2.9	3	<0.1	14.8	1.7	32.9	2.1	1.4	0.6	0.5
Pb	8.9	11.4	2.6	3.8	6.1	3.2	5	11.9	60	12408	3033	415	1577	39
W	1.8	5.5	< 1.2	0.4	1.4	0.7	<0.6	<2.3	<2	29	15	< 1	3	2
Sn	< 0.7	1.4	< 1.3	< 2.6	2.3	0.8	1.2	2	<0.8	1.9	1.1	1.9	0.9	<0.3
Mo	0.5	1	0.7	0.8	1.7	0.3	5	0.7	2.6	2	1.4	0.5	2.5	1.4
Sb	n.a	n.a	n.a	n.a	n.a	n.a	n.a	n.a	n.a	51	7.6	2.9	3.1	0.4
La	n.a	n.a	n.a	n.a	n.a	n.a	n.a	n.a	n.a	1.3	1.8	0.7	1.1	0.7
Ce	n.a	n.a	n.a	n.a	n.a	n.a	n.a	n.a	n.a	4	4	<3	4	< 3
Nd	n.a	n.a	n.a	n.a	n.a	n.a	n.a	n.a	n.a	< 5	< 5	< 5	< 5	< 5
Sm	n.a	n.a	n.a	n.a	n.a	n.a	n.a	n.a	n.a	0.3	0.5	0.3	0.3	0.3
Eu	n.a	n.a	n.a	n.a	n.a	n.a	n.a	n.a	n.a	< 0.2	< 0.2	< 0.2	< 0.2	< 0.2
Gd	n.a	n.a	n.a	n.a	n.a	n.a	n.a	n.a	n.a	< 1	< 1	< 1	< 1	< 1
Tb	n.a	n.a	n.a	n.a	n.a	n.a	n.a	n.a	n.a	< 5	< 5	< 5	< 5	< 5
Yb	n.a	n.a	n.a	n.a	n.a	n.a	n.a	n.a	n.a	< 0.2	0.3	< 0.2	< 0.2	< 0.2
Lu	n.a	n.a	n.a	n.a	n.a	n.a	n.a	n.a	n.a	<.05	<.05	<.05	<.05	<.05

* = Miniki Gol unmineralised marble; ° = Besti Gol mineralised marble. Be and Li were analysed by ICP-ES and B, Cs, U, Hf, Ta, Sb, Hg, Ag and REE by INAA. All the other elements were analysed by XRF.

- The Miniki Gol unmineralised marble is represented by SiO_2 (7-13 %), Al_2O_3 (2-5 %), FeO (1-2 %), MgO (1-2 %), MnO up to (0.1 %), CaO up to (54 %), Na_2O up to (0.2 %) and K_2O up to (1 %). The major element chemistry of the Pb-Zn-bearing marble at Besti Gol has not been analysed by XRF. It is difficult to make the fusion beads of the sulphide-bearing marble as the sulphur in these sulphide minerals corrode the platinum crucible. However, some of the major elements of the Besti Gol mineralised marble are analysed by INAA and contains average Ca (44 %), Fe (0.5 %) and Na (0.1 %).
- The trace element chemistry of the Miniki Gol unmineralised marble is similar to the Besti Gol mineralised marble, except Sr, Pb and Zn which are very high in the latter rocks. The maximum concentrations of Zn, Pb, and Sr are 2.5 %, 1.2 %, 0.7 % respectively.
- The Besti Gol marble is enriched in As, Ba, Sc, Sb, Ag (up to 15 ppm), Hg (up to 110 ppm) in addition to S, Zn and Pb (Table 5.7) compared with the average carbonates data of Graf (1960) and Turekian and Wedepohl (1961).
- Arsenic has a strong positive correlation with Ba (r= 0.81), with Sc (r = 0.69) and weak correlation with Sr (0. 28), indicating that As, Ba, Sc and to lesser extent Sr may have been introduced during hydrothermal alteration. There is no correlation between As and Sb.
- The strong positive correlation of Sr with CO_2 (r = 0.79) and weak positive correlation of Ba with S (0.22) and lack of correlation of Ba with CO_2 suggest that Sr may exists as a carbonate and Ba partly as $BaSO_4$.
- A strong positive correlation between Zn and S (r = 0.91) and inverse relationship with CO_2 (r = - 0.03) reflect that most of the Zn occur as ZnS and some as hydro-zincite.
- The strong positive correlation between As and Zn (r = 0.96), indicating a similar geochemical behaviour during the alteration.
- No relationship has been found between Pb and S.

Major elements of the proposed marble are comparable with a sedimentary origin of carbonates. However, a strong positive correlation between As and Fe (r = 0.78) in the Besti Gol mineralised marble indicate some of the Fe has been introduced by metasomatic activity. Although Mg was not determined in the Besti Gol marble, the Miniki Gol marble contains up to 2 % MgO, demonstrating that the marble is mainly composed of calcite.

According to Graf (1960) pure sedimentary carbonates do not show any marked concentration of minor elements except Sr which can reach more than 6000 ppm. In addition, sedimentary carbonates contain only a few ppm As and Sc (1-2 ppm) as well as

Ba (10-190 ppm) see (Turekian and Wedepohl 1961). Although carbonates contain up to 1 % Ba (e.g. Scottish sedimentary carbonates, Graf 1960). In contrast, the investigated marble contains As up to 410 ppm and Sc up to 65 ppm and Ba up to 2050 ppm. The similar correlation among the As, Ba and Sc probably, imply that these elements are concentrated during the later hydrothermal activity. The occurrence of arsenopyrite in the adjacent quartz veins also indicates hydrothermal activity.

5.8 REE

The REE abundances of the Miniki Gol granite, schist, calc-silicate quartzite, psammite, tourmalinites and marble are given in (Table 5.1, 5.3, 5.4, 5.5, 5.7) and chondrite normalised pattern are shown in (Fig 5.8 A-D).

5.8.1 Leucogranite

The Miniki Gol leucogranite contains very low level of both the REE (Table 5.1). The La / Yb ratios in these granites are less than 10, which shows the depletion of LREE relative to HREE. Out of 11 samples, only two analyses (ZC 20, ZM 1) have ratios of more than 10. Most of the analyses display negative Eu anomalies. The minimum and maximum Eu / Eu* in the proposed leucogranite is recorded as 0.29 and 1.16 respectively (see ZM 52, ZM 70 Fig. 5.8 A). Where Eu / Eu* is a measure of the depletion or enrichment of the europium relative to the neighbouring REE, samarium and gadolinium. A strong positive correlation exist between Zr and LREE (r = 0.86) in the leucogranite (Fig. 5.9 A), indicating the similar relationship of the least mobile elements. Negative Eu anomalies and the enrichment of LREE are generally considered as the characteristic features of the anatectic leucogranite (Harris and Inger 1992). In contrast, France-Lanord and Le Fort (1988), have argued that very low abundance of LREE together with the negative Eu anomalies is a prominent feature of the leucogranitic magma acquired either at partial melting stage or early fractionation of monazite and biotite.

The very low content of the total REE and particularly the depletion of LREE over HREE in the studied leucogranite could be the result of hydrothermal alteration. Alderton et al. (1980) have attributed the bulk loss of REE and Zr and loss of LREE to the hydrothermal alteration such as tourmalisation and chloritization respectively in the granite of SW England. The strong positive correlation between Zr and LREE (Fig. 5.9 A) is consistent with the above interpretation. Such an enrichment of HREE and the depletion of LREE has also been recorded by Öhlander et al. (1989) during greisenisation in the granite of Rostberget, northern Sweden. In addition, Cullers and Graf (and references therein 1984) have argued that H_2O and CO_2-rich fluid may facilitate the transportation

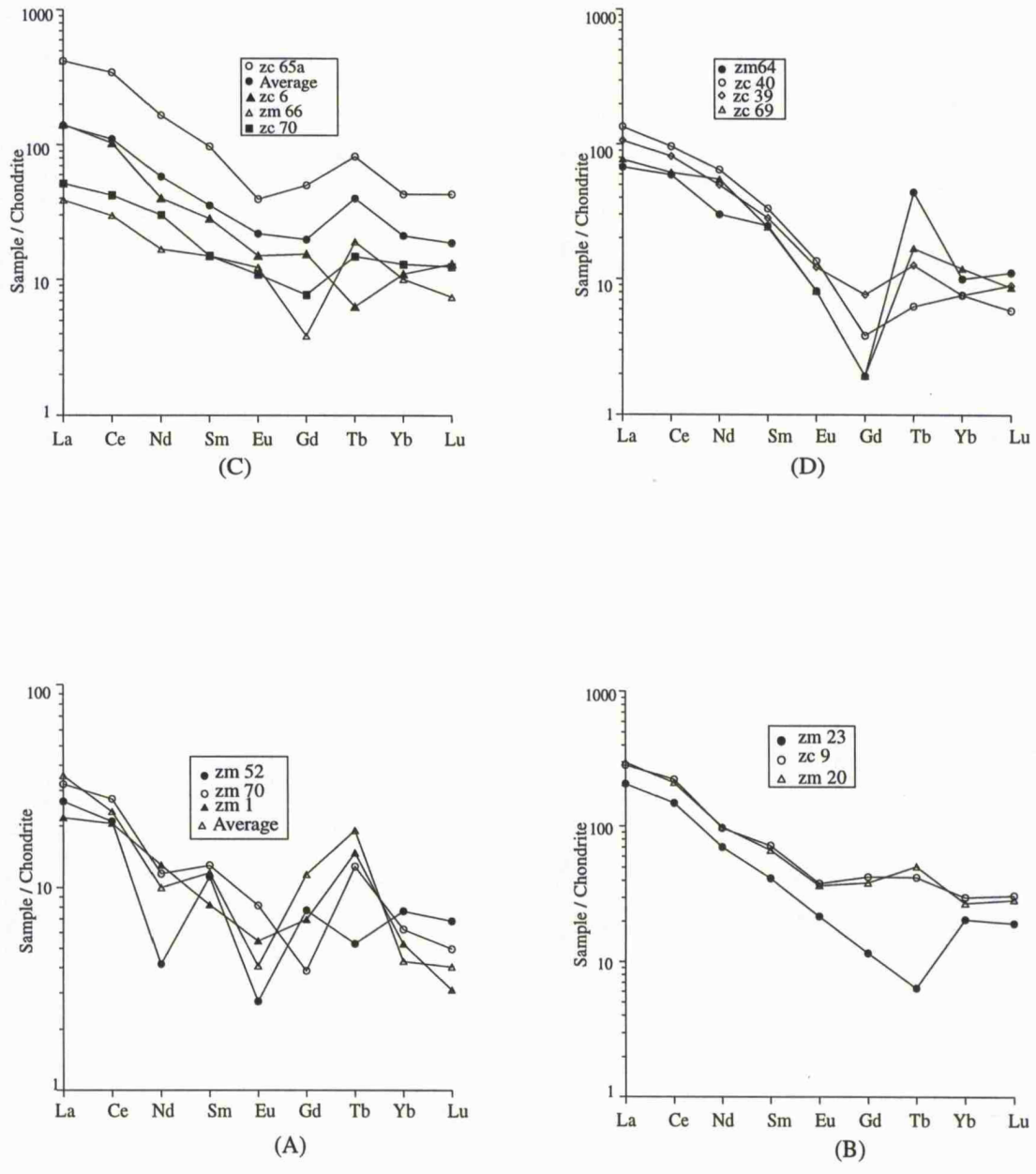

Fig. 5.8: Chondrite-normalised REE pattern of **(A)** Miniki Gol leucogranite **(B)** schist **(C)** calc-silicate quartzite (zc 65a, zm 66, zc 70 and psammite (zc 6) and **(D)** tourmalinite. Chondrite values taken from Boynton (1984).

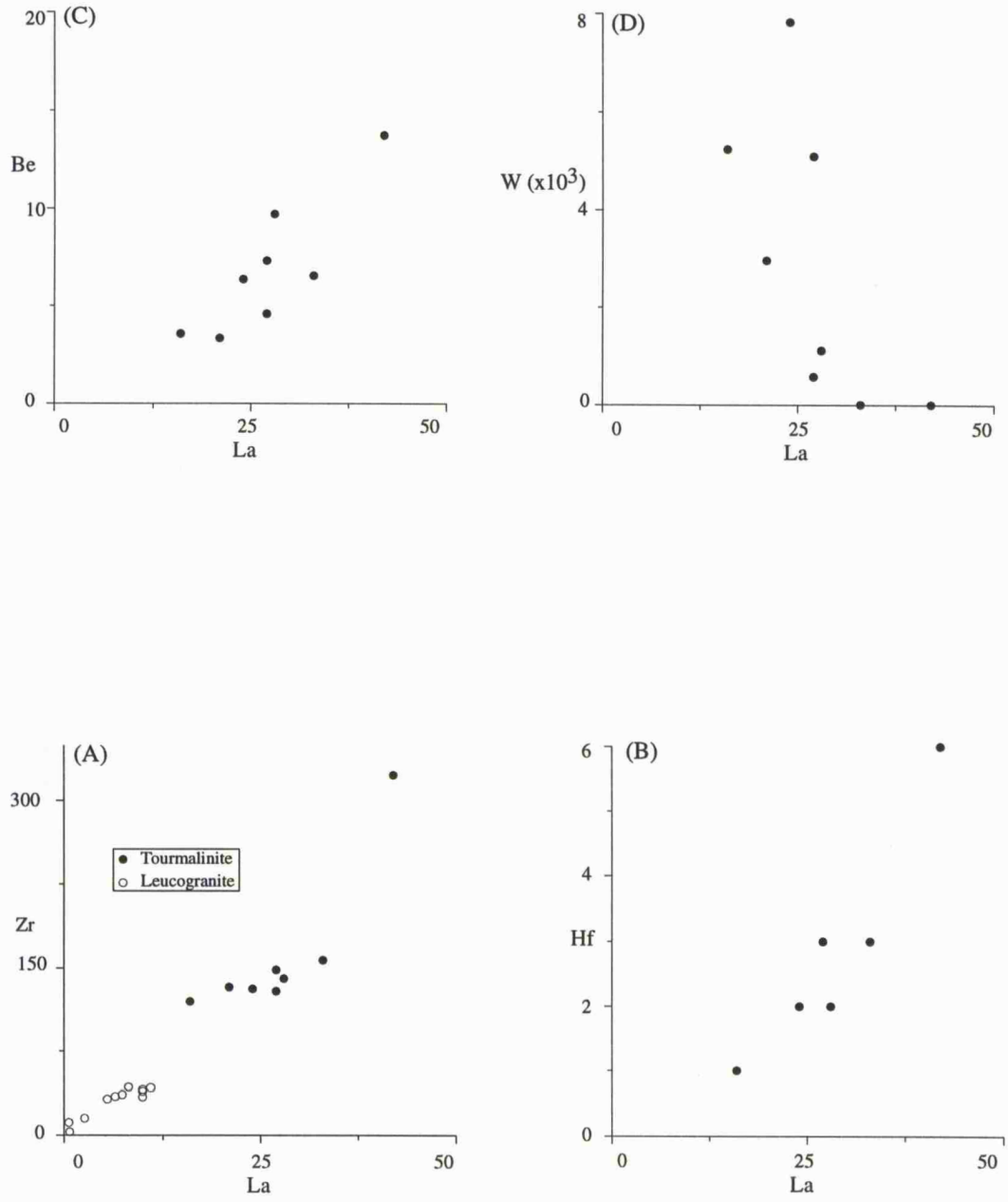

Fig. 5.9: Relationship of La (ppm) with **(A)** Zr (ppm) in lecuogranite and tourmalinite, **(B)** Hf (ppm), **(C)** Be (ppm) and **(D)** with W (ppm) in tourmalinite. The same relationship holds for other LREE elements. Data taken from **Appendix (5.2, 5.5).**

of the LREE in the hydrothermal regime. As discussed above, the investigated leucogranite is depleted in LREE over HREE contents and also total REE is extremely depleted compared with the metasediments (see Table 5.1, 5.3, Fig 5.8 A-B). This is inconsistent with the Harris and Inger (1992) model that pelite-derived granite should exhibit large LREE / HREE ratios. However, such a depletion of LREE and Eu in the Manaslu leucogranite relative to the source metasediments is attributed by Vidal et al. (1982) to circulation of large volumes of fluid.

5.8.2 Schist

The REE contents of the Miniki Gol metasediments are significantly higher (Table 5.3, Fig. 5.8 B) than the North American shale (see Taylor and McLennan 1985). The maximum Eu / Eu* and chondrite-normalised La_N / Yb_N ratios in the studied schist is observed as 0.99 and 10.85 respectively which is higher than the North American shale (0.7 and 7) respectively.

The REE mobility in the metamorphic rocks is poorly understood (see Grauch 1989) and many investigators such as Cullers et al. (1974) and Lottermoser (1989a) believe that REE pattern is unaffected during the progressive metamorphism. However, partial melting and retrogressive metamorphism do change (loss or gain) the REE pattern (cf. Lottermoser 1989a). The enrichment of REE abundances in the proposed metasediments relative to the North American shale, indicates metasomatic activity associated with retrogressive metamorphism.

5.8.3 Calc-silicate rocks

The summary of the rare elements data of the calc-silicate quartzite and psammite is presented in Table 5.5 and Fig 5.8 C. The following are the main characteristics of the REE pattern of the studied calc-silicate quartzite and psammite.

- The Miniki Gol calc-silicate quartzite is enriched in all REE contents compared with the North American shale (see Taylor and McLennan 1985).
- The total REE abundances in the scheelite-bearing calc-silicate quartzite are relatively high as compared to the psammite (mica quartzite). Maximum REE contents (ppm) in the scheelite-bearing calc-silicate quartzite are as follow La (130), Ce (280), Nd (100), Sm (19), Eu (2.9), Gd (13), Tb (3.9), Yb (9) and Lu (1.39) and are shown in (Table 5.5, Fig. 5 .8 C, ZC 65 A).
- Almost half of the scheelite-bearing calc-silicate quartzite rocks exhibit positive Eu anomalies. The unmineralised psammites exhibit negative Eu anomalies (Fig. 5.8 C, ZC 6) as do the scheelite-bearing calc-silicate quartzite rocks (Fig. 5.8 C, ZC 65 A).

- The calc-silicate quartzite rocks are represented by low chondrite normalised $(La/Lu)_{CN}$ ratios (< 10) whereas the most of the analyses of the psammite and metasediments have $(La / Lu)_{CN}$ ratios greater than 10.
- Most of the scheelite-bearing calc-silicate quartzite rocks (13 out of 21) are enriched in HREE. This enrichment is apparent from the LA/Yb ratio, recorded less than 10. Whereas the LA/Yb ratio in the psammite is noted very high (maximum 19).
- A strong positive correlation exist among the REE and Zr, Hf, Nb, Y, Ta together with a weak linear relationship with F (Fig. 5.10 A-F). However, no correlation has been found between REE and ore elements such as W and Sn.

Keeping in view the above geochemical characteristics of the rare-earth elements in the calc-silicate quartzite, it can be said confidently that the calc-silicate rocks have undergone extensive hydrothermal alteration. The positive correlation among the elements of the LREE and HREE is consistent with hydrothermal activity in these rocks. Similarly, the positive correlation between the elements of hydrothermal character Zr, Hf, Nb, Y, Ta, F and REE also indicate that REE were highly mobile in the hydrothermal alteration. The mobility of the REE during hydrothermal alteration was discussed by Lottermoser (1992) and Wood (1990). According to Wood (1990) the fluoride and carbonate complexes significantly facilitate the transportation of the REE along with Y in the hydrothermal regime. The mobility of the REE appears to increases with the change from early-magmatic to late-stage hydrothermal solutions (Lottermoser 1992).

The mobility of Zr, Ti, U, Th, Y along with REE in the presence of alkali-rich-fluorine and phosphorus complexes from the calc-silicate assemblages (Bergell and Adamello contact aureoles, Italy) has also been reported by Giere (1990) during the hydrothermal activity. Rubin et al. (1993) have also argued that Zr together with Be, Y, Nb, Ta, U, Th and REE, are highly mobile in the hydrothermal systems rich in alkalis and fluorine. Moreover most of these elements have been found high in the peri-anatectic W mineralisation, especially in the case of skarn (see Sonnet et al. 1985).

According to Lottermoser (1989b) HREE enrichment and low $(La / Lu)_{CN}$ ratios demonstrate hydrothermal alteration. Lottermoser (1989b) has also expressed that the HREE and Eu enrichment and the depletion of LREE could be related to the dissolution of carbonate minerals and scheelite deposition with the decreasing temperature of the hydrothermal fluid. Positive Eu anomalies have also been reported by Sonnet et al. (1985) in the scheelite-bearing calc-silicate rocks of peri-granitic origin.

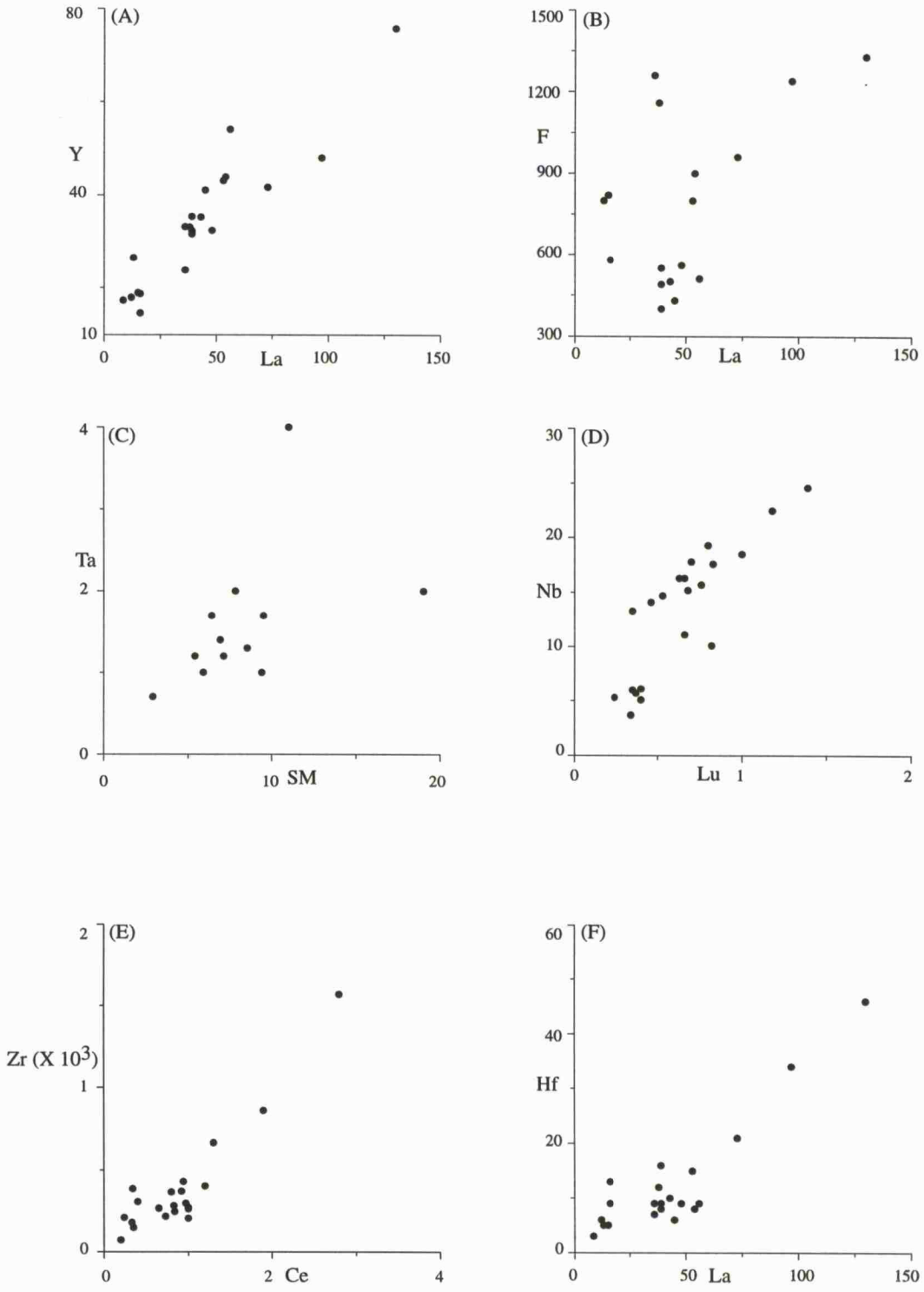

Fig. 5.10: Relationship of REE (ppm) in calc-silicate quartzite with **(A)** Yttirum (ppm), **(B)** Flourine (ppm), **(C)** Tantalum (ppm), **(D)** Niobium (ppm), **(E)** Zirconium (ppm) and **(F)** Hafnium (ppm). A similar relationship holds for other REE with the corresponding elements in the above Figures. Data taken from Appendix 5.4.

The high levels of REE, Zr and Y in the scheelite-bearing calc-silicate quartzites probably, indicates that the these elements may have been incorporated in the scheelite as 0.3 wt % Zr have been found in scheelite (see section 4.4.9). However, no relationship has been found between W and REE, indicating these elements may have been accommodated in titanite, as 3 wt % Y has been found in titanite (Janeczek and Sachanbinski 1992).

5.8.4 Tourmalinites

The REE abundances of the tourmalinites are presented in Table 5.6 and Fig 5.8 D. The REE pattern shows a LREE enrichments with most La / Yb ratios are greater than 10. Gd in most of the samples is below detection limit and when found, very low in these rocks (Fig. 5.8 D). Like other units in the study area, LREE also display a linear relationship with Zr, Hf and more interestingly Be (Fig. 5.9 A-C) indicating identical geochemical behaviour of REE together with Zr, Hf and Be during the metasomatic activity. However, an inverse relationship has been found between LREE and W (Fig. 5.9 D), whereas no relationship exist between REE and boron. A strong correlation also exist between La and Ce (Fig. 5.7 F) reflects a similar geochemical behaviour during the regional metamorphism and hydrothermal alteration. The REE contents are quite different from the Broken Hill tourmalinites (Table 5.6) of exhalative origin. The Broken Hill tourmalinites are rich in REE content compare to tourmalinites in the study area and also HREE in the Broken Hill are slightly elevated relative to LREE (Slack et al. 1993). Moreover the Broken Hill exhalites and tourmalinites display both prominent positive and negative Ce anomalies (see Lottermoser 1989a).

5.8.5 Marble

The concentration of most of the REE in the marble is below detection limit and is difficult to comment on it (see Table 5.7).

5.9 Conclusion

- The Miniki Gol leucogranites are pelite-derived granites and can be considered as fractionated and potentially ore-bearing granite.
- The hydrothermal alteration has significantly affected the trace elements data within the leucogranite.
- The rock units such as metasediments, tourmalinites and psammite have undergone hydrothermal alteration and this alteration is prominent in the calc-silicate rocks.

- The hydrothermal activity has significantly changed the trace elements distribution and even the immobile elements such as Zr, Y, Hf, Nb, REE and incompatible elements Ta, Sn, Li and W have been remobilised probably, in the presence of phosphorus and fluoride complexes.
- The background levels of W both in the Miniki Gol metasediments, Pakistan and Cornubian pelite, S W England are slightly higher than the average shale and rules out the possibility of pre-granitic enrichment of these elements in the study area.

Chapter Six

FLUID INCLUSIONS

6.1 Introduction

Fluid inclusions are an integral part of any rocks and minerals. Primary fluid inclusions are trapped by host minerals at the time of their deposition (see Roedder 1984). Thus these fluid inclusions are considered to be truly representative portions of the fluid, present during the primary growth of the mineral (Shepherd et al. 1985).

The study of fluid inclusions provides direct evidence about the genesis of the enclosing rocks as well as the nature and source of ore-forming fluids. The objects of the fluid inclusion study in this chapter are as follows:

- To determine the temperature of formation for both scheelite mineralisation and associated gangue minerals.
- To distinguish between metamorphic, magmatic and post-magmatic fluids in the investigated area.
- To understand the composition and source of ore-forming fluid.
- To study the possible effect of hydrothermal solutions accompanying retrograde metamorphism on the pre-existing minerals.

6.2 Sample preparation

This study was mainly carried out on the primary granular quartz grains, as fluid inclusions are more clearly visible in the quartz crystals than the other minerals in the project area.

In order to know the nature of the fluid in different lithologies, representative samples from leucogranites, pegmatites, scheelite-bearing calc-silicate quartzites, mica schists, tourmalinites and Pb-Zn-bearing marble were selected from both Miniki Gol and Besti Gol area. Some of the samples were also chosen from quartz veins at Besti Gol as these veins are closely associated with Pb-Zn-bearing marble. In all a total of 36 doubly polished wafers of about 200 μm in thickness from these rocks were prepared. These wafers were then studied using transmitted light microscope in search of suitable fluid inclusions. Suitable inclusions were found mainly within the quartz grains in leucogranites, pegmatites, scheelite-bearing calc-silicate quartzites and quartz veins. Fluid inclusions in the mica schist, tourmalinite and marble are very rare and when present, very small. No fluid inclusions were observed in the marble-hosted lead-zinc mineralisation, although

quartz veins spatially associated with the mineralised marble at Besti Gol, contain numerous fluid inclusions.

Out of these 36 doubly polished sections, only 9 were selected for the fluid inclusion study (Table 6.1), as the fluid inclusions found in these samples were very small.

Table 6.1: Locations and description of the samples used in fluid inclusions study (See Fig. 4 A-C for the sample locations).

Sample No.	Description	Locality
ZM 109	Quartz veins associated with Pb-Zn mineralisation	Besti Gol mineralised zone
ZS 19	Quartz grains in leucogranite	Garam Chashma road
ZC 20	Quartz grains in leucogranite	Miniki Gol
ZC 21	Quartz grains in pegmatite	Miniki Gol
ZC 23	Quartz grains in pegmatite	Umkosh Gol
ZC 65	Quartz grains in scheelite-bearing calc-silicate rocks	Miniki Gol mineralised zone
ZC 67	Quartz grains in scheelite-bearing calc-silicate rocks	Miniki Gol mineralised zone
ZC 67A	Quartz grains in scheelite-bearing calc-silicate rocks	Miniki Gol mineralised zone
ZC 70	Quartz grains in scheelite-bearing calc-silicate rocks	Miniki Gol mineralised zone

6.3 Analytical techniques

The fluid inclusion studies were carried out at Royal Holloway and Bedford New College, University of London, under the supervision of Dr. David Alderton. For the thermometric studies (i.e. heating and freezing), doubly polished wafers were analysed using a Linkam TH 600 programmable heating-freezing stage attached to a Zeiss transmitted-light microscope. The stage has a wide range of temperature between -180^{o}C and 600^{o}C with the following accuracy;

-180^{o}C to -20^{o}C = ± 0.1^{o}C

-20^{o}C to + 50^{o}C = ± 0.2^{o}C

50^{o}C to 500^{o}C = ± 0.5^{o}C

The stage was calibrated using synthetic fluid inclusions in quartz crystals. The various abbreviations and terminology used in this study for the microthermometric measurements are as follows:

- (T_M) Temperature of the final ice melting: this temperature is mainly used to estimate the salinity of aqueous two phase inclusions. Salinity is determined from the phase diagram of Shepherd et al. (1985) for the system (NaCl + H_2O) and graphical presentation of Crawford (1981a). For CO_2-bearing fluid inclusions, (liquid H_2O, liquid

CO_2 and vapour CO_2) salinity is estimated using $T_M$clath measurements. T_M is not recommended for the estimation of salinity as pointed out by Collins (1979), that during the cooling, the gas (CO_2-CH_4) hydrates form in the fluid, increases the salinity in the residual aqueous phase. The measurement of T_M in the CO_2-bearing fluid inclusions give inaccurate salinity estimation.

- (T_{FM}) Temperature of the first ice melting: this temperature is used to estimate the composition of salt-H_2O solutions (e.g. NaCl, KCl, $CaCl_2$, and $MgCl_2$). The T_{FM} is not determined in this study as the fluid inclusions were too small to record the T_{FM}.
- ($T_M CO_2$) Temperature of final melting of solid CO_2: these temperature measurements show the presence of gas content (such as CH_4 and N_2) in the fluid inclusions. The melting temperature of pure CO_2 (-56.6°C) is lowered by the presence of CH_4 and N_2. Any temperature lower than -56.6°C, indicates the presence of volatile compounds other than CO_2.
- ($T_M$clath) Temperature of final melting of clathrate (formation of gas hydrate, CO_2. 5.75 H_2O): these measurements are used to determine the salinity of CO_2-bearing fluid inclusions. The final temperature of the CO_2 clathrate dissociation is recorded up to 10°C or above. The measurement $T_M$clath at temperature above 10°C indicates the presence of other gasses in fluid inclusions, in addition to CO_2 (Collins 1979).
- ($T_h CO_2$) Temperature of partial homogenisation of CO_2-rich phase: this temperature is used to estimates the density of CO_2 phase in the fluid inclusions.
- (T_H) Temperature of total homogenisation: this measurement gives us the minimum temperature of mineral growth.

The total density of the fluid inclusion was determined from the degree of fill (F) i.e. the ratio of vapour and liquid following the graphical representation of Shepherd et al. (1985). The wt % of CO_2 of these CO_2-bearing fluid inclusions, was also calculated following the formula of Shepherd et al. (1985).

6.4 Fluid inclusions characteristics

Both primary and secondary inclusions (Roedder 1984; Shepherd et al. 1985) were recognised in the study area. Primary inclusions were identified as shown by their occurrence within the quartz crystal whereas secondary inclusions occur along grains boundaries and as trail or planar groups (see Fig. 6.4 B). Primary inclusions were found mostly in the granular quartz grains. Microthermometric measurements were carried out on the primary inclusions, although the total homogenisation temperatures were also noted in some of secondary fluid inclusions.

6.4.1 Primary inclusions.

The studied primary fluid inclusions were subdivided into non-aqueous gas inclusions and aqueous H_2O inclusions. The following is the subdivision of these fluid inclusions in different rock types.

6.4.1 (A) Quartz veins

Three phase inclusions (liquid H_2O, liquid CO_2 and vapour $CO_2 \pm CH_4$), have been identified in the quartz veins spatially associated with marble-hosted lead-zinc mineralisation at Besti Gol (Fig. 6.1 A-B, ZM 109, Table 6.2). Aqueous fluid inclusions were also found in these quartz veins. The size of these fluid inclusions ranges from 15 to 40 μm in diameter. These fluid inclusions are relatively CO_2-rich compared with the inclusions in the muscovite pegmatite.

6.4.1 (B) Pegmatites

Only aqueous fluid inclusions occur in the quartz grains of the tourmaline pegmatite (ZC 23, Table 6.2) however, both CO_2-bearing and aqueous fluid inclusions were recognised in the quartz grains of the muscovite pegmatite (ZC 21, Table 6.2, Fig. 6.4 A). These muscovite pegmatite patches are located within the Miniki Gol leucogranite at the mouth of Miniki Gol roughly 400 m away from scheelite mineralisation (Fig. 1.1). Fluid inclusions vary in size, ranging from 5 to 35 μm in diameter.

6.4.1 (C) Leucogranites

Primary aqueous fluid inclusions with liquid H_2O and vapour H_2O are relatively abundant in the Miniki Gol leucogranite (Fig. 6.2). No CO_2-bearing fluid inclusions were observed within the Miniki Gol leucogranite. These aqueous fluid inclusions range from 20 to 25 μm in diameter.

6.4.1 (D) Scheelite-bearing calc-silicate quartzites

As in leucogranite, only aqueous fluid inclusions were found in the Miniki Gol scheelite-bearing calc-silicate quartzites (Fig. 6.3) and no CO_2-bearing fluid inclusions were observed within the scheelite-bearing calc-silicate quartzite. The fluid inclusions in these rocks are relatively smaller than those found in the pegmatite and leucogranite, ranging from 15 to 20 μm in diameter. Aqueous fluid inclusions in the scheelite-bearing calc-silicate quartzite such as sample ZC 65, ZC 67 and ZC 67A (Table 6.1), have been found in the granular quartz grains with well-defined grain boundaries. These quartz grains are intergrown with clinozoisite and scheelite crystals (Fig. 4.2 B). As mentioned in

chapter 4 these quartz grains particularly in scheelite-bearing calc-silicate quartzite, do not exhibit any deformation, indicating annealing (i.e. cooling down from high temperature).

6.4.2 Secondary inclusions

These fluid inclusions comprise of two-phase and mono-phase fluid inclusions. Two phase aqueous fluid inclusions were noted in the Miniki Gol leucogranite (6.4B), whereas mono-phase inclusions occur in leucogranite, pegmatite and scheelite-bearing calc-silicate quartzite (Fig. 6.2 B, 6.3 B).

6.4.3 Microthermometry

Fluid inclusion data from the study area are summarised in the Table 6.2. The data such as (salinity, freezing temperature and the gas contents) of quartz veins from Besti Gol are significantly different from those of Miniki Gol rocks (Table 6.2).

The final melting of clathrate ($T_M$clath) of the primary CO_2-bearing fluid inclusions in the quartz vein at Besti Gol, is recorded between 1.5 and 9.5^oC, corresponding to salinities between 2 to 14 wt % NaCl equivalent (Table 6.2). These CO_2-bearing fluid inclusions were frozen down to -165^oC because at this temperature every phase was solidified. During the reheating, the first melt of solid CO_2 appeared at - 79^oC and the final melting (T_MCO_2) was completed at temperatures, ranging from -56.6^oC to -71^oC. This temperature is well below the melting temperature of pure solid CO_2 (-56.6^oC), indicating the presence of volatile compounds such as CH_4, N_2 or even H_2S, in addition to CO_2 (Almeida and Noronha 1988). The presence of CH_4 was also confirmed as the final clathrate dissociation ($T_M$clath) of the CO_2-bearing fluid inclusions occurred at 16^oC (Table 6.2). However, nothing can be said about the amount of N_2 and H_2S as they have not been analysed and also their behaviour is not fully known. The CO_2 content of these fluid inclusions reaches up to 28.6 wt %. Total densities of the fluid inclusions and CO_2 were calculated as 0.52 and 0.4 g cm^{-3} respectively. The partial homogenisation temperature (T_hCO_2) of the CO_2-bearing fluid inclusions in the quartz veins, were recorded between 30.9^oC and 31.1^oC (Table 6.2). The total homogenisation (T_H) in the Besti Gol quartz vein, occurred at temperature between 240^oC and 415^oC (Fig 6.5 B), with the maximum decrepitation temperature (T_D) 410^oC. It should be noted, that the study on the quartz veins at Besti Gol is preliminary as it was carried out on only three CO_2-bearing fluid inclusions in one sample.

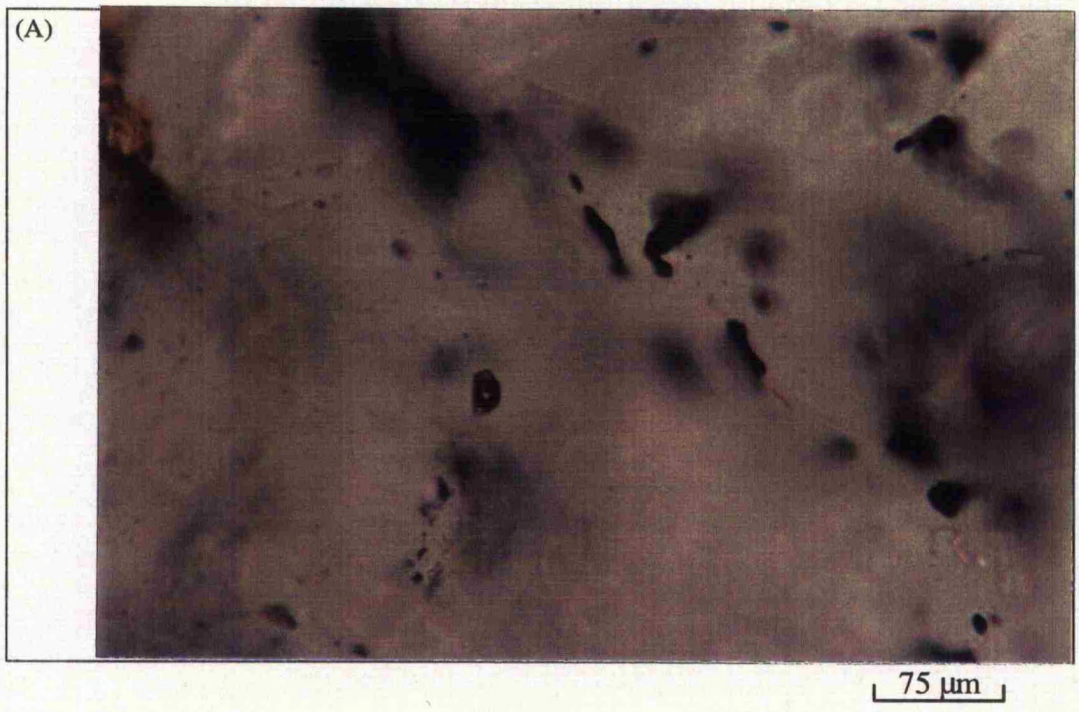

Fig. 6.1: CO_2-rich inclusions in Besti Gol quartz vein (sample ZM 109): **(A)** CO_2-bearing fluid inclusions with degree of fill (F) =0.5. **(B)** CO_2-bearing fluid inclusions of various size (15 µm to 40 µm).

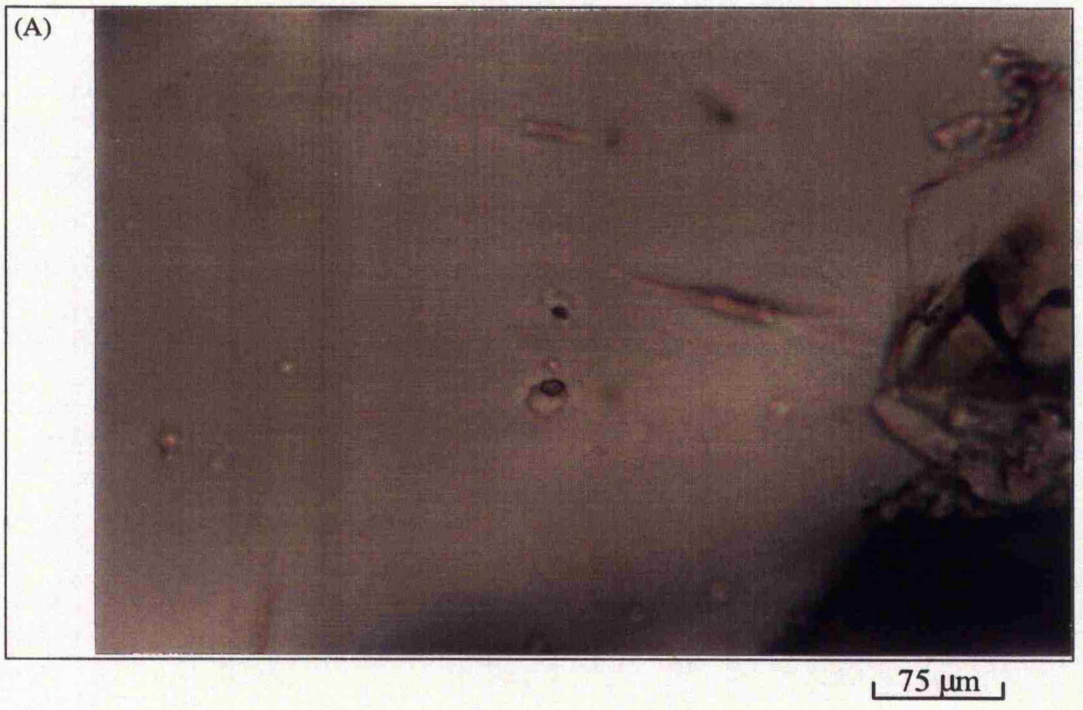

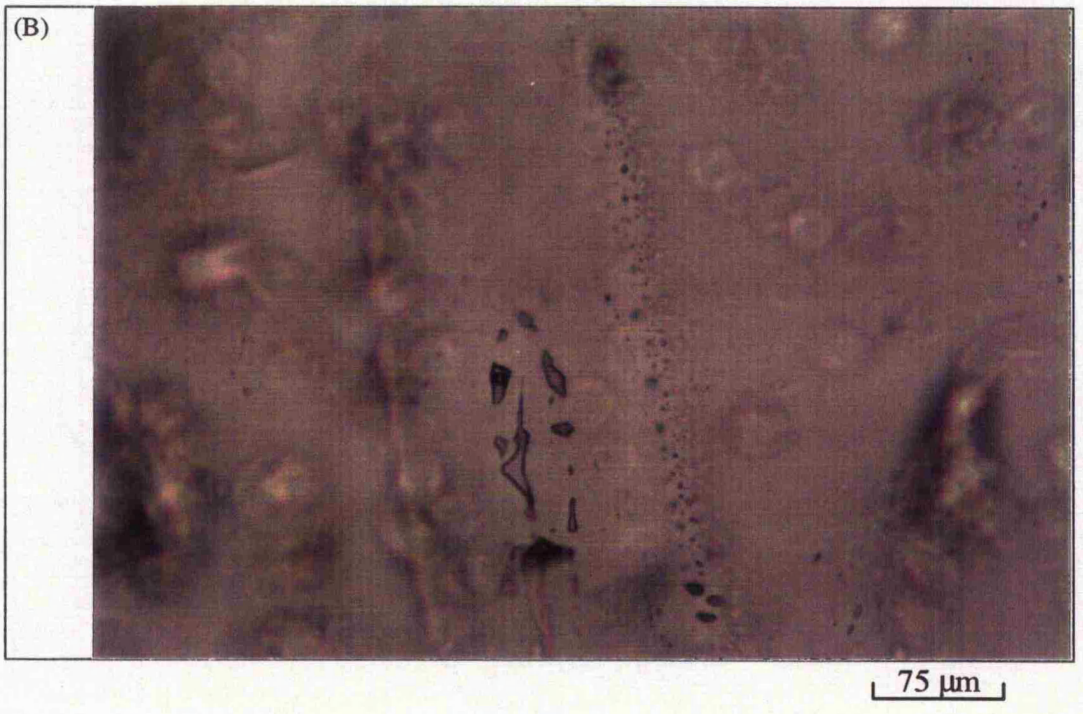

Fig. 6.2: Aqueous fluid inclusions in leucogranite: **(A)** Aqueous fluid inclusions in the quartz of Miniki Gol leucogranite (sample ZC 20). **(B)** Two-phase and mono-phase aqueous fluid inclusions in the quartz of leucogranite at Garam Chashma (sample ZS 19).

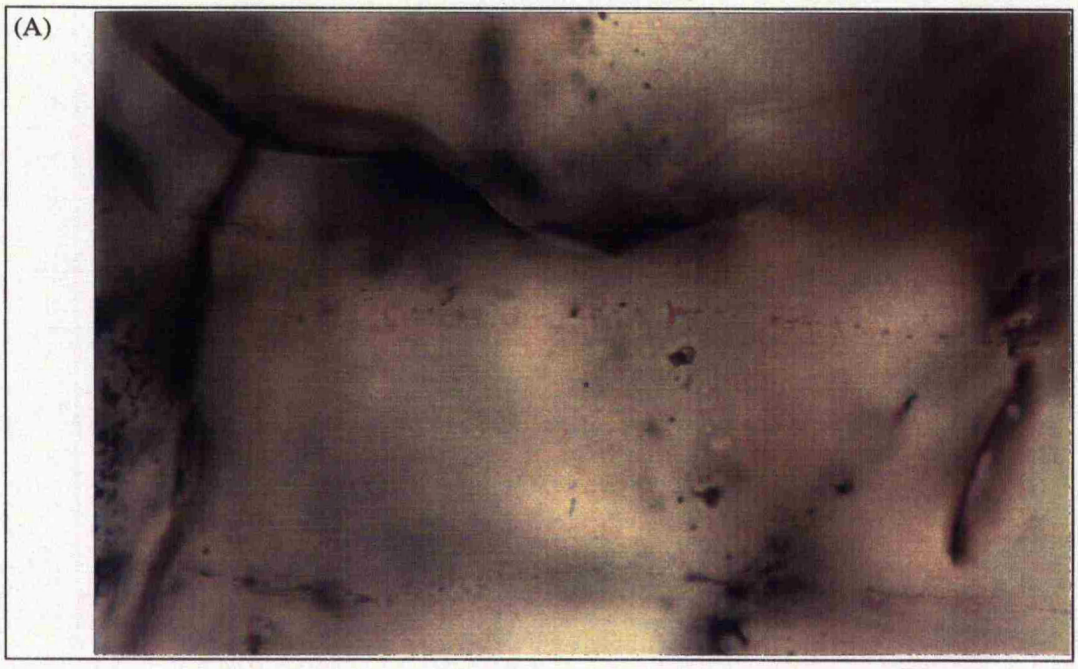

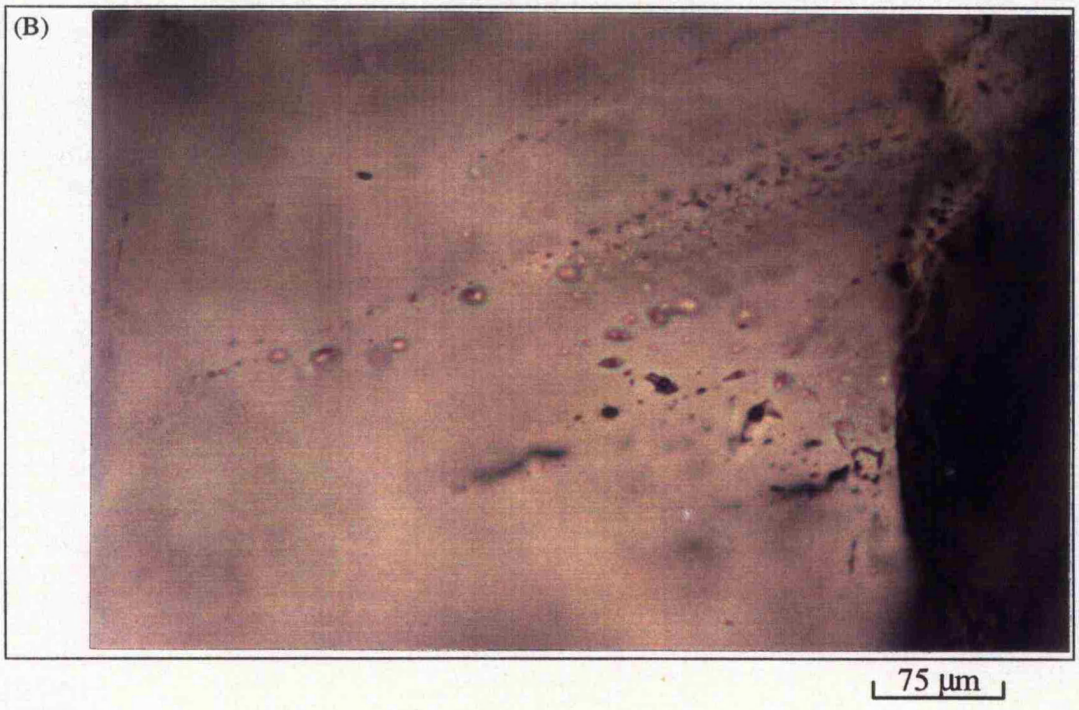

Fig. 6.3: Aqueous fluid inclusions in the scheelite-bearing calc-silicate quartzite at Miniki Gol: **(A)** Fluid inclusions in the granular quartz (sample ZC 67A). **(B)** Series of fluid inclusions along with mono-phase fluid inclusions in the quartz grains (sample ZC 67).

Fig. 6.4: Aqueous fluid inclusions: **(A)** Primary fluid inclusions in quartz of muscovite pegmatite at Miniki Gol (sample ZC 21). **(B)** A trail of secondary fluid inclusions in the quartz of Miniki Gol leucogranite (sample ZC 20).

The salinity of CO_2-bearing fluid inclusions in the muscovite pegmatite at Miniki Gol ranges from 8 to 10 wt % NaCl equivalent (Table 6.2). However, aqueous fluid inclusions both in the muscovite and tourmaline pegmatite show low salinity, ranging from 0.5 to 8 wt % NaCl equivalent, with the exception of one analysis of 13 wt % NaCl equivalent (Table 6.2, Fig. 6.6 B). The final melting of solid CO_2 (T_MCO_2) was recorded at temperature -56.6°C, along with ($T_M$clath below + 10°C), indicating a pure CO_2 gas. These fluid inclusions are characterised by a low fluid density (0.3 g cm^{-3}) and relatively high CO_2 density (0.6 g cm^{-3}) with 20.4 wt % CO_2. The partial homogenisation temperature (T_hCO_2) occurred between 29.3°C and 31.1°C. The non-aqueous fluid inclusions in the pegmatite homogenised at maximum temperature 495°C with (T_D 390°C), whereas in the aqueous fluid inclusions it occurred at between 100 and 400°C (Fig 6.5 A).

The Miniki Gol leucogranite contains both primary and secondary aqueous fluid inclusions. The primary fluid inclusions are characterised by relatively low salinity (between 2 and 8 wt % NaCl equivalent), and with T_H, ranging from 100°C up to 440°C (Table 6.2, Fig. 6.5 C, 6.6 B). The salinity of the secondary fluid inclusions in the studied leucogranite was not recorded, however they homogenised at temperature between 150-200°C with leakage up to 330°C (Fig. 6.6 B). Some melt inclusions have also been found in the analysed leucogranite.

The aqueous fluid inclusions in the scheelite-bearing calc-silicate quartzite, is represented by very low salinity and the maximum value is noted as 2 wt % NaCl equivalent (Table 6.2). The homogenisation of two phases in these inclusions, occurred at temperature between 160 and 500°C (6.6 A). It is also worth mentioning that the salinity progressively decreases from pegmatite through leucogranite to scheelite-bearing calc-silicate quartzite at Miniki Gol (Table 6.2). The prominent features of the studied fluid inclusions are summarised as follow;

- The maximum depositional temperature of the quartz is as follows: quartz vein at Besti Gol 415°C, Miniki Gol pegmatite 495°C, leucogranite 440°C and scheelite-bearing calc-silicate quartzite 500°C.
- The salinity is very low in the scheelite-bearing calc-silicate quartzite compared with pegmatite and leucogranite.
- The fluid inclusions in the quartz vein at Besti Gol are predominantly CO_2-rich.
- The fluid inclusions in the quartz vein at Besti Gol contain substantial amounts of CH_4 whereas fluid inclusions in the Miniki Gol pegmatite contain mainly CO_2 gas.

Table 6.2: Microthermometric analyses of the fluid inclusions from Miniki and Besti Gol area.

Description	Type	Composition	T_MCO_2	T_M	$T_M$clath	Salinity Wt. %NaCl equ.	T_hCO_2	T_H
ZM 109 (Quartz vein)	Primary	CH_4-CO_2-H_2O-NaCl	-60°C	—	1.5°C	14	30.9°C	412°C
ZM 109 (Quartz vein)	"	CH_4-CO_2-H_2O-NaCl	-64°C	—	—	—	31.1°C	415°C
ZM 109 (Quartz vein)	"	CH_4-CO_2-H_2O-NaCl	-71°C	—	16°C	—	31.1°C	415°C
ZM 109 (Quartz vein)	"	CO_2-H_2O-NaCl	-56.6°C	—	9.5°C	2	—	270°C
ZM 109 (Quartz vein)	"	CO_2-H_2O-NaCl	—	—	—	—	—	240°C
ZM 109 (Quartz vein)	"	CO_2-H_2O-NaCl	—	—	—	—	—	255°C
ZM 109 (Quartz vein)	"	CO_2-H_2O-NaCl	—	—	—	—	—	390°C
ZC 21 (Muscovite pegmatite)	"	CO_2-H_2O-NaCl	-56.6°C	—	-2°C	—	31.1°C	—
ZC 21 (Muscovite pegmatite)	"	"	—	—	6.1°C	8	31.1°C	450°C
ZC 21 (Muscovite pegmatite)	"	"	-56.6°C	—	5.5°C	9.5	30.5°C	495°C
ZC 21 (Muscovite pegmatite)	"	"	-56.6°C	—	5.5°C	9.5	30.8°C	—
ZC 21 (Muscovite pegmatite)	"	"	-56.6°C	—	5.5°C	9.5	29.3°C	—
ZC 21 (Muscovite pegmatite)	"	"	-56.6°C	—	5.0°C	10	30.5°C	—
ZC 21 (Muscovite pegmatite)	"	"	-56.6°C	—	5.5°C	9.5	31.1°C	—
ZC 21 (Muscovite pegmatite)	"	"	-56.6°C	—	5.5°C	9.5	30.8°C	—
ZC 21 (Muscovite pegmatite)	"	H_2O-NaCl	—	-9°C	—	13	—	209°C
ZC 21 (Muscovite pegmatite)	"	"	—	-0.5°C	—	1	—	205°C
ZC 21 (Muscovite pegmatite)	"	"	—	—	—	—	—	400°C
ZC 21 (Muscovite pegmatite)	"	"	—	—	—	—	—	140°C
ZC 21 (Muscovite pegmatite)	"	"	—	—	—	—	—	200°C
ZC 21 (Muscovite pegmatite)	"	"	—	—	—	—	—	230°C
ZC 21 (Muscovite pegmatite)	"	"	—	—	—	—	—	200°C
ZC 23 (Tourmaline pegmatite)	"	"	—	-2.4°C	—	4.5	—	—
ZC 23 (Tourmaline pegmatite)	"	"	—	-1.7°C	—	3	—	—
ZC 23 (Tourmaline pegmatite)	"	"	—	-0.3°C	—	0.5	—	183°C
ZC 23 (Tourmaline pegmatite)	"	"	—	-2.7°C	—	5	—	182°C
ZC 23 (Tourmaline pegmatite)	"	"	—	-1.1°C	—	2	—	154°C
ZC 23 (Tourmaline pegmatite)	"	"	—	-0.7°C	—	1.5	—	220°C
ZC 23 (Tourmaline pegmatite)	"	"	—	-6.5°C	—	10	—	100°C
ZC 23 (Tourmaline pegmatite)	"	"	—	-4.5°C	—	8	—	175°C
ZC 23 (Tourmaline pegmatite)	"	"	—	-0.7°C	—	1.5	—	200°C

Table 6.2. (Contd.)

Description	Type	Composition	T_M	Salinity (Wt. % NaCl equivalent)	T_H
ZS 19 (Leucogranite)	Primary	H_2O-NaCl	-4.5^oC	8	170^oC
ZS 19 (Leucogranite)	Primary	H_2O-NaCl	-3.5^oC	6.5	100^oC
ZS 19 (Leucogranite)	Secondary	H_2O only	0.0^oC	0.0	150^oC
ZS 19 (Leucogranite)	Secondary	H_2O only	0.0^oC	0.0	200^oC
ZS 19 (Leucogranite)	Secondary	H_2O only	0.0^oC	0.0	—
ZS 19 (Leucogranite)	Secondary	H_2O-NaCl	-2.5^oC	5	330^oC
ZC 20 (Leucogranite)	Primary	H_2O-NaCl	-1^oC	2	390^oC
ZC 20 (Leucogranite)	Primary	H_2O-NaCl	—	—	440^oC
ZC 20 (Leucogranite)	Primary	H_2O-NaCl	—	—	390^oC
ZC 20 (Leucogranite)	Primary	H_2O only	0.0^oC	0.0	—
ZC 65 (Calc-silicate quartzite)	"	H_2O only	0.0^oC	0.0	280^oC
ZC 65 (Calc-silicate quartzite)	"	—	—	—	260^oC
ZC 65 (Calc-silicate quartzite)	"	—	—	—	250^oC
ZC 65 (Calc-silicate quartzite)	"	—	—	—	210^oC
ZC 67 (Calc-silicate quartzite)	"	—	—	—	396^oC
ZC 67 (Calc-silicate quartzite)	"	—	—	—	500^oC
ZC 67 (Calc-silicate quartzite)	"	H_2O only	0.0^oC	0.0	—
ZC 67A (Calc-silicate quartzite)	"	H_2O-NaCl	-1^oC	2	400^oC
ZC 67A (Calc-silicate quartzite)	"	H_2O only	0.0^oC	0.0	160^oC
ZC 70 (Calc-silicate quartzite)	"	—	—	—	296^oC
ZC 70 (Calc-silicate quartzite)	"	—	—	—	450^oC
ZC 70 (Calc-silicate quartzite)	"	H_2O only	0.0^oC	0.0	205^oC
ZC 70 (Calc-silicate quartzite)	"	H_2O only	0.0^oC	0.0	390^oC
ZC 70 (Calc-silicate quartzite)	"	—	—	—	220^oC

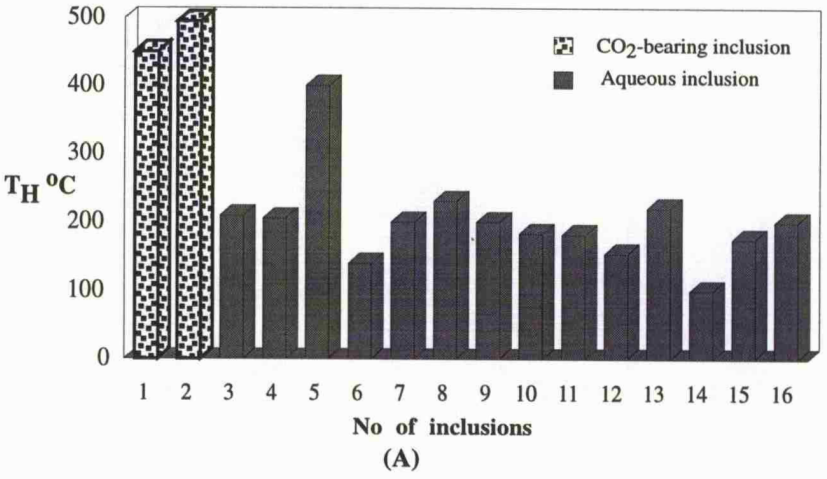

(A)

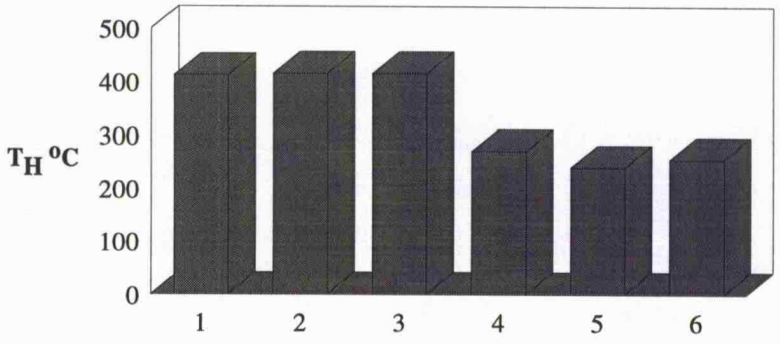

(B)

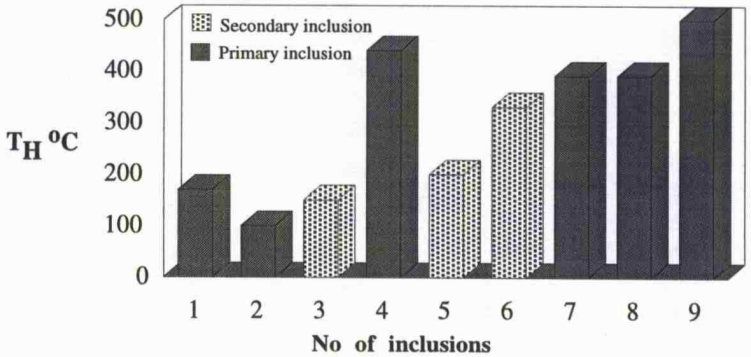

(C)

Fig. 6.5: Charts showing total homogenisation temperature (T_H): **(A)** Primary CO_2-bearing and aqueous fluid inclusions in pegmatite at Miniki Gol. **(B)** Primary CO_2-bearing fluid inclusions in the Besti Gol quartz vein **(C)** Primary and secondary fluid inclusions in the Miniki Gol leucogranite. Data taken fromTable 6.2.

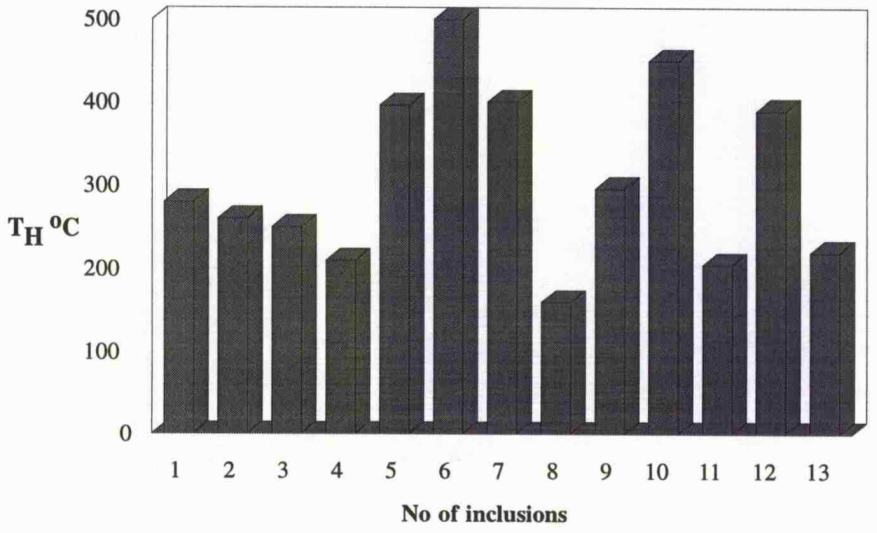

(A)

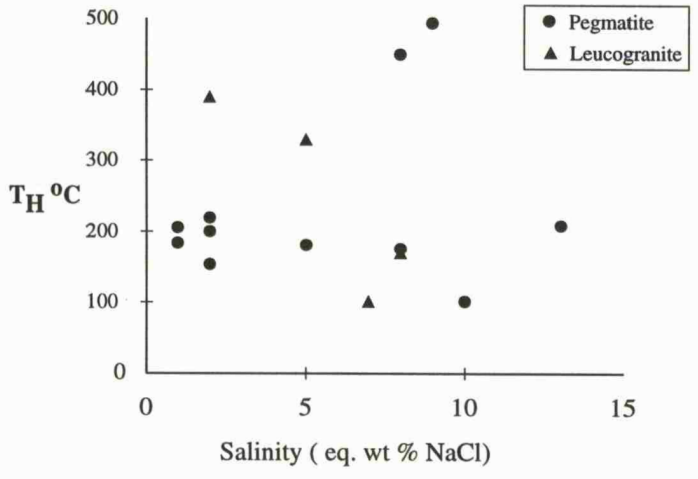

(B)

Fig. 6.6: **(A)** Total homgenisation temperature (T_H) of Miniki Gol scheelite-bearing calc-silicate quartzite. **(B)** Relationship of salinity with (T_H) of Miniki Gol leucogranite and pegmatite. Data taken fromTable 6.2.

- With the exception of the pegmatite, the fluid inclusions in the Miniki Gol leucogranite and scheelite-bearing calc-silicate quartzite are aqueous.
- The CO_2-bearing fluid inclusions in the quartz vein at Besti Gol are quite abundant compared with the Miniki Gol pegmatite.

6.5 Discussion

Fluid inclusion studies in rocks which have undergone several phases of deformation and metamorphism are difficult to interpret. As discussed earlier, the study area has experienced at least two deformational events accompanying metamorphism up to upper amphibolite facies. The emplacement of the leucogranite appears to be contemporaneous with the peak of metamorphism, which was followed by retrogression. Many ingredients may have been added to the trapped fluid or lost during these tectonic events.

The formation of fluid inclusions in metamorphic rocks is discussed by many authors. According to Roedder (1984), primary fluid inclusions in metamorphic rocks form with difficulty as material is added very slowly along the grain boundaries during metamorphism. However, when found, they are normally in vugs or quartz veins, representing fractures along which fluid escaped (Poutiainen 1990). Most of the fluid inclusions in metamorphic rocks are formed during retrogressive metamorphism and are secondary in nature (Roedder 1984). The source of these metamorphic fluids has been discussed by many authors. According to Roedder (1984) it could be the interstitial porewater of detrital sediments and muds, released during devolatilization. Thompson and Connolly (1992) and Newton (1989) argued that the main source of metamorphic fluid is structurally-bound volatiles.

There is a general consensus among workers that the fluid inclusions found in the low to medium-grade metamorphic rocks generally contain CO_2, CH_4 and N_2 trapped from sedimentary rocks containing organic matter, graphite or hydrocarbons (Mullis 1979; Crawford 1981b and 1992; Poutiainen 1990; Bottrell et al. 1988; Wilkinson 1990; Roedder 1984). In contrast, the CH_4 and N_2 contents in fluid inclusions from granite or shallow intrusive rocks are low. These fluid inclusions are mostly aqueous or CO_2-rich (Weisbrod 1981; Bottrell and Yardley 1988; Rankin and Alderton 1985; Kinnaird et al. 1985).

As far as the fluids associated with scheelite-bearing rocks are concerned, most of the fluid inclusions in the scheelite or quartz associated with scheelite deposits in the world, are predominantly CO_2-rich. However, fluid inclusions in some scheelite deposits, particularly greisen-related deposits such as the tungsten-molybdenum deposit of New

Brunswick, Canada (Davis and Williams-Jones 1985), and many deposits in China (cf. Giuliani et al. 1988) are predominantly aqueous.

Keeping in view the above scenario, the fluid inclusions in quartz veins at Besti Gol contains CH_4 and possibly N_2 in addition to CO_2. These veins, most likely post-date the associated Pb-Zn bearing marble and are not spatially associated with the leucogranite, because no plutons are exposed in the vicinity of Besti Gol lead-zinc mineralisation. The presence of the volatiles such as methane and N_2 probably suggest that these quartz veins are metamorphosed. The alternate explanation would be, that these volatiles may have been incorporated in the quartz veins from the adjacent marble or associated graphitic schist during their emplacement. We could not trace out any fluid inclusions in the marble-hosted lead-zinc mineralisation. However, the fluid inclusion study of the adjacent quartz veins suggests indirectly, that the fluids in the marble may contain $CH_4 \pm N_2$ in addition to CO_2.

In contrast, the fluid inclusions in the quartz from the leucogranite, pegmatite and scheelite-bearing calc-silicate quartzite at Miniki Gol are aqueous in general. Although, in one sample of the granite-hosted pegmatite the fluids are non aqueous, containing CO_2-bearing fluid inclusions.

The striking feature of the aqueous fluid inclusions from the scheelite-bearing calc-silicate quartzite is their very low salinity, lower than that of leucogranite. Moreover, the salinity of the CO_2-bearing fluid inclusions in the Miniki Gol pegmatite is relatively higher than the aqueous fluid inclusions. The general falling temperature trend from CO_2-bearing fluid inclusions to aqueous fluid inclusions within the Miniki Gol pegmatite, is correlated with a decline in salinity (Table 6.2). This probably, demonstrates that these fluids are mixed with meteoric water. Such phenomenon is the characteristic feature of many hydrothermally (including greisen) related tungsten deposits such as Xihuashan tungsten deposits, China (Giuliani et al. 1988) and Cligga Head, SW England (Spooner 1981). The low salinity could also be related to lack of albite in the scheelite-bearing calc-silicate rocks. Some authors have related the variation of salinity to the metamorphic grade and according to Poutiainen (1990) the salinity of aqueous solutions decreases with the increase in metamorphic grade. However, Crawford (1981b) argued that the variation of the salinity of the fluids could not be correlated with a grade of metamorphism.

The scarcity of CO_2-bearing fluid inclusions in the scheelite-bearing calc-silicate rocks and the association of clinozoisite with the scheelite signify that the fluids at the time of growth of these minerals, were predominantly aqueous. This is in a good agreement with Manning and Henderson's (1984) experimental observation that tungsten partitions preferentially in favour of melt in the presence of carbonate solution and also in

accordance with the laboratory experiments of Keppler and Wyllie (1991), that solubility of W is very high in the presence of water as the only volatile.

It is evident that the Miniki Gol scheelite precipitated from very low-saline solutions suggesting that the salinity of the fluid in the investigated scheelite-bearing rocks is reduced due to the probable influx of meteoric water. However, it is inconsistent with Manning and Henderson's (1984) laboratory experiments that with chloride and phosphate solutions tungsten partitions strongly into the aqueous phase.

The presence of CO_2-bearing fluid inclusions in many of the world's tungsten deposits, has led several workers to advocate high X_{CO_2} activity in the hydrothermal regime. According to Jianming et al. (1982 and references therein), the complex anion of tungsten $(WO_4)^{2-}$ is only stable together with corresponding cations (Ca^{2+}, Mn^{2+} and Fe^{2+}) under a high partial pressure of CO_2. As the ore-forming solution moves away from the source area, CO_2 is released from the solution along with the decline of CO_2 pressure. The equilibrium of the solution and the stability of metallic complexes are thus lost, resulting in the precipitation of ore minerals.

The occurrence of calcite in scheelite-bearing calc-silicate rocks in the studied area also demonstrates that CO_2 was an essential component of the hydrothermal fluid. The association of tourmaline with scheelite in the tourmalinites also demonstrates that B was also predominant volatile in the hydrothermal fluids. Volatiles such as CO_2, H_2O and B in the Miniki Gol tungsteniferous fluids may have driven away tungsten and brought to the site of deposition (calc-silicate rocks) during the last phase of hydrothermal activity, when pH was relatively high. As pointed out by Absar (1991), clinozoisite usually forms from a high pH and CO_2-deficient fluid whilst calcite precipitates from a CO_2-rich fluid. It is evident that calcite in the studied calc-silicate quartzite fractionated first from the CO_2-rich fluid. The continuous separation and consumption of CO_2 by calcite from the hydrothermal fluids may have increased the pH of the fluid. This has facilitated the deposition of clinozoisite together with scheelite from the CO_2-deficient fluid. It would, however, be a mere speculation to propose two separate fluids, responsible for the deposition of calcite and clinozoisite. The time gap of these events and also the paragenetic sequence between the precipitation of scheelite in the subordinate tourmalinites and calc-silicate rocks are very hard to establish.

It is also very difficult to assess whether the fluid inclusions, trapped in the granular quartz grains of the Miniki Gol scheelite-bearing calc-silicate quartzite, represent the true composition of the fluids at the time of growth. CO_2 may have been lost during the deformational events. Crawford (1981b and references therein) argued that retrogressive reactions may change the composition of the fluid (such as removal of CO_2).

Keeping in view the above discussion, it can be said that the fluid inclusion data are not compatible with those formed by regional metamorphic fluids. As most of fluid inclusions from the world's metamorphosed scheelite deposits, such as Felbertal scheelite deposit (Schenk et al. 1990) and metamorphic scheelite deposit in N. Norway (Larsen 1991), contain CH_4 and N_2 in addition to CO_2.

The occurrence of secondary fluid inclusions, low-temperature aqueous fluid inclusions (~ 150°C, Table 6.2) and mono phase inclusions within the leucogranite also indicate low-temperature hydrothermal activity within the leucogranite and pegmatite. The presence of kaolin in the pegmatite is also consistent with low-temperature activity. Such a low-temperature and low-salinity fluid has also been reported in the kaolinized St. Austell granite, SW England. According to Alderton and Rankin (1983) this represents the influx of meteoric water through cooled granite during or after the last phase of hydrothermal activity.

Two sets of temperature i.e. high and low temperature have been recorded in the granite, pegmatite and scheelite-bearing rocks (Table 6.2). The drop in temperature in these rocks could indicate the influx of meteoric water. The maximum temperature recorded in the scheelite-bearing rocks is 500°C. This temperature corresponds to the temperature range, which was calculated by plagioclase-amphibole geothermometry in the scheelite-bearing calc-silicates (see section 4.4.4).

6.6 Conclusion

The fluid inclusion study of the Miniki Gol tungsten deposits and Besti Gol lead-zinc deposits shows the presence of two contrasting hydrothermal fluids. The former was dominantly aqueous whilst the later contains substantial amounts of CO_2 together with CH_4 and possibly N_2. The aqueous fluid inclusions in the leucogranite and scheelite-bearing calc-silicate quartzite are similar in nature, indicating a possible genetic linkage between these two fluids. The salinity of the hydrothermal fluid decreases from leucogranite and pegmatite to scheelite-bearing calc-silicate quartzite indicating an influx of possible meteoric water. The aqueous fluid inclusions in the scheelite-bearing calc-silicate quartzite and leucogranite (pegmatite) homogenise into the liquid or vapour phase between 100 and 500°C. The falling temperature could be related to the mixing of ground water with the hydrothermal fluid. The kaolinisation in the pegmatite and secondary low-temperature fluid inclusions closely correlate with the above interpretation.

On the basis of thermometric data, a temperature of 450 ± 50°C is proposed for the growth of scheelite in the study area.

The presence of CO_2 in the Miniki Gol pegmatite and the occurrence calcite in the calc-silicate rocks probably demonstrate two phases of the same fluid, the earlier CO_2-rich and later aqueous fluid. The CO_2 and B may have played a role in the transportation of W in the ore-forming solution. The precipitation of scheelite is favoured by the removal of CO_2, followed by increase in pH in the tungsteniferous fluid.

Chapter Seven

DISCUSSION AND CONCLUSIONS

7.1 *DISCUSSION*

7.1.1 Introduction

As mentioned in previous chapters, the main purpose of this study is, to deduce genetic models for the tungsten and lead-zinc mineralisations in the Miniki and Besti Gol areas, Chitral, Northern Pakistan. In order to achieve these objects, a detailed discussion and interpretations have been made at the end of some chapters. In this chapter a generalised view of geological events (in sequential order) is presented to help in understanding the evolution and genesis of the W and Pb-Zn mineralisation in the project area.

The genesis of the Miniki Gol scheelite mineralisation and its protolith is very difficult to assess as the study area has suffered multiple episodes of deformation and metamorphism followed by the intrusion of leucogranite and post-magmatic hydrothermal activity. In particular, the protoliths of the metamorphosed sequence are difficult to investigate in the view of the absence of the paleontological information and the loss of sedimentary structures during the metamorphism.

On the basis of high levels of Mn, Zn and low levels of K and Rb in the tourmaline quartz gneiss compared with adjacent schists, Leake et al. (1989) have considered these tourmaline-rich rocks as siliceous chemical precipitates. These authors have ascribed a sedimentary / exhalative or diagenetic origin to the Miniki Gol scheelite mineralisation and argued that the subsequent metamorphism has recrystallised the tungsten as scheelite prior to the emplacement of leucogranite. A detailed study has not been performed in the past on the Miniki Gol leucogranites, emplaced 400 m away from the scheelite mineralisation at Miniki Gol. During the present study the role of Miniki Gol leucogranite in the formation of scheelite mineralisation has been addressed. The following is a summary of the geological events at Miniki Gol.

7.1.2 Deformation and metamorphism

The Miniki Gol and surrounding area has undergone at least two major deformational events (D1, D2) associated with the formation of foliations (S1, S2) and with the folds (F1, F2) shown in Fig. 3. 2 and 3.3. According to Leake et al. (1989) the first deformation is related to the collision between Kohistan complex and Asian plate along the Northern suture during the late Cretaceous. The second deformation is probably associated with the regional metamorphism and granite emplacement as result of a second

collision between Indian plate and Kohistan complex along Main Mantle Thrust during the Eocene (Fletcher 1985). However, leucogranites in the study area post-date the final collision (around 45 Ma) between Indian plate and Kohistan complex as K-Ar dating of the Garam Chashma plutons gives 20 Ma (Searle 1991). Moreover, post-collisional Oligocene-Miocene deformation D_3 and D_4 have also been reported in the Karakoram terrane (Searle and Tirrul 1991).

The area has suffered a regional metamorphism up to an upper amphibolite facies and Leake et al. (1989) referred to it as Barrovian type of metamorphism. Based on petrographic study, at least two metamorphic zones, a garnet zone at north and staurolite zone at the south and west of the Miniki Gol can be identified. Using a relationship between external and internal schistosity (Leake et al. 1989), textural relationship and mineral stability field (Miyashiro 1973) a paragenetic sequence of minerals can be discerned. Muscovite, chlorite, calcite with minor sphalerite and galena crystallised at the early stage of metamorphism and were joined by amphibole and staurolite at later stage of the first deformation. At the start of D2 deformation, tourmaline, hornblende, staurolite, biotite, garnet, cordierite and andalusite formed. These minerals heralded partial melting and the emplacement of leucogranite followed by retrograde metamorphism, when hydrous minerals such as clinozoisite, actinolite, secondary muscovite and chlorite, biotite, sphene and scheelite crystallised.

An almost similar deformational history has been reported by Raith and Prochaska (1995) from the granite-related tungsten deposits at Namaqualand, South Africa, where deformation overprints hydrothermal activity associated with tungsten mineralisation.

7.1.3 Leucogranite

The Miniki Gol leucogranite can be characterised as peraluminous and S-type granite. Its mineralogy and mineral chemistry of biotite, muscovite and garnet together with the aluminium saturation index, are consistent with a two-mica leucogranite (see section 5. 2). The Miniki Gol leucogranite displays high levels of Rb, Li, Be, Sn, W, Pb, Ta, U and Rb / Sr ratio and low concentrations of Zr, Hf, Y, Th, Sr, Ba, Zn, V, Co, Cr, Ni, TiO_2 / Ta, K / Rb and Mg / Li. The geochemical data of these leucogranites are very similar to the ore bearing granites of the Tischendorf (1977), Plant et al. (1985), and Boissavy-Vinau and Roger (1980). Although a number of geochemical features are common both in the unmineralised leucogranite and ore-bearing granite such as Miniki Gol. However, the Miniki Gol leucogranite can be delineated from leucogranites such as Manaslu, Himalaya (France-Lanord and Le Fort 1988; Le Fort et al. 1987) by its low levels of Cs, Co, B, and Th and high values of Mo, W, Sn, Ta and Be. The high

concentrations of Li, Be, Sn, W and Ta in the Miniki Gol granite highlight its metallogenic significance and it can, therefore, be regarded as a potential ore-bearing leucogranite.

A strong positive correlation between Sn and Ta has been found in these leucogranites (see Fig. 5.3 D). According to Schwartz (1992) and Boissavy-Vinau and Roger (1980) the evolution trend between Sn and Ta increases with the increasing degree of magmatic differentiation. These authors argued that the enriched elements (Sn and Ta) can be considered as essential parameters for Sn-W bearing granites.

Apart from the leucogranite in the area of under investigation, the associated pegmatites are also enriched in B, Be, Sn, Rb and Na. The high concentration of these elements in the Miniki Gol pegmatite signify its metallogenic character. The beryl deposits in the pegmatite and granite at the south of Garam Chashma (study area) and the occurrences of the Li-Ta-Be-Sn deposits within pegmatite throughout the Hindu Kush and Pamir belts (Rossovskiy 1991) indicate the metallogenic character of these pegmatites.

The depletion of Zr, Y, Ba, Sr and the enrichment of Be, Li, Ta, Sn, Cs and Rb in the leucogranite indicate a very evolved magmatic signature (Vidal et al. 1982; Chappell et al. 1987). The high Rb / Sr ratios (3.4) and low Sr / Ba ratios (0.4) together with negative Eu anomalies indicate that the Miniki Gol leucogranites were derived from a pelitic protolith (see Harris and Inger 1992). The high Rb and low Sr and Ba contents in the leucogranite relative to the metapelites and their overlap further suggest the derivation of these leucogranites from a pelitic source.

7.1.4 Hydrothermal alteration

7.1.4 (A) Leucogranite

The Miniki Gol leucogranite and its protolith rocks (metasediments) have undergone a certain degree of metasomatic activity. Hydrothermal alteration such as chloritization (i.e. growth of chlorite at the expense of biotite) and the presence of the abundant albite (albitization) can be recognised within the studied leucogranite. Similarly kaolinisation, tourmalinisation (development of tourmaline) and the partial sericitization of the plagioclase within the pegmatite also demonstrate the role of hydrothermal fluids in these rocks. However, these alterations are not extensive within the leucogranites and pegmatites.

The trace element chemistry also appears to be affected by the hydrothermal activity. The hydrothermal fluids appear to have leached elements such as Zr, Hf, Y, Th, Sr, Ba, Zn, V, Co, Cr, Ni and REE, particularly LREE, from the leucogranite, as these elements are low in the Miniki Gol leucogranite (Table 5.1).

7.1.4 (B) Schist

The high concentrations of F, Li, Cs, and to a lesser extent Be, W, Sn, Pb, Th, Zr, Y, Hf and Nb in Miniki Gol schist (Table 5.3), compared with the average shale (Turekian and Wedepohl 1961), suggest that these elements have been introduced by metasomatic fluids. The enrichment of these elements provide clear expression of metasomatic activity (Leake et al. 1989; Van de Haar et al. 1993), in the Miniki Gol schist.

7.1.4 (C) Calc-silicate rocks

Hydrothermal activity seems to have an obvious effect on the calc-silicate rocks as the scheelite-bearing calc-silicate quartzite is characterised by high values of Zr, Hf, Be, Sn, W, Th, U, Ga, Nb and Y compared with the unmineralised calc-silicate quartzite, psammite and schist. The F content is also higher in the calc-silicate quartzite than the psammite (Table 5.5).

The positive correlation between Ga and Nb, Y and Zr (Fig. 5.7 C-D) and between Sn and W ($r = 0.2$) in the scheelite-bearing calc-silicate quartzite indicate the similar geochemical behaviour of these elements during the hydrothermal regime. Very low concentrations of B, Hg, Sb, Mn and Fe may be considered as an indication of the negligible role of volcano sedimentary activity (Sonnet et al. 1985; Plimer 1984; Maucher 1976) in the calc-silicate quartzites.

Hydrothermal activity has also affected the REE pattern of the Miniki Gol calc-silicate quartzite. Some of the scheelite-bearing calc-silicate quartzites, such as ZC 65 A and ZC 17 (Fig. 5.8 C and Appendix 5.4), are rich in all REE (with positive Eu anomalies) whereas some, such as ZC 70, are depleted in total REE (Fig. 5.8 C). This enrichment and depletion of the REE in the scheelite-bearing calc-silicate quartzite and enrichment of HREE over LREE indicate pronounced metasomatic activity in these rocks. Positive Eu anomalies have also been reported by Sonnet et al. (1985) in the scheelite-bearing calc-silicate rocks of peri-granitic origin. The strong correlation between the elements such as Zr, Hf, Nb, Y, Ta, F and REE (see Fig. 5.10) indicates an identical geochemical behaviour of the these elements in the calc-silicate quartzite and also suggests that REE were highly mobile in the aqueous fluids. The mobility of the REE during hydrothermal alteration has been discussed by Lottermoser (1992) and Wood (1990). According to Wood (1990) fluoride and carbonate complexes can significantly facilitate the transportation of the REE along with Y in the hydrothermal regime. The mobility of the REE appears to increase with the change from early-magmatic to late-stage hydrothermal solutions (cf. Lottermoser 1992).

The mobility of Zr, Ti, U, Th, Y along with REE in the presence of alkali-rich-fluorine and phosphorus complexes have also been reported by Giere (1990), from hydrothermally-altered calc-silicate assemblages in the Bergell and Adamello contact aureoles, Italy. Rubin et al. (1993) have also argued that Zr together with Be, Y, Nb, Ta, U, Th and REE, is highly mobile in the hydrothermal system rich in alkalis and fluorine. Moreover, most of these elements have been found high in the peri-anatectic tungsten mineralisation, especially in skarns (Sonnet et al. 1985). Flynn and Burnham (1978) have also shown experimentally that the presence of chloride and fluoride ion increases the partitioning of the individual REE into the vapour phase, while CO_2 has negligible effect on the transportation of these elements.

The occurrence of Zr within the Miniki Gol scheelite (see section 4.4.9) and high concentrations of F up to (1430 ppm) in the scheelite-bearing calc-silicate rocks, are in a good agreement with theoretical studies of transportation of these elements in the hydrothermal regime. Foster (1977) noticed that the possible migration of W as fluoro-tungsten complex species can not be ruled out.

7.1.4 (D) Tourmalinite

LREE also display a linear relationship with Zr, Hf and more interestingly, Be, in the tourmalinite (Fig. 5.9 A-C) indicating similar geochemical behaviour of REE along with Zr, Hf and Be during the metasomatic activity. The REE abundances in the Miniki Gol tourmalinites are significantly different from the Broken Hill tourmalinites of exhalative origin (Table 5.6).

7.1.5 Tourmalinisation

Tourmalinites have been defined by Slack (1982) as containing 15-20 % or more tourmaline by volume. The Miniki Gol tourmalinites are characterised by extreme enrichment of boron (with up to 80 % tourmaline). The enrichment and possible sources of boron will be addressed in the following section.

The presence of graphitic schist, carbonaceous material and a thick unit of calcite overlying the pelitic schist, apparently without structural discontinuity (Leake et al. 1989), support a marine depositional environment. A submarine exhalative model for Miniki Gol tourmalinite has many difficulties as supportive evidences from sedimentary structures which might indicate exhalation, have been lost during metamorphism. According to Slack et al. (1984) tourmaline precipitates directly from exhalative hot hydrothermal fluid on the sea floor during exhalation. However, Slack et al. (1993) argued that submarine hydrothermal fluids contain very small amounts of Al (Von Damm et al. 1985) and

exhalative fluid precipitating tourmaline would consume so much alumina initially that the fluids would be undersaturated with respect to later tourmaline. The scarcity of Al-rich silicate phase in the vicinity of submarine vents (Boström et al. 1969) also indicate that the direct precipitation of tourmaline would not be possible during the exhalation. The limited strike length of the Miniki Gol tourmalinite (reported only at three locations within 2 km strike length) is inconsistent with the exhalative model. In contrast, the Broken Hill exhalites cover over 330 km strike length distance (Lottermoser 1989 a).

An evaporitic-sabkha model for the Miniki Gol tourmalinite is unlikely due to lack of evidence for the presence of evaporites or a lacustrine environment. The absence of metamorphosed products of the proposed evaporites, such as Cl-rich scapolite, abundant magnetite (product of oxidised red beds), sillimanite and andalusite-corundum (metamorphosed bauxite or laterites) which are likely to form during metamorphism of evaporite (Slack et al. 1993), rule out the possibility of a coastal sabkha environment. The absence of secondary halides also indicates a non-evaporitic environment.

Suggesting a metamorphic origin for the Miniki Gol tourmalinite, where B is leached and brought to the site of deposition has also major difficulties. Firstly, the leaching and transportation of the boron over a large distance (few kilometres) and its concentration at particular site of deposition probably would not be possible under the progressive regional metamorphism and needs extensive boron metasomatism. Secondly, tourmaline can be formed easily in situ by the diagenetic modification of evaporitic borate (Raith 1988). This contrasts with Leake et al. (1989) observations that the Miniki Gol tourmalinites crystallised during the second phase of deformation, suggesting that sufficient B was not available for these tourmalinites during diagenesis.

A boron-rich clay is also an inadequate precursor as clay minerals are not known to contain more than 2000 ppm of boron (Slack et al. 1984). This amount of boron would only be sufficient for 9 % tourmaline by volume (Plimer 1986), whereas Miniki Gol tourmalinites contain up to 80 % tourmaline by volume.

Leucogranite may be considered as a potential source of boron for these tourmalinites. The mineral chemistry of tourmaline, although not conclusive, can provide some constraints on any genetic relationship between the leucogranite and tourmalinisation. The FeO content of the tourmaline progressively increases from the leucogranite to that of pegmatite in the study area, indicating an iron-enrichment trend (Fig. 4.11 B). This iron-enrichment trend can also be noticed in the tourmaline of xenoliths within the pegmatite as well as tourmalinites, showing that excessive Fe in these tourmalinites could have been introduced from post-magmatic hydrothermal fluids. This iron-enrichment trend in tourmaline is regarded as a function of late-stage evolved

magmatic differentiation (Benard et al. 1985; Taylor et al. 1992). The Miniki Gol tourmaline iron-enrichment trend is also similar to tourmaline from Cornish granite and pegmatite (Lister 1979), from northern Portugal (Neiva 1974), from the Hub Kapong batholith of Thailand (Manning 1982) and from the Karagwe-Ankolean belt, Tanzania (Taylor et al. 1992). The positive correlation between the Fe and Aly in the tourmaline of pegmatite, xenolith and tourmalinites (Fig. 4.12), probably demonstrates similar geochemical behaviour during the post-magmatic hydrothermal fluid. Excessive Al is considered as a common feature of the pegmatite and occasionally correlated with magmatic evolution (Jolliff et al. 1986; Linnen and Williams-Jones 1993). In addition, the FeO # (FeO / (FeO + MgO) of the tourmalines from study area (0.6) is similar to the tourmaline from hydrothermal (greisen-related) Sn-W deposits at Witkop and Van Rooi localities, South Africa (Pirajno and Smithies 1992) and Kirwana Hill and Doctor Hill, New Zealand (Mackenzie 1983).

The preferred orientation of these tourmalinites can be explained due to the fact that the granite-related tourmalinisation was contemporaneous with the post-granitic deformation as the Miniki Gol leucogranite itself was deformed. The similarity of spessartine-rich garnet both in tourmalinite and leucogranite (see Table 4.3) also provide evidence for the role the post-magmatic hydrothermal fluids in the growth of these rocks.

7.1.6 Nature of the mineralising fluid

The evolution of fluids in the rocks of the project area, which have undergone several phases of deformation and metamorphism, is difficult to interpret. Based on the evidences discussed previously, the study area is interpreted to have experienced at least two deformational events accompanying metamorphism up to upper amphibolite facies, then followed by emplacement of leucogranite and retrogression. Many ingredients may have been added to the mineralising fluids or lost during these tectonic events.

The fluid inclusions in quartz vein associated with marble and graphitic schist at Besti Gol area, contain CH_4 and possibly N_2, in addition to CO_2 and theses volatiles are significantly different from those found in the Miniki Gol rocks. Their occurrence probably indicate the local remobilization of the aqueous fluid from the associated marble during the emplacement of the quartz veins. Due to the association of graphitic schist with the Miniki Gol mineralised calc-silicate rocks, one might expect the occurrence of CO_2, CH_4 and N_2 in the fluid inclusions of these rocks. However, these gases have not been found in these rocks because they were lost during the progressive metamorphism or alternatively, the fluid inclusions found in these rocks represent the later phases of hydrothermal alteration.

The fluid inclusions in the quartz from leucogranite, pegmatite and scheelite-bearing calc-silicate quartzite at the Miniki Gol area, are predominantly aqueous together with minor CO_2 in the pegmatite. Aqueous fluid inclusions in the scheelite-bearing calc-silicate quartzite are of very low salinity and this salinity is also lower in granite as well. Moreover, the salinity of the CO_2-bearing fluid inclusions in the Miniki Gol pegmatite is higher than the aqueous fluid inclusions in granite and scheelite-bearing calc-silicate quartzite. A general decreasing trend of the homogenisation temperatures from CO_2-bearing fluid inclusions to aqueous fluid inclusions within the Miniki Gol pegmatites correlates with decrease in salinity (Table 6.2). This suggests that any magmatic fluids were probably mixed with meteoric water. Such a phenomenon is characteristic feature of many hydrothermally and greisen related deposits such as Xihuashan tungsten deposits, China (Giuliani et al. 1988) and Cligga Head, SW England (Spooner 1981).

The scarcity of the CO_2-bearing fluid inclusions in the scheelite-bearing calc-silicate rocks and the association of clinozoisite with the scheelite signify that the fluid at the time of growth of these minerals, was predominantly aqueous. This is in a good agreement with the experimental observations of Manning and Henderson (1984) that tungsten partitions preferentially in favour of melt in the presence of carbonate-rich solution and also in accordance with the laboratory experiments of Keppler and Wyllie (1991), that solubility of W is very high in the presence of water as the sole volatile.

It is apparent that at Miniki Gol tungsten precipitated from very low-saline solution, suggesting that the salinity of the fluid in the scheelite-bearing rocks is low due to the possible influx of meteoric water. However, this is inconsistent with the Manning and Henderson (1984) laboratory experiments that in the presence of chloride and phosphate solutions tungsten partitions strongly into aqueous phase.

The presence of CO_2-bearing fluid inclusions in many of the world's tungsten deposits, has led several workers to advocate high X_{CO_2} activity in the associated hydrothermal regimes. According to Jianming et al. (1982 and references therein), the complex anion of tungsten $(WO_4)^{2-}$ is only stable together with corresponding cations (Ca^{2+}, Mn^{2+} and Fe^{2+}) under high partial pressures of CO_2. As the ore-forming solution moves away from the source area, CO_2 is released from the solution along with the decline of CO_2 pressure. The equilibrium of the solutions and the stability of metallic complexes are thus lost, resulting in the precipitation of ore minerals.

The occurrence of calcite in the Miniki Gol scheelite-bearing calc-silicate rocks also demonstrates that CO_2 was present at the early stage of the hydrothermal fluids. Tungsten has brought to the site of deposition (calc-silicate rocks) probably at the last phase of hydrothermal activity, when pH was relatively high. As pointed out by Absar (1991),

clinozoisite usually forms from high pH and CO_2-deficient fluid whilst calcite precipitates from CO_2-rich fluids. It is likely that the secondary calcite in the studied calc-silicate quartzite fractionated in the early stages from the CO_2-rich fluid. The continuous separation and consumption of CO_2 by calcite from the hydrothermal fluid may have increased the pH of the fluid and has facilitated the deposition of clinozoisite together with scheelite from the CO_2-deficient fluid. An alternative model for the occurrence of calcite and clinozoisite is that, there were two separate hydrothermal fluids. However, the timing of these events and also the paragenetic sequence between the precipitation of scheelite in the subordinate tourmalinites and calc-silicate rocks are very hard to establish.

Keeping in view the above discussion, it can be said with great confidence, that the fluid inclusion data at Miniki Gol are not compatible with those formed by regional metamorphic fluids. Most fluid inclusions from the world's metamorphosed scheelite deposits such as Felbertal scheelite deposit (Schenk et al. 1990) and metamorphic scheelite deposit in N. Norway (Larsen 1991), contain CH_4 and N_2 in addition to CO_2.

The occurrence of secondary fluid inclusions, low-temperature aqueous fluid inclusions (Table 6.2) and mono-phase inclusions within the leucogranite indicate later low-temperature hydrothermal activity within the leucogranite and pegmatite.

7.1.7 Pressure-temperature estimates

The fluid inclusion study of the scheelite-bearing rocks shows two sets of homogenisation temperatures (400-500^{o}C and 160-390^{o}C). Whereas higher estimates of the metamorphic temperatures (650-725^{o}C and 490-530^{o}C) have been obtained from amphibole-plagioclase geothermometry within these rocks (see section 4.4.4). These temperatures corresponds to the upper-amphibolite and upper-green schist facies metamorphism respectively. The falling temperature trend of fluid inclusions within the scheelite-bearing rocks, is probably due to the influx of meteoric water. It can be inferred from these studies that tungsten partitioned as scheelite around 450 ± 50^{o}C and continued till the lower-green schist facies.

A low pressure (2-3 kbar) is proposed for the precipitation of the scheelite. This pressure is obtained from the mol % spessartine of the garnet from the tourmalinite (see section 4.5.3) and also from the occurrence of primary muscovite within the leucogranite (Miller et al. 1981). Similar pressure-temperature estimates have also been reported from other mineralised skarns (Einaudi et al. 1981).

7.1.8 Evolution of calc-silicate quartzite

Hydrothermal solutions have brought about changes in the mineralogy and chemistry of the mica quartzite and psammite, containing layers of marble and possibly calcic plagioclase-rich rocks. The formation of both barren and scheelite-bearing calc-silicate bands within the mica quartzite and psammite clearly suggest the occurrence of pre-existing calcium-rich rocks. During the formation of calc-silicate quartzites Al, Fe, and probably some Ca, were added whereas K and Na were lost (Table 5.5). The CaO content is very high (up to 15.3 %) in the calc-silicate quartzite, expressing a Ca-metasomatism in these rocks and corresponds with the calc-silicate mineralogy consisting of calcic-amphibole (hornblende-actinolite), clinozoisite, calcite, sphene or titanite, calcite, anorthite, grossular garnet, diopside and scheelite. These are typical mineral assemblages found in the skarn environment. Except for diopside and grossular garnet, these mineral compositions appear to show a consistent and common trend through out the deposits.

The clinozoisite seems to be formed by the complete breakdown of plagioclase, as evident from its pistacite (100 Fe^{3+} / (Fe^{3+} + Al) content ranging from 2.95 to 16 (Table 4.2) and is compatible with the occurrence of epidote formed by alteration of plagioclase (Tulloch 1979). The presence of grossular garnet (mol % grossular up to 87) in the garnet of calc-silicate quartzite, ZC 8 (Table 4.3), clearly shows a calcium metasomatism in the Miniki Gol area. Grossular garnet is considered by Deer et al. (1982) as the typical garnet found in the skarn or occurring in the rocks which have undergone calcium metasomatism.

The lack of regular zoning in the five generations of calcic-amphibole and the occurrence of tschermakitic-hornblende and actinolitic-hornblende within a single grain of the calc-silicate quartzite (Fig. 4.15, Table 4.4), suggest that equilibrium has not been attained during the formation of the calc-silicate quartzite. The occurrence of secondary (spherulitic) actinolite in these rocks, depicts a retrogressive environment. Such retrogression is generally attributed to the late stage igneous-hydrothermal solutions or metasomatic metamorphism (Deer et al. 1992).

The occurrence of Mg-rich biotite and chlorite (especially in the scheelite-bearing quartzite), appears to be the function of hydrothermal activity in these rocks (Brimhall et al. 1977). The Fe^{2+}/ (Fe^{2+} + Mg) ratio of biotite in the scheelite-bearing quartzite is similar to the biotite of the Var (France) calc-silicate quartzite-hosted tungsten mineralisation of metasomatic origin (Sonnet et al. 1985). These data are more or less consistent with the Morocco skarn-related stratiform-scheelite-biotite mineralisation (Cheilletz 1985).

The chemistry of the sphene from both the studied scheelite-bearing and barren calc-silicate rocks with the exception of ZC 27 (Table 4.7), correlates with the sphene

from skarns and igneous rocks of Victoria Range, New Zealand, (Tulloch 1979). Titanite along with orthoclase has also been found in the skarn calc-silicate assemblages of Var, France (Sonnet et al. 1985).

The scheelite-bearing calc-silicate rocks are also enriched in Fe, W, Sn, Be, F and to a lesser extent Mn (Table 5.5). This enrichment is considered as a salient feature in distinguishing metasomatic skarns from metamorphic skarn (Einaudi et al. 1981; Kwak 1987; Newberry et al. 1986). The large thickness of the calc-silicate bands are also consistent with metasomatic skarns (Kwak 1987). According to Newberry et al. (1986) metasomatic skarn is represented both by progressive and retrogressive metamorphic assemblages, whereas metamorphic skarns exhibit equilibrium assemblages. The conversion of hornblende into marginal actinolite, biotite into chlorite and plagioclase into clinozoisite in the scheelite-bearing rocks are consistent with metasomatic skarn.

7.1.9 Scheelite mineralisation

Scheelite is the only tungsten mineral identified in the Miniki Gol area, and occurs in a variety of rocks, the most important of which is calc-silicate quartzite. Tourmalinites also contain substantial amount of scheelite but the lateral extension of these tourmalinites is very limited. Scheelite occurs as discontinuous patches, stringers and conformable small veins within the calc-silicate quartzite (Fig. 3.3 A, 3.4) and can be considered as stratabound scheelite (Hosking 1982; Leake et al. 1989), although minor scheelite veins also cross-cut the calc-silicate quartzite beds (Fig. 3.3 A). It should be noted that not all the calc-silicate quartzite beds are mineralised and also that there is a considerable variation in the concentration of scheelite both laterally and vertically within the calc-silicate quartzite beds.

Both the continuity and distribution of scheelite mineralisation seems to be influenced by the internal structure in the calc-silicate quartzite and tourmalinites. Scheelite in the tourmalinites seems to be partitioned along both overprint penetrative foliation as well as crenulation foliation (Fig. 3.3 B). Some of the cross-cutting quartz veins also contain scheelite patches. Dames and Moore (1987) have also reported scheelite grains in the drag-folded sequence of calc-silicate quartzite. The concentration of some scheelite grains in hinges of the kink folds (Fig. 3.3 B) can also be interpreted as the fractured hinges as loci for the epigenetic mineralising fluids (Dames and Moore 1987). The foliation planes may also have acted as channel ways for the epigenetic mineralising fluids. According to Leake et al. (1989), scheelite, together with clinozoisite and garnet crystals, developed mimetically along this foliation and therefore must have formed post D1.

The concentration of scheelite in the drag folded sections and the emplacement of scheelite bearing quartz veins along the axial plane of F2 folds indicate a genetic relationship between the scheelite mineralisation during the deformation and intrusion of Miniki Gol granite. Scheelite grains are concentrated in those calc-silicate quartzites, which contain substantial amount of amphibole and clinozoisite. However some small veins cross-cut the clinozoisite grains (Fig. 4.6 B) and postdate the main clinozoisite phase. Moreover scheelite-bearing calc-silicate quartzite loses schistosity or metamorphic layering at the onset of clinozoisite and scheelite.

The most interesting feature of the Miniki Gol scheelite is, the occurrence of zirconium and to lesser extent tantalum, recorded up to 0.46 and 0.35 wt % respectively (Table 4.9). Zirconium and tantalum are usually related to igneous activity and the concentration of these elements, is notably high in plutonic rocks rich in Na_2O or alkaline igneous rocks (Deer et al. 1982; Tukiainen 1988).

7.1. 10 Source of tungsten

The average background tungsten content of the metasediments in study area is 2.6 ppm and reaches up to 7 ppm (Table 5.3, Appendix 5.3). This value is relatively higher than the one found in the average shale (1.8 ppm) of Turekian and Wedepohl 1961). However, the background tungsten levels of the Miniki Gol metapelite are not anomalous and does not support the possibility of a pre-granitic or exhalative source for tungsten concentration.

It is likely that partial melting of pelites with relatively high contents of W (up to 7 ppm) have yield a granitic melt with 5-10 or even more ppm of W (see also Lehmann 1990). Miniki Gol pelite-derived leucogranites contain tungsten up to 10 ppm, corresponds to this interpretation. The later fractionation may have further enriched the tungsten in the most evolved part of these leucogranites. The post-magmatic hydrothermal tungsteniferous fluids enriched with volatiles such as CO_2, H_2O, B and F, were driven away from the leucogranite into the Miniki Gol metasediments. These fluids may have leached Al, Fe and some Ca from the metasediments and reconcentrated within the most reactive rocks such as marble within the mica-quartzite and psammite. Zr and Ta may have incorporated in the scheelite during the post-magmatic hydrothermal activity.

7.1.11 Marble-hosted stratiform Pb-Zn mineralisation

As discussed earlier, the Besti Gol lead-zinc mineralisation is concordantly interbedded with the enclosing marble and occurs as conformable, continuous veins within the marble beds. Based on the continuity and conformability of these mineralised veins, it

can be classified as stratiform and stratabound mineralisation (see Fig. 3.5 A-B). Zinc minerals (sphalerite and hydrozincite) are more common and widespread than the Pb in the Besti Gol area. The mineralisation is confined to a 65 m thick marble horizon at Singlasht in the Besti Gol area, whereas other marble beds in the Besti Gol area are unmineralised (Fig. 1.3). Moreover, the one kilometre thick marble unit at Miniki Gol is also devoid of any lead-zinc mineralisation.

Sphalerite is the dominant sulphide with subordinate galena and pyrite. Sphalerite and galena appear to be recrystallised and coarsened during the course of metamorphism as indicated by triple junction textures (Fig. 4.8 A). Sphalerite and galena, at their margin are altered to (probable) hydrozincite and plattnerite respectively (Fig. 4.8 A, 4.9 A). In contrast, Pyrite seems to be altered to zinc-bearing magnetite or hydrous iron oxide (Fig. 4. 9 B).

Sphalerite shows consistent chemical compositions from core to margin of the grain. However, two generations of sphalerite (Fe-poor, 2.85 to 3.65 wt % and relatively Fe-rich 6-7 wt %) have been found in different grains (Table 4.10). The amount of FeS in the metamorphosed sphalerite is regarded as a function of pressure, temperature and sulphur activity when buffered by pyrite (Scott and Barnes 1971; Scott 1983; Moles 1983). The 5-12 mole % FeS content in the Besti Gol sphalerite indicates a wide but generally high pressure and temperature range (Scott and Barnes 1971; Deer et al. 1992). The pale blue fluorescence seen in the outcrop, could be related to hydrozincite or to sphalerite itself. The formation of zincite can easily be explained as during high temperature CO_2 and H_2O are lost, leaving ZnO as zincite (Frondel and Baum 1974; Palache et al. 1951) or the mineral may be formed as a result of supergene enrichment. Galena is the minor phase in the sulphide mineralisation and only few grains of galena have been spotted. Galena, at places, appears to be altered, possibly to plattnerite (PbO_2).

The Besti Gol marble shows high levels of As, Ba, Sc, Sb, S, Zn and Pb (Table 5.7), Ag (up to 15 ppm), Hg (up to 110 ppm) compared with the average carbonates data of Graf (1960) and Turekian and Wedepohl (1961). The strong positive correlation of As with Ba, Sc and Sr may indicates that these elements were introduced during the hydrothermal alteration.

The major element chemistry of the marble seems to be of sedimentary origin. However, a strong positive correlation between As and Fe ($r = 0.78$) in the Besti Gol mineralised marble could be secondary, indicating some of the Fe was introduced by hydrothermal activity. Although the Mg was not determined in the Besti Gol marble, the Miniki Gol Marble contains up to 2 % MgO, showing that the marble is predominantly composed of calcite.

So in summary, the conformability of the sulphide mineralisation with host marble indicates that this mineralisation precipitated in of synsedimentary environment. Subsequent metamorphism has induced distinct textural changes in sphalerite and thus the original sedimentary layering has been obliterated. The coarse grain size, the euhedral crystal and triple junction in the calcite also correspond to metamorphism.

7.1.12 Comparison of Miniki Gol (Chitral) W mineralisation with Cornubian (SW England) Sn-W deposits

The Miniki Gol (Chitral) W mineralisation is different in character from the Cornubian (S-W England) Sn-W deposits, however some similarities also exist in these two regions. The following are main points of differences and similarities.

- Both tungsten deposits of Miniki Gol and SW England are associated with crustally derived S-type granites.
- The major part of SW England province is composed of porphyritic biotite granites (Exley and Stone 1982), whereas the Miniki Gol leucogranite predominantly contains muscovite with a minor phase of biotite.
- The granite of SW England is enriched in volatiles such as F, Li, B and P (Manning 1986), whilst the Miniki Gol leucogranite is enriched mainly in P and to a lesser extent F and Li.
- Tungsten mineralisation occur almost always in the form of wolframite associated with, and subordinate to cassiterite in SW England, whereas tungsten in the Miniki Gol is present as scheelite.
- Wolframite occur mainly in the hydrothermal vein systems and is closely associated with greisenisation and tourmalinisation at SW England (Beer and Ball 1987; Manning 1986). The Chitral tungsten mineralisation is precipitated mainly in the calc-silicate quartzite (skarn assemblages) and subordinate tourmalinites, 400 to 500 m away from leucogranite. Although kaolinisation and partial sericitization have been recorded in the pegmatite, however, these alterations are not extensive.
- The original REE abundances of the SW England granite were lost during the hydrothermal alteration (tourmalinisation) and LREE altered during chloritization and argillic alteration (Alderton et al. 1980). Likewise the bulk REE and particularly LREE are depleted during the hydrothermal alteration of the Miniki Gol leucogranite.
- Fractional crystallisation is the dominant mechanism at SW England granite and these plutons are distinguished into B (Biotite rich granite), C (Biotite and muscovite rich granite), zinnwaldite-albite bearing granite (D-E type) and fluorite-topaz-albite rich

granite (F type) (Stone and Exley 1986; Beer and Ball 1987). The C-type granite is considered to be derived from the B-type magma, whereas (D, E and F type) magma are derived from (B-C type magma). The Miniki Gol leucogranite is relatively less fractionated with an homogenous composition throughout the study area and with only minor variation of muscovite, biotite and tourmaline.

- Tungsten mineralisation in SW England has also been reported (although less commonly) from pegmatites (Manning 1986), whereas the pegmatites especially at Miniki Gol are devoid of any scheelite mineralisation.

7.2 Conclusions

7.2.1 Genesis of Miniki Gol scheelite

Although a number of plausible genetic models, a regional tungsten skarn type origin, a prograde metamorphic origin and exhalative-sedimentary origin, can be considered for the Miniki Gol scheelite mineralisation, but they are not recommended. On the basis of the evidences, cited during the course of this study the author favours a post-magmatic hydrothermal model for the scheelite mineralisation. The evidences for this model are summarised as follows:

7.2.1A Tourmalinites

The most striking feature of the Miniki Gol scheelite mineralisation is, its association with tourmalinites. These tourmalinites have been found as small pockets within the tourmaline-bearing schist at three locations around 2 km strike length. According to Leake et al. (1989) these tourmalinites are not laterally extensive and have sharp contacts with adjacent rocks. It should also be noted that scheelite is not associated with tourmaline-bearing schist at Miniki Gol. Moreover, tourmaline grains are concentrated only in schist at Miniki Gol and decrease towards the Garam Chashma away from the Miniki Gol. Tourmaline grains are almost rare or absent elsewhere within the schist at the study area.

The Miniki Gol tourmalinites contain up to 3.1 % K_2O, up to 190 ppm Rb, up to 700 ppm Ba and low levels (up to 2.6 %) of MnO and up to 150 ppm Zn (Appendix 5.5). These levels are not markedly different from the associated schist and thus can not be considered as siliceous chemical precipitates (exhalites) as suggested by Leake et al. (1989). The limited extent of these tourmalinites is inconsistent with the occurrence of exhalites as the Broken Hill exhalites cover over 330 km strike length distance (Lottermoser 1989 a). It should also be noted that the background levels of W are slightly

higher than those of the average shale (Turekian and Wedepohl 1961), and does not support the pre-granitic enrichment of tungsten. The lack of Sb, Hg, Ag, F and P in the tourmalinites (Appendix 5.5) and the very low level of B, Mn together with Hg, Ag and Sb in the calc-silicate quartzite are also not consistent with exhalative activity in the study area.

If the tourmalinites are not exhalites then the Miniki Gol leucogranite is a possible source for both the W and B. This is supported by the structural observations that the tourmalinites were formed after the first deformation, probably contemporaneous or after the emplacement of the leucogranite. The chemical composition of the tourmaline and spessartine-rich garnet of the tourmalinites is similar to that of tourmaline and spessartine-rich garnet of the leucogranite (Fig. 4.11 A, 4.14 A), further support a genetic linkage.

7.2.1B Calc-silicates

The occurrence of clinozoisite, sphene, actinolitic-hornblende, grossular garnet and the chemistry of biotite and chlorite within the calc-silicate rocks all favour post-magmatic hydrothermal activity. The presence of Zr and Ta in the scheelite also indicate a magmatic signature. The enrichment of Zr, Hf, Be, Sn, W, Th, U, Ga, Nb, Y, and REE in the scheelite-bearing calc-silicate quartzite compared with the unmineralised calc-silicate quartzite, psammite and schist, also indicate pronounced post-magmatic hydrothermal activity. The occurrence of scheelite-bearing skarn at one locality at the eastern margin of the marble at Miniki Gol also reflects a genetic relationship between scheelite and leucogranite.

7.2.1C Granite chemistry

The Miniki Gol leucogranites can be categorised as fractionated and potential ore-bearing granites as levels of Be, Li, Ta, Sn, Cs and Rb are very high. They can be differentiated from other Himalayan leucogranites by the high levels of Sn and Ta at Miniki Gol. According to Schwartz (1992) and Boissavy-Vinau and Roger (1980) Sn and Ta increase with the increasing degree of magmatic differentiation and are essential parameters for W-bearing granites. High concentration of Sn has also been found in the most evolved granites (type E and F) from the Cornubian batholith, SW England (Stone and Exley 1986) and Bolivian fractionated tin granites (Lehmann 1990).

7.2.1D Fluid inclusions

The consistency of the fluid inclusions both within leucogranites and calc-silicate rocks establishes a genetic link between the scheelite mineralisation and post-magmatic hydrothermal fluids.

7.2.1E Deformation

As discussed previously the study area has suffered several phases of deformation, however, foliation has been lost within the scheelite-bearing calc-silicate rocks. The intergrown scheelite and clinozoisite grains seem to be undeformed, although, scheelite-bearing tourmalinites are strongly deformed. This probably, suggests that post-granitic deformation overprints hydrothermal activity associated with scheelite mineralisation, which is evident from the deformation within the Miniki Gol leucogranite. All the above evidences indicate that both B and W were introduced during the post-magmatic hydrothermal activity and hydrothermal fluids follow weak structural zones.

7.2.2 Other conclusions

- Lead-zinc mineralisation is concordantly interbedded with the enclosing marble and hence classified as stratiform and stratabound mineralisation.
- Lead-zinc mineralisation were precipitated as sphalerite and galena in synsedimentary environment. Subsequent metamorphism has induced distinct textural changes in sulphide mineralisation including recrytallisation, coarsening of the grain size and changes in chemical composition.
- Sphalerite, galena and pyrite seems to be altered to hydrozincite, plattnerite and zinc-bearing magnetite respectively during the hydrothermal alteration.

7.3 Recommendation for future studies

In order to confirm the origin of W and Pb-Zn mineralisations, the following further studies are suggested.

- Stable isotopic study of boron in tourmalinites, oxygen etc. in scheelite and radiometric dating ($^{40}Ar/^{39}Ar$, K-Ar geochronology or Rb-Sr isotopic data) of the leucogranite is needed. This study will resolve the timing of mineralisation and the emplacement of leucogranite.
- The determination of REE abundances within the scheelite which will establish a possible genetic link between the scheelite and the leucogranite.

- A detailed study including field relations, geochemistry, fluid inclusion and radiometric dating (Pb^{206}/Pb^{204} of galena) is needed to produce a complete genetic model for the lead-zinc mineralisation as the conclusions drawn in this study, are preliminary.
- The alteration mechanisms of sphalerite, galena and pyrite into hydrozincite, plattnerite and zinc-bearing magnetite should be investigated further.
- The causes of fluorescence in the lead-zinc mineralisation should be confirmed.

Appendix 4.1: List of the samples studied during the course of present investigation.

The following is the list of samples collected during the two field trips to the study area. Letters (ZC) were assigned to the samples as an identification in the first field work followed by ZS and ZM in the second field trip. Samples ZM 100 to ZM 133 were collected from Besti Gol, ZS 1 to ZS 19C from Garam Chashma-Shoghor section, ZM 85-87 from Kafiristan granodiorite, ZM 92-95 from Tirich Mir and the rest are taken from Miniki Gol and surrounding area (see Fig. 4.1 A-C, 5.4). A brief mineralogy based on field and petrographic observation is also presented.

Sample	Mineralogy
ZC 1	Mica schist (muscovite, staurolite, plagioclase, biotite, chlorite, graphite and quartz).
ZC 1	Mica quartzite (quartz, biotite and muscovite).
ZC 2	Mica schist (muscovite, quartz, staurolite, chlorite, plagioclase and garnet).
ZC 3	Micaceous psammite (quartz, biotite and plagioclase).
ZC 3A	Micaceous psammite (quartz, biotite and plagioclase).
ZC 4	Calc-silicate quartzite (quartz, clinozoisite, hornblende-actinolite, sphene, biotite, garnet and plagioclase).
ZC 4A	Micaceous psammite (quartz, biotite, plagioclase, chlorite and graphite).
ZC 5	Calc-silicate quartzite (quartz, clinozoisite, hornblende-actinolite, sphene and biotite).
ZC 6	Micaceous psammite (quartz, biotite and plagioclase).
ZC 7	Calc-silicate quartzite (quartz, clinozoisite, biotite and plagioclase).
ZC 8	Calc-silicate quartzite (quartz, clinozoisite, garnet and plagioclase).
ZC 9	Mica schist (muscovite, staurolite, plagioclase, biotite, garnet and quartz).
ZC 10	Micaceous psammite (quartz, biotite, muscovite and plagioclase).
ZC 11	Mica schist (garnet over 50 %, biotite, muscovite, plagioclase and quartz).
ZC 12	Micaceous psammite (quartz, biotite, muscovite and plagioclase).
ZC 13	Micaceous psammite (quartz, muscovite and plagioclase).
ZC 13A	Micaceous psammite (quartz, muscovite and plagioclase).
ZC 14	Micaceous psammite (quartz, muscovite and plagioclase).
ZC 15	Micaceous psammite (quartz, biotite, muscovite and plagioclase).
ZC 16	Micaceous psammite (quartz, biotite, muscovite plagioclase, chlorite, clinozoisite and sphene).
ZC 17	Calc-silicate quartzite (quartz, clinozoisite over 50 % and scheelite).
ZC 18	Micaceous psammite (quartz, biotite, muscovite, clinozoisite and plagioclase).
ZC 19	Micaceous psammite (quartz, muscovite and plagioclase).
ZC 20	Leucogranite (plagioclase, orthoclase, quartz, garnet and muscovite).
ZC 21	Pegmatite (plagioclase, quartz and muscovite).
ZC 23	Tourmaline pegmatite.
ZC 25	Mica schist (muscovite, chlorite and quartz).

Appendix 4.1 (contd.)

Sample	Mineralogy
ZC 26	Amphibolite (plagioclase, hornblende-actinolite and quartz).
ZC 27	Calc-silicate quartzite (quartz, clinozoisite, epidote, titanite, chlorite, and plagioclase) containing cross-cutting chlorite vein.
ZC 28	Feldspathic gneiss (plagioclase, quartz, garnet and muscovite).
ZC 29	Micaceous psammite (quartz, biotite, and plagioclase).
ZC 30	Calc-silicate quartzite (quartz, clinozoisite, chlorite and muscovite).
ZC 31	Leucogranite (plagioclase, orthoclase, quartz, garnet and muscovite).
ZC 32	Banded Calc-silicate quartzite (quartz, clinozoisite, chlorite and hornblende-actinolite).
ZC 33	Banded Calc-silicate quartzite (quartz, clinozoisite, titanite, biotite and garnet).
ZC 34	Calc-silicate quartzite (quartz, clinozoisite, chlorite and biotite).
ZC 35	Calc-silicate quartzite (quartz, clinozoisite, chlorite, biotite and hornblende-actinolite).
ZC 36	Mica schist (biotite, muscovite, chlorite, quartz and plagioclase).
ZC 37	Mica schist (muscovite, staurolite, plagioclase, biotite, chlorite, garnet and quartz).
ZC 38	Leucogranite (plagioclase, orthoclase, quartz, garnet, muscovite and biotite).
ZC 39	Tourmaline gneiss (tourmaline, garnet and quartz).
ZC 40	Tourmalinite (tourmaline up to 80 %, quartz and garnet).
ZC 41	Calc-silicate quartzite (quartz, clinozoisite, hornblende-actinolite, sphene, garnet and scheelite).
ZC 42	Banded calc-silicate quartzite (quartz, clinozoisite, and hornblende-actinolite).
ZC 43	Calc-silicate quartzite (quartz, clinozoisite, hornblende-actinolite, sphene, muscovite and scheelite).
ZC 44	Mica schist (biotite, garnet ,quartz and actinolite).
ZC 45	Banded calc-silicate quartzite (biotite, quartz, clinozoisite and garnet).
ZC 46	Phyllite (muscovite, chlorite, biotite, quartz and garnet).
ZC 46A	Phyllite (muscovite, chlorite, biotite, quartz and garnet).
ZC 48	Phyllite (muscovite, chlorite, biotite, quartz, clinozoisite and garnet).
ZC 49	Banded calc-silicate quartzite (quartz, clinozoisite, hornblende-actinolite and sphene).
ZC 50	Calc-silicate quartzite (quartz, clinozoisite, chlorite and biotite).
ZC 51	Banded calc-silicate quartzite (quartz, clinozoisite, chlorite and biotite).
ZC 52	Phyllite (muscovite, chlorite, biotite, quartz and garnet).
ZC 53	Phyllite (muscovite, chlorite, biotite, quartz and garnet).
ZC 54	Mica quartzite (biotite, quartz and chlorite).
ZC 55	Phyllite (muscovite, chlorite, biotite, quartz and garnet).
ZC 56B	Marble (calcite, quartz and muscovite).

Appendix 4.1 (contd.)

Sample	Mineralogy
ZC 57	Marble (calcite, biotite and muscovite).
ZC 57A	Marble (calcite, biotite and muscovite).
ZC 57B	Marble (calcite, biotite and muscovite).
ZC 58	Phyllite (muscovite, chlorite, biotite and quartz).
ZC 59	Phyllite (muscovite, chlorite, biotite, quartz and graphite).
ZC 60	Marble.
ZC 60A	Marble.
ZC 61	Phyllite (muscovite, chlorite, biotite and quartz).
ZC 62	Phyllite (muscovite, chlorite, biotite and quartz).
ZC 63	Mica schist (garnet, biotite, muscovite, chlorite and quartz).
ZC 64	Mica schist (biotite, muscovite, chlorite and quartz).
ZC 65A	Calc-silicate quartzite (quartz, clinozoisite, chlorite, hornblende-actinolite, biotite, sphene, zircon, apatite and scheelite).
ZC 65B	Calc-silicate quartzite (calcite, quartz, clinozoisite, hornblende-actinolite, sphene and scheelite).
ZC 65C	Calc-silicate quartzite (calcite, quartz, clinozoisite, hornblende-actinolite, sphene and scheelite).
ZC 66	Calc-silicate quartzite (calcite, quartz, clinozoisite, hornblende-actinolite and scheelite).
ZC 67	Calc-silicate quartzite (calcite, quartz, clinozoisite, hornblende-actinolite, and scheelite).
ZC 67A	Calc-silicate quartzite (quartz, clinozoisite, hornblende-actinolite, calcite, sphene and scheelite).
ZC 67B	Calc-silicate quartzite (quartz, clinozoisite, hornblende-actinolite, calcite, sphene and scheelite).
ZC 68	Mica schist (garnet, biotite, muscovite, chlorite and quartz).
ZC 69	Tourmalinite (tourmaline, garnet, quartz and scheelite).
ZC 69A	Tourmalinite (tourmaline, garnet, quartz and scheelite).
ZC 70	Calc-silicate quartzite (quartz, clinozoisite, hornblende-actinolite and scheelite).
ZC 71	Leucogranite (plagioclase, orthoclase, quartz, muscovite and biotite).
ADIT 3	Calc-silicate quartzite (hornblende-actinolite over 40 %, clinozoisite, quartz, calcite, biotite, plagioclase and scheelite).
TREN 132	Calc-silicate quartzite (hornblende-actinolite, clinozoisite, quartz, calcite, biotite, plagioclase and scheelite).
ZS 1	Slate.
ZS 2	Slate (muscovite, chlorite, quartz and calcite).
ZS 3	Slate.
ZS 4	Mica schist.
ZS 5	Mica schist.
ZS 6	Mica schist.

Appendix 4.1 (contd.)

Sample	Mineralogy
ZS 7	Leucogranite.
ZS 8	Leucogranite (plagioclase, orthoclase, quartz and muscovite).
ZS 9	Leucogranite (plagioclase, orthoclase, quartz, muscovite and biotite).
ZS 10	Leucogranite (plagioclase, quartz, orthoclase, biotite, muscovite and tourmaline).
ZS 11	Mica schist.
ZS 11A	Pegmatite (tourmaline, quartz, kaolin and muscovite).
ZS 12	Pegmatite (tourmaline, quartz, plagioclase and muscovite).
ZS 13	Calc-silicate quartzite.
ZS 14	Leucogranite.
ZS 15	Calc-silicate quartzite.
ZS 16	Calc-silicate quartzite.
ZS 17	Leucogranite (plagioclase, orthoclase, quartz, muscovite, garnet and biotite).
ZS 18	Calc-silicate quartzite.
ZS 19A	Mica schist.
ZS 19B	Mica quartzite.
ZS 19C	Leucogranite (plagioclase, orthoclase, quartz, muscovite, garnet and biotite).
ZM 1	Leucogranite (plagioclase, quartz, orthoclase, biotite and muscovite).
ZM 2	Leucogranite (plagioclase, quartz, orthoclase, biotite and muscovite).
ZM 3	Leucogranite (plagioclase, quartz, orthoclase, perthite, biotite and muscovite).
ZM 4	Banded calc-silicate quartzite.
ZM 5	Mica schist.
ZM 6	Mica schist.
ZM 7	Mica schist.
ZM 8	Mica schist.
ZM 9	Mica schist.
ZM 10	Mica schist.
ZM 11	Mica schist.
ZM 12	Calc-silicate quartzite.
ZM 13	Mica schist.
ZM 14	Calc-silicate quartzite.
ZM 14A	Calc-silicate quartzite.
ZM 15	Calc-silicate quartzite.
ZM 16	Tourmaline-bearing schist.
ZM 17	Calc-silicate quartzite.
ZM 18	Mica schist.
ZM 19	Mica schist.
ZM 20	Mica schist.

Appendix 4.1 (contd.)

Sample	Mineralogy
ZM 21	Mica schist.
ZM 22	Calc-silicate quartzite.
ZM 23	Mica schist.
ZM 24	Tourmalinite.
ZM 24A	Calc-silicate quartzite.
ZM 25	Tourmaline gneiss (tourmaline and quartz).
ZM 26	Mica schist.
ZM 27	Tourmaline-bearing schist (biotite, muscovite, tourmaline and garnet).
ZM 28	Tourmalinite.
ZM 29	Tourmalinite.
ZM 30	Mica schist.
ZM 31	Tourmalinite.
ZM 32	Tourmalinite.
ZM 34	Mica schist.
ZM 35	Mica schist.
ZM 36	Mica schist.
ZM 37	Scheelite-bearing calc-silicate quartzite.
ZM 38	Scheelite-bearing calc-silicate quartzite.
ZM 39	Mica schist (biotite, muscovite, quartz and garnet).
ZM 40	Mica quartzite (biotite, muscovite and quartz).
ZM 41	Mica quartzite (biotite, muscovite and quartz).
ZM 42	Mica schist (biotite, muscovite, quartz, chlorite and graphite).
ZM 43	Calcareous schist.
ZM 44	Phyllite.
ZM 47	Phyllite.
ZM 48	Graphitic schist.
ZM 51	Leucogranite (plagioclase, quartz, orthoclase, biotite and muscovite).
ZM 52	Leucogranite (plagioclase, quartz, orthoclase, garnet, biotite and muscovite).
ZM 53	Leucogranite (plagioclase, quartz, orthoclase, biotite and muscovite).
ZM 54	Amphibolite.
ZM 55	Mica schist.
ZM 56	Leucogranite (plagioclase, quartz, orthoclase, biotite and muscovite).
ZM 57	Mica schist.
ZM 58	Quartz vein.
ZM 59	Mica schist.
ZM 60	Calc-silicate quartzite.
ZM 61	Mica schist.
ZM 62	Tourmalinite.
ZM 63	Tourmalinite (garnet over 50 %, tourmaline and quartz).
ZM 64	Tourmalinite (garnet over 50 %, tourmaline and quartz).

Appendix 4.1 (contd.)

Sample	Mineralogy
ZM 64A	Tourmalinite.
ZM 65	Scheelite-bearing calc-silicate quartzite.
ZM 66	Scheelite-bearing calc-silicate quartzite.
ZM 67	Leucogranite (plagioclase, quartz, orthoclase, perthite, biotite and muscovite).
ZM 68	Mica quartzite.
ZM 69	Leucogranite (plagioclase, quartz, orthoclase, biotite and muscovite).
ZM 70	Leucogranite (plagioclase, quartz, orthoclase, perthite, garnet, biotite and muscovite).
ZM 71	Pegmatite (plagioclase and quartz).
ZM 85	Porphyritic granodiorite (plagioclase, orthoclase, quartz and biotite).
ZM 86	Porphyritic granodiorite (plagioclase, orthoclase, quartz and biotite).
ZM 87	Porphyritic granodiorite.
ZM 92	Porphyritic granodiorite (plagioclase, orthoclase, quartz and biotite).
ZM 93	Porphyritic granodiorite (plagioclase, orthoclase, microcline quartz and biotite).
ZM 94	Porphyritic granodiorite.
ZM 95	Porphyritic granodiorite.
ZM 100	Phyllitic schist.
ZM 101	Phyllitic schist.
ZM 102	Calcareous schist.
ZM 103	Calcareous schist.
ZM 104	Calcareous schist.
ZM 105	Calcareous schist (calcite, quartz, chlorite, biotite, plagioclase, epidote, actinolite and muscovite).
ZM 106	Green schist (chlorite, quartz, biotite, plagioclase, epidote, actinolite, calcite and muscovite).
ZM 107	Calcareous schist (calcite, quartz, chlorite, biotite, plagioclase, epidote, actinolite and muscovite).
ZM 108	Green schist (chlorite, quartz, biotite, plagioclase, epidote, actinolite, calcite and muscovite).
ZM 109	Quartz vein.
ZM 110	Quartz vein.
ZM 111	Hornblende gneiss.
ZM 112	Phyllitic schist (biotite, chlorite, muscovite and quartz).
ZM 113	Quartz vein.
ZM 114	Quartz vein.
ZM 115	Marble.
ZM 116	Quartz vein.
ZM 117	Phyllitic schist.
ZM 118	Phyllitic schist (biotite over 50 %, muscovite, chlorite and quartz).

Appendix 4.1 (contd.)

Sample	Mineralogy
ZM 119	Marble.
ZM 120	Marble.
ZM 121	Quartz vein (containing arsenopyrite and pyrite grains).
ZM 122	Quartz vein.
ZM 123	Quartz vein (containing xenolith of schist).
ZM 124	Quartz vein.
ZM 125	Quartz vein (containing tourmaline grains).
ZM 126	Phyllitic schist.
ZM 127	Marble (calcite, quartz, muscovite, sphalerite, hydrozincite, galena and pyrite).
ZM 128	Marble (calcite, quartz, muscovite, sphalerite, hydrozincite, galena and pyrite).
ZM 129	Marble (calcite, quartz, muscovite, sphalerite, hydrozincite, galena and pyrite).
ZM 130	Marble (calcite, quartz, muscovite, sphalerite, hydrozincite, galena and pyrite).
ZM 131	Marble (calcite, quartz, muscovite, sphalerite, hydrozincite, galena and pyrite).
ZM 132	Phyllitic schist.
ZM 133	Phyllitic schist.
NMG 1	Leucogranite (plagioclase, quartz, orthoclase, garnet, tourmaline, biotite and muscovite).
NMG 2	Calc-silicate quartzite.
NMG 3	Calc-silicate quartzite.
NMG 4	Pegmatite (plagioclase and quartz).
NMG 5	Mica schist.

Appendix 4.2: Details of the analytical techniques used for microprobe analyses.

The analyses were performed through Jeol Superprobe model JXA-8600 with an on-line computer for ZAF corrections. Quantitative analyses were obtained using wavelength dispersive system under the following operating conditions: 15 kV (25 kV for the scheelite analyses) accessory voltage; 30 x 10^{-9} A probe current; 20 (2 x 10) seconds peak, 10 (2 x 5) seconds negative background and 10 (2 x 5) seconds positive background counting times. The diameter of the X-ray beam varied according to the type, nature and grain size of the analysed phase. Except plagioclase (15 μm) and garnet (10 μm), 5 μm diameter was used for most of the silicate and oxide phase.

The silicate phase and some oxides were analysed for major and minor oxide such as SiO_2, TiO_2, Al_2O_3, FeO (total), MnO, MgO, CaO, Na_2O, K_2O, Cr_2O_3 and NiO. Scheelite was analysed by a program consisting of CaO, WO_3, MoO_2, SnO_2, FeO (total), MnO, MgO, Y_2O_3, TiO_2, ZrO_2, Nb_2O_5, and Ta_2O_5. Sulphide were analysed for S, Fe, Zn, Pb, Cd, Ge, Ag and As.

The following standards were used during these microprobe analyses: wollastonite (natural for Si, and Ca); rutile (natural for Ti); jadeite (natural for Al and Na); magnetite (synthetic for Fe); Fe (pure synthetic for Fe in case of sulphide); rhodonite (natural for Mn); MgO (synthetic for Mg); microcline (natural for K); YF_3 (synthetic for Y). Pure synthetic metals were used for each of W, Mo, Sn, Nb, Ta, Cd, Ge, Ni, Co, Cr, Cu, Pb, Ag, Zr and As. Synthetic ZnS was used for the determination of both Zn and S. The accuracy of the ZAF correction is generally better than 2 %. A correction has been made to the ZrO_2 figures based on measurement of Zr in pure tungsten metal and 0.4 % ZrO_2 was deducted from each of the scheelite analyses. The minimum detection limits (MDL) (3 sigma) and degree of precision (2 sigma) for the minor oxides analysed within the scheelite are as follows:

Oxides	MDL %	Precision %
MoO_2	0.09	0.15
SnO_2	0.07	0.10
FeO	0.03	0.03
MnO	0.03	0.03
MgO	0.02	0.03
Y_2O_3	0.05	0.09
TiO_2	0.06	0.07
ZrO_2	0.10	0.19
Nb_2O_5	0.10	0.16
Ta_2O_5	0.06	0.07

The minimum detection limits for the oxides analysed within the silicates, albite (Alb), chlorite (Chl), biotite (Bio), muscovite (Musc), amphibole (Amp), garnet (Gt), sphene (Sph), epidote (Epi) and tourmaline (Tour) are as follows:

Oxides	Alb	Chl	Bio	Musc	Amp	Gt	Sph	Epi	Tour
SiO_2	0.02	0.02	0.03	0.02	0.02	0.03	0.03	0.03	0.02
TiO_2	0.04	0.05	0.04	0.05	0.05	0.06	0.06	0.06	0.04
Al_2O_3	0.02	0.02	0.02	0.02	0.02	0.02	0.02	0.02	0.02
Cr_2O_3	0.04	0.04	0.05	0.04	0.04	0.06	0.06	0.06	0.04
FeO	0.04	0.05	0.05	0.05	0.05	0.06	0.06	0.06	0.04
MnO	0.05	0.05	0.05	0.04	0.05	0.06	0.06	0.06	0.04
MgO	0.02	0.02	0.02	0.02	0.02	0.02	0.02	0.02	0.02
CaO	0.03	0.03	0.03	0.03	0.03	0.03	0.03	0.03	0.03
Na_2O	0.02	0.02	0.02	0.02	0.02	0.02	0.02	0.02	0.02
K_2O	0.02	0.02	0.02	0.02	0.02	0.03	0.03	0.03	0.02
NiO	0.05	0.05	0.05	0.05	0.05	0.07	0.07	0.07	0.05

Appendix 5.1: Analytical techniques used for geochemical analyses.

All the fresh rock samples were cleaned and crushed to small pieces (~ 1 mm across), by using a hardened steel fly-press. The crushed samples were powdered in a Podmore agate tema for about 10-20 minutes depending on the hardness of the samples. The powdered samples were stored individually in a sealed plastic bag and labelled.

X-ray Fluorescence Spectrometry

The major element analyses were performed on glass discs (fusion beads) and each bead was prepared as follows:

Roughly 5 gm of each of the powdered samples were dried out overnight at ~110^{o}C to remove absorbed moisture. The loss of ignition values (LOI) was determined by weighing individual dried sample, heated in a muffle furnace at 950^{o}C for 90 minutes, and reweighed after cooling in a dessicator. 1 gm of the ignited sample was mixed with 5 gm of flux (JM 100B, a eutectic mixture of lithium metaborate and lithium tetraborate). A weight loss of ignition of the flux was determined each day and was added to 5 gm of the flux, used for making a bead.

The mixture (flux + sample) was then fused in a platinum-gold crucible in a vertical tube furnace at 1100^{o}C for 20-25 minutes. During this period, the crucible was taken out periodically and swirled over a burner to eliminate the gas bubbles and ensure a thorough mixing of the melt. After the complete fusion, the melt was cast between aluminium discs, annealed and gradually cooled to room temperature. The bead, then was labelled and stored in a polythene bag.

The fusion beads were analysed for SiO_2, TiO_2, Al_2O_3, Fe_2O_3, MnO, MgO, CaO, Na_2O, K_2O and P_2O_5. The analyses were carried out through a Philips 1400 X-ray tube spectrometer and ARL 8420+ spectrometer, each equipped with a rhodium anode X-ray tube. Standard including AN-G, MRG-1, BE-N, Ga, GH, W-1, JA-1, BCR-1, BOB-1, NIM-G and AC-E were used alternatively with each batch of samples to monitor the precision and accuracy of the XRF technique.

The minor and trace element analyses of the sample were performed on powder pellets. The method used for the preparation of each pellet is as follows:

Powdered sample weighing 15 gm was mixed in a glass beaker with mount (10-20 drops) of Mowiol 88 (a solution of polyvinyl alcohol in a 1: 5 mix of methanol and distilled deionised water). This mixture was then placed in a small die and pressed into the shape of pellet by exerting a 15 ton hydraulic pressure. The pellet was allowed to dry overnight before labelling and storing in a plastic bag.

The powder pellets were run through a Philips Pw 1400 XRF spectrometer equipped with either a 3 kW rhodium anode tube or a tungsten anode tube. Each of the samples was analysed for the following set of elements: Ga, Sc, Co, Ni, Cr, V, Cu, Mo, Sn, W, As, Pb, Zn, Th, Ba, Rb, Sr, Nb, Y, Zr, La, Ce, Nd, F, Cl and S. A set of international and internal standards was run with each batch of samples to monitor the accuracy of the technique. It is observed during the course of this study that except for La, Ce and Nd the precision and accuracy of methods and instrument used are high for the other elements. The elements which are run by both XRF and INAA and also the analyses of international standard from different runs were found comparable to each other and close to their general agreed values. The minimum detection limits (MDL), the international standard run by XRF and the recommended values for theses standards are given below:

Oxides	**MDL**	**MRG-1***	**Recom.[1]**	**NIM-G***	**Recom.[2]**
SiO_2	0.01 %	40.02 %	39.12 %	76.17 %	75.7 %
TiO_2	0.001 %	3.79 %	3.77 %	0.1 %	0.09 %
Al_2O_3	0.005 %	8.36 %	8.47 %	12.14 %	12.08 %
Fe_2O_3 ◊	0.002 %	17.7 %	17.02 %	2.02 %	1.88 %
MnO	0.002 %	0.17 %	0.17 %	0.03 %	0.02 %
MgO	0.011 %	14.11 %	13.55 %	0.07 %	**0.06 %**
CaO	0.003 %	14.52 %	14.7 %	0.79 %	0.78 %
Na_2O	0.016 %	0.56 %	0.74 %	3.23 %	3.36 %
K_2O	0.002 %	0.17 %	0.18 %	4.98 %	4.99 %
P_2O_5	0.002 %	0.07 %	0.08 %	0.01 %	0.01 %
Elements	**(ppm)**	**(ppm)**	**(ppm)**	**(ppm)**	**(ppm)**
F	50	650	240	2960[a]	2840[a]
Cl	50	360	170	280[a]	78[a]
S	50	340	610	1.3 % [a]	1.77 % [a]
As	2	0.9	0.73	14.5	15
Ba	1.3	70	61	107	120
Rb	0.4	7	8.5	324	320
Sr	0.6	269	266	10	10
Th	1.3	< 1.3	0.93	49	51
Zr	0.6	109	108	300	300
Nb	0.5	22	20	61	53
Y	0.5	14	14	151	143

Sc	3.8	60	55	0.3	1
V	3.5	610	526	1.7	2
Cr	3	526	430	25	12
Co	2.4	91	87	6.6	4
Ni	1	184	193	12	8
Cu	2	126	134	12	12
Zn	2	197	191	67	50
Ga	1.8	19	17	27	27
Pb	2	7.4	10	38	40
W	2	0.2	0.3	5.9	---
Sn	2	2.6	**3.6**	5	4
Mo	2	2.2	0.87	2.7	3

◊ = Considered as total Iron; * = Reference sample analysed by XRF during this study; 1 and 2 = Recommended values for samples MRG-1 and NIM-G respectively, the underlines are proposed values whereas bold numbers are information values. a = reference sample (GRX-4).

Inductively Coupled Plasma Emission Spectrometry

The powdered samples were also analysed for the Be and Li values by the method of Inductively Coupled Plasma Emission Spectrometry (ICPES). The procedure used for the analysing these samples are as follows:

0.1 gm of each sample was weighed into a labelled PTFE test-tube and 2 ml of HNO_3 (70 %) added to each sample. After a gentle swirling, all the test-tubes were put in a heating block at 50°C and left overnight. Then 1 ml of $HClO_3$ (60 %) and 5 ml of HF (40 %) was added to each tube and mixed gently. This was followed by heating of the tubes in the block successively at 100°C for three hours, 140°C for three hours and 190°C overnight. After this, 1 ml of conc. HCl was added and the tubes were heated at 50°C in the heating block for 30 minutes. Each of the samples was mixed thoroughly with ml of deionised water using a "whirly mixer". All the tubes were left to allow the sediments to settle down and then decanted into 10 ml labelled vials.

The solutions were run through a Philips PV 8050 spectrometer linked to a PV 8490 source. To know about the possible contamination during the sample preparation process, 4 % blank samples out of the total samples, were run. The degree of precision and accuracy of the method was quantified by repeating 10 % of the analysed samples and 5 % of an internal standard. In order to minimise the interference effect on other elements, the samples containing high Ca content, were ten-times diluted. To monitor the effects of inter-element interferences, solutions of known concentrations were analysed with each

batch of samples. These estimates were later used to correct the data with the help of an "Excel Macro".

Keeping in view the effect of the partial dissolution, the accuracy of the machine is fairly good on the international reference materials with the approximate degree of precision as determined by multiple analyses on international reference materials and Arif (1994) is better than 10 % for the Li and Be. The detection limits for Li and Be are 11 ppm and 0.1 ppm respectively.

Instrumental Neutron Activation Analysis

About 70 samples, representing different lithologies (including mineralised and unmineralised calc-silicate quartzites and tourmalinites, psammites, leucogranites, marble and schists) were analysed for the following elements; Au, Ag, As, B, Ba, Br, Ca, Ce, Co, Cr, Cs, Eu, Fe, Gd, Hf, Hg, Ir, La, Lu, Mo, Na, Nd, Ni, Rb, Sb, Sc, Se, Sm, Sn, Sr, Ta, Th, Tb, U, W, Yb and Zn. Out of these elements, only REE, B, Ag, Cs, Hf, Hg, Sb, Ta, Th, U and W were included. Other elements are taken from XRF analyses whereas Li and Be from ICPES. The analyses were conducted through the Activation Laboratories in Ontario, Canada by the procedure described by Lindstrom and Anderson (1985). In this method 0.5 to 30 gm of sample is encapsulated in a polythene vial and is placed in a beam of thermalised neutrons. Samples are counted with a high purity Ge detector and loss free counting system for the Doppler prompt gamma at 477.6 KeV. Net peak areas are adjusted for Na interference. The minimum detection limits (MDL)of elements analysed by INAA are as follows:

Elements	MDL	Elements	MDL
B	2 ppm	Nd	5 ppm
Ag	5 ppm	Sm	0.1 ppm
Cs	1 ppm	Eu	0.2 ppm
Hf	1 ppm	Gd	1 ppm
Hg	1 ppm	Tb	0.5 ppm
Sb	0.1 ppm	Yb	0.2 ppm
Ta	0.5 ppm	Lu	0.05 ppm
Th	0.2 ppm		
U	0.5 ppm		
W	1 ppm		
La	0.5 ppm		
Ce	3 ppm		

Appendix 5.2: Major and trace element chemistry of the Miniki Gol leucogranite.

No	1	2	3	4	5	6	7	8	9	10
Sample	ZC20	ZC31	ZC38	ZC71	ZS 8	ZS 9	ZS 10	ZS 14	ZS 17	ZS 19C
SiO_2	77.55	75.94	75.27	75.36	72.92	70.16	74.43	n.a	76.76	75.00
TiO_2	0.07	0.00	0.19	0.05	0.18	0.46	0.04	n.a	0.03	0.02
Al_2O_3	13.76	15.97	14.17	14.62	14.76	15.55	15.42	n.a	14.82	14.54
Fe_2O_3	0.72	0.66	1.54	0.87	1.32	2.95	0.25	n.a	0.58	0.48
MnO	0.03	0.10	0.02	0.04	0.02	0.04	0.02	n.a	0.05	0.07
MgO	0.21	0.06	0.37	0.04	0.30	0.83	0.05	n.a	0.07	0.05
CaO	0.56	0.22	1.17	0.63	0.82	1.83	0.66	n.a	0.69	0.53
Na_2O	3.10	4.28	3.16	3.71	2.82	3.47	3.21	n.a	4.87	4.11
K_2O	4.44	2.25	3.32	4.24	6.07	4.70	6.01	n.a	2.55	4.04
P_2O_5	0.16	0.12	0.24	0.26	0.31	0.35	0.13	n.a	0.13	0.11
Total	100.59	99.62	99.47	99.81	99.51	100.36	100.22	n.a	100.55	98.95
ASI	1.70	2.37	1.85	1.70	1.52	1.55	1.56	n.a	1.83	1.68
Trace elements (ppm)										
B	17	15	n.a	n.a	n.a	n.a	15	n.a	n.a	n.a
F	460	170	880	430	900	1100	740	970	830	780
Cl	50	50	120	50	210	230	270	210	210	210
S	20	0.0	0.0	0.0	40	40	60	40	40	40
As	n.a	1.1	n.a	2.2	2.7	1.9	5.6	2.2	2.1	2.3
Li	99.1	26.8	258.3	383.9	35.6	106.2	24	115.2	82.5	105.3
Be	15	172.6	15.4	9.2	1.2	2.6	2	23.5	6.6	1.9
Cs	22	8	n.a	n.a	n.a	n.a	n.a	n.a	n.a	n.a
Ba	203.7	16	231.4	125.2	317	454.9	386.8	4	29.1	53.5
Rb	312.7	259.9	262.6	298.5	195.8	212.8	157.3	207.8	141	172
Sr	85.8	41.4	100.6	50	116.9	167.7	140.9	19.9	22.3	25.4
Th	2.4	0.9	n.a	n.a	n.a	n.a	n.a	n.a	n.a	n.a
U	3	5.7	n.a	n.a	n.a	n.a	n.a	n.a	n.a	n.a
Zr	38.8	11.2	103	34.1	68.8	185.1	15.3	32.1	36	33.1
Hf	2	2	n.a	n.a	n.a	n.a	n.a	n.a	n.a	n.a
Ta	4.4	19	n.a	n.a	n.a	n.a	n.a	n.a	n.a	n.a
Nb	15.7	19.4	13.1	19.4	6.6	15.7	2.8	25	12.2	4.7
Y	17.9	7.2	14.4	16.6	16.9	27.8	9.5	11.5	14.8	9
Sc	5.6	0.8	5.5	1.4	6.6	10.3	3.8	3.6	3.5	4.9
V	4.6	0.1	2	8.3	18.2	39.6	1.8	1.4	9.6	4.9
Cr	< 3.6	< 0.9	5.3	< 0.3	7.6	10.1	< 2.3	9.1	2.6	< 5.7
Co	0.4	0.0	2.3	0.3	0.1	8.2	< 2.4	< 1	< 3	< 2.5
Ni	< 4.3	< 1.4	0.3	10	4	5.7	3	0.7	2.2	2.2
Cu	< 0.1	< 3.1	< 1.8	< 1.6	0.0	2	< 2.5	< 4.4	< 2.8	< 1.8
Zn	22.8	9.6	67.1	40.7	36.3	59.7	< 4.1	11.7	9.8	1.3
Ga	16.6	20.4	22.5	17.5	13	16.6	10.6	23.6	16.6	15.2
Pb	44.4	17.9	35.3	38.3	62.2	48.3	77.5	28.3	26.6	36.6
W	< 1	2	n.a	n.a	n.a	n.a	n.a	n.a	n.a	n.a
Sn	37.7	67.3	23.6	33.2	1.25	2.32	2.42	6	3.16	1.9
Mo	1.6	1.7	< 0.6	< 1.4	< 1.1	< 0.7	< 1.1	< 1.4	< 1.2	< 0.9
Sb	0.5	< 0.1	n.a	n.a	n.a	n.a	n.a	n.a	n.a	n.a
La	10.	0.6	n.a	n.a	n.a	n.a	n.a	n.a	n.a	n.a
Ce	29	< 3	n.a	n.a	n.a	n.a	n.a	n.a	n.a	n.a
Nd	< 5	< 5	n.a	n.a	n.a	n.a	n.a	n.a	n.a	n.a
Sm	1.8	< 0.1	n.a	n.a	n.a	n.a	n.a	n.a	n.a	n.a
Eu	0.6	< 0.2	n.a	n.a	n.a	n.a	n.a	n.a	n.a	n.a
Gd	< 1	< 1	n.a	n.a	n.a	n.a	2	n.a	n.a	n.a
Tb	< 0.5	< 0.5	n.a	n.a	n.a	n.a	n.a	n.a	n.a	n.a
Yb	1	< 0.2	n.a	n.a	n.a	n.a	n.a	n.a	n.a	n.a
Lu	0.12	< 0.05	n.a	n.a	n.a	n.a	n.a	n.a	n.a	n.a

Appendix 5.2 (Contd.)

No.	11	12	13	14	15	16	17	18	19	20	21
Sample	**ZM 1**	**ZM 2**	**ZM 3**	**ZM 51**	**ZM 52**	**ZM 53**	**ZM 56**	**ZM 67**	**ZM 69**	**ZM 70**	**NMG 1**
SiO_2	74.71	75.85	74.70	73.12	73.20	80.23	79.01	72.56	74.29	74.78	75.74
TiO_2	0.08	0.06	0.08	0.10	0.10	0.08	0.02	0.09	0.07	0.08	0.03
Al_2O_3	15.46	15.06	14.29	15.14	15.23	12.62	15.05	15.07	14.84	14.76	14.71
Fe_2O_3	1.08	0.86	1.01	0.60	1.33	0.60	0.90	0.98	0.63	0.91	0.56
MnO	0.04	0.04	0.05	0.03	0.06	0.01	0.16	0.04	0.03	0.04	0.04
MgO	0.2	0.15	0.19	0.13	0.25	0.10	0.11	0.22	0.13	0.18	0.00
CaO	0.74	0.54	0.73	0.70	0.75	0.48	0.38	0.64	0.59	0.78	0.57
Na_2O	3.35	2.98	3.37	3.82	3.40	3.81	1.31	3.56	3.52	3.53	3.50
K_2O	3.348	4.23	4.08	4.82	4.53	1.89	3.15	4.39	4.63	4.58	4.20
P_2O_5	0.52	0.24	0.25	0.23	0.34	0.33	0.14	0.27	0.27	0.23	0.14
Total	99.53	100.00	98.74	98.70	99.18	100.15	100.21	97.83	99.01	99.85	99.47
ASI	2.08	1.94	1.75	1.62	1.75	2.04	3.11	1.75	1.70	1.66	1.78
Trace elements (ppm)											
B	21	10	12	8	16	18	23	12	16	12	16
F	1370	960	910	n.a	n.a	n.a	n.a	n.a	n.a	n.a	n.a
Cl	200	210	210	n.a	n.a	n.a	n.a	n.a	n.a	n.a	n.a
S	40	40	40	n.a	n.a	n.a	n.a	n.a	n.a	n.a	n.a
As	1.6	2.2	2.5	n.a	n.a	n.a	n.a	n.a	n.a	n.a	n.a
Li	283.7	453.1	154.1	78.8	334.6	58.7	71.7	215.1	98.9	183	190.1
Be	6.5	6.2	7	13.5	12.1	11.3	86.7	7.1	7.7	8.6	6.2
Cs	15	9	22	14	29	5	13	13	11	23	19
Ba	79.8	101.3	197.5	508.5	106	148.5	114.9	214.3	235.7	247.7	22.8
Rb	305.7	244.6	256.3	326.3	295.6	135.8	284.2	251	278.7	240.9	242.4
Sr	21.9	44.8	81.1	135.8	50.9	64.1	57.9	88.6	77.3	86.8	33.5
Th	5.4	2.6	3.4	3.2	3.4	4.4	0.6	3.5	3.7	4.1	1.3
U	46	3.2	7.8	5.6	4.4	12	1.2	5.1	13	4.2	12
Zr	42.2	38.8	40.7	32.1	42.8	35.5	2.9	34.4	36.1	34.1	15.1
Hf	2	2	2	2	3	2	<1	1	1	2	2
Ta	7.7	<0.5	3.4	3.1	4.4	<0.5	21	4.4	4.8	3.8	3.8
Nb	27.7	14.5	14.1	12.5	17.8	8.6	32.3	14.8	12.3	11.7	13.4
Y	24.7	22.4	21.9	12.1	17.5	10.9	<1.3	14	12.4	13.8	2.1
Sc	2.6	8.4	5.8	8.2	4.9	6.1	6.1	6.5	4.2	5.6	3
V	7	8.4	8.9	9.1	9	9.3	5.4	7.1	7.1	8.7	9.2
Cr	< 1.8	1.6	2.2	22.3	9.6	< 1.6	< 8	6.2	5.5	5.8	3.8
Co	< 0.4	0.4	< 0.2	< 1.8	0.4	0.0	< 0.1	0.6	< 0.7	< 0.1	< 0.4
Ni	3.7	5.3	2.6	1.1	< 0.1	< 0.5	0.6	1	0.1	< 0.2	< 1
Cu	< 1.4	< 1.7	< 2.8	0.7	< 1.2	1.4	< 3.3	0.1	0.9	< 1.6	< 2.5
Zn	35.2	24.9	30.7	17.4	46.3	17.3	10.8	26.9	20.4	29.5	16.2
Ga	20.6	16.3	15.8	16.4	19.1	12.3	24	17.7	15.8	14.5	17.2
Pb	20.3	36.4	43.6	52.9	36.2	9.8	20.5	38	34.9	49.1	38.6
W	4	3	< 1	4	< 1	5	3	9	10	4	9
Sn	22.7	5.23	5.78	22.4	33.1	21.8	76.6	26.4	31	18.2	18
Mo	< 1.2	< 0.6	<1	< 0.7	< 0.7	< 1.2	< 1.3	<0.8	< 1.1	< 1.1	< 0.9
Sb	0.3	0.3	0.5	< 0.1	0.6	< 0.1	0.3	0.4	0.4	0.6	0.2
La	11	8	10	5.5	8.2	7.7	0.7	6.5	7.4	10	2.6
Ce	19	11	20	15	17	16	< 3	11	16	22	7
Nd	6	< 5	15	7	< 5	< 5	< 5	< 5	6	7	< 5
Sm	2.3	1.7	2.1	1.5	2.2	1.8	0.1	1.6	1.5	2.5	0.3
Eu	0.3	0.4	0.7	0.6	0.2	0.4	0.3	0.4	0.4	0.6	0.2
Gd	3	1	< 1	2	2	1	< 1	2	< 1	1	2
Tb	0.9	< 0.5	< 0.5	0.6	< 0.5	< 0.5	< 0.5	< 0.5	< 0.5	0.6	< 0.5
Yb	0.9	1.1	1.3	1.2	1.6	0.9	< 0.2	1.2	1.1	1.3	0.5
Lu	0.13	0.16	0.17	0.16	0.22	0.1	< 0.05	0.17	0.13	0.16	0.1

ASI= Aluminium Saturation Index (Al_2O_3 / (CaO + Na_2O + K_2O).

Appendix 5.3: Major and trace element geochemical data of the schist from Miniki Gol and surrounding area.

No.	1	2	3	4	5	6	7	8	9	10	11	12	13	14
Sam.	**ZC2**	**ZC9**	**ZC11**	**ZC25**	**ZC36**	**ZC37**	**ZC44**	**ZC59**	**ZC63**	**ZC64**	**ZC68**	**ZS4**	**ZS5**	**ZS6**
SiO_2	58	59.7	63.37	53.74	n.a	64.2	67.38	70.84	67.48	63.57	n.a	n.a	n.a	n.a
TiO_2	1.02	1.2	0.65	0.96	n.a	1	0.84	0.9	0.87	0.95	n.a	n.a	n.a	n.a
Al_2O_3	21.44	21.7	15.4	23.52	n.a	17.24	14.81	14.1	18.01	17.95	n.a	n.a	n.a	n.a
Fe_2O_3	8.96	9.66	11.71	12.21	n.a	8.38	6.16	5.5	7	6.9	n.a	n.a	n.a	n.a
MnO	0.18	0.09	2.09	0.04	n.a	0.2	0.09	0.04	0.13	0.07	n.a	n.a	n.a	n.a
MgO	2.74	2.23	2.36	4.14	n.a	2.37	1.45	1.92	1.71	2.64	n.a	n.a	n.a	n.a
CaO	2.1	1.33	3.1	0.95	n.a	2.15	6.5	2.07	1.01	2.54	n.a	n.a	n.a	n.a
Na_2O	2.58	2.07	2.09	1.01	n.a	1.21	1.51	2.26	0.97	1.48	n.a	n.a	n.a	n.a
K_2O	2.82	3.2	1.17	3.68	n.a	3.07	1	2.94	3.37	3.47	n.a	n.a	n.a	n.a
P_2O_5	0.2	0.3	0.15	0.18	n.a	0.18	0.1	0.17	0.11	0.15	n.a	n.a	n.a	n.a
Total	100.05	101.43	102.08	100.45	n.a	100.02	99.86	100.75	100.68	99.8	n.a	n.a	n.a	n.a
Trace elements in ppm														
B	n.a	47	n.a	n.a	n.a	n.a	n.a	n.a	n.a	n.a	n.a	n.a	n.a	n.a
F	n.a	n.a	960	n.a	820	910	n.a	n.a	910	840	840	n.a	n.a	n.a
Cl	n.a	n.a	60	n.a	140	140	n.a	n.a	60	100	60	n.a	n.a	n.a
S	n.a	n.a	0	n.a	400	60	n.a	n.a	60	10	0	n.a	n.a	n.a
Li	188.8	299.4	64.2	160.5	112.8	97.1	135.4	27.5	73.5	61.9	165.4	30.5	33.2	32.1
Be	4.2	3.8	5.7	3	2.8	3.5	3.8	<1.1	3.7	4.1	5.4	1.5	1.7	1.8
Cs	n.a	9	n.a	n.a	n.a	n.a	n.a	n.a	n.a	n.a	n.a	n.a	n.a	n.a
Ba	448.2	680	166.6	475.4	263.5	336.1	119.3	438.7	483.5	566.5	597.3	595.3	485.8	427.3
Rb	206.1	173.2	122	190.4	135.2	145.6	113.8	126.5	186.1	169.4	175.8	104.5	98.8	107.9
Sr	428.7	346.2	238.9	161.4	240.1	110.3	206.5	125.7	159.5	299.8	468.7	119.1	79.6	82.6
Th	21	22.4	19.3	26.2	26.7	14.6	17	13.8	18	17.2	21.3	10	9.1	5.6
U	n.a	4.2	n.a	n.a	n.a	n.a	n.a	n.a	n.a	n.a	n.a	n.a	n.a	n.a
Zr	151.3	207.8	111.4	144	465.6	227.9	277.6	325.1	193.3	183.7	113.6	157.2	251.4	199.6
Hf	n.a	8	n.a	n.a	n.a	n.a	n.a	n.a	n.a	n.a	n.a	n.a	n.a	n.a
Ta	n.a	2	n.a	n.a	n.a	n.a	n.a	n.a	n.a	n.a	n.a	n.a	n.a	n.a
Nb	20.6	23.2	14.1	22.7	19.7	19.6	16.6	21.9	20	20.2	23.6	6.9	10.8	7.6
Y	39.4	46	30.8	41.4	49.6	35.3	44.6	26.9	35.1	33.5	37.7	29.6	30.7	28.4
Sc	17.3	16.7	13.3	17.7	9.7	10.5	15.6	11.8	14.1	15.9	19.9	13.3	13.8	12.9
V	131.6	153.7	85.2	122.1	89.1	148.7	77.4	131.5	91.7	121.1	134	87.1	85.1	75.4
Cr	136.8	138	107.8	132.1	79.4	124.4	81.4	82.2	96.8	112.6	145.9	57	41	41.4
Co	23.7	25	15.3	33.8	15.7	25.1	17.2	19.5	17	20.6	26.9	11.6	10.5	10.1
Ni	34.9	48.8	47.2	71.4	56.9	60	49.3	40.4	20.3	65.8	64.1	24.6	19.2	21.6
Cu	18.7	26.5	11.8	12.8	24.7	17.1	20.7	18.4	12.5	10.1	8.5	31.7	1.2	11
Zn	138.5	107.3	100.6	50.5	60.5	256.9	80.9	123.3	93.7	96.5	104.4	62.3	55.4	71.2
Ga	26.1	26.7	18.1	33.7	21.7	25.2	21.2	24.5	24.2	23.3	32	17.4	18.1	16.9
Pb	39.1	27.8	27.7	25.1	22.5	25.8	17.3	21.4	36.4	22.8	37.1	10.4	6.7	9.6
W	1.3	0.6	1.6	<0.2	5.5	3.7	3.8	2.2	2.5	2.6	3.3	1.6	1	1.6
Sn	3.5	4.4	1.3	5.2	5.9	7.4	12.1	3.7	2.34	2.8	2.8	1.4	2.2	1.8
Mo	2.6	0.8	1.7	2.2	2.4	2.8	0.7	3.4	<0.1	0.1	<0.4	<0.1	0.2	<0.5
Sb	n.a	<0.1	n.a	n.a	n.a	n.a	n.a	n.a	n.a	n.a	n.a	n.a	n.a	n.a
La	n.a	88	n.a	n.a	n.a	n.a	n.a	n.a	n.a	n.a	n.a	n.a	n.a	n.a
Ce	n.a	180	n.a	n.a	n.a	n.a	n.a	n.a	n.a	n.a	n.a	n.a	n.a	n.a
Nd	n.a	58	n.a	n.a	n.a	n.a	n.a	n.a	n.a	n.a	n.a	n.a	n.a	n.a
Sm	n.a	14	n.a	n.a	n.a	n.a	n.a	n.a	n.a	n.a	n.a	n.a	n.a	n.a
Eu	n.a	2.8	n.a	n.a	n.a	n.a	n.a	n.a	n.a	n.a	n.a	n.a	n.a	n.a
Gd	n.a	11	n.a	n.a	n.a	n.a	n.a	n.a	n.a	n.a	n.a	n.a	n.a	n.a
Tb	n.a	2	n.a	n.a	n.a	n.a	n.a	n.a	n.a	n.a	n.a	n.a	n.a	n.a
Yb	n.a	6.3	n.a	n.a	n.a	n.a	n.a	n.a	n.a	n.a	n.a	n.a	n.a	n.a
Lu	n.a	1	n.a	n.a	n.a	n.a	n.a	n.a	n.a	n.a	n.a	n.a	n.a	n.a

Appendix 5.3: (Contd.)

No.	15	16	17	18	19	20	21	22	23	24	25	26	27	28
Sam.	**ZS11**	**ZS19A**	**ZM5**	**ZM6**	**ZM7**	**ZM8**	**ZM9**	**ZM10**	**ZM11**	**ZM13**	**ZM16**	**ZM18**	**ZM19**	**ZM20**
SiO_2	n.a	61.22	n.a	n.a	n.a	n.a	n.a	47.27	n.a	n.a	72.13	n.a	n.a	n.a
TiO_2	n.a	0.84	n.a	n.a	n.a	n.a	n.a	1.23	n.a	n.a	0.42	n.a	n.a	n.a
Al_2O_3	n.a	19.97	n.a	n.a	n.a	n.a	n.a	29.43	n.a	n.a	13.71	n.a	n.a	n.a
Fe_2O_3	n.a	6.57	n.a	n.a	n.a	n.a	n.a	11.5	n.a	n.a	5.18	n.a	n.a	n.a
MnO	n.a	0.092	n.a	n.a	n.a	n.a	n.a	0.116	n.a	n.a	0.05	n.a	n.a	n.a
MgO	n.a	1.63	n.a	n.a	n.a	n.a	n.a	2.61	n.a	n.a	2.47	n.a	n.a	n.a
CaO	n.a	0.95	n.a	n.a	n.a	n.a	n.a	1.3	n.a	n.a	4.16	n.a	n.a	n.a
Na_2O	n.a	2.93	n.a	n.a	n.a	n.a	n.a	0.99	n.a	n.a	1.05	n.a	n.a	n.a
K_2O	n.a	5.521	n.a	n.a	n.a	n.a	n.a	5.091	n.a	n.a	1.638	n.a	n.a	n.a
P_2O_5	n.a	0.211	n.a	n.a	n.a	n.a	n.a	0.301	n.a	n.a	0.2	n.a	n.a	n.a
Total	n.a	99.94	n.a	n.a	n.a	n.a	n.a	99.82	n.a	n.a	101.01	n.a	n.a	n.a
Trace elements in ppm														
B	184	17	n.a	n.a	n.a	n.a	n.a	n.a	n.a	n.a	35	n.a	n.a	67
F	1340	n.a	1310	1500	1130	1120	950	1590	1520	1310	3210	1750	1320	1000
Cl	220	n.a	210	210	220	210	220	220	210	230	90	60	120	50
S	130	n.a	120	170	650	110	180	100	40	60	1390	170	0	0
Li	274.7	335.4	281.9	200.3	222.7	224.7	258.3	391.1	205.7	282.8	266.6	353.9	368.2	250.9
Be	4.1	6.9	2	3.3	3.3	4.7	3.5	9.5	3	3.2	20.9	5.5	7.1	3.7
Cs	n.a	n.a	n.a	n.a	n.a	n.a	n.a	n.a	n.a	n.a	83	n.a	n.a	29
Ba	472.2	949.7	816.3	761.5	198.8	228	209.5	795.8	903.6	372.6	742.8	527.3	571.8	777.1
Rb	152.8	420.7	216.7	203.6	127.2	131	64.8	254.5	235.2	215.6	203	302.5	297.7	218.1
Sr	378.5	155.4	148.4	242.5	285.5	330.7	451.5	394.5	279.4	229.7	227.2	269.8	277.2	189.1
Th	25.7	13.7	22.2	22.6	18.6	18	29.8	28.2	25	15.3	4.8	22	23	22.5
U	n.a	n.a	n.a	n.a	n.a	n.a	n.a	n.a	n.a	n.a	1.8	n.a	n.a	6.4
Zr	184.9	201.9	228.1	128	290.2	199.7	451	149.6	136.1	178	109.8	192.5	184.9	180.8
Hf	n.a	n.a	n.a	n.a	n.a	n.a	n.a	n.a	n.a	n.a	3	n.a	n.a	7
Ta	n.a	n.a	n.a	n.a	n.a	n.a	n.a	n.a	n.a	n.a	2.5	n.a	n.a	3.1
Nb	20.3	31.1	21.3	19.7	17.4	17.7	18.7	23.5	19.6	16.2	8.9	18.5	19.8	23.5
Y	38.6	30.3	43.5	32.5	38.9	35.6	45.2	32.6	33.9	28.2	19.9	36.6	35.5	52.1
Sc	18.5	9.4	18	18.1	13	21.2	22.1	19	17	15.4	16.9	16.8	20.4	21.5
V	141.1	81.6	106.7	128.6	73.6	90.3	110.3	138.6	128.5	75.1	87.6	94.8	105.6	123.5
Cr	150	88.1	116.1	137.7	75.8	94.5	128.7	173	141.5	90.6	31.3	116.5	124.3	147.7
Co	25.9	17	12.3	18.5	17.4	19	27.5	29.2	24.3	13.8	13.5	15.5	22.2	27.6
Ni	55.6	36.8	18.4	18.6	54.9	31.3	45	38.4	54.8	28.1	54.5	21.8	36	59.2
Cu	28.9	3.9	15.2	20.9	29.8	36.5	12.2	23	22.9	21.3	24.4	7.8	16.3	39.1
Zn	110.1	158.1	87.5	103.9	79.3	93.8	165.3	162.7	119.2	72.9	140.8	89.3	102.8	116.4
Ga	24.4	26.3	27.9	31	20.1	20.1	27.5	39.4	31.1	17.2	11.3	23.2	24	30.4
Pb	60.1	24.9	25.3	31.7	33.7	37.2	35.8	41.3	38.7	28.8	19	38.2	41.3	32.4
W	1.4	6.9	4.6	2.9	1.3	1	2.9	4.9	4	3.5	8	2.7	3.6	7
Sn	2.9	10.4	2.7	2.8	2.02	1.8	2.14	3.6	3.54	3.9	10.6	6.10	8.7	2.84
Mo	0.1	0	0	0.5	0.4	<0.1	1.4	0.6	0.6	0.5	0.2	0.2	0.3	0.6
Sb	n.a	n.a	n.a	n.a	n.a	n.a	n.a	n.a	n.a	n.a	2.9	n.a	n.a	2.6
La	n.a	n.a	n.a	n.a	n.a	n.a	n.a	n.a	n.a	n.a	17	n.a	n.a	92
Ce	n.a	n.a	n.a	n.a	n.a	n.a	n.a	n.a	n.a	n.a	42	n.a	n.a	170
Nd	n.a	n.a	n.a	n.a	n.a	n.a	n.a	n.a	n.a	n.a	14	n.a	n.a	59
Sm	n.a	n.a	n.a	n.a	n.a	n.a	n.a	n.a	n.a	n.a	2.9	n.a	n.a	13
Eu	n.a	n.a	n.a	n.a	n.a	n.a	n.a	n.a	n.a	n.a	0.8	n.a	n.a	2.7
Gd	5	2	n.a	n.a	n.a	n.a	n.a	n.a	n.a	n.a	2	n.a	n.a	10
Tb	n.a	n.a	n.a	n.a	n.a	n.a	n.a	n.a	n.a	n.a	<0.5	n.a	n.a	2.4
Yb	n.a	n.a	n.a	n.a	n.a	n.a	n.a	n.a	n.a	n.a	1.9	n.a	n.a	5.7
Lu	n.a	n.a	n.a	n.a	n.a	n.a	n.a	n.a	n.a	n.a	0.3	n.a	n.a	0.9

Appendix 5.3: (Contd.)

No.	29	30	31	32	33	34	35	36	37	38	39	40	41	42	43
Sam.	ZM21	ZM23	ZM26	ZM27	ZM30	ZM34	ZM35	ZM36	ZM39	ZM42	ZM48	ZM55	ZM57	ZM59	ZM61
SiO_2	n.a	n.a	57.28	49.83	53.57	n.a	n.a	n.a	n.a	n.a	n.a	n.a	n.a	66.06	n.a
TiO_2	n.a	n.a	0.98	1.07	1.07	n.a	n.a	n.a	n.a	n.a	n.a	n.a	n.a	0.82	n.a
Al_2O_3	n.a	n.a	22.56	26.6	24.16	n.a	n.a	n.a	n.a	n.a	n.a	n.a	n.a	16.86	n.a
Fe_2O_3	n.a	n.a	9.51	9.44	7.45	n.a	n.a	n.a	n.a	n.a	n.a	n.a	n.a	6.75	n.a
MnO	n.a	n.a	0.275	0.2	0.481	n.a	n.a	n.a	n.a	n.a	n.a	n.a	n.a	0.16	n.a
MgO	n.a	n.a	1.88	2.55	3.18	n.a	n.a	n.a	n.a	n.a	n.a	n.a	n.a	1.54	n.a
CaO	n.a	n.a	0.6	1.48	2.48	n.a	n.a	n.a	n.a	n.a	n.a	n.a	n.a	5.63	n.a
Na_2O	n.a	n.a	0.9	2.54	4.34	n.a	n.a	n.a	n.a	n.a	n.a	n.a	n.a	2.19	n.a
K_2O	n.a	n.a	4.55	5.457	1.803	n.a	n.a	n.a	n.a	n.a	n.a	n.a	n.a	0.587	n.a
P_2O_5	n.a	n.a	0.129	0.142	0.291	n.a	n.a	n.a	n.a	n.a	n.a	n.a	n.a	0.107	n.a
Total	n.a	n.a	98.67	99.3	98.81	n.a	n.a	n.a	n.a	n.a	n.a	n.a	n.a	100.71	n.a
Trace elements in ppm															
B	n.a	100	n.a	n.a	n.a	n.a	n.a	n.a	n.a	n.a	n.a	n.a	n.a	n.a	n.a
F	960	960	1010	1570	710	1090	630	860	n.a	550	270	n.a	n.a	n.a	n.a
Cl	60	40	50	60	40	60	60	50	n.a	50	60	n.a	n.a	n.a	n.a
S	0	0	0	50	10	20	0	50	n.a	0	0	n.a	n.a	n.a	n.a
Li	193.5	180.8	179.3	469	205	295.6	108.2	130.1	344.3	80.8	41.9	171.1	111.2	95.1	174.8
Be	2.7	3	3.4	8	4.8	<4.5	3.7	2.7	4.6	2	1	4.3	7.6	2.2	3.2
Cs	n.a	11	n.a	n.a	n.a	n.a	n.a	n.a	n.a	n.a	n.a	n.a	n.a	n.a	n.a
Ba	509.5	564.8	575.4	492.6	170.9	286.1	392.7	607	611.3	529.3	239.6	479.4	55.1	190.2	746.1
Rb	173.3	163.9	177.1	417.6	69.8	288.8	135.1	208.5	288.4	123.7	67.8	204.6	14	92.7	230.2
Sr	180.6	212.4	193.3	402	712.8	275.2	216.6	155.3	359.5	170.5	40.8	143.5	625.3	199.7	193.1
Th	20.4	23.9	22	31.6	22.7	20.6	18.9	22	24.3	8.4	9.7	20.6	23.6	16.7	25.9
U	n.a	6.3	n.a	n.a	n.a	n.a	n.a	n.a	n.a	n.a	n.a	n.a	n.a	n.a	n.a
Zr	164.8	198.8	129.3	168.6	164.3	185.9	135.1	162.7	147.2	238	658	144.5	267.3	233.9	180.8
Hf	n.a	7	n.a	n.a	n.a	n.a	n.a	n.a	n.a	n.a	n.a	n.a	n.a	n.a	n.a
Ta	n.a	-0.5	n.a	n.a	n.a	n.a	n.a	n.a	n.a	n.a	n.a	n.a	n.a	n.a	n.a
Nb	20.7	20.3	19.9	24.9	19.8	19.2	16.7	19.5	18.4	13.4	15.2	17.5	19.5	17.4	21
Y	36	33.2	39.5	48.3	57.7	30.5	26.2	32.1	33.2	29.6	29.3	29.3	38.3	35.2	32.3
Sc	14.3	14.5	18	21.2	22.7	20.8	18.8	20.3	16.9	17.1	11.5	16.8	23.3	16.7	15.4
V	102.2	106.3	122.5	138.6	105.6	81.9	95.7	107.3	113.5	109.6	53.3	103.1	107.2	92.6	120.8
Cr	114.9	114.8	127.3	152.6	140.8	101.9	124.3	111.3	122.6	94.7	60.5	136.1	127.3	90.6	143.2
Co	30.6	19.7	41.3	34	15.2	21.6	12	20.2	18.8	13.5	9.6	20.9	19.6	15.5	21.4
Ni	74.4	35.9	71	42.2	30.3	25.9	12.4	15.6	13	14.1	8.5	21.9	19.3	28.1	33.4
Cu	74.2	24.8	n.a	n.a	3.2	30.6	3.6	52.4	34.1	17.3	26.8	23.1	21	32.4	21.6
Zn	129.1	93.8	120	99.7	60.5	91.2	63.3	70.5	90.3	64.6	67.7	103.5	99.2	80.1	90.1
Ga	26.3	26.9	28.5	32.8	27.5	22.7	21.8	29.2	29.2	19.7	11.9	30.1	22.4	22.8	32.5
Pb	32.9	37.2	29	47.8	42.9	50	40.1	27.2	40.3	16.5	18.2	29.2	55.6	22.1	34.8
W	2.9	5	5.5	6.5	4.9	<1.2	<0.2	1.5	0.4	<0.5	1.2	<1.1	<1.2	<2.5	1.7
Sn	3.6	3.6	2.7	10.4	30.1	5.05	4.8	8	16.5	5.3	4.7	5.8	2.1	2.4	5.7
Mo	0.3	0.1	<0.4	0.4	0.7	0.2	0.1	0.2	0.3	0.9	1.2	0.4	0.6	0.6	0.8
Sb	n.a	2.2	n.a	n.a	n.a	n.a	n.a	n.a	n.a	n.a	n.a	n.a	n.a	n.a	n.a
La	n.a	64	n.a	n.a	n.a	n.a	n.a	n.a	n.a	n.a	n.a	n.a	n.a	n.a	n.a
Ce	n.a	120	n.a	n.a	n.a	n.a	n.a	n.a	n.a	n.a	n.a	n.a	n.a	n.a	n.a
Nd	n.a	42	n.a	n.a	n.a	n.a	n.a	n.a	n.a	n.a	n.a	n.a	n.a	n.a	n.a
Sm	n.a	8.1	n.a	n.a	n.a	n.a	n.a	n.a	n.a	n.a	n.a	n.a	n.a	n.a	n.a
Eu	n.a	1.6	n.a	n.a	n.a	n.a	n.a	n.a	n.a	n.a	n.a	n.a	n.a	n.a	n.a
Gd	n.a	3	n.a	n.a	n.a	n.a	n.a	n.a	n.a	n.a	n.a	n.a	n.a	n.a	n.a
Tb	n.a	<0.5	n.a	n.a	n.a	n.a	n.a	n.a	n.a	n.a	n.a	n.a	n.a	n.a	n.a
Yb	n.a	4.3	n.a	n.a	n.a	n.a	n.a	n.a	n.a	n.a	n.a	n.a	n.a	n.a	n.a
Lu	n.a	0.6	n.a	n.a	n.a	n.a	n.a	n.a	n.a	n.a	n.a	n.a	n.a	n.a	n.a

Appendix 5.4: Major, minor and trace element chemistry of the Miniki Gol calc-silicate quartzite (1-44) and psammite (45-63).

No.	1	2	3	4	5	6	7	8	9	10	11	12	13
Sample	**ZC4**	**ZC5**	**ZC7**	**ZC8**	**ZC17**	**ZC27**	**ZC30**	**ZC32**	**ZC33**	**ZC34**	**ZC35**	**ZC41**	**ZC42**
SiO_2	92.2	n.a	n.a	n.a	68.19	69.24	91.75	71.8	n.a	n.a	73.36	64.56	n.a
TiO_2	0.24	n.a	n.a	n.a	0.67	0.81	0.27	0.75	n.a	n.a	0.67	0.58	n.a
Al_2O_3	3.59	n.a	n.a	n.a	15.71	14	3.52	11.2	n.a	n.a	10.92	13.56	n.a
Fe_2O_3	0.9	n.a	n.a	n.a	5	6.08	0.93	4.06	n.a	n.a	3.78	3.82	n.a
MnO	0.5	n.a	n.a	n.a	0.245	0.07	0.05	0.1	n.a	n.a	0.12	0.09	n.a
MgO	0.27	n.a	n.a	n.a	1.07	1.7	0.3	1.3	n.a	n.a	1.18	0.86	n.a
CaO	3.33	n.a	n.a	n.a	6.02	6.25	3.51	9.5	n.a	n.a	9.04	13.29	n.a
Na_2O	0.03	n.a	n.a	n.a	1.62	0.89	0.21	1.28	n.a	n.a	0.35	0.12	n.a
K_2O	0.13	n.a	n.a	n.a	0.498	1.63	0	0.18	n.a	n.a	0.22	0.11	n.a
P_2O_5	0.06	n.a	n.a	n.a	0.13	0.09	0.07	0.11	n.a	n.a	0.1	0.15	n.a
Total	100.8	n.a	n.a	n.a	99.14	100.79	100.64	100.28	n.a	n.a	99.76	97.18	n.a
Trace elements in ppm													
B	n.a	6	4	n.a	4	6	n.a	n.a	n.a	n.a	n.a	3	n.a
F	n.a	n.a	n.a	n.a	510	900	130	460	770	670	430	490	590
Cl	n.a	n.a	n.a	n.a	110	70	50	60	80	60	60	50	40
S	n.a	n.a	n.a	n.a	130	550	0	20	40	0	0	0	0
As	n.a	n.a	2.2	n.a	n.a	n.a	n.a	n.a	n.a	n.a	n.a	n.a	n.a
Li	5.2	164	12.3	31.9	92.7	135.1	9.3	19.1	94.5	75	24.9	13.2	11.2
Be	0.9	3.1	1.5	2.2	3.4	3.7	0.8	1.9	3	2.8	2.1	1.8	2.4
Cs	n.a	11	7	n.a	8	11	n.a	n.a	n.a	n.a	2	<1	n.a
Ba	8.2	452.1	94.9	186.3	126.9	343.3	6.7	33.2	351.5	167.6	32.8	17.2	18.8
Rb	n.a	101	48.3	50.3	57.7	129.3	n.a	8.9	93.9	68.7	12.5	10.6	n.a
Sr	118	242.2	135.6	199.8	180.2	279.5	128.2	299.7	296.1	289.9	225.6	277	370.8
Th	4.7	17	14	11.5	16	24	6.9	17	17.5	15.1	19	17	8.7
U	n.a	5.3	4	n.a	3.8	5.2	n.a	n.a	n.a	n.a	3.6	3.3	n.a
Zr	423.8	279.7	306.5	316.3	269.2	261.3	480.6	322.5	314	315.9	369.3	244.8	243.9
Hf	n.a	9	n.a	n.a	9	8	n.a	n.a	n.a	n.a	6	8	n.a
Ta	n.a	<0.5	n.a	n.a	<0.5	2	n.a	n.a	n.a	n.a	1.4	<0.5	n.a
Nb	6.9	13.3	6.1	9.8	18.5	17.8	7.2	16.4	17	18.2	16.3	16.3	12.1
Y	13.4	23.8	14.6	28	54.1	43.9	13.8	37.7	38.5	47.6	41.1	35.4	31.7
Sc	<1.7	5.3	4.8	6.1	7.9	16.8	<0.2	12.3	10.8	10	12.5	10.8	6.9
V	18.9	55.1	18.5	38.8	81.6	74.9	16.2	51.1	67.2	65.6	45.6	54.8	62.2
Cr	6.9	51.2	24.1	33.2	63.2	78.5	2.9	55.4	65.3	62.2	48	46.4	27.2
Co	<0.8	8.9	1.8	10.5	18.8	21.7	2.2	12.4	10.5	13.8	13.2	8.1	9.7
Ni	6.5	19	7.3	25.3	89.2	74	2.8	26	25.7	59.4	44.1	11.8	8.4
Cu	<1.1	4.9	13.2	15.4	46.8	35.7	<2.2	7.3	10.3	9	3.4	4.8	4.5
Zn	8.3	47	6.7	29.3	73.7	93.3	8	48.1	54.5	66.8	53.3	24.1	36.6
Hg	n.a	< 1	n.a	n.a	< 1	< 1	n.a	n.a	n.a	n.a	< 1	< 1	n.a
Ag	n.a	< 5	n.a	n.a	< 5	< 5	n.a	n.a	n.a	n.a	< 5	< 5	n.a
Ga	7.4	12	3.8	9.3	38.9	18.4	12.4	17.5	22.4	16.7	17.6	36.4	34
Pb	13.4	27.8	14.8	12.2	21.6	27.8	2	19.2	24.8	18.6	17.8	22	25.2
W	<1.6	11	0.9	193.4	3525.5	11	0.6	2.6	1.7	1.5	37.4	933.4	0.7
Sn	16.6	5.9	<1.4	1.6	34.1	4	7	15.8	9.5	9.9	14.9	30.7	212.3
Mo	1.5	2	0	2.1	0.8	1.8	3	0.5	0.6	0.5	3.3	<0.1	0.1
Sb	n.a	0.3	n.a	n.a	0.7	0.3	n.a	n.a	n.a	n.a	<0.1	0.2	n.a
La	n.a	36	n.a	n.a	56	54	n.a	n.a	n.a	n.a	45	39	n.a
Ce	n.a	83	n.a	n.a	100	100	n.a	n.a	n.a	n.a	92	84	n.a
Nd	n.a	33	n.a	n.a	40	39	n.a	n.a	n.a	n.a	35	41	n.a
Sm	n.a	5.2	n.a	n.a	9.7	7.8	n.a	n.a	n.a	n.a	6.9	7.3	n.a
Eu	n.a	1.5	n.a	n.a	2.5	1.8	n.a	n.a	n.a	n.a	1.7	1.9	n.a
Gd	n.a	5	n.a	n.a	7	6	n.a	n.a	n.a	n.a	8	4	n.a
Tb	n.a	<0.5	n.a	n.a	3.5	<0.5	n.a	n.a	n.a	n.a	1.3	1.8	n.a
Yb	n.a	2.3	n.a	n.a	7	4.2	n.a	n.a	n.a	n.a	4.4	4.7	n.a
Lu	n.a	0.4	n.a	n.a	1	0.7	n.a	n.a	n.a	n.a	0.6	0.7	n.a

Appendix 5.4: (Contd.)

No.	14	15	16	17	18	19	20	21	22	23	24	25	26
Sample	**ZC43**	**ZC45**	**ZC49**	**ZC50**	**ZC51**	**ZC65**	**ZC65A**	**ZC66**	**ZC67**	**ZC67A**	**ZC70**	**ZS13**	**ZS15**
SiO_2	64.05	69.03	68.11	n.a	66.51	68	76.6	73.36	66.48	60.29	n.a	n.a	n.a
TiO_2	0.48	0.73	0.66	n.a	0.69	0.77	1.3	0.67	0.41	0.45	n.a	n.a	n.a
Al_2O_3	15.49	12.3	12.5	n.a	16.2	12.72	6.63	10.35	12.94	17.08	n.a	n.a	n.a
Fe_2O_3	2.83	4.9	3.6	n.a	4.08	2.67	2.89	4.36	4.51	4.44	n.a	n.a	n.a
MnO	0.1	0.1	0.1	n.a	0.104	0.072	0.07	0.07	0.09	0.097	n.a	n.a	n.a
MgO	0.59	1.31	0.94	n.a	0.74	0.32	0.92	0.96	0.9	0.47	n.a	n.a	n.a
CaO	14.27	7.88	12.45	n.a	12.33	10.95	8.34	9.4	12.29	15.27	n.a	n.a	n.a
Na_2O	0.15	0.42	0.32	n.a	0.13	0.26	0.05	0.22	0.27	0.19	n.a	n.a	n.a
K_2O	0	1.2	0.03	n.a	0.426	0.141	0.02	0.22	0.08	0.069	n.a	n.a	n.a
P_2O_5	0.09	0.11	0.1	n.a	0.164	0.988	0.67	0.35	0.67	1.18	n.a	n.a	n.a
Total	98.06	98	98.9	n.a	101.36	96.89	97.5	100	98.7	99.54	n.a	n.a	n.a
Trace elements in ppm													
B	3	n.a	n.a	n.a	n.a	n.a	7	4	n.a	n.a	3	n.a	n.a
F	550	n.a	500	n.a	810	960	1330	800	1160	1430	580	n.a	960
Cl	50	n.a	30	n.a	50	50	50	80	80	60	40	n.a	220
S	0	n.a	0	n.a	0	90	0	280	0	0	0	n.a	60
As	n.a	n.a	0.8	n.a	n.a	n.a	1	2.5	1.6	1.7	n.a	0.8	1.6
Li	12.2	111.9	9.9	25.6	49.5	22.9	11.7	30.9	32	24.4	28	32.6	48.9
Be	12.6	3.2	1.5	1.5	2.3	3.1	2.7	3.5	3.1	2.5	3	0.7	2
Cs	<1	n.a	1	n.a	n.a	2	<1	2	2	n.a	2	n.a	n.a
Ba	28.8	246.7	20	38.6	176.6	49.6	13.4	43.8	23.2	25	31.2	132.1	114.3
Rb	n.a	94.9	0.1	25.6	37.1	13.3	n.a	14.9	6.4	4.8	0.9	39.2	24.1
Sr	227.8	278.5	243.2	256.4	291.8	232.7	299.4	210.8	297.5	328.6	228.8	48.7	270.3
Th	17	12.3	19	9.9	15	45	81	29	20	10.8	8.2	5.3	23
U	2.7	n.a	4.8	n.a	n.a	12	17	8.2	7.8	n.a	5.9	n.a	n.a
Zr	264.3	311.3	294.5	339.8	349.8	664.6	1567.6	401.3	364.5	190.5	384.1	220.4	427.3
Hf	9	n.a	10	n.a	n.a	21	46	15	12	n.a	13	n.a	n.a
Ta	1	n.a	<0.5	n.a	n.a	1	2	1.7	1.7	n.a	0.7	n.a	n.a
Nb	15.2	15.5	15.7	20.1	16.2	17.6	24.6	19.3	14.1	13.4	6.1	8.4	15.5
Y	31.6	38.4	35.3	36.6	44.3	41.7	75.7	43.1	33.1	26.3	14.6	20.3	38.1
Sc	10.2	10.1	10.2	11.2	10.4	7.2	2.5	13.8	10.4	19.4	0.2	6.7	15.2
V	46.6	66.1	53	76.3	70.6	54.3	26.2	65.2	35.6	60.8	24.2	42.8	64.7
Cr	30.4	53	49.7	61.7	65	41.9	29.6	49.3	29.8	16.9	14.3	50.4	71.1
Co	5.8	14.9	10.4	14	10.7	7.9	11.4	12.2	9.1	10.5	10.4	7.4	11.1
Ni	14.9	37.9	<56	25.6	21.4	35.4	45.2	33.4	36.8	30.1	22.8	22.9	31.1
Cu	6.3	5.6	2.9	6.2	6.2	12.6	6.5	6.9	9.7	8.9	11.6	<1.3	10.3
Zn	<7	74.3	24.4	37.5	35.4	<22	59	42.9	44.8	29.3	<3.5	16.5	32.3
Hg	< 1	n.a	< 1	n.a	n.a	< 1	< 1	< 1	< 1	n.a	< 1	n.a	n.a
Ag	< 5	n.a	< 5	n.a	n.a	< 5	< 5	< 5	< 5	n.a	< 5	n.a	n.a
Ga	40.2	24.9	25.2	27.8	30.4	25.6	70.5	<47.5	<65.9	35.9	28.7	7.3	15.3
Pb	18.2	24.2	26.2	24	35.1	26.7	16.8	23.8	29.9	37	32.7	4.8	8.5
W	11584.7	2.1	54	0.4	7.8	23808.1	1175.8	26	2821.9	478.1	16132.5	<1.5	2.4
Sn	421.9	12.9	61.7	22.7	106.8	34.1	15.3	20.9	110	108	90.9	1.2	2.5
Mo	0.6	2.3	2.2	2.4	0.2	3	3.2	0.1	0.9	0.2	1.5	<0.2	0.9
Sb	<0.1	n.a	<0.1	n.a	n.a	<0.1	0.5	<0.1	0.3	n.a	<0.1	n.a	n.a
La	39	n.a	43	n.a	n.a	73	130	53	38	n.a	16	n.a	n.a
Ce	65	n.a	97	n.a	n.a	130	280	120	80	n.a	34	n.a	n.a
Nd	30	n.a	35	n.a	n.a	46	100	49	44	n.a	18	n.a	n.a
Sm	5.9	n.a	7.2	n.a	n.a	9.4	19	9.5	6.4	n.a	2.9	n.a	n.a
Eu	1.5	n.a	1.6	n.a	n.a	2.1	2.9	2	2	n.a	0.8	n.a	n.a
Gd	4	n.a	3	n.a	n.a	9	13	7	6	2	2	n.a	n.a
Tb	1.2	n.a	1.2	n.a	n.a	1.6	3.9	1.5	<0.5	n.a	0.7	n.a	n.a
Yb	4.8	n.a	4.8	n.a	n.a	5.9	9	5.2	4	n.a	2.7	n.a	n.a
Lu	0.7	n.a	0.8	n.a	n.a	0.8	1.4	0.8	0.5	n.a	0.4	n.a	n.a

Appendix 5.4: (Contd.)

No.	27	28	29	30	31	32	33	34	35	36	37	38	39
Samp.	**ZS16**	**ZS18**	**ZM4**	**ZM12**	**ZM14**	**ZM14A**	**ZM15**	**ZM17**	**ZM22**	**ZM24A**	**ZM37**	**ZM60**	**ZM65**
SiO_2	n.a	n.a	n.a	n.a	n.a	88.44	87.57	n.a	n.a	75.46	77.98	n.a	75.67
TiO_2	n.a	n.a	n.a	n.a	n.a	0.15	0.71	n.a	n.a	0.79	0.45	n.a	0.07
Al_2O_3	n.a	n.a	n.a	n.a	n.a	5.63	5.5	n.a	n.a	11.62	9.73	n.a	6.81
Fe_2O_3	n.a	n.a	n.a	n.a	n.a	2.56	1.73	n.a	n.a	7.22	3.35	n.a	1.57
MnO	n.a	n.a	n.a	n.a	n.a	0.07	0.033	n.a	n.a	0.27	0.22	n.a	0.115
MgO	n.a	n.a	n.a	n.a	n.a	0.55	0.48	n.a	n.a	1.77	0.54	n.a	0.22
CaO	n.a	n.a	n.a	n.a	n.a	3.84	4.03	n.a	n.a	3.57	8.31	n.a	14.2
Na_2O	n.a	n.a	n.a	n.a	n.a	0.3	0.15	n.a	n.a	0.59	0.21	n.a	0.02
K_2O	n.a	n.a	n.a	n.a	n.a	0.117	0.27	n.a	n.a	0.378	0.018	n.a	0.01
P_2O_5	n.a	n.a	n.a	n.a	n.a	0.058	0.07	n.a	n.a	0.046	0.06	n.a	0.224
Total	n.a	n.a	n.a	n.a	n.a	101.72	100.53	n.a	n.a	101.72	100.86	n.a	98.87
Trace elements in ppm													
B	n.a	n.a	n.a	2	n.a	n.a	n.a	n.a	n.a	n.a	n.a	n.a	14
F	740	n.a	1310	800	820	1090	460	1260	500	680	400	n.a	n.a
Cl	210	n.a	210	210	210	220	40	40	50	50	50	n.a	n.a
S	50	n.a	390	40	520	160	0	20	140	350	20	n.a	n.a
As	2.2	2.2	3.8	2	0.7	1.3	1.2	1.3	0.9	0.5	2.4	1	n.a
Li	83.8	146.6	204.4	24.1	50.1	34	48.4	51	64.7	95.5	18.5	25.1	49
Be	1.1	1.7	4.4	0.5	3.6	2.1	1.9	3.6	0.5	2.1	0.6	0.5	51.5
Cs	n.a	n.a	n.a	<1	3	n.a	n.a	1	n.a	n.a	<1	<1	1
Ba	50.4	367	179.9	0.8	28.4	7.7	111	12	29.2	31.3	<1.4	40.7	16.5
Rb	60.1	167.7	121.2	2.5	18.1	10.8	30	2.9	35.4	42.8	0.7	16	2.2
Sr	217	160.5	419.3	142.8	70.6	100.7	134.7	311.9	46.9	137	180	153.9	151.1
Th	12.7	28.1	23.6	6.3	5.1	5	16.1	13	3.6	22.4	19	8.9	3.7
U	n.a	n.a	n.a	2.3	1.7	n.a	n.a	4.3	n.a	n.a	4	3.1	2.8
Zr	237.9	621.2	263.8	177.1	146.1	146	690.4	214.5	217.9	314.7	428.1	305.4	70.9
Hf	n.a	n.a	n.a	5	5	n.a	n.a	7	n.a	n.a	16	9	3
Ta	n.a	n.a	n.a	<0.5	<0.5	n.a	n.a	1.2	n.a	n.a	1.2	<0.5	0.7
Nb	6.9	11.6	16.2	5.1	5.7	3.4	16.4	14.7	3.9	9.5	10.1	6	3.7
Y	21.1	34	35.5	26.5	18.9	21.9	26.6	33.2	12.3	46.5	32.3	18.7	17.3
Sc	9.6	7.9	15.4	11.4	5.1	9.3	11	18.1	4.5	11.4	14.9	7.1	9.3
V	37.2	45.1	81.7	27.4	32.3	24.5	35.7	73.2	11.8	84.7	25.6	30.7	14
Cr	57.3	61.1	92.2	17.3	12	14.7	61.7	49	11.6	80.8	23.9	12.8	48.1
Co	8.9	7.6	17.7	8.4	10.6	6.7	4.6	19.7	5.7	27.9	8	5	4.9
Ni	11.5	18.3	28.4	14.1	20.5	36.4	17.7	29.5	5.5	70.2	6.2	3.6	22.2
Cu	6.9	<1.1	31.7	5.6	19.8	6.1	2.4	19	49.2	n.a	4.2	0.4	4.4
Zn	20.6	45.3	58.8	14	23.1	33.3	7.9	58.8	17	84.2	26.3	10.2	15.6
Hg	n.a	n.a	n.a	< 1	< 1	n.a	n.a	< 1	n.a	n.a	< 1	< 1	< 1
Ag	n.a	n.a	n.a	< 5	< 5	n.a	n.a	< 5	n.a	n.a	< 5	< 5	<5
Ga	8.8	11.9	18.6	12.8	10.3	7	8.1	26.5	4.6	15.3	15.6	11.2	12.5
Pb	24.3	20.4	48.7	12.1	10.3	8.3	12.2	28.7	6.7	15.4	18.8	11	9.2
W	<2.3	1	0.5	41.8	79	1.3	6.5	686.2	<0.3	1.3	474.7	7	4507.1
Sn	1.5	2.8	1.22	4.52	43.2	7.12	20.9	130.3	1.9	2.14	13.9	8.8	451.6
Mo	<0.6	0.8	0.1	<0.6	<0.6	<0.7	0.8	0.6	<0.3	0.7	0	0	0.6
Sb	n.a	n.a	n.a	0.3	1	n.a	n.a	1.8	n.a	n.a	2	1.3	0.7
La	n.a	n.a	n.a	13	15	n.a	n.a	36	n.a	n.a	39	16	8.4
Ce	n.a	n.a	n.a	33	35	n.a	n.a	73	n.a	n.a	94	40	20
Nd	n.a	n.a	n.a	16	14	n.a	n.a	35	n.a	n.a	40	16	10
Sm	n.a	n.a	n.a	4.2	3.2	n.a	n.a	5.4	n.a	n.a	7.1	3.3	2.9
Eu	n.a	n.a	n.a	1.6	1	n.a	n.a	1.3	n.a	n.a	1.7	0.9	0.9
Gd	n.a	n.a	n.a	<1	4	n.a	n.a	4	n.a	n.a	5	2	3
Tb	n.a	n.a	n.a	0.8	0.7	n.a	n.a	1.5	n.a	n.a	<0.5	<0.5	4.9
Yb	n.a	n.a	n.a	2.4	2.3	n.a	n.a	3.4	n.a	n.a	4.8	2	2.6
Lu	n.a	n.a	n.a	0.4	0.4	n.a	n.a	0.5	n.a	n.a	0.8	0.4	0.3

Appendix 5.4: (Contd.)

No.	40	41	42	43	44	45	46	47	48	49	50	51
Sample	**ZM66**	**TR132**	**ADIT3**	**NMG2**	**NMG3**	**ZC1**	**ZC3**	**ZC3A**	**ZC6**	**ZC10**	**ZC12**	**ZC13**
SiO_2	80.37	n.a	61.62	n.a	n.a	n.a	78.02	81.26	n.a	85.86	n.a	94.9
TiO_2	0.11	n.a	0.53	n.a	n.a	n.a	0.56	0.47	n.a	0.44	n.a	0.24
Al_2O_3	8.01	n.a	16.71	n.a	n.a	n.a	9.5	8.34	n.a	7.8	n.a	3.03
Fe_2O_3	1.23	n.a	4.79	n.a	n.a	n.a	2.58	2.2	n.a	0.49	n.a	0.4
MnO	0.068	n.a	0.124	n.a	n.a	n.a	0.12	0.1	n.a	0	n.a	0
MgO	0.16	n.a	0.88	n.a	n.a	n.a	0.88	0.74	n.a	0.2	n.a	0.18
CaO	6.67	n.a	14.24	n.a	n.a	n.a	4.03	3.4	n.a	0.98	n.a	0
Na_2O	0.4	n.a	0.06	n.a	n.a	n.a	1.6	1.82	n.a	3.25	n.a	0.2
K_2O	0.189	n.a	0.048	n.a	n.a	n.a	0.61	0.8	n.a	0.25	n.a	1.74
P_2O_5	0.14	n.a	0.157	n.a	n.a	n.a	0.1	0.32	n.a	0.08	n.a	0.03
Total	97.35	n.a	99.17	n.a	n.a	n.a	98	99.45	n.a	99.33	n.a	100.76
Trace elements in ppm												
B	6	2	n.a	n.a	n.a	n.a	n.a	n.a	5	n.a	n.a	n.a
F	n.a	1240	560	n.a	n.a	n.a	n.a	n.a	n.a	130	n.a	70
Cl	n.a	50	50	n.a	n.a	n.a	n.a	n.a	n.a	50	n.a	40
S	n.a	230	0	n.a	n.a	n.a	n.a	n.a	n.a	70	n.a	0
As	n.a	n.a	n.a	n.a	n.a	n.a	n.a	n.a	n.a	n.a	n.a	n.a
Li	20.3	55.3	27.9	144.9	137.6	12.1	56.8	81	73.8	17.7	105	33.6
Be	37	2.4	1.3	1.5	1.3	0.8	3	8.5	2.3	2.2	1.6	0.6
Cs	3	4	2	n.a	n.a	n.a	n.a	n.a	3	n.a	n.a	n.a
Ba	68.2	177.2	14.1	107.7	196.6	21	333.6	239.9	130.8	32.6	74.3	390.7
Rb	25.7	51.4	2.2	119.6	55.1	10.8	48.7	64.4	26.9	5.2	19.4	55.6
Sr	177.7	273.2	247.1	72.9	104.8	28.3	330.7	283.7	380.4	322.4	238.5	45.6
Th	5	64	20	4.4	8.3	1	15.1	12.7	17	12.8	17.3	6.3
U	<1	<2.4	3.5	n.a	n.a	n.a	n.a	n.a	3.3	n.a	n.a	n.a
Zr	207.9	858.5	203.1	166.1	239.5	6	364.5	277.7	276	382.4	445.9	249.4
Hf	6	34	9	n.a	n.a	n.a	n.a	n.a	11	n.a	n.a	n.a
Ta	<0.5	4	1.3	n.a	n.a	n.a	n.a	n.a	<0.5	n.a	n.a	n.a
Nb	5.3	22.5	11.1	8.4	12.3	1.1	13.4	10.4	7.5	10.1	9.3	4.4
Y	17.9	48	32.4	15.8	23.5	3	34.7	29.6	21.6	22.5	21.2	10.9
Sc	7.6	20.9	19.8	6.8	10.7	<0.1	8.4	5.3	4.8	9.9	4.4	<0.1
V	24.8	82.1	69.4	51.6	93.6	4.2	49.9	38.9	27.6	24.5	24.2	14.7
Cr	14.5	90.5	68.1	62	166.7	<2.3	50.1	33.9	36.2	31	17.4	13.6
Co	6.8	10.7	9.7	8.6	15.8	0.5	8.7	5.2	4.8	1.4	2	1.1
Ni	75.7	28.3	18.6	21.7	32.2	3.3	20.4	34.7	12	6.2	23.7	<1.6
Cu	5.6	18.6	6.7	2.3	12.4	<3.3	5.6	3.9	1.2	<1.3	<2.7	<1.6
Zn	<37.1	<63.4	38.8	48	36.3	<0.5	30.5	39.4	10.1	2.2	4.8	5.5
Hg	< 1	< 1	< 1	n.a	n.a	n.a	n.a	n.a	< 1	n.a	n.a	n.a
Ag	< 5	< 5	< 5	n.a	n.a	n.a	n.a	n.a	< 5	n.a	n.a	n.a
Ga	14.8	32.3	27.8	7.8	11.8	3	13.8	11.3	10.2	8.7	7.6	4.8
Pb	15.6	32	40.8	16.5	7.7	2.5	11.2	15.7	6.7	9.6	18.2	11
W	21186.9	30556.9	2253.6	<1.4	2.1	<1.1	2.2	2.8	0.2	0.3	0.1	1
Sn	396.8	255.1	38	3.3	3.6	1	5.2	39.6	3.3	2.1	1.2	1.1
Mo	1.6	5	0.5	<0.4	0.5	0.6	3	1.8	0.9	1.7	1.7	2.3
Sb	<0.1	<0.1	0.3	n.a	n.a	n.a	n.a	n.a	0.9	n.a	n.a	n.a
La	12	97	48	n.a	n.a	n.a	n.a	n.a	44	n.a	n.a	n.a
Ce	24	190	100	n.a	n.a	n.a	n.a	n.a	83	n.a	n.a	n.a
Nd	10	<5	46	n.a	n.a	n.a	n.a	n.a	24	n.a	n.a	n.a
Sm	1.6	11	8.5	n.a	n.a	n.a	n.a	n.a	5.5	n.a	n.a	n.a
Eu	0.6	2.2	1.9	n.a	n.a	n.a	n.a	n.a	1.1	n.a	n.a	n.a
Gd	1	8	4	n.a	n.a	n.a	n.a	n.a	4	n.a	n.a	n.a
Tb	0.9	<0.5	2.8	n.a	n.a	n.a	n.a	n.a	<0.5	n.a	n.a	n.a
Yb	2.1	8.9	5.1	n.a	n.a	n.a	n.a	n.a	2.3	n.a	n.a	n.a
Lu	0.2	1.2	0.7	n.a	n.a	n.a	n.a	n.a	0.4	n.a	n.a	n.a

Appendix 5.4: (Contd.)

No.	52	53	54	55	56	57	58	59	60	61	62	63
Sample	**ZC13A**	**ZC14**	**ZC15**	**ZC16**	**ZC18**	**ZC19**	**ZC29**	**ZC54**	**ZS19B**	**ZM40**	**ZM41**	**ZM68**
SiO_2	92.86	87.9	n.a	63.91	81.55	n.a	n.a	n.a	n.a	80.26	n.a	77.61
TiO_2	0.3	0.57	n.a	0.8	0.33	n.a	n.a	n.a	n.a	0.6	n.a	0.48
Al_2O_3	4.17	6.62	n.a	17.65	6.92	n.a	n.a	n.a	n.a	10.51	n.a	11.28
Fe_2O_3	0.47	0.78	n.a	4.9	1.8	n.a	n.a	n.a	n.a	0.9	n.a	3.22
MnO	0	0.02	n.a	0.08	0.05	n.a	n.a	n.a	n.a	0.02	n.a	0.02
MgO	0.22	0.24	n.a	1.5	0.59	n.a	n.a	n.a	n.a	0.48	n.a	0.63
CaO	0	0.6	n.a	4.01	1.6	n.a	n.a	n.a	n.a	2.62	n.a	1.93
Na_2O	0.29	1.99	n.a	4.14	1.73	n.a	n.a	n.a	n.a	2.75	n.a	3.01
K_2O	2.25	0.9	n.a	2.24	2.21	n.a	n.a	n.a	n.a	0.626	n.a	1.036
P_2O_5	0.03	0.04	n.a	0.2	0.16	n.a	n.a	n.a	n.a	0.075	n.a	0.141
Total	100.66	99.67	n.a	99.44	96.92	n.a	n.a	n.a	n.a	98.85	n.a	99.35
Trace elements in ppm												
B	n.a	n.a	n.a	n.a	n.a	n.a	n.a	n.a	n.a	n.a	n.a	6
F	120	210	110	710	920	110	340	n.a	n.a	n.a	410	n.a
Cl	50	40	50	80	50	40	80	n.a	n.a	n.a	50	n.a
S	0	0	0	0	0	0	80	n.a	n.a	n.a	0	n.a
As	n.a	n.a	n.a	n.a	n.a	n.a	n.a	n.a	1.3	n.a	n.a	1.4
Li	48.8	56.6	25.7	224.5	73	35.6	90.5	47.3	113.4	23.7	14.8	100.1
Be	1	2.1	0.7	5.5	4.3	0.5	1.9	1.4	3.9	1.2	0.7	2.5
Cs	n.a	n.a	n.a	n.a	n.a	n.a	n.a	n.a	n.a	n.a	n.a	9
Ba	532.6	300.6	183.7	1295.7	597.3	398.5	284.6	129.5	260.1	238.4	362	390.2
Rb	81.4	39.8	23	130.4	120.7	53.6	42.2	54.2	78.4	26	28.5	66.4
Sr	57.5	196	62.3	484.9	231.6	49.1	282.1	106.3	197	1148.6	555.1	320.5
Th	13.8	19.2	7.4	25	12.6	8.6	12.4	5.6	18.3	8.8	10.8	18
U	n.a	n.a	n.a	n.a	n.a	n.a	n.a	n.a	n.a	n.a	n.a	6.5
Zr	309.8	562.1	157	526.5	238.8	273.9	303.2	253.5	411.6	405.1	342.1	386.8
Hf	n.a	n.a	n.a	n.a	n.a	n.a	n.a	n.a	n.a	n.a	n.a	16
Ta	n.a	n.a	n.a	n.a	n.a	n.a	n.a	n.a	n.a	n.a	n.a	2.3
Nb	6.1	10.1	3.4	18.1	10.7	5	6.9	10.1	9.5	12.3	13.2	8.9
Y	11.7	19.3	8.7	37.6	20.8	10.2	36.7	23.1	21.6	30	22.9	20.3
Sc	5.9	7.2	0.5	16.2	8.4	6.4	6.8	2.7	10.9	15.1	13.8	10.1
V	19.1	24.6	14.2	77.2	32.7	8.7	35.6	50	40.1	48.4	58.6	42.3
Cr	12	26.7	10.6	78	23.6	12.9	28.3	64.8	32.7	67.9	74.1	51
Co	<2.6	0.6	1.2	13	4.7	1.2	4.9	9.7	5.7	1.9	4.6	4.7
Ni	2.3	2.6	<3	24.2	8.8	<1.4	6.8	24	12	3.9	2.7	2.1
Cu	<0.9	<1.4	<2.7	10.7	6.1	<1.7	2.4	11.6	<2.1	4.2	18.3	13.3
Zn	5.9	4.8	2.2	62.1	22.3	1.4	13.6	38	32.4	25.1	193.8	45.9
Hg	n.a	n.a	n.a	n.a	n.a	n.a	n.a	n.a	n.a	n.a	n.a	< 1
Ag	n.a	n.a	n.a	n.a	n.a	n.a	n.a	n.a	n.a	n.a	n.a	< 5
Ga	6.4	7.5	3.3	20.4	8.1	4	7.1	9.3	9.9	7.9	9.1	12
Pb	15.4	18.2	4.1	35.1	24.7	11.7	30.4	6.3	13.4	23.8	206.9	53
W	0.5	<0.9	<0.7	6.1	1	<0.9	1	0.4	0.4	0.1	<0.2	21
Sn	1.9	8.1	1.2	1.2	23.9	<0.2	<0.2	4.1	1.7	6.1	5.8	1.2
Mo	2.8	2.4	2.1	1.9	1.3	1	3.2	2.7	0.1	0.1	0.9	2.1
Sb	n.a	n.a	n.a	n.a	n.a	n.a	n.a	n.a	n.a	n.a	n.a	0.3
La	n.a	n.a	n.a	n.a	n.a	n.a	n.a	n.a	n.a	n.a	n.a	39
Ce	n.a	n.a	n.a	n.a	n.a	n.a	n.a	n.a	n.a	n.a	n.a	86
Nd	n.a	n.a	n.a	n.a	n.a	n.a	n.a	n.a	n.a	n.a	n.a	30
Sm	n.a	n.a	n.a	n.a	n.a	n.a	n.a	n.a	n.a	n.a	n.a	5.8
Eu	n.a	n.a	n.a	n.a	n.a	n.a	n.a	n.a	n.a	n.a	n.a	1.6
Gd	n.a	n.a	n.a	n.a	n.a	n.a	n.a	n.a	n.a	n.a	n.a	5
Tb	n.a	n.a	n.a	n.a	n.a	n.a	n.a	n.a	n.a	n.a	n.a	0.7
Yb	n.a	n.a	n.a	n.a	n.a	n.a	n.a	n.a	n.a	n.a	n.a	3
Lu	n.a	n.a	n.a	n.a	n.a	n.a	n.a	n.a	n.a	n.a	n.a	0.5

Appendix 5.5: Major, minor and trace element composition of the tourmalinites from the study area.

No.	1	2	3	4	5	6	7	8	9	10	11	12	13
Sample	**ZC40**	**ZC69**	**ZC69A**	**ZM 24**	**ZM 25**	**ZM28**	**ZM 29**	**ZM 31**	**ZM 32**	**ZM 62**	**ZM 63**	**ZM 64**	**ZM 64A**
SiO_2	48.1	47.5	46.8	49.2	61.7	n.a	50	55.8	58.5	50.2	47.6	48.7	49.9
TiO_2	0.7	0.9	0.9	1.5	0.8	n.a	1.2	1.1	1	0.8	0.9	0.8	0.8
Al_2O_3	29.5	22.2	23.4	23.3	21	n.a	26.7	24.4	22.7	21.8	24	23.5	22
Fe_2O_3	6.8	13.3	13	8.6	6.6	n.a	7.7	6.3	6.6	12.8	12.5	12.5	10.8
MnO	0	2.4	2.6	0.1	0.1	n.a	0.1	0.1	0.1	2.1	2.1	1.6	1.7
MgO	3.3	3.2	2.7	2.5	2.3	n.a	3.7	2.6	2.3	3.1	2.7	4.5	4.3
CaO	3.7	2.9	3.6	1.9	0.5	n.a	0.8	0.3	0.8	2.5	3.2	1.9	1.9
Na_2O	2.8	1.4	1.8	3.3	1.1	n.a	2.2	1.1	1.2	1.6	2.1	1.5	1
K_2O	0.3	0.1	0.2	0.5	1.7	n.a	1.6	3.1	2.8	0.1	0.2	0.1	0.1
P_2O_5	0.1	0.2	0.2	0.1	0.1	n.a	0.1	0	0.1	0.2	0.2	0.1	0.2
Total	95.4	94.2	95.2	90.9	95.8	n.a	94	94.8	96	95	95.4	95.1	92.6
Minor and trace elements in ppm unless and otherwise mentioned.													
B (%)	1.37	1.196	1.06	n.a	1.09	n.a	n.a	1.04	0.931	1.18	1.07	1.48	1.41
F	n.a	1090	880	1350	980	1220	1330	790	950	n.a	n.a	n.a	n.a
Cl	n.a	50	60	50	50	40	40	40	70	n.a	n.a	n.a	n.a
S	n.a	0	0	140	230	40	280	0	180	n.a	n.a	n.a	n.a
As	n.a	< 4.3	0.7	1.1	1.5	2.4	1.6	0.9	1.5	2	1	n.a	n.a
Li	37.7	52.4	56	69.8	91.7	172.7	104.9	113.2	102.4	68	64.4	51	50
Be	13.7	6.4	9.7	10.7	4.6	4.9	5.7	2.8	6.6	4.6	7.3	3.3	3.6
Cs	< 1	< 1	< 1	n.a	n.a	n.a	n.a	n.a	4	< 1	< 1	< 1	< 1
Ba	16.5	20.7	21.7	72.7	406.3	719.7	228.8	568.5	560.5	5.6	19.1	9.1	4.9
Rb	25.2	8.3	15.1	30.2	74.6	187.8	72.8	125.3	113.5	6	11	2.1	1.1
Sr	520.7	237.8	284.6	355.5	247.6	395.6	388	237.4	240.7	200.4	254.5	284.2	262.4
Th	20	13	14	31	16.3	19.3	41.6	2.5	16	16	16	12	9.7
U	5.8	< 0.6	4.7	n.a	n.a	n.a	n.a	n.a	4.2	4.7	4.5	4.7	3.9
Zr	323.1	131.4	140.7	249.3	106	181.4	189.1	192.4	157.1	129.3	148.4	133	120
Hf	6	2	2	n.a	n.a	n.a	n.a	n.a	3	< 1	3	< 1	< 1
Ta	< 0.5	1.5	< 0.5	n.a	n.a	n.a	n.a	n.a	1.1	< 0.5	< 0.5	< 0.5	1.4
Nb	4.9	17	16.8	31.9	14.1	33.1	19.4	23.2	22.6	13.1	16.1	15.5	14.2
Y	38.1	35	41.8	43.4	17.5	13	27.7	6.3	29.9	35.4	35.6	44.9	39.4
Sc	11.5	19.9	17.1	13.7	15.2	26.2	21.8	19.4	21.4	18.3	20.5	16.7	16.6
V	114.8	106.9	96.9	80.4	105	170.4	151.7	127	102.3	98.2	102.4	114.9	110.6
Cr	113.7	130.2	129.6	175.1	102	202.8	161.8	143.6	132.9	139.6	142.2	167.7	115.5
Co	10.2	19.6	20	13.9	28.2	11.3	14.5	13	11.8	26.1	19.8	17.2	29.7
Ni	11.7	42.6	37.7	11.8	32.5	23.7	25.8	13.3	26.8	48.2	45.8	29.5	47.2
Cu	11.9	11.3	8.9	7.3	n.a	2.5	2.8	1.4	10.6	20.4	12.5	13.6	36.2
Zn	141.8	132.5	142.5	136.3	150.3	129.9	97.7	124.1	119.3	107.6	119.9	153.4	129.9
Hg	< 1	< 1	< 1	n.a	n.a	n.a	n.a	n.a	< 1	< 1	< 1	< 1	< 1
Ag	< 5	< 5	< 5	n.a	n.a	n.a	n.a	n.a	< 5	< 5	< 5	< 5	< 5
Ga	31	22.5	21.7	24.8	28.5	42.2	32.4	30.2	28.9	22.3	22.4	26.3	25.9
Pb	39	16.7	24.6	27.7	17.8	36.3	27.8	28	21.9	17.7	26.3	20.1	18.4
W	0.3	7833.6	1117.7	1.9	4.1	5.6	4	4.9	6.3	5100.4	582.2	2963.9	5242.9
Sn	16.3	5.33	3.8	4.6	11.6	17.7	12.3	11.4	12.9	18.2	12.7	23.1	21.9
Mo	1.1	1.1	0.1	0.1	< 0.3	< 0.5	< 0.3	0.1	0.6	0.8	0.2	0	0.6
Sb	< 0.1	< 0.1	0.4	n.a	n.a	n.a	n.a	n.a	1.7	1.3	< 1	0.3	< 1
La	42	24	28	n.a	n.a	n.a	n.a	n.a	33	27	27	21	16
Ce	78	50	57	n.a	n.a	n.a	n.a	n.a	66	54	57	48	31
Nd	39	33	25	n.a	n.a	n.a	n.a	n.a	30	17	21	18	16
Sm	6.5	4.7	4.9	n.a	n.a	n.a	n.a	n.a	5.5	5.3	4.9	4.8	3.9
Eu	1	0.6	0.6	n.a	n.a	n.a	n.a	n.a	0.9	0.9	0.6	0.6	0.5
Gd	1	< 0.1	< 0.1	n.a	< 0.1	n.a	n.a	< 1	2	< 1	1	< 1	< 1
Tb	< 0.5	0.8	0.9	n.a	n.a	n.a	n.a	n.a	0.6	2.7	< 0.5	2.1	< 0.5
Yb	1.6	2.5	2.1	n.a	n.a	n.a	n.a	n.a	1.6	2.2	2	2.1	1.8
Lu	0.2	0.3	0.4	n.a	n.a	n.a	n.a	n.a	0.3	0.3	0.4	0.4	0.3

Appendix 5.6: Description of the samples from SW England.

Sample	Rock	Location
SW 1	Acidic Volcanics	Whympston
SW 2	Slate	Wadham
SW 3	Pyrite-bearing rock	Wadham
SW 4	Schist	Wadham
SW 5	Black Shale	Jennyclift Bay
SW 6	Sandstone	Jennyclift Bay
SW 7	Slate	Bigbury,
SW 8	Greisen	Hemerdon mine
SW 10	Black Shale	Bridestowe
SW 11	Volcanics	Burley Wood
SW 12	Black Shale	Burley Wood
SW 13	Agglomerate	Brentor
SW 14	Volcanics	Tintagel Castle
SW 15	Quartz vein in Volcanics	Tintagel Castle
SW 16	Slate	Tintagel Castle
SW 17	Siltstone	Cansford quarry
SW 19	Chert	Egloskerry quarry
SW 20	Ultramafic rock	Polyphant quarry
SW 21	Pyrite-bearing Dolerite	Colvannick
SW 22	Background Dolerite	Colvannick
SW 23	Tourmaline pegmatite	Colvannick
SW 24	Dolerite associated with mica schist	Penroseburden
SW 25	Dolerite	Michaelstow
SW 26	Slate	Tregildrans
SW 27	Pisolitic Dolerite	Tregildrans
SW 28	Slate	Waderidge
SW 29	Slate	Pentire
SW 30	Volcanics	Pentire
SW 31	Slate	Trevose
SW 32	Dolerite	Trevose
SW 33	Volcanics	Trevose
SW 34	Calcareous rocks	Withiel
SW 35	Meta Volcanics	Polgrain

Appendix 5.6 (Contd.)

SW 36	Granite	Roche
SW 37	Pegmatite	Roche
SW 40	Volcanics	Pendeen
SW 41	Tourmalinites	Botallack
SW 42	Mafic rocks	Potalloack
SW 43	Feldspar Granite	Porthleddon
SW 44	Tourmaline Granite	Porthleddon
SW 45	Hornfels	Porthleddon
SW 46	Leucogranite	Porthleven
SW 47	Slate	Porthleven

Appendix 5.7: Trace element chemistry of the studied rocks from SW England.

Sample	SW1	SW2	SW3	SW4	SW5	SW6	SW7	SW8	SW10	SW11
As	6.9	42.3	87.7	3.1	51.9	1.1	6.0	25.5	17.2	1.0
Li	8.1	247.7	100.8	92.2	127.6	29.3	98.2	407.5	63.9	17.6
Be	1.1	1.8	0.7	2.6	2.8	1.0	3.1	4.5	1.7	0.7
Ba	581.1	735.3	1075.6	574.3	475.6	211.5	462.8	165.0	949.5	33.7
Rb	238.4	171.3	200.3	151.7	158.9	60.0	195.2	802.8	77.6	5.3
Sr	20.9	130.0	84.9	71.2	134.7	222.2	83.8	11.4	907.4	660.4
Th	28.7	5.0	2.3	12.6	17.3	8.8	13.4	6.3	8.8	0.1
Zr	99.2	179.9	134.3	248.9	205.3	268.5	214.0	67.5	100.6	7.9
Nb	27.5	15.4	12.1	20.3	20.7	9.4	21.0	11.9	9.5	<1.5
Y	29.7	37.6	23.6	38.6	41.9	30.1	38.0	16.8	32.0	2.2
Sc	4.3	23.2	23.9	16.3	17.5	13.9	14.8	8.1	19.2	18.3
V	4.3	190.1	174.3	113.1	146.3	61.8	157.4	19.9	86.5	74.9
Cr	7.7	52.1	53.1	150.6	118.0	57.5	140.9	11.0	100.7	18.3
Co	<0.1	36.1	22.0	18.8	28.9	11.0	17.3	<1	13.7	2.1
Ni	4.0	48.3	39.9	61.0	71.0	26.3	54.6	3.1	50.0	17.8
Cu	1.2	26.3	662.2	8.1	32.8	2.7	4.4	2.2	24.5	7.6
Zn	6.8	112.9	37.7	67.0	99.1	14.8	110.5	45.2	170.3	28.6
Ga	15.4	19.4	14.0	20.3	24.2	8.7	25.6	40.8	13.2	2.1
Pb	4.5	13.1	11.3	9.1	34.5	4.1	14.9	5.9	45.9	3.0
W	1.1	2.3	9.7	2.2	5.4	1.1	3.4	110.2	1.6	<0.8
Sn	2.64	1.25	1.2	2.24	2.1	1.07	2.15	238	1.42	1.27
Mo	<0.1	0.9	<0.1	0.1	2.3	<0.4	0.2	<0.4	5.7	1.8
La	24.3	23.5	15.4	34.9	41.5	21.3	11.4	8.1	33.1	4.5
Ce	42.4	36.9	22.6	64.8	81.6	43.1	24.0	14.5	46.4	5.5
Nd	12.7	14.5	8.0	27.3	29.7	22.2	10.0	3.5	18.1	<0.3

Sample	SW12	SW13	SW14	SW15	SW16	SW17	SW19	SW20	SW21	SW22
As	5.9	9.3	18.6	422.7	5.7	11.3	0.5	53.8	67.4	94.1
Li	133.7	71.7	194.6	94.9	140.5	68.8	32.8	180.7	493.1	227.4
Be	3.7	2.1	2.1	0.9	3.4	2.1	0.4	1.3	10.7	6.2
Ba	915.1	393.0	145.8	43.0	598.0	278.8	16.5	23.1	61.1	147.5
Rb	186.6	136.0	48.0	13.4	232.5	83.7	6.3	3.4	50.9	151.8
Sr	76.4	62.9	210.5	12.8	141.3	37.2	1.8	311.0	7.7	257.1
Th	15.2	5.7	4.8	29.7	15.9	8.8	3.2	4.0	20.3	2.7
Zr	148.5	232.3	191.5	26.9	152.0	277.1	18.7	78.8	688.8	352.2
Nb	14.1	69.0	27.9	0.3	17.2	13.5	2.9	9.2	102.5	66.1
Y	38.9	52.0	22.3	13.3	33.3	33.4	6.8	17.2	122.2	68.0
Sc	18.5	21.6	24.3	7.1	18.5	11.0	<0.3	25.5	3.2	30.5
V	121.3	133.8	170.2	2.8	140.9	74.9	19.6	222.3	54.2	220.5
Cr	93.0	417.3	242.4	2.0	121.4	68.8	9.5	348.2	2.6	19.1
Co	10.8	33.7	22.7	17.0	24.9	23.1	8.6	39.1	46.7	33.5
Ni	52.0	70.7	64.1	39.5	57.7	46.6	14.9	138.7	9.3	15.2
Cu	140.3	12.3	6.4	179.8	24.3	26.2	18.2	23.2	955.8	104.5
Zn	91.8	93.6	216.1	31549.4	152.1	56.6	21.3	127.9	438.6	329.8
Ga	24.0	19.7	20.2	12.9	28.8	15.2	3.2	17.1	44.4	29.0
Pb	8.0	13.6	29.8	6632.0	41.6	13.2	9.0	9.0	11.5	11.7
W	4.0	2.3	4.4	<83.8	2.9	1.0	1.8	<0.2	26.4	17.6
Sn	2.8	1.8	2.42	0.9	2.54	1.7	0.8	1.3	51	30
Mo	<0.1	1.1	0.7	3.0	0.3	0.5	<1.3	0.4	3.0	3.4
La	40.6	47.1	11.9	30.8	40.7	27.1	3.9	9.0	96.1	28.1
Ce	65.2	74.9	30.4	108.8	84.0	51.2	12.8	10.2	199.9	65.7
Nd	26.3	33.5	12.8	39.0	33.2	22.6	2.0	3.3	93.0	39.2

Appendix 5.7 (Contd.)

Sample	SW23	SW24	SW25	SW26	SW27	SW28	SW29	SW30	SW31	SW32	SW33	SW34
As	154.8	11115.0	24.8	31.2	10.7	32.8	59.1	48.7	82.9	3.7	11.6	17.6
Li	291.0	60.4	58.1	146.5	226.2	116.8	45.5	242.8	312.4	179.8	206.0	74.6
Be	51.6	1.9	1.0	3.0	2.4	3.1	3.2	2.2	3.2	1.0	3.3	2.1
Ba	-2.0	96.8	51.8	478.5	184.7	422.5	258.3	40.8	104.8	153.4	212.7	60.9
Rb	7.2	35.6	8.1	218.3	19.1	209.1	81.5	6.2	31.9	37.0	123.2	13.7
Sr	4.8	494.7	272.5	20.1	140.6	175.2	139.1	122.9	20.6	425.1	127.4	123.5
Th	13.4	5.9	2.2	12.1	9.5	9.2	1.0	7.0	14.3	0.3	<0.1	7.4
Zr	109.0	278.3	100.8	152.8	146.6	161.4	231.8	468.9	121.6	64.4	98.2	153.7
Nb	28.3	37.4	3.2	16.3	14.9	17.6	48.5	82.7	14.7	5.0	7.7	11.5
Y	20.1	48.3	16.1	41.7	34.2	37.6	33.3	45.4	36.9	17.0	17.9	32.1
Sc	2.0	33.8	35.3	18.9	16.2	21.1	14.5	15.4	19.2	25.6	33.3	22.7
V	15.7	360.7	255.9	167.8	156.8	151.9	256.6	126.1	227.0	187.5	280.8	76.9
Cr	5.5	8.5	103.4	130.1	121.6	138.8	132.8	<0.8	148.0	224.9	332.9	115.4
Co	6.7	50.0	52.8	32.8	28.1	26.3	45.8	40.5	115.6	43.2	44.6	32.2
Ni	4.1	23.9	50.3	116.2	101.4	79.4	110.8	10.7	129.9	69.9	92.7	58.0
Cu	100.3	100.4	92.7	41.6	40.7	35.4	66.9	20.9	104.3	83.6	32.1	15.9
Zn	61.4	245.4	101.1	161.9	126.0	141.5	239.6	188.7	81.9	507.0	92.6	334.0
Ga	7.4	24.9	19.8	24.5	22.9	24.8	28.8	25.8	47.0	17.7	25.5	17.9
Pb	16.3	23.0	21.0	26.5	22.5	30.7	55.3	5.5	20.1	6.4	10.0	20.6
W	16.6	6.0	1.0	1.3	1.5	2.9	6.8	<0.6	3.7	<2.9	0.5	3.5
Sn	6.8	55	2	1.8	1.6	2.54	2.44	2.24	3.1	1.7	1.6	60
Mo	31.3	5.2	0.6	0.9	<0.3	0.1	3.1	2.0	4.4	0.4	4.6	1.3
La	11.3	28.8	8.3	39.5	34.4	40.6	33.4	50.5	55.1	2.3	8.9	50.3
Ce	30.9	380.9	19.4	84.8	72.8	87.4	91.4	118.3	98.6	14.5	11.4	102.3
Nd	8.8	38.6	12.1	35.3	31.8	36.7	41.3	61.2	39.4	9.2	5.3	47.9

Sample	SW35	SW36	SW37	SW40	SW41	SW42	SW43	SW44	SW45	SW46	SW47
As	10.8	0.8	1.0	13.5	17.1	18.5	66.1	13.2	90.3	6.1	7.8
Li	138.7	102.6	87.8	162.7	195.9	112.1	110.4	103.7	310.7	3069.8	180.4
Be	2.0	1.2	1.2	4.0	5.8	2.9	1.5	2.1	2.6	6.4	2.6
Ba	33.9	4.2	<2.3	712.2	<2.2	81.9	356.3	<6.9	590.7	28.8	456.5
Rb	50.7	2.5	1.9	175.7	13.1	77.0	460.5	5.1	222.0	1700.9	191.4
Sr	6.1	17.7	8.0	341.7	594.6	16.9	97.0	3.4	64.5	26.3	183.5
Th	6.7	4.6	9.0	19.0	2.2	4.0	13.3	34.5	11.4	2.8	16.8
Zr	181.3	27.9	54.6	481.9	155.1	167.5	103.1	37.2	201.0	22.4	229.8
Nb	6.7	3.1	15.0	27.0	28.1	40.0	14.1	22.2	21.1	77.5	20.4
Y	13.4	4.1	3.9	94.8	25.7	17.6	17.6	12.2	27.3	23.1	36.7
Sc	4.0	5.0	5.1	28.2	41.2	41.3	8.2	1.7	17.5	11.0	18.6
V	40.8	11.1	15.0	133.8	665.3	342.4	25.1	7.5	155.5	15.6	104.7
Cr	77.0	<1.4	4.2	58.6	69.4	75.7	11.5	2.2	162.8	7.6	102.5
Co	12.2	12.2	8.9	19.5	19.7	68.4	2.5	8.5	13.7	<4.7	16.5
Ni	34.9	6.5	5.7	34.0	127.5	55.1	4.6	4.0	36.1	4.2	35.3
Cu	23.9	<0.7	<1	61.3	50.4	111.1	3.9	4.2	62.3	<2.4	28.1
Zn	245.6	128.9	89.3	92.7	149.7	300.2	31.7	70.0	43.5	25.7	85.6
Ga	12.8	31.2	27.8	27.9	68.1	31.0	21.0	34.8	27.7	40.5	21.4
Pb	5.4	5.7	4.9	6.8	14.2	14.9	29.3	7.5	2.6	4.7	19.6
W	2.1	<0.5	0.6	5.0	31.8	13.8	2.0	13.0	9.9	34.0	2.2
Sn	30.32	8.0	1.84	9.83	827	118	4.18	3.41	13.6	20.6	3.6
Mo	<0.1	<1	<1	2.3	0.2	5.6	<0.2	<0.8	0.0	<0.9	0.5
La	17.0	5.7	3.5	51.6	17.3	23.0	18.8	3.5	38.3	10.5	36.6
Ce	44.5	8.2	5.0	111.9	23.2	22.1	41.6	5.9	87.8	7.7	76.5
Nd	19.3	0.8	2.3	53.4	19.1	27.4	14.1	1.9	30.5	<1.2	33.3

Be and Li were analysed by ICP-ES. All other elements were analysed by XRF.

References

Abdel-Rahman, A. M. (1995). Chlorites in a spectrum of igneous rocks: mineral chemistry and paragenesis. Min. Mag., **59**, 129-141.

Absar, A. (1991). Hydrothermal epidote- an indicator of temperature and fluid composition. J. Geol. Soc. India, **38**, 625-628.

Akcay, M. (1994). Genesis of the stibnite-cinnabar-scheelite deposits of the Gumusler area, Nigde, central Turkey and implications on their gold potential. Unpubl. Ph.D. thesis, Univ. Leicester.

Alderton, D. H. M. & Jackson, N. J. (1978). Discordant calc-silicate bodies from the St. Just aureole, Cornwall. Min. Mag., **42**, 427-434.

Alderton, D. H. M. & Moore, F. (1981). New determination of tin and tungsten in granites from south-west England. Min. Mag., **44**, 354-356.

Alderton, D. H. M., Pearce, J. A. & Potts, P. J. (1980). The rare earth element mobility during granite alteration: evidence from SW England. Ear. Plan. Sci. Let., **49**, 149-165.

Alderton, D. H. M. & Rankin, A. H. (1983). The character and evolution of hydrothermal fluids associated with the kaolinized St. Austell granite, SW England. J. Geol. Soc. London, **140**, 297-309.

Alexandrov, E. A. (1962). A review of a Russian paper on the rhythmic banding of granitoid bodies. Econ. Geol., **57**, 1271-1272.

Almeida, A. & Noronha, F. (1988). Fluids associated with W and Ag-Au deposits of the Mirandale area, NE Portugal: an example of peri-granitic zoning. Bull. de Min., **111**, 331-341.

Anderson, J. L. & Rowley, M. C. (1981). Synkinematic intrusion of peraluminous and associated metaluminous granitic magmas, Whipple mountains, California. Can. Min., **19**, 83-101.

Arif, M. (1994). Mineralogy, geochemistry and stable isotope studies of the ultramafic rocks from the Swat valley ophiolite, Northwestern Pakistan: Implications for the genesis of emerald and nickeliferous opaque phases. Unpubl. Ph.D. thesis, Univ. Leicester.

Asrarullah. (1982). Investigations for tungsten in Pakistan. In: Hepworth, J. V. (eds) Tungst. Geol. Symp. Jiangxi. China, (ESCAP RMRDC), Bandung, Indonesia, 9-13.

Austromineral. (1978). Mineral exploration and mine development, Chitral District. Report for Sarhad Development Authority, Peshawar.

Ball, T. K., Fortey, N. J. & Shepherd, T. J. (1985). Mineralisation at the Carrock Fell tungsten mine, N. England: Paragenetic, fluid inclusion and geochemical study. Mineral. Deposita, **20**, 57-65.

Bailey, S. W. (1988). Chlorites: structures and crystal chemistry. In: hydrous phyllosilicates (exclusive of micas). S. W. Bailey (eds), Min. Soc. America, Rev. in min., **19**, 347-403.

Barazangi, M. & Ni, J. (1982). Velocities and propagation characteristics of P_n and S_n beneath the Himalayan arc and Tibetan plateau: possible evidence for underthrusting of the Indian continental lithosphere beneath Tibet. Geology, **10**, 179-185.

Barbarin, B. (1990). Granitoids: main petrogenetic classifications in relation to origin and tectonic setting. Geo. J., **25**, 227-238.

Bard, j. P., Maluski, H., Matte, P. & Proust, F. (1980). The Kohistan sequence: crust and mantle of an obducted island arc. Geol. Bull. Univ. Peshawar, **13**, 87-94.

Barker, A. J. (1990). Introduction to metamorphic textures and microstructures. Chapman and Hall, New York.

Beer, K. E. & Ball, T. K. (1986). Tin and tungsten in pelitic rocks from S.W. England and their behaviour in contact zones of granites and in mineralised areas. Ussher, Soc., 330-337.

Beer, K. E. & Ball, T. K. (1987). Tungsten mineralisation and magmatism in SW. England. Chron. Rech. Min., n° **487**, 53-62.

Benard, F., Moutou, P. & Pichavant, M. (1985). Phase relations of tourmaline leucogranites and the significance of tourmaline in silicic magmas. J. Geology, **93**, 271-291.

Beran, A., God, R., Gotzinger, M. & Zemann, J. (1985). A scheelite mineralization in calc-silicate rocks of the Moldanubicum (Bohemian Massif) in Austria. Mineral. Deposita, **20**, 16-22.

Boissavy-Vinau, M. & Roger, G. (1980). The TiO2 / Ta ratio as an indicator of the degree of differentiation of Tin granites. Mineral. Deposita, **15**, 231-236.

Boström, K., Peterson, M. N. A., Joensuu, O. & Fisher, D. E. (1969). Aluminum-poor ferromanganoan sediments on active ocean ridges. J. Geophys. Res., **74**, 3261-3270.

Bottrell, S. H., Carr, L. P. & Dubessy, J. (1988). A nitrogen-rich metamorphic fluid and coexisting minerals in slates from North Wales. Min. Mag., **52**, 451-457.

Bottrell, S. H. & Yardley, B. W. D. (1988). The composition of a primary granite-derived ore fluid from S.W. England, determined by fluid inclusion analysis. Geoch. Cosm. Acta, 52, 585-588.

Boyle, R. W. & Jonasson, I. R. (1973). The geochemistry of arsenic and its use as an indicator element in geochemical prospecting. J. Geoch. Exp., 2, 251-296.

Boynton, W. V. (1984). Cosmochemistry of the rare earth elements: meteorite studies. In: Henderson, P. (eds.), Rare earth element geochemistry. Elsevier, Amsterdam, 63-114.

Brimhall, G. H., Jr. (1977). Early fracture-controlled disseminated mineralisation at Butte Montana. Econ. Geol., 72, 37-59.

Brimhall, G. H., Agee, C. & Stoffregen, R. (1985). The hydrothermal conversion of hornblende to biotite. Can. Min., 23, 369-379.

Brookfield, M. E. & Reynolds, P. H. (1990). Miocene Ar^{40}/Ar^{39} ages from the Karakoram batholith and Shyok melange, N. Pakistan, indicate late Tertiary uplift and southward displacement. Tectonophysics, 172, 155-167.

Buchroithner, M. F. & Gamerith, H. (1986). On the geology of the Tirich Mir area, central Hindu Kush (Pakistan). Jb. Geol. B. A., 128, 367-381.

Calkins, J. A., Jamiluddin, S., Bhuyan, K. & Hussain, A. (1981). Geology and mineral resources of the Chitral-Partsan area, Hindu Kush range, Northern Pakistan. U. S. Geol. Surv. Prof. Paper, 716-G, 33.

Chalokwu, C. I. & Kuehner, S. M. (1992). Mineral chemistry and thermobarometry of a southern Appalachian amphibolite with epidote + quartz symplectite. Am. Min., 77, 617-630.

Chappell, B. W. & White, A. J. R. (1974). Two contrasting granite types. Pac. Geol., 8,173-174.

Chappell, B. W. & White, A. J. R. (1992). I- and S-type granites in the Lachlan fold belt. In: Brown, P. E & Chappell, B. W (eds.), The second Hutton symposium on the origin of granites and related rocks. Trans. R. Soc. Edinburgh Ear. Sci., 83, 1-26.

Chappell, B. W., White, A. J. R. & Wyborn, D. (1987). The importance of the residual source material (restite) in granite petrogenesis. J. Pet., 28, 1111-1138.

Cheilletz, P. A. (1985). Les minéralisations stratiformes à scheelite-biotite du Djebel Aouam (Maroc Central). Exemple de skarn d'infiltration dévelopé par remplacement de séries sédimentaires gréso-pélitiques. Bull. De Min., 108, 367-376.

Christensen, O. D., Capuano, R. A. & Moore, J. N. (1983). Trace-element distribution in an active hydrothermal system, Roosevelt hot springs thermal area, Utah. J. Vol. Geoth. Res., **16**, 99-129.

Clarke, D. B. (1981). The mineralogy of the peraluminous granites: a review. Can. Min., **19**, 3-17.

Clemens, J. D. & Vielzeuf, D. (1987). Constraints on melting and magma production in the crust. Earth Plan. Sci. Let., **86**, 287-306.

Collins, P. L. F. (1979). Gas hydrates in CO_2-bearing fluid inclusions and the use of freezing data for estimation of salinity. Econ. Geol., **74**, 1435-1444.

Coward, M. P., Jan, M. Q., Rex, D., Tarney, J. Thirlwall, M. & Windley, B. F. (1982). Geotectonic framework of the Himalaya N. Pakistan. J. Geol. Soc. London, **139**, 299-308.

Coward, M. P., Windley, B. F., Broughton, R. D., Luff, I. W., Petterson, M. G., Pudsey, C. J., Rex, D. C. & Asif Khan, M. (1986). Collision tectonics in the NW Himalayas. In: Coward, M. P. & Ries, A. C. (eds.), Collision tectonics. Geol. Soc. Spec. Pub., **19**, 203-219.

Crawford, M. B. (1988). Leucogranites of the northwest Himalayas. Unpubl. Ph.D. thesis, Univ. Leicester.

Crawford, M. L. (1981a). Phase equilibria in aqueous fluid inclusions. In: Hollister, L. S. & Crawford, M. L. (eds.), Short course in fluid inclusion: Applications to petrology, **6**, Miner. Ass. Canada, 75-100.

Crawford, M. L. (1981b). Fluid inclusions in metamorphic rocks- low and medium grade In: Hollister, L. S. & Crawford, M. L. (eds.), Short course in fluid inclusion: Applications to petrology, **6**, Miner. Ass. Canada, 157-181.

Crawford, M. L. (1992). Fluid inclusions-what can we learn? Earth Sci. Rev., **32**, 137-139.

Crawford, M. B. & Searle, M. P. (1992). Field relationships and geochemistry of pre-collisional (India-Asia) granitoid magmatism in the central Karakoram, northern Pakistan. Tectonophysics, **206**, 171-192.

Crawford, M. B. & Searle, M. P. (1993). Collision-related granitoid magmatism and crustal structure of the Hunza Karakoram, N. Pakistan. In: Treloar, P. J & Searle, M. P. (eds), Himalayan tectonics. Geol. Soc. Spec. Pub., **74**, 53-68.

Cullers, R. L. & Graf, J. L. (1984). Rare earth elements in igneous rocks of the continental crust: intermediate and silicic rocks-ore petrogenesis. In: Henderson, P. (eds.), Rare earth element geochemistry. Elsevier, Amsterdam, 275-316.

Cullers, R. L., Yeh, L. T., Chaudhuri, S. & Guidotti, C. V. (1974). Rare earth elements in Silurian pelitic schist from N. W. Maine. Geoch. Cos. Acta, 38, 389-400.

Dames & Moore. (1987). A report of ministry of planning and development, mineral sector development study, N. W. F. P., Pakistan. United consultant (Pvt) Ltd.

Davis, W. J. & Williams-Jones, A. E. (1985). A fluid inclusion study of the porphyry-greisen, tungsten-molybdenum deposit at Mount Pleasant, New Brunswick, Canada. Mineral. Deposita, 20, 94 -101.

Debon, F., Le port, P., Dautel, D., Sonet, J. & Zimmermann, J. L. (1987). Granites of western karakoram and northern Kohistan (Pakistan): a composite Mid-Cretaceous to Upper Cenozoic magmatism. Lithos, 20, 19-40.

Deer, W. A., Howie, R. A. & Zussman, J. (1962). Rock-forming minerals, sheet silicates. Vol. 3, Longman, London.

Deer, W. A., Howie, R. A. & Zussman, J. (1982). Rock-forming minerals, orthosilicates. Vol. 1A, Longman, London.

Deer, W. A., Howie, R. A. & Zussman, J. (1986). Rock-forming minerals, Disilicates and ring silicates. Vol. 1B, Longman, London.

Deer, W. A., Howie, R. A. & Zussman, J. (1992). An introduction to the rock-forming minerals. Longman, England.

Desio, A. (1959). Cretaceous beds between Karakoram and Hindu Kush ranges (Central Asia). Riv. Ital. di Paleont. and Strat., 65, 221-229.

Desio, A. (1979). Geologic evolution of the Karakoram. In: Farah, A. and Dejong, K. A. (eds), Geodynamics of Pakistan, Geol. Surv. Pakistan, Quetta, 111-1124.

Desio, A. & Zanettin, B. (1970). Geology of the Baltoro basin. Italian expeditions to the Karakoram (K2) and Hindu Kush (leader A. Desio), Scien. Rep. Sec. 11, 2, Brill, Leiden, 308.

Desio, A., Tongiorgi, E. & Ferrara, G. (1964). On the geological age of some granites of the Karakoram, Hindu Kush and Badakhshan (Central Asia). Rep. on 22nd Int. Geol. Congr., 11, 479-496.

Dewey, J. F., Cande, S. & Pitman III, W. C. (1989). Tectonic evolution of the India / Eurasia collision zone. Eclog. Geol. Helv., 82, 717-734.

DiPietro, J. A. & Lawrence, R. D. (1991). Himalayan structure and metamorphism south of the Main Mantle Thrust, Lower Swat, Pakistan. J. Metam. Geol., 9, 481-495.

Doolan, B. L., Zen, E. An. & Bence, A. E (1978). Highly aluminous hornblendes: composition and occurrences from southwestern Massachusetts. Am. Min., 63, 1088-1099.

Dymek, R. F. (1983). Titanium, aluminium and interlayer cation substitutions in biotite from high-grade gneisses, West Greenland. Am. Min., **68**, 880-899.

Edwards, R. & Atkinson, K. (1986). Ore deposit geology. Chapman and Hall, London.

Einaudi, M. T. & Burt, D. M. (1982). Introduction-terminology, classification, and composition of skarn deposits. Econ. Geol., **77**, 745-754.

Einaudi, M. T., Meinert, L. D. & Newberry, R. J. (1981). Skarn deposits. Econ. Geol., **75th Anniv. Vol.**, 317-391.

Engel, A. E. J & Engel, C. G. (1962). Hornblendes formed during progressive metamorphism of amphibolites, northwestern Adirondack Mountains, New York. Bull. Geol. Soc. Am., **73**, 1499-1514.

England, P. C. & Mckenzie, D. P. (1982). A thin viscous sheet model for continental deformation. Geophys. J. Roy. Astron. Soc., **70**, 295-321.

Ernst, W. G. (1972). Ca-amphibole paragenesis in the Shirataki District, Central Shikoku, Japan. Geol. Soc. Am. Mem., **135**, 73-94.

Evans, A. M. (1993). Ore geology and industrial minerals An introduction. Blackwell Scientific Publications, Oxford.

Exley, C. S. & Stone, M. (1982). Petrology of the granites and minor intrusions. In: Sutherland, D. S. (eds), Igneous rocks of the British Isle, John Wiley & Sons, 293-302.

Farrow, C. E. G. & Barr, S. M. (1992). Petrology of high-Al-hornblende- and magmatic-epidote-bearing plutons in the southeastern Cape Breton Highlands, Nova Scotia. Can. Min., **30**, 377-392.

Fletcher, C. J. N. (1985). Gold, antimony and tungsten mineralisation in the Chitral District, Northwest Frontier Province, Pakistan. Report for Sarhad Development Authority, Peshawar.

Flynn, R. T. & Burnham, W. (1978). An experimental determination of rare earth partition coefficients between a chloride containing vapor phase and silicate melts. Geoch. et Cos. Acta, **42**, 685-701.

Foster, M. D. (1962). Interpretation of the composition and a classification of the chlorites. US. Geol. Sur. Prof. Paper., **414-A**, 1-33.

Foster, R. P. (1977). Solubility of scheelite in hydrothermal chloride solutions. Chem. Geol., **20**, 27-43.

France-Lanord, C. & Le Fort, P. (1988). Crustal melting and granite genesis during the Himalayan collision orogenesis. Trans. R. Soc. Edinburgh Ear. Sci., **79**, 183-195.

Franklin, J. M., Lydon, J. W. & Sangster, D. F. (1981). Volcanic-associated massive sulfide deposits. Econ. Geol., **75th Anniv. Vol.**, 485-627.

Franz, G. & Spear, F. S. (1985). Aluminous titanite (sphene) from the eclogite zone, south-central Tauern Window, Austria. Chem. Geol., **50**, 33-46.

Frondel, C. & Baum, J. L. (1974). Structure and mineralogy of the Franklin zinc-iron-manganese deposits, New Jersey. Econ. Geol., **69**, 157-180.

Fyfe, W. S. (1960). Stability of epidote minerals. Nature, **187**, 497.

Garzanti, E., Baud, A. & Mascle, G. (1987). Sedimentary record of northward flight of India and its collision with Eurasia (Ladakh Himalaya, India). Geodin. Acta, **1**, 297-312.

Giere, R. (1990). Hydrothermal mobility of Ti, Zr and REE: examples from the Bergell and Adamello contact aureoles (Italy). Terra Nova, **2**, 60-67.

Giuliani, G., Li, Y. D. & Sheng, T. F. (1988). Fluid inclusion study of Xihuashan tungsten deposit in the southern Jiangxi province, China. Mineral. Deposita, **23**, 24-33.

Goldsmith, J. R. (1982). Review of the behaviour of plagioclase under metamorphic conditions. Am. Min., **67**, 643-652.

Graf, D. L. (1960). Geochemistry of carbonate sediments and sedimentary carbonate rocks. **Part 3**, Illinois State Geol. Surv. Circ., 301.

Grauch, R. I. (1989). Rare earth elements in metamorphic rocks. In: Lipin, B. R. & McKay, G. A. (eds.), Geochemistry and mineralogy of rare earth element. Min. Soc. America, Rev. in min., **21**, 147-167.

Green, T. H. (1977). Garnet in silicic liquids and its possible use as a P-T indicator. Contr. Min. Pet., **65**, 59-67.

Gustafson, L. B. & Williams, N. (1981). Sediment-hosted stratiform deposits of copper, lead, and zinc. Econ. Geol., **75th Anniv. Vol.**, 139-178.

Hall, A. (1971). Greisenisation in the granite of Cligga Head, Cornwall. Proc. Geol. Ass., **82**, 209 - 230.

Hall, A. (1990). Geochemistry of the Cornubian tin province. Mineral. Deposita, **25**, 1-6.

Harris, N. B. W. & Inger, S. (1992). Trace element modelling of pelite-derived granites. Cont. Min. Pet., **110**, 46-56.

Hayden, H. H. (1915). Notes on the geology of Chitral, Gilgit and the Pamirs. Records Ind. Geol. Surv., **45**, 271-235.

Henry, D. J. & Guidotti, C. V. (1985). Tourmaline as a petrogenetic indicator mineral: an example from the staurolite grade metapelites of NW Maine. Am. Min., **70**, 1-15.

Higgins, N. C. (1985). Wolframite deposition in a hydrothermal vein system: The Grey River Tungsten Prospect, Newfoundland, Canada. Econ. Geol., **80**, 1297 - 1327.

Higgins, J. B. & Ribbe, P. H. (1976). The crystal chemistry and space groups of natural and synthetic titanites. Am. Min., **61**, 878-888.

Honegger, K., Dietrich, V., Frank, W., Gansser, A., Thoni, M. & Trommsdorff, V. (1982). Magmatism and metamorphism in the Ladakh Himalaya (the Indus-Tsangpo suture zone). Earth Planet. Sci. Let., **60**, 253-292.

Hosking, K. F. G. (1982). A general review of the occurrence of tungsten in the world. In: Hepworth, J. V. & Zhang, Y. H. (eds), Tungsten Geology Jiangxi. China, (ESCAP RMRDC), Bandung Indonesia, 59-86.

Höy, T. (1976). Calc-silicate isograds in the Riondel area, southeastern British Columbia. Can. J. Ear. Sci., **13**, 1093-1104.

Impeokparia, E. G. (1985). Rare metal mineralisation in granitic rocks of the Tongolo anorogenic complex - Northern Nigeria. Mineral. Deposita, **20**, 81 - 88.

Itaya, T., Brothers, R. N. & Black, P. M. (1985). Sulfides, oxides and sphene in high-pressure schists from New Caledonia. Con. Min. Pet., **91**, 151-162.

Jambor, J. L. (1964). Studies of basic copper and zinc carbonates: synthetic zinc carbonates and their relationship to hydrozincite. Can. Min., **8**, 92-108.

James, D. W. & Ineson, P. R. (1993). Critique of exhalative hypothesis of tungsten skarn formation. Trans. Inst. Min. metall. (Sect. B: Appl. Earth Sci.), **102**, B205-B210.

Jan, M. Q. (1979). Petrography of pyroxene granulites from northern Swat and Kohistan. Geol. Bull. Univ. Peshawar, Spec. Issue, **11**, 65-87.

Jan, M. Q. (1980). Petrology of the obducted mafic-ultramafic metamorphites from the southern part the Kohistan island arc sequence. Geol. Bull. Univ. Peshawar, Spec. Issue, **13**, 95-108.

Jan, M. Q. (1988). Geology of amphibolites from the southern part of the Kohistan arc, N. Pakistan. Min. Mag., **52**, 147-159.

Jan, M. Q. & Howie, R. A. (1982). Hornblendic amphiboles from basic and intermediate rocks of Swat-Kohistan, norhwest Pakistan. Am. Min., **67**, 1155-1178.

Janeczek, J. & Sachanbinski, M. (1992). Babingtonite, Y-Al-rich titanite, and zoned epidote from the Strzegom pegmatites, Poland. Fur. J. Min., **4**, 307-319.

Jeffery, P. G. (1959). The geochemistry of tungsten, with special reference to the rocks of the Uganda Protectorate. Geoch. Cos. Acta, **16**, 278-295.

Jianming, C., Ruolan, L. & Guangsheng, Z. (1982). Study on fluid inclusion and its relation to mineralisation of Pangushan tungsten deposit, Jiangxi Province, China. In: Hepworth, J. V. & Zhang, Y. H. (eds), Tungsten Geology Jiangxi, China, (ESCAP RMRDC), Bandung, Indonesia, 233-243.

Jolliff, B. L., Papike, J. J. & Shearer, C. K. (1986). Tourmaline as a recorder of pegmatite evolution: Bob Ingersoll pegmatite, Black Hill, South Dakota. Am. Min., **71**, 472-500.

Kazmi, A. H., Lawrence, R. D., Dawood, H. Snee, L. W. & Hussain, S. S. (1984). Geology of the Indus suture zone in the Mingora-Shangla area of Swat, N. Pakistan. Geol. Bull. Univ. Peshawar, 17, 127-144.

Keppler, H. & Wyllie, P. J. (1991). Partitioning of Cu, Sn, Mo, W, U and Th between melt and aqueous fluid in the systems haplogranite-H_2O-HCl and haplogranite-H_2O-HF. Cont. Min. Pet., 109, 139-150.

Khaliq, A. (1991). Primary geochemistry and secondary dispersion from gold prospect in the Karakoram and Hindu Kush, N. Pakistan. Unpubl. Ph.D. thesis, Univ. Leicester.

Khan, M. A., Jan, M. Q., Windley, B. F., Tarney, J. & Thirlwall, M. F. (1989). The Chilas mafic-ultramafic igneous complex; the root of the Kohistan island arc in the Himalaya of northern Pakistan. Geol. Soc. America, Spec. Paper, 232, 75-94.

Kinnaird, J. A., Batchelor, R. A., Whitley, J. E. & Mackenzie, A. B. (1985). Geochemistry, mineralisation and hydrothermal alteration of the Nigerian high heat producing granites. In: High heat production (HHP) granites, hydrothermal circulation and ore genesis. Inst. Mini. Met., 169-195.

Koh, Y. K., Choi, S. G., So, C. S., Choi, S. H. & Uchida, E. (1992). Application of arsenopyrite geothermometry and sphalerite geobarometry to the Taebaek Pb-Zn (-Ag) deposit at Yeonhwa I mine, Republic of Korea. Mineral. Deposita, 27, 58-65.

Krauskopf, K. B. (1967). Introduction to geochemistry. McGraw-Hill.

Kwak, T. A. P. (1987). W-Sn skarn deposits and related metamorphic skarns and granitoids. Dev. Econ. Geol., 24, Elsevier, Amsterdam.

Labotka, T. C. (1983). Analysis of the compositional variations of biotite in pelitic hornfelses from northeastern Minnesota. Am. Min., 68, 900-914.

Lalonde, A. E. & Bernard, P. (1993). Composition and color of biotite from granites: two useful properties in the characterisation of plutonic suite from the Hepburn internal zone of Wopmay orogen, northwest territories. Can. Min., 31, 203-217.

Large, D. E. (1981). Sediment-hosted submarine exhalative lead-zinc deposits - a review of their geological characteristics and genesis. In: Wolf, K. H. (eds), Handbook of strata-bound and stratiform ore deposits. Elsevier, Amsterdam, 9, 469-507.

Larsen, R. B. (1991). Tungsten skarn mineralizations in a regional metamorphic terrain in northern Norway: a possible metamorphic ore deposit. Mineral. Deposita, 26, 281-289.

Leake, B. E. (1965). The relationship between tetrahedral aluminium and the maximum possible aluminium in natural calciferous amphiboles. Am. Min., 50, 843-851.

Leake, B. E. (1978). Nomenclature of amphiboles. Am. Min., 63, 1023-1053.

Leake, R. C. (1983). Mineralisation within the Chitral District and adjacent areas of N.W.F.P., Pakistan. Report for Sarhad development Authority, Peshawar.

Leake, R. C., Fletcher, C. J. N., Haslam, H. W., Khan, B. & Shakirullah. (1989). Origin and tectonic setting of stratabound tungsten mineralisation within the Hindu Kush of Pakistan. J. Geol. Soc. London, 146, 1003-1016.

Leake, R. C. & Haslam, H. W. (1985). Tungsten and other mineralization in the Hindu Kush, Chitral District, Northwest Frontier Province, Pakistan. Report for Sarhad Development Authority, Peshawar.

Lee, D. E., Mays, R. E., Van Loenen, R. E. & Rose, H. J. Jr. (1969). Accessory sphene from hybrid rocks of the Mount Wheeler mine area, Nevada. Prof. Paper Geol. Surv., 650-B, 41-46.

Le Fort, P. (1981). Manaslu leucogranite: a collision signature of the Himalaya, a model for its genesis and emplacement. J. Geoph. Res., 86, 10545-10568.

Le Fort, P. (1986). Metamorphism and magmatism during the Himalayan collision. In: Coward, M. P. & Ries, A. C. (eds.), Collision tectonics. Geol. Soc. Spec. Pub., 19, 159-172.

Le Fort, P., Debon, F. & Sonet, J. (1980). The "Lesser Himalayan" cordierite granite belt, typology and age of the pluton of Mansehra, Pakistan. Geol. Bull. Univ. Peshawar, Spec. Issue, 13, 51-61.

Le Fort, P., Cuney, M., Deniel, C., France-Lanord, C., Sheppard, S. M. F., Upreti, B. N. & Vidal, P. (1987). Crustal generation of the Himalayan leucogranites. Tectonophysics, 134, 39-57.

Lehmann, B. (1990). Metallogeny of tin. In: Bhattacharji, S., Friedman, G. M., Neugebauer, H. J. & Seilacher, A. (eds), Lectures notes in earth sciences, 32. Springer-Verlag, Berlin.

Lindstrom, R. M. & Anderson, D. L. (1985). Analytical neutron-capture gamma-ray spectroscopy: status and prospects. In: Ramau, S. (eds), Capture Gamma-ray Spectroscopy and related topic, 810.

Linnen, R. L. & Williams-Jones, A. E. (1993). Mineralogical constraints on magmatic and hydrothermal Sn-W-Ta-Nb mineralization at the Nong Sua aplite-pegmatite, Thailand. Eur. J. Min., 5, 721-736.

Lister, C. J. (1979). Quartz-cored tourmalines from Cape Cornwall and other localities. Proc. Ussher Soc., 4, 402-418.

Lottermoser, B. G. (1989a). Rare-earth element study of exhalites within the Willyama Supergroup, Broken Hill Block, Australia. Mineral. Deposita, 24, 92-99.

Lottermoser, B. G. (1989b). Rare-earth element behaviour associated with stratabound scheelite mineralisation (Broken Hill, Australia). Chem. Geol., 78, 119-134.

Lottermoser, B. G. (1992). Rare earth elements and hydrothermal ore formation processes. Ore Geol. Rev., 7, 25-41.

Mackenzie, I. F. (1983). The geology and geochemistry of tungsten mineralisation at Doctor Hill and Falls Creek, Central Westland, New Zealand. Unpubl. M.Sc. Thesis, Victoria University, Wellington.

MacLellan, H. E. & Taylor, R. P. (1989). Geology and geochemistry of the Burnthill granite and related W-Sn-Mo-F mineral deposits, central New Brunswick. Can. J. Earth Sci., 26, 499-514.

Manning, D. A. C. (1982). Chemical and morphological variation in tourmalines from the Hub Kapong batholith of peninsular Thailand. Min. Mag., 45, 139-147.

Manning, D. A .C. (1986). Contrasting styles of Sn-W mineralisation in peninsular Thailand and SW England. Mineral. Deposita, 21, 44 - 52.

Manning, D. A. C. & Henderson, P. (1984). The behaviour of tungsten in granitic melt-vapour system. Cont. Min. Pet., 86, 286-293.

Martin, R. F. & Bowden, P. (1981). Peraluminous granites produced by rock-fluid interaction in the Ririwai nonorogenic ring-complex, Nigeria: mineralogical evidence. Can. Min., 19, 65-82.

Maucher, A. (1976). The stratabound cinnabar-stibnite-scheelite deposits (discussed with examples from the Mediterranean region). In: Wolf, K. H. (eds), Handbook of stratabound and stratiform ore deposits. Elsevier, 10, 477-503.

Migisha, C. J. R. & Both, R. A. (1991). Mineralogy and genesis of the Trench tungsten-molybdenum deposit, Mount Mulgine, Western Australia. Mineral. Deposita, 26, 247-256.

Miller, C. F. (1985). Are strongly peraluminous magmas derived from pelitic sedimentary sources. J. Geol., 93, 673-689.

Miller, C. F. & Stoddard, E. F. (1981). The role of manganese in the paragenesis of magmatic garnet: an example from the Old Woman-Piute Range, California. J. Geology, 89, 233-246.

Miller, C. F., Stoddard, E. F., Bradfish, L. J. & Dollase, W. A. (1981). Composition of plutonic muscovite: genetic implications. Can. Min., 19, 25-34.

Miyashiro, A. (1973). Metamorphism and metamorphic belts. Unwin Limited, London.

Moles, N. R. (1983). Sphalerite composition in relation to deposition and metamorphism of the Foss stratiform Ba-Zn-Pb deposit, Aberfeldy, Scotland. Min. Mag., 47, 487-500.

Molnar, P. & Tapponnier, P. (1975). Cenozoic tectonics of Asia: effects of a continental collision. Science, **189**, 419-426.

Moody, J. B., Jenkins, J. E. & Meyer, D. (1985). An experimental investigation of the albitization of plagioclase. Can. Min., **23**, 583-596.

Mullis, J. (1979). The system methane-water as a geologic thermometer and barometer from the external part of the Central Alps. Bull. Miner., **102**, 526-536.

Neinavaie, H., Thalmann, F., Ataii, B. & Beran, A. (1989). Wolframite- and scheelite-bearing carbonate rocks of the Nock mountains, Austria: a new type of tungsten mineralisation in the eastern Alps. Mineral. Deposita, **24**, 14-18.

Neiva, A. M. R. (1974). Geochemistry of tourmaline (schorlite) from granites, aplites and pegmatites from Northern Portugal. Geo. et Cos. Acta, **38**, 1307-1317.

Newberry, R. J. (1982). Tungsten-bearing skarns of the Sierra Nevada. I. the Pine Creek mine, California. Econ. Geol., **77**, 823-844.

Newberry, R. J., Dillon, J. T. & Adams, D. D. (1986). Regionally metamorphosed, calc-silicate-hosted deposits of the Brooks Range, Northern Alaska. Econ. Geol., **81**,1728-1752.

Newton, R. C. (1989). Metamorphic fluids in the deep crust. Ann. Rev. Earth Planet. Sci., **17**, 385-412.

Niedermayr, G. & Schroll, E. (1983). The tungsten distribution in rocks of the Western Hohe Tauern. In: Schneider, H. J. (eds), Mineral deposits of the Alps and of the Alpine Epoch in Europe. Springer-Verlag, Berlin, 240-248.

Öhlander, B., Billstrom, K. & Hålenius, E. (1989). Geochemistry of the Proterozoic wolframite-bearing greisen veins and the associated granite at Rostberget, northern Sweden. Chem. Geol., **78**, 135-150.

Oosterom, M. G., Bussink, R. W. & Vriend, S. P. (1984). Lithogeochemical studies of aureoles around the Panasqueira Tin-tungsten deposit, Portugal. Mineral. Deposita, **19**, 283-288.

Palache, C., Berman, H. & Frondel, C. (1944). Dana's system of mineralogy. **Vol**. 1, John Wiley & Sons, New York.

Palache, C., Berman, H. & Frondel, C. (1951). Dana's system of mineralogy. **Vol**. 2, John Wiley & Sons, New York.

Parrish, R. R. & Tirrul, R. (1989). U-Pb age of the Baltoro granite, northwest Himalaya, and implications for zircon inheritance and monazite U-Pb systematics. Geology, **17**, 1076-1079.

Pascoe, E. H. (1924). General report of the Geological Survey of India for the year 1923. India Geol. Surv. Rec., **55**.

Patriat, P. and Achache, J. (1984). India-Eurasia collision chronology and its implications for crustal shortening and driving mechanisms of plates. Nature, **311**, 615-621.

Pearce, J. A. & Norry, M. J. (1979). Petrogenetic implications of Ti, Zr, Y, and Nb variations in volcanic rocks. Cont. Min. Pet., **69**, 33-47.

Perchuk, L. L. (1966). Temperature dependence of the coefficient of distribution of calcium between coexisting amphibole and plagioclase. Dokl. Acad. Sci. USSR, Earth Sci. Sec., **169**, 203-205.

Petterson, M. G. & Windley, B. F. (1985). Rb-Sr dating of the Kohistan arc-batholith in the Trans-Himalaya of N. Pakistan, and tectonic implications. Earth Planet. Sci. Let., **74**, 45-57.

Pierce, J. W. (1978). The northward motion of India since the late Cretaceous. Geophys. J. R. Astr. Soc., **52**, 277-311.

Pirajno, F. & Smithies, R. H. (1992). The FeO / (FeO + MgO) ratio of tourmaline: a useful indicator of spatial variations in granite-related hydrothermal mineral deposits. J. Geoch. Exp., **42**, 371-381.

Plant, J. A., O'Brien, C., Tarney, J. & Hurdley, J. (1985). Geochemical criteria for the recognition of high heat production granites. In: High Heat Production (HHP) Granites, Hydrothermal Circulation and Ore Genesis. Inst. Min. Met., 263-386.

Plimer, I. R. (1980). Exhalative Sn and W deposits associated with mafic volcanism as precursors to Sn and W deposits associated with granite. Mineral. Deposita, **15**, 275-289.

Plimer, I. R. (1984). The role of fluorine in the submarine exhalative systems with special reference to Broken Hill, Australia. Mineral. Deposita, **19**, 19-25.

Plimer, I. R. (1986). Tourmalinites from the golden dyke dome, Northern Australia. Mineral. Deposita, **21**, 263-270.

Plimer, I. R. (1987a). The association of tourmalinite with stratiform scheelite deposits. Mineral. Deposita, **22**, 282-291.

Plimer, I. R. (1987b). Fundamental parameters for the formation of granite-related tin deposits. Geol. Rundschau, **76**, 23-40.

Plyusnina, L. P. (1982). Geothermometry and geobarometry of plagioclase-hornblende bearing assemblages. Contr. Min. Pet., **80**, 140-146.

Poutiainen, M. (1990). Evolution of a metamorphic fluid during progressive metamorphism in the Joroinen-Sulkava area, southeastern Finland, as indicated by fluid inclusions. Min. Mag., **54**, 207-218.

Powell, C. M. (1979). A speculative tectonic history of Pakistan and surroundings: some constraints from Indian ocean. In: Farah, A. and Dejong, K. A. (eds), Geodynamics of Pakistan, Geol. Surv. Pakistan, Quetta, 5-24.

Pudsey, C. J. (1986). The Northern Suture, Pakistan: margin of a Cretaceous island arc. Geol. Mag., **123**, 405-423.

Pudsey, C. J., Coward, M. P., Luff, I. W., Shackleton, R. M., Windley, B. F. & Jan, M. Q. (1985). Collision zone between the Kohistan arc and the Asian plate in NW Pakistan. Trans. Roy. Soc. Edinburgh, **76**, 463-479.

Puziewicz, J. (1990). Post-magmatic origin of almandine-spessartine garnet in the Strzeblow alaskite (Strzegom-Sobotka granitic massif, SW Poland). N. Jb. Min. Mh., **4**, 168-175.

Raase, P. (1974). Al and Ti contents of hornblende, indicators of pressure and temperature of regional metamorphism. Contr. Min. Pet., **45**, 231-236.

Raith, J. G. (1988). Tourmaline rocks associated with stratabound scheelite mineralization in the Austroalpine Crystalline Complex, Austria. Min. Pet., **39**, 265-288.

Raith, J. G. & Prochaska, W. (1995). Tungsten deposits in the Wolfram schist, Namaqualand, South Africa: strata-bound versus granite-related genetic concepts. Econ. Geol., **90**, 1934-1954.

Rambaldi, E. R. (1973). Variation in the composition of plagioclase and epidote in some metamorphic rocks near Bancroft, Ontario. Can. J. Ear. Sci., **10**,852-868.

Rankin, A. H. & Alderton, D. H. M. (1985). Fluids in granites from southwest England. In: High heat production (HHP) granites, hydrothermal circulation and ore genesis. Inst. Mini. Met., 287-299.

Rao, A. T. & Rao, K. S. R. (1971). Clinozoisite from pegmatite near Kandali, Nellore District, Andhra Pradesh. Indian Min., **12**, 78-80.

Raynolds, R. G. H., Johnson, G. D., Johnson, N. M. & Opdyke, N. D. (1980). The Siwalik molasse: a sedimentary record of orogeny. Geol. Bull. Univ. Peshawar, **13**, 47-50.

Rex, A. J., Searle, M. P., Tirrul, A., Crawford, M. B., Prior, D. J., Rex, D. C. & Barnicoat, A. (1988). The geochemical and tectonic evolution of the central Karakoram, N. Pakistan. Phil. Trans. Roy. Soc. London, Ser. A, **326**, 229-255.

Ringwood, A. E. (1974). The petrological evolution of island arc system. J. Geol. Soc. London, **130**, 183-204.

Roberts, D. E. (1983). Metasomatism and the formation of greisen in Grainsgill, Cumbria, England. Geol. J., **18**, 43 - 52.

Robert, F. M. (1972). Stability of biotite: a discussion. Am. Min., **57**, 300-316.

Robinson, P. (1982). The amphibole formula. In: Veblen, D. R & Ribbe, P. H. (eds), Amphiboles: petrology and experimental phase relations. Min. Soc. America, Rev. Min., **9B**, 3-6.

Robinson, P., Schumacher, J. C. & Spear, F. S. (1982). Formulation of electron probe analyses. In: Veblen, D. R & Ribbe, P. H. (eds), Amphiboles: petrology and experimental phase relations. Min. Soc. America, Rev. Min., **9B**, 6-9.

Roedder, E. (1984). Fluid inclusions. Min. Soc. America, Rev. Min., **12**.

Rossi, P. H., Cocherie, A., Meyer, G., Fouillac, A. M. & Autran, A. (1988). Metallogenic W and Sn granites: genesis and main distinguishing features. In: Boissonnas, J. & Omenetto, P. (eds), Mineral deposits within the European community. Springer-Verlag, Berlin, 3-28.

Rossovskiy, L. N. (1991). Metallogenic specificity of pegmatite belts in the Pamirs and the Hindu Kush. Dok. Aka. Nauk SSSR, **319**, 447-450.

Rubin, J. N., Henry, C. D. & Price, J. G. (1993). The mobility of zirconium and other "immobile" elements during hydrothermal alteration. Chem. Geol., **110**, 29-47.

Saunders, C. M., Strong, D. F. & Sangster, D. F. (1992). Carbonate-hosted lead-zinc deposits of western Newfoundland. Geol. Surv. Canada, Bull., **419**, 1-78.

Schärer, U. (1984). The effect of initial ^{203}Th equilibrium on young U-Pb ages: the Makalu case, Himalaya. Earth Planet. Sci. Let., **67**, 191-204.

Schenk, P., Höll, R., München, Ivanova, G. F., Naumov, V. B. & Kopneva, L. A. (1990). Fluid inclusion studies of the Felbertal scheelite deposit. Geol. Rundschau, **79**, 451-466.

Schwartz, M. O. (1992). Geochemical criteria for distinguishing magmatic and metasomatic albite-enrichment in granitoids - example from the Ta-Li granite Yichun (China) and the Sn-W deposit Tikus (Indonesia). Mineral. Deposita, **27**, 101-108.

Scott, S. D. (1983). Chemical behaviour of sphalerite and arsenopyrite in hydrothermal and metamorphic environments. Min. Mag., **47**, 427-435.

Scott, S. D. & Barnes, H. L. (1971). Sphalerite geothermometry and geobarometry. Econ. Geol., **66**, 653-669.

Searle, M. P. (1991). Geology and tectonics of the Karakoram mountains. John Wiley & Sons, Chichester.

Searle, M. P. & Tirrul, R. (1991). Structural and thermal evolution of the Karakoram crust. J. Geol. Soc. London, **148**, 65-82.

Searle, M. P., Cooper, D. J. W. & Rex, A. J. (1988). Collision tectonics of the Ladakh-Zanskar Himalaya. Phil. Trans. Roy. Soc. London, Ser. A, **326**, 117-150.

Searle, M. P., Rex, A. J., Tirrul, R., Rex, D. C., Barnicoat, A. & Windley, B. F. (1989). Metamorphic, magmatic, and tectonic evolution of the central of the central Karakoram in the Biafo-Baltoro-Hushe regions of northern Pakistan. Geol. Soc. Am. Spec. Paper, **232**, 47-73.

Searle, M. P., Windley, B. F., Coward, M. P., Cooper, D. J. W., Rex, A. J., Rex, D. C., Li Tingdong, Xiao Xuchang, Jan, M. Q., Thakur, V. C. & Kumar, S. (1987). The closing of the Tethys and the tectonics of the Himalayas. Geol. Soc. Am., **98**, 678-701.

Shaw, S. E. & Flood, R. H. (1981). The New England batholith, eastern Australia: geochemical variations in space and time. J. Geoph. Res., **86**, 10530-10544.

Shepherd, T. J., Rankin, A. H. & Alderton, D. H. M. (1985). A practical guide to fluid inclusion studies. Blackie & Son Ltd, Glasgow.

Shikazono, N. (1984). Compositional variations in epidote from geothermal areas. Geoch. J., **18**, 181-187.

Shimazaki, H. (1977). Grossular-spessartine-almandine garnets from some Japanese scheelite skarns. Can. Min., **15**, 74-80.

Shvolman, V. A. (1978). Relics of the Mesotethys in the Pamirs. Hima. Geology, **8**, 369-378.

Siddiqui, R. H., Khan, Z. & Hussain, S. A. (1986). Xenothermal alteration and tungsten mineralization in Saindak area, Baluchistan, Pakistan. Act. Min. Pakistanica, **2**, 74-77.

Slack, J. F. (1982). Tourmaline in Appalachian-Caledonian massive sulphide deposits and its exploration significance. Trans. Inst. Min. metall. (Sect. B: Appl. Earth Sci.), **91**, B81-B89.

Slack, J. F., Herriman, N., Barnes, R. G. & Plimer, I. R. (1984). Stratiform tourmalinites in metamorphic terranes and their geologic significance. Geology, **12**, 713-716.

Slack, J. F., Palmer, M. R., Stevens, B. P. J. & Barnes, R. G. (1993). Origin and significance of tourmaline-rich rocks in the Broken Hill District, Australia. Econ. Geol., **88**, 505-541.

Smith, D. C. (1980). Highly aluminous sphene (titanite) in natural high-pressure hydrous eclogite facies rocks from Norway and Italy, and in experimental runs at high pressure. Abst. 26th Inter. Geol. Congr. Paris.

Sonnet, P., Verkaeren, J. & Crevola, G. (1985). Scheelite bearing calc-silicate gneisses in the Provence crystalline basement (Var, France). Bull. De Min., **108**, 377-390.

SOQUEM. (1984). Geological visit to mineral properties of Sarhad Development Authority. Report for Sarhad Development Authority, Peshawar.

Spear, F. S. (1980). NaSi⇔CaAl exchange equilibrium between plagioclase and amphibole. Contr. Min. Pet., 72, 33-41.

Spooner, E. T. C. (1981). Fluid inclusion studies of hydrothermal ore deposits. In: Hollister, L. S. & Crawford, M. L. (eds.), Short course in fluid inclusion: Applications to petrology, 6, Miner. Ass. Canada, 209-240.

Stanton, R. L. (1972). Ore petrology. McGraw-Hill Inc., New York.

Stemprok, M., Burnol, L. & Tischendorf, G. (1977). Metallization associated with acid magmatism. Geol. Surv. Czechoslovakia, 2, 41-96.

Stone, M. (1988). The significance of almandine garnets in the Lundy and Dartmoor granites. Min. Mag., 52, 651-658.

Stone, M. & Exley, C. S. (1986). High heat production granites of Southwest England and their associated mineralisation: A review. Trans. Inst. Min. Metal., 95, B25-36.

Sultan, S. (1990). A study of scheelite mineralisation in the Miniki Gol area, Chitral, Northern Pakistan. Unpubl. M.Sc. Thesis, Univ. Leicester.

Tahirkheli, R. A. K. (1982). Geology of the Himalaya, Karakoram and Hindu Kush in Pakistan. Geol. Bull. Univ. Peshawar, 15, 1-51.

Talent, J. A., Conaghan, P. J., Mawson, R., Molloy, P. D. & Pickett, J. W. (1982). Intricacy of tectonics in Chitral (Hindu Kush): faunal evidence and some regional implications. Geol. Surv. India Miscel. Pub., 41, 77-101.

Taylor, R. P., Ikingura, J. R., Fallick, A. E., Yiming, H. & Watkinson, D. H. (1992). Stable isotope compositions of tourmalinites from granites and related hydrothermal rocks of the Karagwe-Ankolean belt, northwest Tanzania. Chem. Geol., 94, 215-227.

Taylor, S. R. (1965). The application of trace element data to problems in petrology. Phys. Chem. Earth, 6, 135-213.

Taylor, S. R. & McLennan, S. M. (1985). The Continental crust: its composition and evolution. Blackwell Scientific Publications, Oxford.

Thakur, V. C. (1980). Tectonics of the central crystallines of western Himalaya. Tectonophysics, 62, 141-154.

Thalhammer O. A. R, Stumpfl, E. F. & Jahoda, R. (1989). The Mittersill scheelite deposit, Austria. Econ. Geol., 51, 1153-1171.

Thompson, A. B., & Connolly, J. A. D. (1992). Migration of metamorphic fluids: some aspects of mass and heat transfer. Earth Sci. Rev., 32, 107-121.

Tischendorf, G. (1977). Geochemical and petrographic characteristics of silicic magmatic rocks associated with rare-element mineralisation. In: Stemprok, M. Burnol, L.

Tischendorf, G. (eds) IGCP metallization associated with acid magmatism. Geol. Surv. Czechoslovakia, Prague. 2, 41-58.

Tukiainen, T. (1988). Niobium-tantalum mineralisation in the Motzfeldt Centre of the Igaliko nepheline syenite complex, South Greenland. In: Boissonnas, J & Omenetto, P. (eds), Mineral deposits within the European Community. Springer-Verlag, Berlin, 230-246.

Tulloch, A. J. (1979). Secondary Ca-Al silicates as low-grade alteration products of granitoid biotite. Contr. Min. Pet., 69, 105-117.

Turekian, K. K. & Wedepohl, K. H. (1961). Distribution of the elements in some major units of the earth crust. Geo. Soc. Am. Bull., 72, 175-192.

Tweto, O. (1960). Scheelite in the Precambrian gneisses of Colorado. Econ. Geol., 55, 1406-1428.

Van de Haar, A. J., Vriend, S. P. & van Gaans, P. F. M. (1993). Hydrothermal alteration of the Beira schist around the W-Sn specialised Regoufe granite, NW Portugal. J. Geoch. Exp., 46, 335-347.

Vidal, Ph., Cocherie, A. & Le Fort, P. (1982). Geochemical investigations of the origin of the Manaslu leucogranite (Himalaya, Nepal). Geoch. Cos. Act., 46, 2279-2292.

Von Damm, K. L., Edmond, J. M., Measures, C. I. & Grant, B. (1985). Chemistry of submarine hydrothermal solutions at Guaymas Basin, Gulf of California. Geo. et Cos. Acta, 49, 2221-2237.

Weisbrod, A. (1981). Fluid inclusions in shallow intrusives. In: Hollister, L. S. & Crawford, M. L. (eds.), Short course in fluid inclusion: Applications to petrology, 6, Miner. Ass. Canada, 241-271.

White, A. J. R. & Chappell, B. W. (1988). Some supracrustal (S-type) granites of the Lachlan fold belt. Trans. R. Soc. Edinburgh Ear. Sci., 79, 169-181.

Wilkinson, J. J. (1990). The role of metamorphic fluids in the development of the Cornubian ore field: fluid inclusion evidence from south Cornwall. Min. Mag., 54, 219-230.

Willner, A. P. (1992). Tourmalinites from the stratiform peraluminous metamorphic suite of the Central Namaqua mobile belt (South Africa). Mineral. Deposita, 27, 304-313.

Wood, S. A. (1990). The aqueous geochemistry of the rare earth elements and yttrium: 2. Theoretical predictions of speciation in hydrothermal solutions to 350°C at saturation water vapor pressure. Chem. Geol., 88, 99-125.

Woodsworth, G. J. (1977). Homogenization of zoned garnets from pelitic schists. Can. Min., 15, 230-242.

Yeats, R. S. & Lawrence, R. D. (1983). Tectonics of the Himalayan thrust belt in Northern Pakistan. In: Haq, B.U. and Milliman, J.D. (eds), Marine geology and oceanography in the Arabian Sea and coastal Pakistan. Van Nostrand Reinhold, New York, 177-198.

Zeschke, G. (1961). Prospecting for ore deposits by panning heavy minerals from river sands. Econ. Geol., 56, 1250-1257.